The role of Rho GTPases in ~~the~~ regulation of macrophage motility and morphology

by

Ann Wheeler

A thesis submitted to the University of London for the degree of Doctor of Philosophy, February 2005

Ludwig Institute of Cancer Research
91 Riding House Street
London W1W 7BS

Laboratory for Molecular Cell Biology
University College London
Gower Street
London WC1E 6BT

ProQuest LLC
789 East Eisenhower Parkway
P.O. Box 1346
Ann Arbor, MI 48106-1346

Abstract

Rho GTPases are important regulators of cell motility and morphology. Mammals have three highly homologous Rho proteins, RhoA, RhoB and RhoC. The aim of this thesis was to determine whether individual isoforms of Rho have unique functions in the regulation of cell motility using primary bone marrow-derived macrophages (BMM) as a model system. BMMs were shown to express RhoA, RhoB but not RhoC.

BMMs were analysed to determine the role of RhoA and RhoB in motility and morphology. A comparison between RhoA and RhoB-null was carried out using a combination of RhoB-null BMMs, and BMM treated with the pan Rho inhibitor C3-transferase and the Rho kinase inhibitor Y27632. RhoB-null BMMs moved faster and had a smaller spread area than wild-types. Whereas BMM treated with C3-transferase and Y27632 had reduced migration. The RhoB-null BMMs did not change shape following CSF-1 withdrawal unlike wild-type cells. Analysis of BMM spreading and adhesion revealed that deletion of *RhoB* caused defects in the initial stages of cell spreading and adhesion. Interestingly in RhoB-null BMMs the GTPase activity of RhoA and Rac1 and phosphorylation of their targets LIMK and MLC was decreased less in response to withdrawal of CSF-1 than in wildtype cells. This suggests that RhoB may be acting as a 'brake' for RhoA activity.

Table of contents

Table of Figures

Table of tables

1 Introduction

1.1 Introduction to cell migration:

Cell migration is an essential part of the development and function of multicellular organisms. Most cell types are capable of movement; some are only motile during part of the life cycle of the organism, for example in embryogenesis or in wound healing. For others, such as cells in the adaptive immune system, motility is an essential part of their function.

Within wounded tissue several processes occur to ensure adequate repair occurs. When a tissue is damaged by wounding or by a pathogenic micro-organism the body firstly initiates an inflammation response. This is marked by the influx of leukocytes to the wounded tissue within hours of injury. Inflammation is a complex series of events that include: Vasodilation, which increases the flow of blood to the affected area, allowing more leukocytes to be brought to the wound; increase in vascular permeability, which facilitates leukocyte movement from capillaries to the site of infected tissue; and chemotaxis of leukocytes to the site of infection followed by phagocytosis of micro-organisms or damaged cells (Fig. 1.1) (Albelda et.al. 1994, Burke and Lewis, 2002). The wounded tissue attracts leukocytes by secreting chemoattractants (Ben-Baruch, 1995; Lee et al. 2000). Neutrophils are the first leukocytes to arrive at a wound. After they arrive at the wound they phagocytose bacteria and they secrete factors (such as CC family chemokines and phospholipids). These then promote the recruitment of macrophages and T lymphocytes to the wounded tissue (Albelda. 1994; Lauber et al. 2003). Together these leukocytes clear the wound of pathogens and promote healing of the wound (Burke and Lewis, 2002).

The regulation of cell motility in a whole organism is crucial to its function, but cell migration also contributes to disease progression. For example, many deaths from cancer are due to the spread of tumours through metastasis. Metastasis is essentially a corruption of cellular function which causes inappropriate cell migration.

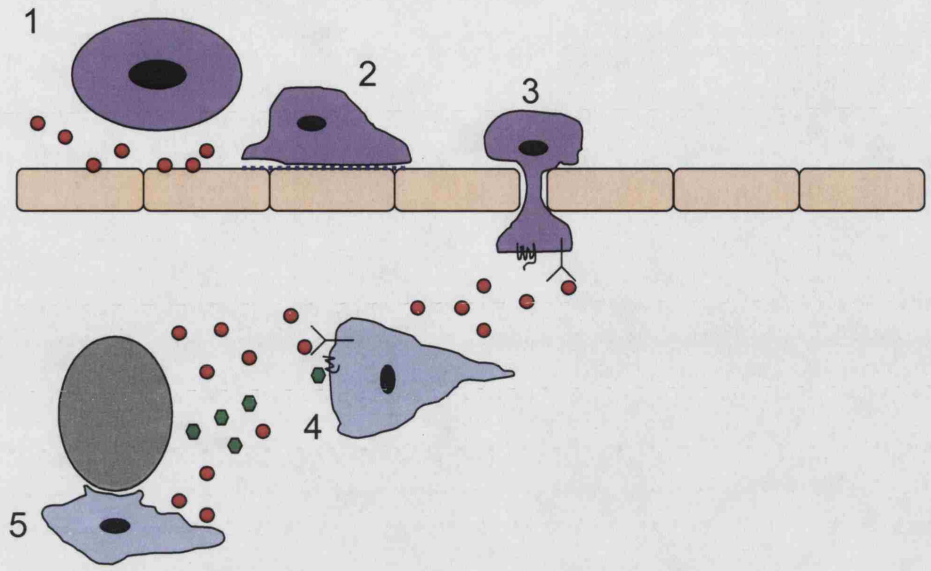

Figure 1.1: Schematic diagram showing monocyte recruitment to an inflammatory site. Monocytes are shown in purple, macrophages are shown in light blue. Chemoattractant molecules secreted by tissues and cells other than apoptotic cells are shown in red, e.g. CSF-1, MCP-1 and complement. Chemoattractants secreted by apoptotic cells are shown in green.

1. Chemo-attractants are presented on the endothelium. If monocytes encounter chemoattracants, such as CSF-1 and MCP-1, presented on the surface of the endothelial cells they begin to attach to the endothelial membrane (Lu et al. 1998; Pixley and Stanley, 2004). 2. The initial interaction between a monocyte and the endothelium is mediated by selectins, this is a weak tethering reaction (Albelda 1994; Ivetic and Ridley, 2004). Monocytes then form firmer adhesions mediated by integrins (Ben-Baruch, 1995; Hogg et al. 2002). 3. Monocytes then bind to the endothelium and move to cell junctions. Next they secrete factors which aid their transmigration through the endothelial membrane and then diapedese through the endothelium (Schenkel et al. 2004; Worthylake, 2001). 4. Monocytes differentiate into macrophages in the interstitial tissue milleu and chemotax towards apoptotic cells (e.g. neutrophils) through the extracellular matrix (ECM). This is mediated by signals secreted by the tissue cells and the apopotic cell itself. (Lauber et al. 2003) 5. Macrophages bind to and phagocytose the apoptotic cells (Leverrier and Ridley, 2001).

The mechanical process controlling cell migration is relatively similar for all mammalian cells. For a cell to migrate, in general, it needs to adopt a polarised morphology. This involves formation and forward movement of the lamella and formation of new adhesions at the front of the cell. Next the cell body needs to move in the direction of polarisation. This involves generation of tractional forces. The final stage in the process is detachment of the rear of the cell. This can either involve disassembly of adhesions at the back of the cell and retraction of the cell tail, or the cell tail can be left behind (Fig. 1.2) (Abercrombie et al. 1971; Mitchison and Cramer, 1996; Ridley, 2004). The methods cells use to orchestrate this motility varies dependent upon cell type. Cells can migrate as individuals or as a group such as epithelial cells in wound repair or in dorsal closure (Wood et al. 2002). The migratory properties of cells, for instance the speed of cell migration and the morphology of cells during migration, can be affected dramatically by its immediate environment (Friedl, 2004).

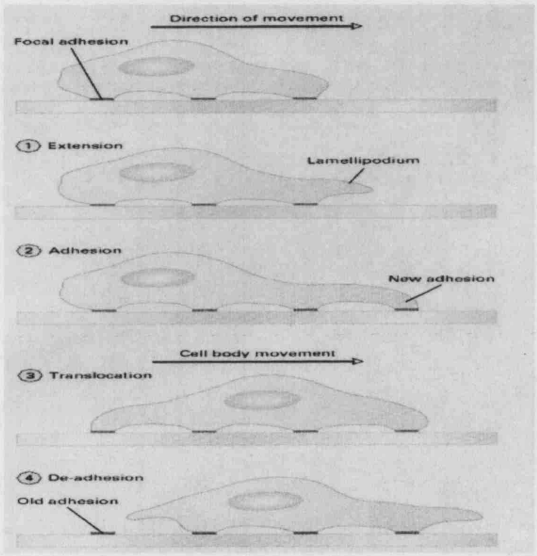

- Protrusion, forward movement of the cell membrane.
- Polarisation, this involves restructuring of the cytoskeleton so that it 'facing' in the direction that it intends to move in and formation of new adhesions.
- Translocation, which involves traction of the cell body in the intended direction of movement.
- Tail retraction and de-adhesion of the cell rear.

Figure 1.2: The cell migration cycle taken from (Mitchison and Cramer, 1996)

1.2The cytoskeleton in cell motility

Cell motility is orchestrated through the cytoskeleton; there are 3 types of cytoskeletal filaments in mammalian cells, actin, microtubule and intermediate filament. These share common properties that are required to make good scaffolding for the cell. The cytoskeleton provides a rigid three-dimensional supportive environment for intracellular function. Actin and microtubule filaments are polarised providing a highway for

transportation and communication within the cell. This also allows the cell to orient itself in three dimensions in response to its environment. Each type of filament has very different biochemical and biophysical properties (Howard, 2001), and this reflects the differences in their contribution to cellular function. Time-lapse fluorescence microscopy of actin and microtubules in migrating cells shows that they are both actively involved in the process of cell locomotion (Ballestrem et al. 1998).

1.2.1 Actin

The actin cytoskeleton has the properties of a viscous gel. It is fluid enough to allow movement of the cell membrane, viscous enough to provide structural support for the cell membrane and sufficiently elastic to allow sufficient force generation for forward movement of the cell membrane. Actin has been shown to be absolutely essential for cell migration (Mitchison and Cramer, 1996). During the process of protrusion of the cell membrane it has been shown that almost no translation of actin mRNA takes place (Higgs and Pollard, 2001). This indicates that all of the actin required for polymerisation is already present within the cell.

Actin filaments are 6 nm in diameter and are polar; with a barbed end and a pointed end. The barbed end nucleates monomeric globular actin (G-actin) more rapidly than the pointed end. Actin polymerisation requires ATP bound actin and Mg^{2+} (Pollard, 1983). Profilin catalyses this process by binding to G-actin and promoting nucleotide exchange to recycle ADP-actin to ATP-actin. Thymosin β4 competes with profilin for actin binding, however Thymosin β4 sequesters G-actin so it cannot polymerise. Therefore this G-actin can be considered to be removed from the actin cycle (Millard et al. 2004). The barbed ends of actin filaments are juxtaposed with the cell membrane. This means that addition of actin onto the barbed end will create force against the cell membrane causing it to move outwards (Millard et al. 2004). This force is regulated by the binding of the barbed ends by capping proteins (e.g. Cap2 and gelsolin). Ena/VASP proteins are present at the edge of lamellipodia and at filopodial tips. Here they compete with capping proteins for binding of barbed ends (Bear et al. 2002). More barbed ends are generated through WASP/Scar mediated activation of the Arp2/3 complex. The Arp2/3 promotes branching of the actin filaments through nucleation of new filaments onto preexisting actin filaments (Millard et al. 2004). Severing of older filaments is necessary to release actin monomers and short filaments for recycling back into the

actin pool and is mediated by proteins such as ADF/cofilin (Mitchison and Cramer, 1996). Proteins such as LIM kinase (LIMK) inhibit ADF/cofilin and can promote protrusion by allowing longer actin filaments to be generated.

Cryoelectron micrographs of the front of the cell show that lamellae, filopodia, microspikes and other structures at the leading edge of a migrating cell are comprised of a complex actin meshwork (Svitkina and Borisy, 1999; Svitkina et al. 1997) (Fig. 1.3). The lamella consists of a spread actin meshwork where a large number of barbed ends face the leading edge (Svitkina and Borisy 1999) (Fig. 1.3a). At the leading edge of the lamellae is the lamellipodia where G actin is nucleated onto preexisting actin filaments (Higgs and Pollard. 2001) (Fig 1.3c). This presumably generates the force required for moving the whole membrane forwards. In filopodia the actin is organised into long filaments which are held together by cross-linking proteins (Svitkina and Borisy. 2003, Biyasheva et al. 2004). The differences in these structures has been attributed to actin bundling and also by the regulation of capping protein and Ena/Vasp (Mejillano et al. 2004; Yamashiro et al. 1998). Actin binding proteins such as the ezrin, radixin and moesin proteins are localised at the tips of microvilli and are important in regulating the morphology of these protrusions (Ivetic and Ridley. 2004).

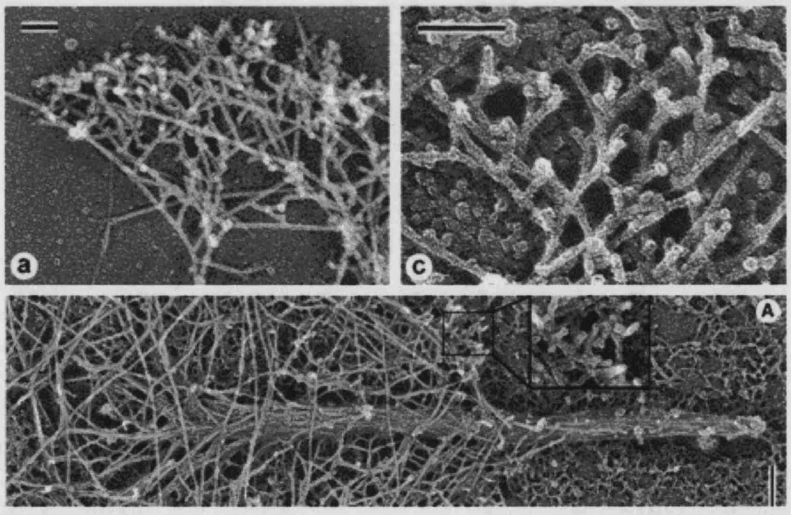

Figure 1.3: Cryo-electron micrographs of the actin cytoskeleton showing:
a) the dendritic filaments of a lamella. c) A close up image of branching actin filaments. (A) A filopodium taken from (Svitkina and Borisy, 1999; Svitkina et al. 2003)

1.2.2 Myosin

Myosin has been understood for a long time to be a key molecule for the generation of force required for cell motility. Using cyro-electron microscopy the structure of the myosin molecule has been resolved to show that it consists of two functional domains. The head domain, which is comprised of a heavy chain which binds actin and generates force through hydrolysis of ATP and a regulatory domain consisting of a regulatory light chain (MLC) and one or more IQ motifs. The tail domain is an association domain, which can bind to another myosin or other molecules (Malik and Gross, 2004). Myosin II (conventional myosin) is important in cell motility as it is known to generate local contractility in the cell. This is required in cytokinesis, in cell shape change, cell spreading and in wound healing (Mitcheson and Cramer1996).

1.2.3 Microtubules

Microtubules form pipe like structures. They are made up of tubulin heterodimers and have a diameter of 25 nm. There are 5 types of tubulin, of which α and β dimers make up the microtubules (Fujikawa and Tilney, 1975, Mitcheson 1995). γ tubulin is found at the centrosome, can nucleate microtubules and is important in formation of the mitotic spindle (Zheng et al. 1995). δ tubulin is localised in the basal body of the centriole. ε tubulin is found in the pericentriolar region. The cellular process where the role of microtubules has been best characterised is cell division. The mitotic spindle is formed of microtubules which exert tractional forces required for chromosomal segregation (Mitchison, 1995). However microtubules are also essential for determining cell polarity, vesicular locomotion, structural support and intracellular transport.

Microtubules are polar, with the minus ends generally anchored in the microtubule organising centre (MTOC) or centrosome. The + ends grow out as far as the cell periphery in many cell types. This allows transport to and from the periphery of the cell using the microtubule motor proteins kinesin and dynein. In a migrating cell the MTOC is often found to be in front of the nucleus oriented towards the leading edge (Houliston et al. 1987). This facilitates cell polarisation by allowing microtubules to grow into the leading edge. It also allows microtubule-mediated delivery of Golgi-derived vesicles containing proteins and membrane into the area where the cell is actively polarising (Etienne-Manneville, 2004). In general microtubule + ends within the lamella maintain

a constant distance from the lamellipodium, there is a large amount of turnover of microtubules in the lamella and this process is known as dynamic instability (Rodriguez et al. 2003).

1.2.4 Intermediate filaments

Intermediate filaments (IF), with a diameter of 10 nm are made up of intertwined protein strands and are more rope like in structure. Unlike actin and microtubules, IF are comprised of proteins with no known enzymatic activity. They are also very heterogeneous in their make up, particularly their non α-helical amino and carboxyl terminus domains. Over 50 different types of IF are present in humans (Fuchs and Cleveland, 1998). They vary considerably in their properties and are highly tissue specific in their expression; as such they can be used as cytoskeletal identity cards that allow one cell type to be distinguished from another. IF radiate through the cell in all directions and are important in relaying mechanical information across the cell (Chang and Goldman, 2004). IF may provide a signalling scaffold across the cell, and are phosphorylated by several kinases including Rho kinase (ROCK), protein kinase C (PKC), p21-activated kinase (PAK), and p38 mitogen activated protein kinase (MAPK) (Chang and Goldman, 2004). During the early stages of cell spreading in fibroblasts and nerve cells the IF system is present as discrete particulate structures in the cytoplasm. Later these particles fuse into squiggles, which then condense into filamentous structures. The movement of these IF particles is dependent on an intact microtubule cytoskeleton (Prahlad et al. 1998). Some IFs are important for cell motility, e.g. embryonic fibroblasts from a vimentin null mouse have impaired mechanical stability and reduced motility, though the role of vimentin in cell motility has not yet been described. IFs are also present in some cell adhesions such as podosomes (Correia et al. 1999), found in the leading edge of macrophages.

1.3 Introduction to Rho GTPases

Rho GTPases play a central role in regulating cell shape, polarity and locomotion through their effects on actin polymerization, actomyosin contractility, cell adhesion and microtubule dynamics (Ridley, 2001b). Rho GTPases are part of the Ras small GTPase super-family, which, with a few notable exceptions, are molecular switches that cycle between a GTP-bound active and a GDP-bound inactive confirmation (Hall,

2000) (Fig. 1.4A). GTP bound Rho proteins are contacted by effectors wihch activate a plethora of responses. The activity of Rho proteins is promoted by guanine nucleotide exchange factors (GEF), which exchange the GDP moiety on the GTPase for GTP. GTPase activating proteins (GAP) inhibit Rho protein activity by catalysing the hydrolysis of the γ–terminal phosphate group. This causes a conformational change in the GTPases that reduces the efficacy of effector binding (Ihara et al. 1998). The activity of these GEFs and GAPs is regulated by autocrine and paracrine signalling cascades (Hall, 2000). There are over 80 GEFs and 70 GAPs for Rho family GTPases and their activity is tightly regulated and can be highly specific (Bishop and Hall, 2000; Schmidt and Hall, 2002).

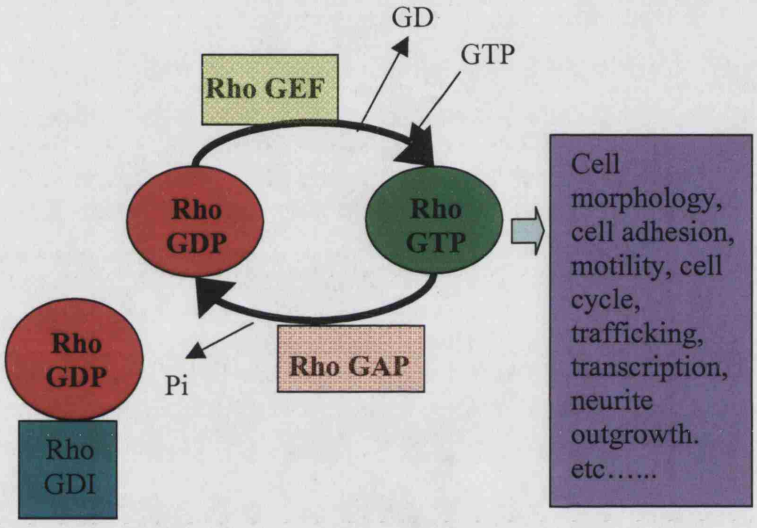

Figure 1.4: A schematic diagram of the regulatory cycle of Rho GTPases

RhoA, Rac1 and Cdc42, have taken centre stage in these functional studies primarily because they were the first to be described as playing an important role in the response of the actin cytoskeleton to extracellular stimuli. Activation of RhoA stimulates formation of stress fibres (Ridley and Hall. 1992). Stress fibres are filaments of actin, which stretch across the basal and dorsal surfaces of some cell types (Fig 1.5). Contraction and relaxation of stress fibres has been shown to mediate cell tension in certain cell types (Kaibuchi et al 1999, Small and Kaverina). Rac stimulates formation of multiple lamella and lamellipodia within cells (Ridley et al. 1992). Lammelae are thin, semicircular, vales of actin found on the dorsal surface of cells, which are made up of a branched network of actin filaments (Chapter 1.2.1 and Fig 1.5) (Svikina and Borisy.1999). The lamellipodia is found at the very edge of the lamellae it is a dynamic

area of cell protrusion, retraction and adhesion turnover. Cdc42 regulates formation of filopodia (Fig. 1.5) (Kozma et al. 1995; Nobes and Hall, 1995). Filopodia are thin bundles of F-actin that protrude from the cell membrane of cells (Svitkina and Borisy. 2001). Filopodia have been associate with axon guidance and dorsal closure (Wood et al 2002).

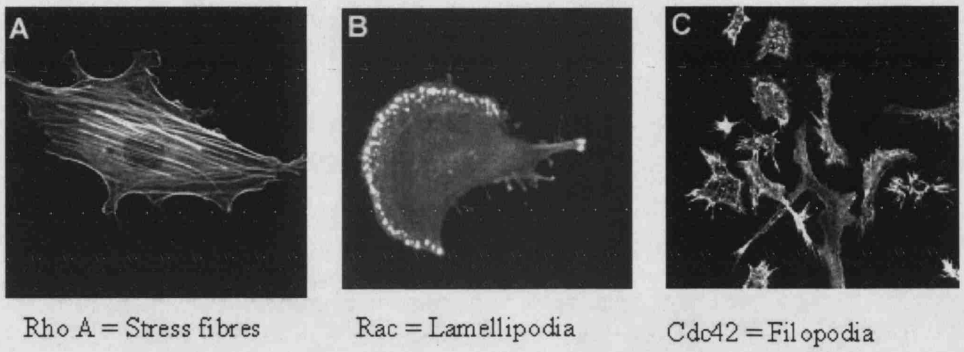

Figure 1.5: Actin morphologies which are stimulated by Rho GTPases.
A) Stress fibres in a NIH3T3 cell. B) Leading lamella and lamellipodia in a cell of the macrophage cell line IC21. C) Filopodia and microspikes in bone marrow macrophage. In all examples F-actin is shown using phalloidin staining.

In higher vertebrates 3 Rho family GTPases are present, RhoA, RhoB and RhoC. These are structurally similar and share 85% amino acid sequence homology. Although RhoB and RhoC were cloned at the same time as RhoA (Madaule and Axel, 1985), they have received less attention because of their extensive homology to RhoA and because over-expression studies indicated that, like RhoA, they induced stress fibres in cells (Hall et al. 1993; Ridley, 1997b; Ridley and Hall, 1992). RhoB was shown to have a different localization to RhoA very early on suggesting a unique function, but despite this it has been relatively little studied (Adamson et al. 1992).

1.4 The evolution of Rho proteins

To determine when each of these Rho proteins emerged in terms of evolution the UNIPROT database was searched with the human RhoA GTPase domain (amino acids 1-90 of RhoA). The results were sorted according to organism, and UNIGENE and BLAST were used to compare the homology of identified genes with Human genes. Results from ten organisms, representing different branches of the evolutionary tree,

show that the number of Rho proteins increase as organisms become more complex (Table 1.1).

Name	Type of organism	No. of Rho family GTPases	RhoA	RhoB	RhoC
Dictyostelium	Protoctisan	9	/	/	/
S.Cerevisiae	Fungi, yeast	6	Y	/	/
C.Elegans	Nematode worm	5	Y	/	/
D.Melanogaster	Arthropod, fly	7	Y	/	/
C.Intestalis	Simple Chordate	15	Y	/	/
D.Rerio	Vertebrate, fish	12	Y	/	Y
X.Laevis	Amphibian, frog	18	Y	/	Y
G.Gallus	Endothermic, bird	20	Y	Y	Y
M.Musculus	Mammal, rodent	20	Y	Y	Y
H.Sapiens	Mammal, Primate	20	Y	Y	Y

Table 1.1: Evolution of RhoA, RhoB and RhoC

A search of bacterial genomes showed that are no proteins with homology to the human RhoA GTPase domain, making emergence of Rho family GTPases a unique step forward in the evolution of eukaryotes. Simple fungi such as *Saccharomyces cerevisiae* (*S. cerevisiae)* and *Saccharomyces Pombe* (*S.* Pombe) contain 5 Rho GTPases; Rho1 is most similar functionally to RhoA and is essential for cytokinesis (Hall, 2000) and Cdc42, required for organising polarised budding (Etienne-Manneville, 2004). Simple fungi do not contain a Rac-like GTPase, but as they are not motile Rac may not be required for survival. In more complex invertebrates the number of Rho GTPases hovers around 6-8. *Dictyostelium discoideum* (*Dictyostelium*) unusually lacks RhoA favouring 8 Rac like genes. *Dictyostelium* also contains the first 'evolutionary incidence' of RhoBTB proteins which are Rho GTPases containing a 400-amino acid C-terminal broad-tramtrack-domain. Interestingly chordate organisms contain nearly twice as many Rho GTPases as their non-chordate compatriots. It is not known why more Rho family proteins are present in chordates. Potentially these novel Rho isoforms may play role in the development and function of the more complex nervous system of chordate organisms (Govek et al. 2005). All invertebrates contain only one *rhoA*-like protein, whereas vertebrates have more than one Rho. In evolutionary terms *rhoC* emerged first, amphibians and fish have a *rhoA* and *rhoC*. So far, in published genomes, *rhoB* has first identified in birds (Wallis et al. 2004). It is unfortunate that at this time a published fully

sequenced genome of *Danio Rerio* and *Xenopus laevis* is unavailible for analysis (Table 1.1).

There are over 20 Rho GTPases present in higher mammals. A comparison of their primary amino acid sequence shows that several them into sub-families (Wherlock and Mellor, 2002) (Fig. 1.6). RhoA, RhoB and RhoC are an example of this. In mouse and human the amino acid sequence of each of these 3 Rho proteins is virtually identical. On a genetic level, however though these 3 homologues are very different. *rhoA* consists of 5 exons, *rhoC* has 5 exons, while *rhoB* contains only 1 exon (Hall, 2000) (Table 1.2).

Rho isoform	Chromosomal location	Gene Bp	No exons	mRNA Bp	Gene product amino acids	Protein kDa
RhoA	3p21.3	52818	5	1792	193	21.74
RhoB	2p21.4	591	1	590	196	22.12
RhoC	1p13.2	5997	5	1067	193	22.01

Table 1.2: Comparison of the genes of Rho

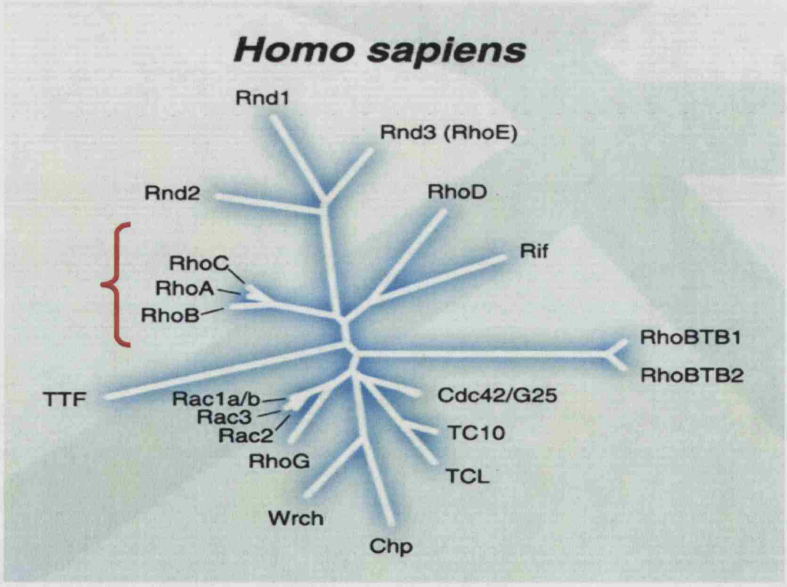

Figure 1.6: The Rho GTPase phylogenetic tree in *Homo Sapiens* taken from (Wherlock and Mellor, 2002)

In humans, rats and mice the three Rho genes are found on different chromosomes (Table 1.2) (Cannizzaro et al. 1990). The *rhoA* gene is longer and contains more exons

and introns than *rhoB* or *rhoC*. Therefore, it is suggested that *rhoC* arose due to an incomplete duplication of *rhoA*. The *rhoB* gene is far smaller and contains only one exon, and is thought to have arisen by reverse transcription (Wherlock and Mellor, 2002). Northern blotting shows that the 3 Rho GTPases are expressed in all tissues tested (Genecards http://www.rzpd.de/cgi-bin/cards/carddisp). However the expression the expression levels of RhoA, RhoB and RhoC vary significantly. For example, *rhoC* is highly up-regulated in metastatic cancers compared to non-metastatic cancers (Kleer and Meravjer 2002). A possibly unique role of *rhoC* in metastasis is indicated by the fact that expression of *rhoC* but not *rhoA* enhanced melanoma cell metastasis in an animal model (Clark et al. 2000). However, *rho*A expression is also increased in some cancers (Ridley, 2004).

1.5 Regulation of Rho expression

In cultured cells, *rhoB* expression but not *rhoA* or *rhoC* is induced by a variety of stimuli such as UV irradiation, cytokines or growth factors, at least in part due to activation of the *rhoB* promoter (Fritz et al. 1995). On the other hand, *rhoB* expression is reduced by Ras via Akt/PKB (Jiang et al. 2004b). RhoB levels vary through the cell cycle, and the *rhoB* transcript has a half-life of 30 minutes, which is substantially shorter than *rhoA* or *rhoC* (Zalcman et al. 1995). This indicates that RhoB's function requires its expression to be highly regulated. Together these results indicate that there are marked differences in gene regulation of the three isoforms of the Rho family, which is likely to reflect different functions for the three proteins.

1.6 Expression in development

Rho proteins are required for processes involving cell migration in development, including neurite outgrowth, dorsal closure, bone formation and myogenesis (Settleman, 2001). The model organisms *Caenorhabditis elegans* (C.Elegans) and *Drosophila melanogaster* (D. Melanogaster) are often used for developmental studies but only have one Rho protein (Redd et al. 2004; Wherlock and Mellor, 2002) (Table 1.1) and so a comparison of the roles of RhoA, RhoB and RhoC in development requires studies on

higher organisms. Studies in which RhoA activity was abrogated through expression of a RhoGDI show that loss of function of Rho is embryonically lethal in mouse development by E7 (Wei et al. 2002). This is attributed to failure in gastrulation and an inability of cells to migrate, a process that has been characterised in more detail in Drosophila (Magie et al. 1999). In contrast, RhoB-null mice are viable and fertile (Liu et al. 2001). Indicating that RhoB plays more specific roles in cell function. RhoB-null mice have defects in retinal development and are not as fertile as wild-type mice. It is not known whether these differences represent defects in migration or cell survival (Adini et al. 2003). *rhoB* has been seen to be transiently expressed in several developing tissues, for example in delaminating neural crest cells (Del Barrio and Nieto, 2004). Its expression has been suggested to play a role in the formation of memory through regulation of long term potentiation in hippocampal cells (O'Kane et al. 2004). Interestingly the peak of *rhoB* expression correlated with adhesion of neurons to the culture surface and the expression of *rhoB* was influenced by the composition of the culture substratum (Laplante et al. 2001).

1.7 Rho structure and regulation

The primary protein sequences of RhoA, RhoB and RhoC are around 85% homologous, with most divergence close to the C-terminus (Fig. 1.7). The N-terminal half of Rho GTPases contains the majority of the amino acids involved in GTP binding and hydrolysis, together with the Switch 1 and 2 regions that change conformation between the GTP-bound and GDP-bound states (Hall, 2000). Several X-ray crystallographic structures of RhoA have been solved at high resolution (Ihara et al. 1998). Amino acids essential for catalytic function (e.g. binding, stabilisation or regulation of GTP hydrolysis) are conserved throughout all Rho isoforms, including Gly14, Thr19, Phe30 and Gln63, (Fig. 1.7). Rho proteins are also targets for a number of bacterial toxins, which modify key conserved amino acids involved in their regulation. These include *Clostridium botulinum* exoenzyme C3-transferase, which inhibits RhoA, B and C through selective ADP ribosylation of Asn 41, blocking effector binding and downstream activity of Rho (Hall, 2000). *Clostridium difficile* toxins A and B are cation-dependent UDP-glucose glucosyltransferases, and inactivate most Rho GTPases through monoglucosylation of Thr37 which prevents guanine nucleotide exchange (Fig. 1.7).

Some sequence divergence between RhoA, RhoB and RhoC is found in the 'insert loop', a helix between amino acids 123 and 137 in Rho that is found in most Rho family members but not other Ras superfamily GTPases (Hall, 2000); (Fig. 1.7). This insert loop has been shown to be essential for NADPH oxidase binding to Rac (Nisimoto et al. 1997). Effector proteins that interact uniquely with the insert loop of RhoA, RhoB or RhoC have not been identified, although deletion of the insert domain of RhoA causes a decrease in protein stability and a reduction in its transforming potential (Zong et al. 1999). However, the differences between the three proteins in this loop could allow them to interact differentially with specific regulators or targets.

The C-terminus of Rho family GTPases is essential for correct localization of the proteins. The major divergence of sequence between RhoA, RhoB and RhoC in this region indicates that their localization is likely to be differentially regulated (Adamson et al. 1992; Shao and Dixon, 2003) (Fig. 1.7). RhoA, RhoB and RhoC are post-translationally modified by both palmitylation and by prenylation of a conserved C-terminal cysteine followed by methylation and proteolytic removal of the last three amino acids (Ridley, 1997a). The prenyl group anchors the GTPase into membranes. This modification is essential for cell growth, transformation and cytoskeleton organisation (Lebowitz and Prendergast, 1998). Prenylation of Rho proteins appears to be important for their stability, as inhibitors of enzymes that synthesize prenyl groups induce a decrease in RhoA or RhoB protein levels and their function (Koch et al. 1997; Stamatakis et al. 2002). However, the length of the prenyl group differs between the Rho proteins: RhoB can be prenylated either with a 15-carbon farnesyl (F) or a 20-carbon geranylgeranyl (GG) group, whereas RhoA and RhoC are only geranylgeranylated (Table 1.3). This difference is reflected in their localization: RhoB localizes on late endosomes and lysosomes and the plasma membrane whereas RhoA and RhoC are found in the cytosol or at the plasma membrane (Table 1.3) (Adamson et al. 1992; Wang et al. 2003b). When RhoB is only geranylgeranylated, which is either achieved through use of farnesyltransferase inhibitors or mutation of the C terminus, RhoB is localised only on the endosomal membrane and the plasma membrane localisation of RhoB is lost (Liu et al. 2000; Wherlock et al. 2004). This indicates that the prenylation of RhoB is essential in determination of its cellular localisation.

	RhoA+C	**RhoB**
Localisation	Cytosol+Plasma Membrane	Endosomes and Lysosome
Prenylation	Geranylgeranylated only	F or GG
CAAX box sequence	Similar to Rac and Cdc42	Similar to N Ras
Over expression in fibroblasts	Changes in actin cytoskeleton	Changes in actin cytoskeleton

Table 1.3: Comparisons between RhoA, RhoB and RhoC.

Figure 1.7: Alignment of the amino acid sequence of RhoA, RhoB and RhoC

Rho GTPases can be sequestered in the cytoplasm by GTPase dissociation inhibitors (RhoGDIs). These bind to the prenyl group of a Rho GTPase preventing its interaction with membranes. RhoGDIs also inhibit GTPase activity and release of GTP. There is some suggestion that the three different mammalian RhoGDIs show differential binding to RhoA and RhoB (Platko et al. 1995), although this has yet to be verified with endogenous proteins in vivo.

1.8 Differences in regulator binding between Rho proteins

There is a small degree of sequence divergence between RhoA, RhoB and RhoC, particularly in the switch 1 and 2 regions (Fig. 1.7). This suggests that there could be differences in their affinities for regulators or target proteins. In fact, few GEFs or GAPs have been compared for their relative activity on RhoA, RhoB and RhoC, and most have been tested just on RhoA. Of those that have been tested, for example Vav, p115RhoGEF, Bcr, p190 RhoGAP, no clear difference between RhoA, RhoB and RhoC has been observed (Schmidt and Hall, 2002). In a unique study, the GEF XPLN has been shown to act on RhoA and RhoB but not RhoC. The difference in specificity is attributed to of a single amino acid difference in RhoC as compared to RhoA and RhoB: Val43 in RhoA and RhoB is essential for forming a Van der Waals interaction with XPLN. Rho C has isoleucine in the place of valine at position 43, which inhibits XPLN binding (Arthur et al. 2002a). XPLN does have a tissue specific expression pattern although its function and intracellular localisation have yet to be fully documented.

As well as differences in affinity for each Rho protein, it is possible that GEFs and GAPs could be differentially localized in cells and that this would make them act specifically on RhoA, RhoB or RhoC (Chikumi et al. 2004). So far, however, the localization of most GEFs and GAPs has not been defined, although it is known that some translocate in response to extracellular stimuli. For example, p190RhoGAP moves from the cytoplasm to the plasma membrane following activation by v-Src or integrin engagement (Chang et al. 1995; Sharma, 1998). p115RhoGEF also translocates to the plasma membrane following stimulation of Gα13 (Bhattacharyya and Wedegaertner, 2003). Expression of some RhoGEFs is tissue-specific, and some can form homo- and hetero-oligomeric complexes, which may complicate studies on their isoform specificity and regulation (Chikumi et al. 2004).

1.9 Differences in effector binding between Rho proteins

To date at least 11 proteins have been identified which directly interact with RhoA (Govek et al. 2005) (Table 1.4). Some of these have been shown to contribute to specific responses downstream of Rho proteins (Narumiya et al. 1997). Similarly to GEFs and GAPs, effectors bind to Rho both mainly through the Switch 1 and 2 regions. However, the amino acids involved in interaction with each target differ and effectors

can interact with other regions on the Rho proteins (Fujisawa et al. 1998; Maesaki et al. 1999). This is reflected in the different Rho-binding motifs of the targets, which fall into different subgroups. Firstly PRKs (also known as PKNs), Rhotekin and Rhophilin contain Rho-binding regions of 70 amino acids near their N-termini, designated HR1 domains. The HR1 domain has a structure that corresponds to a leucine zipper. Secondly, ROCK1 and ROCK2 contain a different Rho-binding region near their C-termini. Finally, Citron contains a Rho-binding region that is similarly located to that of ROCKs, but has no sequence homology to the ROCK Rho-binding region or HR1 (Fujisawa et al. 1998).

Effector	RhoA	RhoB	RhoC
ROCK 1+2	√	ND	√
mDia	√	ND	√
PRK1/2 PKN	√	√	√
Rhotekin	√	√*	√
Rhophillin	√	√	√
Kinectin	√	ND	ND
Citron Kinase	√	√*	√
MBS	√	ND	ND
p76RBE	√*	√	ND
PKCζ	√	√	√

Table 1.4: Effectors for RhoA, RhoB and RhoC;
√= interaction and ND= not determined. *=weak interaction

Yeast 2-hybrid studies suggest that ROCK and Citron have a higher affinity for RhoC compared to RhoA (Madaule et al. 1995; Matsui et al. 1996). RhoC appears to have a stronger ability to activate ROCK in epithelial cells compared to RhoA (Sahai and Marshall, 2002b). This should have important implications for understanding the respective contribution of RhoA and RhoC to cell motility. So far, however, the sequence differences between RhoA and RhoC that affect their affinity for ROCKs or Citron have not been identified. The VFSKD sequence in switch 1 (residues 20 – 26) (Fig. 1.7) is essential for binding PRKs, ROCK and Citron (Madaule et al. 1995; Fujisawa et al. 1998; Zong et al. 1999). This sequence is identical in RhoA, RhoB and RhoC (Fig. 1.7) and PKN and Citron bind to all 3 isoforms of Rho. ROCK also requires Switch 2 for interaction with Rho proteins, but again this is identical between the three Rho isoforms. There is no evidence that PRKs have different affinities for each of the

Rho isoforms *in vitro*, but the co-localization of PRK1 (Mellor et al. 1998) with RhoB on endosomes suggests that it is a specific target for RhoB (Gampel et al. 1999).

There is only one example of a downstream effector for Rho that is isoform-specific in its binding. p76RBE was initially identified as a protein upregulated in response to thyrotrophin signaling via cAMP. p76RBE contains a PRK-like HR1 Rho-binding domain and a PDZ domain. Yeast 2-hybrid studies showed that p76RBE has the highest affinity for constitutively active RhoB, whereas Rhotekin binds with equal affinity to activated RhoA, RhoB and RhoC (Mircescu et al. 2002; Reid et al. 1996). So far, the function of p76RBE is not known, but it would be interesting to determine whether it co-localizes with RhoB in cells (Table 1.4).

1.10 Functions of Rho proteins

Motility is an important function of Rho proteins and will be discussed at length below, other functions of Rho are:

1.10.1 Cytokinesis

Cytokinesis requires actomyosin-based contraction (Hall and Nobes, 2000). Inhibition of Rho proteins, ROCKs or citron kinase causes defects in cytokinesis resulting in multinucleate cells (Kaibuchi et al. 1999; Tolliday et al. 2002). Diaphanous related formins (DRFs) are also implicated in cytokinesis: in *Saccharomyces Cerevisiae*, the DRF BNI1 is essential for cytokinesis and in mammals the DRF Dia1 localizes to the cleavage furrow during cytokinesis (Wallar and Alberts, 2003). DRFs could contribute to cytokinesis by stimulating local actin polymerization and/or by coordinating microtubules with actin filaments at the site of the contractile ring.

1.10.2 Rho and transcription

As well as regulating the cytoskeleton directly, Rho proteins can induce transcriptional changes that may indirectly impact on cytoskeletal organization. RhoA is known to activate transcription by the MAL/SRF transcription factor complex by reducing the level of monomeric G-actin in cells (Miralles et al. 2003). MAL binds directly to G-actin and is believed to act as a G-actin sensor, inducing SRF-mediated transcription of

several cytoskeletal genes, including α-actin, β-actin and vinculin (Schratt et al. 2002). RhoB and not RhoA also signals to transcription of genes such as transforming growth factor β2 (TGFβ2) and macrophage inhibitory factor (MIF) which form part of macrophage function (Adnane et al. 2002). This indicates that RhoB and RhoA have distinct mechanisms for regulating transcription, and could thereby have different long-term effects on cell motility and the cytoskeleton.

1.10.3 Trafficking

Arfs and Rabs, which are part of the same GTPase superfamily as the Rho GTPases play a central role in the control of vesicle trafficking. However, several Rho family GTPases are also involved in the generation of vesicles, their transport around the cell and regulation of their secretion (Symons and Rusk, 2003). RhoB, RhoD and Cdc42 have been shown to be localised on vesicles which are trafficking through the cell. Rac1 has been found in signalling complexes with Arf6; Arf6 regulates plasma membrane to endosomal trafficking (Symons and Rusk, 2003). Both Rac and Cdc42 are involved in pinocytosis, promoting formation of small invaginations of the membrane through PAK and LIMK, and pinching off budding vesicles though interaction with dynamin and syndapin, via WASP. The formation and trafficking of these pinocytic vesicles is essential for antigen presentation, particularly on dendritic cells (Symons and Rusk, 2003). Rho GTPases have a central regulatory role in phagocytosis, which is important for several biological processes including development and the immune response. Rac1 and Cdc42 are required for control of formation of the phagocytic cup and engulfment of the particle in FcγR mediated phagocytosis (Hall and Nobes, 2000). RhoA is involved in the regulation of complement receptor-mediated phagocytosis. RhoB has been reported to be required for efficient phagocytosis and has been suggested to be recruited to newly formed vesicles (Zhang et al. 2004a).

Interestingly RhoA and RhoB act at different stages of endocytosis: constitutively active RhoA alters the rate of receptor uptake early on in endocytosis (either slowing it down or speeding it up depending on which cell type is investigated) (Rojas et al. 2004; Gampel et al. 1999; Symons and Rusk, 2003). Whereas RhoB has been found to retard the trafficking of epidermal growth factor receptor (EGFR) from the early endosome to the late endosome / lysosome (Gampel et al. 1999). Recruitment of PRK1 to endocytic vesicles by RhoB has been implicated in this process (Mellor et al. 1998). Over-

expression of RhoB also inhibits the recycling of transferrin and IgA (Rojas et al. 2004). Recent work suggests RhoB is required for recruitment of Src to the plasma membrane (Sandilands et al. 2004). The differences in intracellular localisation of RhoA and B have been suggested to be responsible for their effects on endocytosis.

1.10.4 Transformation

Perhaps the clearest indication that there are differences in Rho isoform function is shown in cancer studies. RhoA and RhoB were reported to promote transformation of cultured mouse fibroblasts. RhoA can enhance tumour formation by these fibroblasts in mice. RhoA is over-expressed in several cancer cell lines many of which are either highly metastatic or have defects in growth control (Ridley, 2004). In contrast to RhoA and B, RhoC does not affect fibroblast transformation (Ridley, 2004). However, microarray analysis has shown that expression of RhoC is progressively increased as tumours become more aggressively metastatic and RhoC expression promotes metastasis (Wu et al. 2004). This may be because RhoC is better activator of ROCKs than RhoA, especially since activation or inhibition of ROCK respectively promotes or inhibits tumour cell motility (Sahai and Marshall, 2002a). Interestingly, RhoC has not been found mutated in cancers, indicating that upregulated expression is sufficient for it to contribute to metastasis.

In contrast to RhoC, over-expression of RhoB inhibits migration, invasion and melanoma metastasis (Prendergast, 2001) and in several cancers RhoB expression levels are decreased as the cancer progresses (Ridley, 2004). Recent studies show that RhoB is critical for promotion of stress-induced apoptosis and antineoplastic activity. Over-expression of RhoB in cancer cell lines inhibited anchorage-independent growth and induced apoptosis by inhibiting extracellular regulated kinase (ERK) activity and the insulin like growth factor (IGF-1) activation of Akt (Jiang et al. 2004a). Deletion of RhoB compromises the response of embryonic fibroblasts to stress stimuli (Liu et al. 2001). Interestingly, the role of RhoB in stress responses may depend upon its prenylation status (Allal et al. 2002).

There is a conflict of opinion in the transformation field as to whether the type of prenylation of RhoB affects its transforming potential. Prendergast et al argue that farnesyl transferase inhibitors (FTI) block neoplastic transformation in cell culture

(Prendergast, 2001). FTIs do not affect proliferation of non-transformed cells but they reduce the proliferation of Ras-transformed cells (Lebowitz et al. 1997). Mechanistic investigation of Ras inhibition did not fully explain the anti-proliferative effect of FTIs in Ras-transformed cells (Cox and Der, 2002). Therefore, RhoB was suggested to be a FTI target as FTI treatment inhibits production of RhoB-F (Lebowitz and Prendergast, 1998). FTI treatment caused a gain in function of RhoB-GG, which was sufficient to mediate phenotypic reversion, growth inhibition and apoptosis (Du and Prendergast, 1999). Sebti et al. disagree with this and state that RhoB-F is not a relevant target for farnesyl transferase inhibitors and has the same anti-transformation activity as RhoB-GG (Chen et al. 2000). To investigate the role of RhoB in transformation further the Prendergast laboratory generated a RhoB-null mouse. The deletion of *rhoB* increased the susceptibility of fibroblasts to form tumours (Liu et al. 2001). Together this suggests that RhoB may act as a negative modulator of cell survival (Prendergast, 2001).

1.10.5 Rho and cell-cell adhesions

Rho proteins play a critical role in regulating the integrity of cell-cell adhesions, including both adherens junctions and tight junctions (Arthur et al. 2002b; Braga et al. 1999; Wojciak-Stothard and Ridley, 2002). Loss or weakening of cell-cell junctions is required for the migration of epithelial cells, and may be regulated reciprocally by ROCKs and DRFs (Sahai and Marshall, 2002b). RhoC appears to weaken adherens junctions more than RhoA and this has been attributed to activation of ROCK. RhoA also acts to promote formation of stress fibres in endothelial cells and increases vascular permeability upon leukocyte binding, (Millan and Ridley, 2004).

1.11 Rho proteins and cell motility

The regulation of cell shape change and tension is essential in the migrating cell. The cell needs to generate sufficient force to push forward its membrane at the front of the cell, move its cell body and retract its end. Rho GTPases regulate the process of cell motility on several different levels (Fig. 1.8A+B).

1.11.1 Formation of the lamella

Microinjection of activated Rac into fibroblasts rapidly induces the formation of lamellipodia and dorsal ruffles (Ridley et al. 1992). This effect has been recapitulated in several different cell types (Hall and Nobes, 2000). Rac has been shown to be locally active within the lamellipodia of extending cells (Kraynov et al. 2000). The regulation of actin polymerisation through the Arp2/3 via WASP by Cdc42 and Rac1 has been well characterised (Higgs and Pollard, 2001) (Fig. 1.7). Rac1 is known to activate actin polymerisation through the Scar/WAVE complex. However, the precise mechanism through which, this complex functions is not fully characterised as yet, and seems to vary between different organisms (Millard et al. 2004). The regulation of actin depolymerisation is slightly better characterised, ADF/cofilins are inhibited by phosphorylation which inhibits filament severing (Minamide et al. 1997). Rac1 activates PAK1, which in turn phosphorylates LIMK (Edwards et al. 1999). LIMK phosphorylates ADF cofilin inhibiting its severing activity (Arber et al. 1998). This allows Rho family GTPases to co-ordinate the formation of new filaments with their rate of turnover (Fig. 1.8).

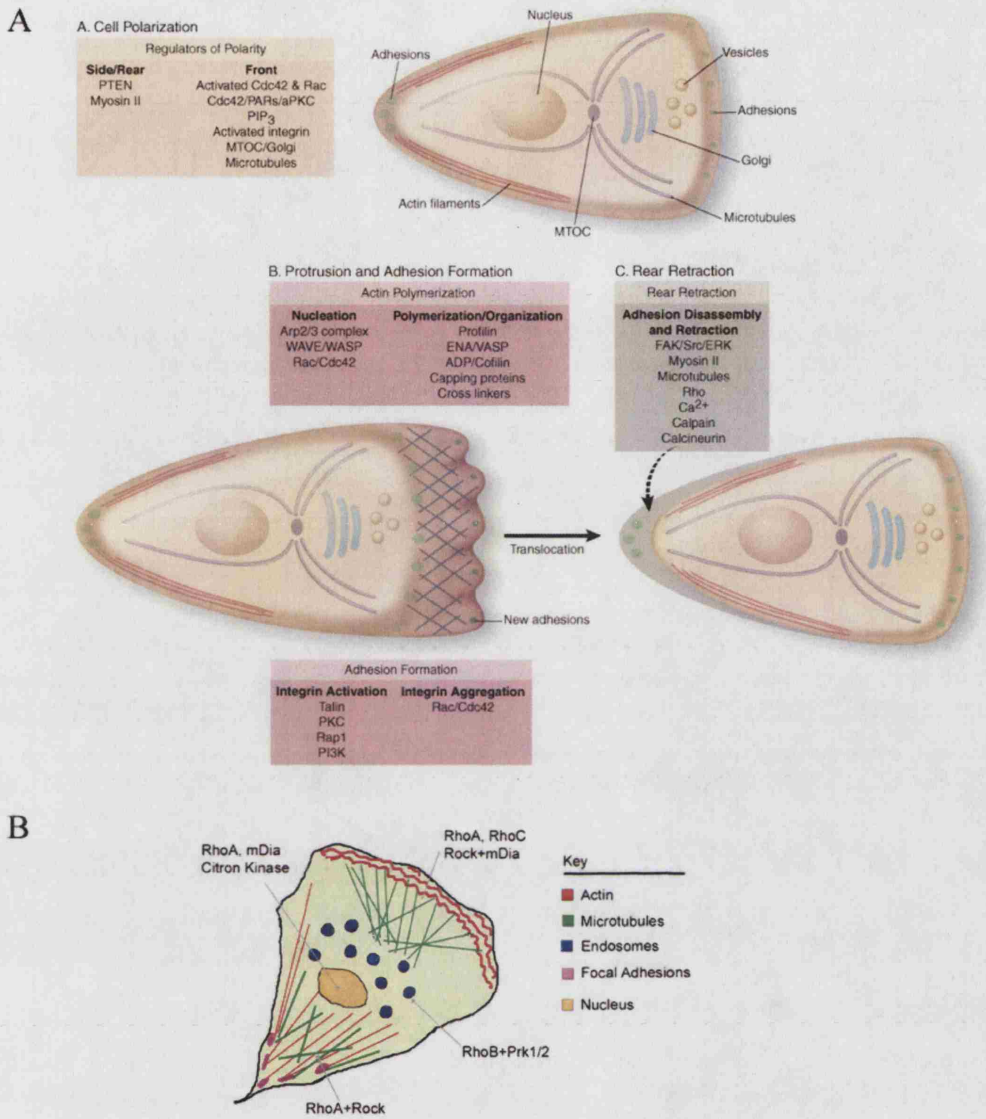

Figure 1.8 (A). The regulation of migration by RhoGTPases and associated proteins. taken from (Ridley et al. 2003) (**B)** The function of Rho A, RhoB and RhoC in a migrating cell.

Microtubule growth also promotes lamellipodial outgrowth by activation of Rac1, which in turn activates actin polymerisation in fibroblasts (Wittmann et al. 2003). Rac1 can also regulate microtubule growth through PAK1 dependent activation of stathmin, which promotes microtubule disassembly. Depolymerisation of microtubules and actin activates RhoA via GEF H1 (Krendel et al. 2002). This may create a cycle where microtubule + ends extension activates Rac1 in the lamellipodium and - ends depolymerisation activates RhoA in the cell body (Rodriguez et al. 2003).

The role of Rac in migration and chemotaxis has been shown to be isoform specific in leukocytes. Neutrophils and macrophages derived from Rac1-null mice have defects in cell spreading and membrane ruffling but not in migration (Glogauer et al. 2003; Wells et al. 2004). Rac1 has also been shown play a key role in regulation of neutrophil chemotaxis (Sun et al. 2004). Intriguingly Rac2-null B lymphocytes, T lymphocytes and neutrophils have severely reduced migration and defects in polarisation due to a disrupted actin cytoskeleton (Croker et al. 2002a; Croker et al. 2002b; Li et al. 2002). This suggests specificity in Rac isoform function in neutrophils, with Rac1 signalling to control the chemotaxis compass allowing cells to follow a persistent path and Rac2 regulating actin polymerisation in neutrophils (Sun et al. 2004, Li et al 2002).

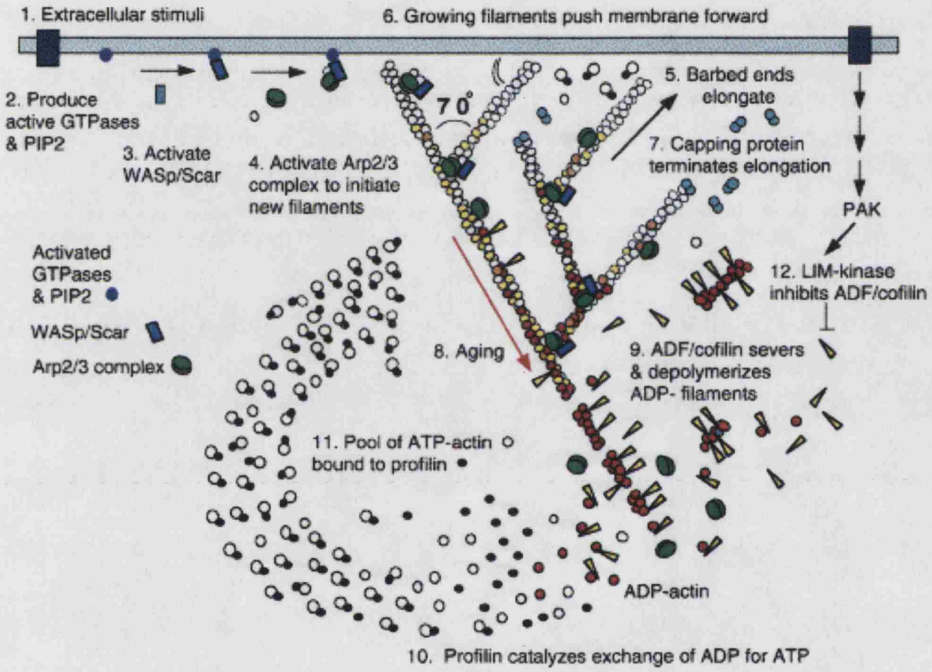

Figure 1.9. The actin cycle taken from (Higgs and Pollard, 2001).

1.11.2 Generation of cell polarity

To prevent a cell migrating to the wrong place the regulation of the direction of cell polarisation is essential. In leukocytes interdependent regulation of cell polarity and migration is essential for chemotaxis. Polarisation of the cell is regulated through Rac, Cdc42, TC10 and RhoG (Etienne-Manneville, 2004). Recent studies show that Cdc42 and cytoplasmic dynein are important in re-orientation of the MTOC during cell polarisation in fibroblasts (Palazzo et al. 2001) (Fig. 1.8). Cdc42 elicits its effects on the MTOC through a complex that consists of Par6 and Par3 and PKCζ, an atypical PKC

(Etienne-Manneville, 2004). The concerted action of ROCK and Dia is essential for regulation of cell polarity and organisation of microtubules. DRFs act to stabilise microtubules and coordination of microtubule orientation is achieved through an integrin/focal adhesion kinase (FAK) pathway which causes localized activation of Rho (Ishizaki et al. 2001; Palazzo et al. 2004).

1.11.3 Generation of tractional forces

Actomyosin contractility is important in migrating cells for detachment of the rear and movement of the cell body (Fig. 1.10). Over expression of RhoA in fibroblasts causes formation of stress fibres, which are indicative of an increase in cell tension. ROCK was implicated in generation of tractional forces as its inhibition leads to fibroblasts being unable to retract their tails (Fig. 1.8). DRFs also act together with ROCKs to mediate Rho-induced stress fibre formation (Pring et al. 2003). ROCK-mediated phosphorylation of LIMK and consequent inhibition of cofilin contributes to the Rho-mediated increase in actin filaments (Maekawa et al. 1999). IF have been shown to be involved in regulation of the localisation of ROCK. ROCK binds to vimentin in serum starved fibroblasts. Following stimulation with serum or sphingosine-1-phosphate ROCK phosphorylates vimentin, causing filament disassembly and reorganisation of vimentin into a juxta-nuclear aggregate (Chang and Goldman, 2004). This also causes liberation of ROCK from the IF. ROCK then migrates to the cell periphery; this translocation of ROCK has been associated with actin stress fibre formation and increased cell contractility. ROCK is also responsible for the disassembly of IF in the cleavage furrow during cytokinesis (Chang and Goldman, 2004). Microtubules and actin also co-operate in force generation. The tensegrity model describes actomyosin push against microtubule scaffolding (Howard, 2001). However as actin and microtubules share several regulatory proteins the tensegrity model may be an oversimplification of the actual process occuring within the cell (Rodriguez et al. 2003).

Tension within the cell is generated by myosin motors moving across actin filaments. Myosin activity is regulated by Rho GTPases, specifically by RhoA. Phosphorylation of the regulatory light chain on Ser 19 and Thr 18 promotes the activity of myosin (Kemp et al. 1983). The phosphorylation of myosin is catalysed by Ca^{2+} using a calmodulin activated myosin light chain kinase (MLCK) or directly by ROCK (Ridley et al. 2003) (although this has only been shown in vitro). Dephosphorylation is catalysed by myosin

phosphatase; Myosin phosphatase is a heterotrimeric enzyme made up of a 38kDa catalytic subunit, a 20kDa subunit and a 110kDa regulatory subunit (MYPT1). The activity of myosin phosphatase is inhibited by ROCK mediated phosphorylation of MYPT1. (Kimura et al. 1996). Therefore it can be seen that RhoA signalling to ROCK promotes myosin mediated cell contractility directly by activation of MLCK and indirectly by inhibition of MYPT1 (Fig. 1.10).

Traditionally Rho has been thought to function at the rear of the cell disassembling adhesions. Rac acts at the front of the cell to stimulate actin-mediated membrane protrusion. However, active Rac is detected at both the front and rear of migrating cells, and the localization of active Rho proteins within migrating cells has not been defined. So it is not clear that migrating cells are really divided into a Rac zone and Rho zone. A recent study has suggested that Rho is selectively degraded at the front of cells (Wang et al. 2003a; Zhang et al. 2004b). p190RhoGAPs have also been shown to deactivate RhoA during cell spreading (Arthur and Burridge, 2001). This would provide an area of low Rho activity and high Rac activity which would promote the formation of adhesions (Ridley et al. 2003; Worthylake and Burridge, 2003). RhoA directly can also stimulate actin polymerization through activation of Dia (Watanabe et al. 1997). Dia, stimulates addition of actin monomers to the barbed, or fast-growing, end of actin filaments (Pring et al. 2003). It has been suggested that microtubule induced suppression of RhoA activity causes inactivation of ROCK. At the front of the cell this could promote focal contact formation and cell ruffling. Interestingly the ruffling response to ROCK inhibition is not seen when Dia is also blocked which may suggest that Dia signals to activate Rac (Tsuji et al. 2002).

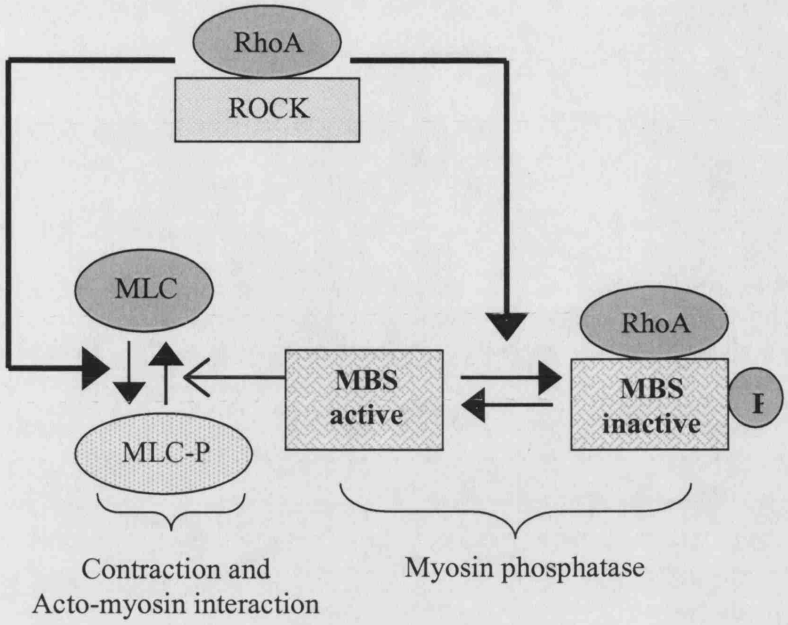

Figure 1.10: Model of the regulation of myosin activity by Rho, ROCK and myosin phosphatase adapted from (Kaibuchi et al. 1999).

Together this may suggest that Dia is important for mediating Rho activity at the front of the cell where adhesions are initially assembled. ROCK may play a more important role at the rear of the cell regulating stress fibre mechanics and turnover of adhesions. As localization of active Rho proteins within migrating cells has not been defined, it is not clear that migrating cells are really divided into a Rac zone and Rho zone. It may be likely that the localisation of Rho effectors such as Dia, ROCK, LIMK and PAK determine the impact of activation of Rho GTPases in different parts of the cell (Fig. 1.8).

1.12 Chemotaxis in leukocytes

Leukocytes are very sensitive to variations in concentrations of chemo-attractant factors and can detect a difference of as little as 0.1% across a cell (Webb et al. 1996). The cell manages to respond to such a shallow change in gradient by an internal process that amplifies the outside chemo-attractant signal. In neutrophils actin is actively polymerised in the region which is closest to a chemoattractant source and actin polymerisation is inhibited in other parts of the cell (Xu et al. 2003). It is clear that gradient sensing and chemotaxis is not depend on a single molecular mechanism, but

consists of several signalling networks acting in concert to generate a polarised cell capable of persistent movement towards a chemokine source (see Fig. 1.1 and 1.8). Chemo-attractants signal either through 7 transmembrane G protein-coupled receptors or tyrosine kinase receptors. These receptors signal to phospho inositide 3 kinases (PI 3-K) activation and also MAPK. Experiments using PI 3-K inhibitors such as LY294002 and wortmannin show that PI 3-K signalling is essential for directed migration towards a chemo-attractant source; conversely MAPK inhibitors do not affect chemotaxis (Merlot and Firtel, 2003). Migration analysis in macrophages derived from PI 3-K knockout mice showed that distinct PI 3-K isoforms signal to cell migration and mitogenic signalling (Vanhaesebroeck et al. 1999). Neutrophils and macrophages derived from mice lacking class1B PI 3-K γ displayed severe defects in chemotaxis. Interestingly chemotaxis in both neutrophils and macrophages derived from PI 3-K γ-null mice is not completely abrogated (Hannigan et al. 2002; Jones et al. 2003), which may suggest that other isoforms of PI 3-K may weakly substitute for PI 3-K γ activity in its absence.

Phosphatidyl inositol-3,4,5-triphosphate (PIP3), which is generated by PI -3K, rapidly recruits PH domain containing proteins to the leading edge of the cell. This results in localised activation of Rho GEFs and GAPs such as PIX and Vav by phosphorylation. This in turn activates Rac/Cdc42 mediated actin polymerisation, formation and turnover of adhesions (Li et al. 2003; Merlot and Firtel, 2003). PIP3 is removed by the phosphatase 'phosphatase and tensin homolog' (PTEN) and PKC. PTEN is found to accumulate at the sides and rear of a migrating *Dictyostelium* (Funamoto et al. 2002) although currently there is no evidence to suggest this occurs in mammalian cells.

1.13 Rho and regulation of adhesion

Adhesions act as the 'feet' of the migrating cell. They serve a dual purpose of attachment of the cell to the substratum and sensing information about the cell's environment and relaying this information to the cell. In order for cells to move, they need to lay down adhesions at the front of the cell to stabilise the protrusions and turn over cell adhesions at the cell rear to allow forward movement. Cell tension and traction is mediated through cytoskeletal interactions with cellular adhesions (Ridley et al. 2003).

1.13.1 Cell- substratum adhesion structure in migrating cells.

Interference reflection microscopy (IRM) showed, several years ago, that fibroblasts do not uniformly attach to a substrate. Instead small specialised foci are spread across the cell membrane at intervals (Curtis, 1964). Time lapse microscopy and IRM of migrating cells show there are many different types of adhesions. In a migrating fibroblast adhesions in the lamellipodium are small and punctuate and are described as focal contacts. If these focal contacts are in the centre of the lamella in fibroblasts they condense to form larger focal adhesions (Bershadsky et al. 2003). The adhesions at the rear of fibroblasts are large and elongated (Small and Kaverina, 2003). These focal adhesions are not static but have a dynamic turnover of proteins (Small and Kaverina, 2003). Initially experiments where the cells were sheared off their substrates were used to identify the components of focal adhesions such as the adaptor vinculin (Geiger et al. 1984). More sophisticated biochemical techniques have now identified over 50 proteins which are involved in focal adhesions (Small and Kaverina, 2003). In general there are four classes of molecules involved in adhesions (Table 1.5).

Molecule	Function
Integrins	Integrins span the cell membrane and contain extracellular domains which interact with the ECM and intracellular domains which interact with the actin cytoskeleton
Adaptor proteins	Vinculin, talin, and paxillin are a few of the adaptor proteins which form a scaffold that link the intracellular domain of the integrin and the cytoskeleton
Cytoskeletal proteins	α-actinin, tubulin and vimentin have been found to be associated with focal adhesions, the link between the cytoskeleton and cellular adhesion is essential in regulation of tension in the cell.
Kinases and phosphatases	Protein kinases of the Src family and FAK family are both found in adhesions. Most adhesions are hotspots of tyrosine phosphorylation. The kinases and phosphatases regulate adhesion assembly and turnover.

Table 1.5: Classes of molecules involved in cell-substratum adhesions.
(Clark et al. 1998; Danen et al. 2002; Hotchin and Hall, 1995; Palazzo et al. 2004).

Not all cell types use the same mechanism of attachment to the substratum as fibroblasts. Neutrophils form an even attachment to the substratum and only appear to use adhesions containing vinculin at the cellular periphery (Yuruker and Niggli, 1992). Similarly, T cells form an even attachment to the substratum, with F actin enriched at the front of the cell and the rear. T cell adhesion has been shown to be dependent upon the integrin LFA-1, though the adhesion complexes used by T cells are too small to be resolved by current optical microscopy techniques (Hogg et al. 2004). Macrophages and

osteoclasts do not contain the focal adhesions seen in fibroblasts but do have small, focal contact like structures evenly distributed over the basal plane of the cell (Pfaff and Jurdic, 2001; Pixley et al. 2001). Certain varieties of adhesion are present only in specific cell types, such as podosomes, which are present only in myeloid cells or transformed cells. These appear to form within the leading lamella and turn over with a half life between 2 and 12 minutes (Evans et al. 2003). It has been suggested that the variety of adhesion used by a cell type for attachment reflects the speed and mechanism of motility of that cell type (Friedl et al. 1998a). Fibroblasts and melanoma cells have slow migratory speeds whereas neutrophils and T cells migrate at a far higher speed and often have a more amoeboid migratory morphology.

1.13.2 Integrins and cell substratum adhesions

Integrins are trans-membrane proteins, their extracellular domain binds directly to the ECM. To date over 30 integrin genes have been described in humans (Hynes, 2002). Integrins form heterodimers consisting of one α and one β subunit. Humans have 9 types of β subunits and 24 types of α subunits. The integrin heterodimer predominantly used in adhesion depends upon the substrate the cell is binding to (Friedl et al. 1998a; Hynes, 2002). The density of the substrate affects the affinity and avidity of integrin binding (Dubin-Thaler et al. 2004; Hogg et al. 2002). When the cell attaches to a substratum integrins cluster and begin to form adhesive complexes increasing the avidity of binding. Avidity is a measure of integrin clustering which has been shown to be required for adhesion (Hogg et al. 2004). Novel techniques such as fluorescent image correlation microscopy, fluorescent recovery after photobleaching and speckle microscopy (Waterman-Storer and Danuser, 2002) allow analysis of the integrin interactions and dynamics during migration that cannot be resolved by more conventional microscopy techniques (Wiseman et al. 2004). The clustering activity of integrins is dependent upon interaction with the actin cytoskeleton and calpain activity (Hogg et al. 2004). Calpain is a protease which cleaves proteins associated with the cytoskeleton and is involved in turnover of adhesions (Franco et al. 2004). Integrin clustering in a motile cell is localised at the leading edge (Kiosses et al. 2001). This promotes signalling to activation of Rac and Cdc42 (Rottner et al. 1999), protein tyrosine phosphorylation and changes in phosphoinositide biosynthesis which regulate the formation and strengthening of adhesions (Geiger and Bershadsky, 2002). Rho proteins may contribute to focal adhesion assembly in part by actomyosin-based

clustering of integrins (Burridge and Wennerberg, 2004) but may also regulate integrin activity and endocytosis (del Pozo et al. 2004; Worthylake et al. 2001).

The cytoplasmic protein talin connects integrins with the interior of the cell (Franco et al. 2004). Talin interacts with the cytosolic portion of β subunit tails though FERM domain mediated contacts (Calderwood and Ginsberg. 2003). A scaffold of signaling and adaptor proteins then bind to talin, including vinculin, paxillin and FAK (Nayall et al. 2004). Adaptor proteins transduce signals to the cell from the ECM and vice versa. For instance paxillin associates with talin and interacts with the GIT/PIX/PAK complex, which can activate Rac and Cdc42 (See section 1.11.1 and 1.12) (Burridge and Wennerberg, 2004).

1.13.3 Protein tyrosine phosphorylation and adhesions

Many proteins in adhesions are tyrosine phosphorylated including paxillin, PYK and focal adhesion kinase (FAK). Turnover of focal adhesions and focal contacts has been shown to be dependent on phosphorylation by FAK: Indeed FAK-null mouse embryonic fibroblasts have severe defects in motility and an increased number of focal adhesions (Parsons, 2003). Protein tyrosine phosphatases cause disassembly of adhesions and stress fibres (Schneider et al. 1998). Together this indicates that regulation of protein tyrosine phosphorylation is essential in the regulation of cell adhesion and therefore motility (Arthur et al. 2002b). Activation of several different cell surface receptors promotes tyrosine phosphorylation of focal adhsion proteins. These can signal directly to regulate adhesions via activation of Src family kinases and also indirectly by activation of Rho GTPases (Parsons and Parsons, 2004).

1.13.4 The regulation of adhesion turnover

As well as protein tyrosine phosphorylation, adhesion turnover is inextricably linked with regulation of cellular motility. Turnover of adhesions at the rear of migrating cells is believed to be dependent upon Rho activity and microtubules (Kaverina et al. 1999; Ridley et al. 2003) (Fig. 1.8). Certainly, inhibition of RhoA and ROCK inhibits deadhesion of the cell tail in fibroblasts and transmigrating monocytes (Kaibuchi et al. 1999; Worthylake and Burridge, 2001). Over-expression of ROCK promotes focal adhesion formation. Microtubules have been proposed to target adhesion complexes to

promote disassembly (Small and Kaverina, 2003). This may be due to microtubule dependent localised Rho inactivation as the activity of p190RhoGAP was shown to be dependent on intact microtubules (Small and Kaverina, 2003). p190RhoGAP is also activated via integrin signaling and this promotes adhesion turnover and protrusion during cell spreading (Arthur and Burridge, 2001).

1.13.5 Cell spreading

The attachment and spreading of leukocytes circulating in the bloodstream to the endothelium is a key part of the inflammatory and immune responses. Circulating leukocytes sporadically contact the endothelial cells which line blood vessels. If leukocytes encounter chemokines and/or cytokines, for example CSF-1 and MCP-1, presented on the surface of endothelial cells they become tethered to the endothelium by an interaction between glycoproteins such as selectins (Lu et al. 1998; Ivetic and Ridley, 2004). Firm adhesion of the cell to the endothelium is mediated by integrins and cellular adhesion molecules (e.g. ICAM-1) and spreading of the cell then follows this (Hogg et al. 2002) (Fig. 1.1). Often there is little distinction made in the literature between adhesion and spreading. This is partly because when fibroblasts contact the substratum they rapidly spread to produce a flattened shape, using a process which is analogous to the forward extension of a lamellipodium and is regulated by Rac1 and Cdc42 (Worthylake and Burridge, 2001).

The lamellipodium of fibroblasts goes through periods of stochastic extension during spreading. The pauses between the extensions are thought to correspond to the time taken for ECM binding and consequent stimulation of force generation against the cell membrane (Dobereiner et al. 2004; Dubin-Thaler et al. 2004). As in migrating cells the rate of rearward movement of F-actin from the front of the lamellipodium is inversely related to the speed of cell edge protrusion in these spreading cells (Giannone et al. 2004; Higgs and Pollard, 2001).

Using total internal reflection fluorescent microscopy (TIRF) some of the physical principles underlying fibroblast spreading have been determined. Fibroblasts have three phases of cell spreading: an initial lag phase where contact with the ECM is thought to be established and secured, a second phase where the cell spreads to at least 60% of its total cell area, and a final slower phase (Dobereiner et al. 2004). As cell spreading is

very similar to the forward movement of the lamellipodium, it is thought that the Rho GTPases will regulate cell spreading through both the ENA/VASP and Scar/WAVE complexes (see section 1.2.1 and 1.11.1). Similarly it has been shown that the density of the cell matrix, which regulates the speed of cell migration, also regulates the speed of extension of the cell membrane in a spreading cell (Dubin-Thaler et al. 2004; Ware et al. 1998). The formation of focal contacts is also shown to be essential for cell spreading (Giannone et al. 2004).

During cell spreading as RhoA activity is low and the rate of cell spreading varies inversely with myosin II activity. The myosin II light chain is dephosphorylated upon contact with the substratum as a result of Rho inactivation during spreading (Wakatsuki et al. 2003). Use of ML-7 an inhibitor of MLCK reduces activity of a broad spectrum of myosins. This inhibits spreading indicating that myosin activity is essential to cell spreading. Studies of GFP-MLCK show that it is present at the front of the lamellipodium of the spreading cell in fibroblasts. However myosin II is known to be located towards the rear of the lamellae of Fibroblasts and T cells (Smith et al. 2003; Matsumura et al. 1998). Together this suggests that the activity of other, non conventional, myosins may be needed for the cell spreading process to occur (Giannone et al. 2004).

1.14 Rho GTPase isoform specificity in cell movement

Much work determining the in vivo functions of Rho and Rac GTPases in cell migration have been carried out in *D. melanogaster*, *C.elegans* or yeast (Redd et al. 2004; Settleman, 2001). However these organisms contain only one Rho isoform. Most studies of Rho function in cell motility have used C3-transferase to inhibit Rho proteins, which does not distinguish between the three isoforms of Rho. Some studies have used dominant-negative, constitutively active or fast cycling RhoA or RhoB to attempt to differentiate between isoforms. However, some of the data from these experiments can be misleading as the intra-cellular localisation of RhoA and RhoB is known to be important for their function and this is perturbed by overexpression (Adamson et al. 1992; Prendergast, 2001; Wherlock et al. 2004). The generation of a RhoB-null mouse allows a more precise determination of the roles of Rho in cell migration and adhesion. However, it is not possible to generate a RhoA null mouse (See section 1.6). Fibroblasts lacking RhoB show defective motility on fibronectin and an impaired wound healing

response (Liu et al. 2001). RhoB-null fibroblasts have a decreased spread area when plated on fibronectin. Recent research reveals that although the peripheral actin structures of RhoB-null fibroblasts were still present there was no Src associated with these structures. It appears that in RhoB null fibroblasts Src is not trafficked to the plasma membrane, and in RhoB-null endothelial cells Akt is mislocalised (Adini et al. 2003; Sandilands et al. 2004). This suggests that RhoA is required to form actin filaments for Src to move through the cytoplasm to the plasma membrane and RhoB activity to target the endosomal trafficking of Src.

1.15 Leukocyte trafficking

Leukocytes share several common properties; many of them are derived from pluripotent haematopoietic cells known as megakaryocytes in the bone marrow stroma (Paul and Seder, 1994). They then migrate from the stroma to their site of function where they are matured for their final function (Table 1.6). All leukocytes to a greater or lesser extent are motile.

Catergory	Cell type	Function
Granulocytes: Contain several secretory vesicles and lobed nuclei	Neutrophils	Phagocytosis of small organisms
	Basophils	Secretion of histamine and mediation of inflammatory reactions
	Eosinophils	Destruction of parasites and modulation of allergic responses
Monocytes: Mononuclear phagocytes	Macrophages	Phagocytosis of apoptotic cells, invading micro-organisms and foreign bodies.
	Osteoclasts	Digestion of bone
Lymphocytes:	B Cells	Matured in the spleen, generation of antibodies
	T Cells	Matured in the thymus, killing of virally infected cells and regulation of the activity of other immune cells
	Natural killer cells	Kill certain type of tumour cells and virally infected cells

Table 1.6: Classes of leukocyte derived from pluripotent haematopoietic stem cells in the bone marrow stroma,

During an inflammatory response there are two key phases of leukocyte recruitment to the wound (See Section 1.1). The first is an influx of neutrophils which mainly express CXC chemokine receptors. These are attracted to infected tissue in response to CXC

ELR+ chemokines and bacterial products (Springer, 1994). Once neutrophils have been recruited to the wound they are thought to promote a switch in the chemoattractants released. Neutrophils and tissue resident macrophages promote the secretion of monocyte chemoattractant protein (MCP-1) (Burke and Lewis, 2002,). MCP-1, as well as other factors secreted by cells within wounded tissue, recruit macrophages to the infected tissue (Lu et al. 1998). Monocytes and macrophages express chemokine receptors of the CC type for instance CCR2, the receptor for the MCP-1 ligand. MCP-1-null mice have severe impairments in the recruitment of monocytes to the wound (Zlotnik. 2000). This indicates that MCP-1 secretion both by neutrophils and by surrounding tissues is crucial in the inflammatory response (Lu et al. 1998).

1.16 Macrophage function

Macrophages carry out a diverse range of functional activities. These include phagocytosis and degradation of foreign antigens, matrix dissolution and tissue remodelling, and production and secretion of cytokines, chemokines and growth factors. As professional phagocytes macrophages play a key role in clearance of pathogens and apoptotic neutrophils from wounded tissue and tissue remodelling (Burke and Lewis, 2002). Macrophage phagocytosis of apoptotic cells is necessary for tissue remodelling during the process of development (Burke and Lewis, 2002). Release of MIP and TGFβ2 by macrophages promotes the switch between the inflammation and proliferation phase of wound healing (Fadok et al. 1998) and cytokines and chemokines released by macrophages help recruit lymphocytes to the wound (Kunkel and Butcher, 2002). In the body there are two basic types of macrophages: circulating macrophages, which move to individual site of infection and inflammation following chemo-attractive cues, and resident macrophages, which reside in tissues that are prone to frequent infection by pathogens (Gordon, 1995). Macrophages however are a physiological double-edged sword. Inappropriate phagocytosis and release of reactive oxygen species by macrophages can cause substantial tissue damage. Macrophages are responsible for the symptoms of several autoimmune diseases and chronic inflammation. Diseases most notably caused by inappropriate activation of macrophages are rheumatoid arthritis and asthma (Burke and Lewis, 2002). Macrophages also contribute to the development of artheriosclerotic plaques (Sheikine and Hansson, 2004). Macrophages are recruited to carcinomas due to production of the macrophage chemoattractant, colony-stimulating factor 1 (CSF-1) by the carcinoma cells (Lin et al. 2001). Macrophages then secrete

EGF which, promotes migration of the carcinoma cells. This forms a paracrine loop, which has been shown to promote metastasis of the carcinoma cells in vivo (Wyckoff et al. 2004).

All types of macrophages share the ability to chemotax and to phagocytose to a greater or lesser extent. Macrophages from different tissues are varied in their phenotype and function due to their adaption to their local environment. This variation in phenotype and function can be observed from the heterogeneity in cytokine production, receptor expression and perioxidatic activity of macrophages in different tissues (Gordon, 1995). Macrophages are often classified by their unique expression of a combination of cell surface markers (Gordon, 1992) (Table 1.7).

Table 1.7: Macrophage cell surface markers

Macrophage marker	Function	Exceptions
c-Fms	CSF-1 receptor, essential for macrophage proliferation, differentiation and survival	Not expressed in thymic macrophages (Dai et al. 2002)
Complement receptor type 3 ($\alpha M\beta 2$)	Recruits macrophages to sites where complement has been activated and also required for adhesion to ICAM-1	Expressed by all leukocytes (Zlotnik, 2000)
F4/80	Not required for development of tissue macrophages, function unknown	Not expressed by splenic white pulp macrophages but expressed by all other types of macrophages. (Gordon, 1995)
Scavenger receptor	Recognises certain anionic polymers and also acetylated low-density lipoproteins, essential for removing older erythrocytes	None but also expressed on neutrophils
Sialoadhesin	Adhesion to the endothelium. (Sialic acid is part of a glycoprotein expressed by CAMs)	Not expressed by splenic white pulp macrophages. (Paulnock, 2000)
MHC class 2	Presentation of antigen from phagocytosed cells to activate T Cells.	Expressed on other leukocytes (Zlotnik, 2000)

1.16.1 Control of macrophage activity

Macrophages have enormous secretory capacity (Table 1.8). Secretion by macrophages is regulated by activation signals such as adhesion, binding of bacterial products such a lipopolysacheride (LPS) and cytokines (Paulnock, 2000). Engagement of all of these activation signals does not only alter the secretory properties of macrophages. LPS, CSF-1 and MCP-1 has been shown to alter the shape, migration and phagocytic index of macrophages (Allen et al. 1997; Jones et al. 2003; Leverrier and Ridley, 2001; Weiss-Haljiti et al. 2004; Wells et al. 2004; Williams and Ridley, 2000). This has implications when experimenting with macrophages as small amounts of contaminants can fundamentally alter the properties of the macrophages.

Secreted molecule	Function
Reactive oxygen species	Locally toxic
Prostaglandins	Paracrine signalling
Tissue factor, Factor IX, X, V	Coagulation of enzymes
C1, C2, C3, C4, C5 and Factor B and C	Complement components
PDGF, EGF, CSF-1	Growth factors
IL-1, IL-6, TNF-α, MCP-1	Pro-inflammatory cytokines
TGFβ, IL-10	Anti-inflammatory cytokines

Table 1.8: Molecules secreted by macrophages

1.16.2 Rho GTPases regulate macrophage migration

Activation of Rac and Cdc42 in macrophages promotes the formation of dorsal ruffles, lamellipodia and filopodia, in a similar fashion to fibroblasts (Allen et al. 1997; Wells et al. 2004). Rho functions in both macrophages to maintain cell shape, activation of RhoA induces Bac1 macrophages to round up and form fine actin cables, and inhibition of Rho caused cell spreading in macrophages (Allen et al. 1997). Cdc42, Rac and RhoA are also involved in regulating phagocytic cups in macrophages (Castellano et al. 2001). Instead of focal adhesions macrophages use focal contacts and small phospho-paxillin rich adhesions for adhesion (Pixley et al. 2001). Microinjection of dominant negative Rac1 and Ccd42 caused loss of focal complexes in macrophages. This shows that, similar to fibroblasts, Rac1 and Cdc42 regulated the formation of adhesions although adhesions do not mature to become focal adhesions (Allen et al. 1997). Macrophages also contain larger punctuate adhesive structures called podosomes. Podosomes are not

the present in all macrophages indicating they are not the primary mechanism for adhesion in macrophages (Evans et al. 2003).

1.17 CSF-1

CSF-1 is a pleiotrophic macrophage growth factor. It stimulates survival, proliferation and differentiation of macrophages. It is also a chemo-attractant and promotes spreading and motility in macrophages (Webb et al. 1996) (Fig. 1.11). Mice that lack the gene for CSF-1 have severe osteoporosis, skeletal defects and tooth eruption failure, (due to a lack of osteoclasts) and have a decrease in tissue macrophages (though macrophages are not completely absent as thymic and lymph node macrophages do not require CSF-1 for survival) (Dai et al. 2002).

CSF-1 exists in three separate forms in vivo: a secreted glycoprotein, a proteoglycan, a membrane spanning cell surface-glycoprotein (Stanley et al. 1997). The circulating CSF-1 isoforms are synthesised by endothelial cells and can recruit macrophages at a distance. The cell surface isoform of CSF-1 and the proteoglycan are synthesised by several different cell types and are involved in local recruitment of macrophages (Stanley et al. 1997). The CSF-1R is encoded by the cFMS proto-oncogene (Sherr et al. 1985). The CSF-1R is a tyrosine kinase, and binding of CSF-1 results in the dimerisation of CSF-1R (Yeung et al. 1987). This causes a wave of tyrosine phosphorylation of proteins directly associated with the receptor within 30 seconds and promotes an increase in tyrosine phosphorylation of cellular proteins, the majority of which are cytoplasmic (Yeung et al. 1998). Activation of the CSF-1R promotes receptor ubiquitination via c-Cbl and the ligand receptor complex is internalised before its intralysosomal degradation (Yeung and Stanley, 2003) (Fig. 1.11).

The activated CSF-1 receptor is tyrosine-phosphorylated. Signaling molecules then associate with receptor through their phosphotyrosine-binding domains. Molecules shown touching specific receptor phosphotyrosines are those that associate directly with a particular phosphotyrosyl sequence motif (Pixley and Stanley, 2004) (Fig 1.11). CSF-1 signalling promotes activation of PI 3-K, which is implicated in the initiation of chemotaxis as (Section 1.12). The CSF-1-PI 3-K Akt/PKB pathway also signals to cell survival (Kelley et al. 1999) and activation of the ERK, NF-κB and the mTOR/S6K pathways (Bhatt et al. 2002; Brach et al. 1991; Glantschnig et al. 2003) (Fig. 1.11).

CSF-1 stimulation promotes formation of new paxillin enriched focal contacts, mediated through Pyk2 (a relative of FAK) (Pixley et al. 2001). Pyk2-null macrophages have motility defects and a loss of polarity, which is consistent with defects in adhesion (Okigaki et al. 2003). Pyk2 is known to be a substrate of Src (Duong et al. 1998), which connects the PI 3-K and the Src signalling pathways in the regulation of macrophage adhesion (Fig 1.11).

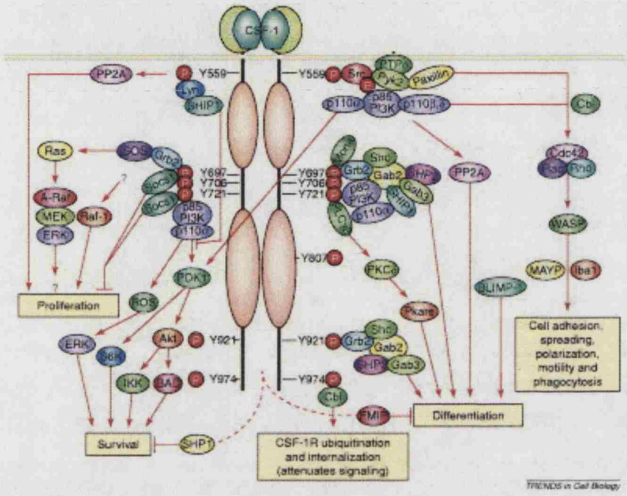

Figure 1.11: Signaling pathways regulated by CSF-1 receptor taken from (Pixley and Stanley, 2004)

1.18 CSF-1 and macrophage migration

Acute stimulation of macrophages with CSF-1 promotes formation of lamellipodia, filopodia and dorsal ruffles (Allen et al. 1997; Wells et al. 2004). When macrophages are placed in a gradient containing CSF-1 they rapidly become polarised along the axis of that gradient and show strong positive chemotaxis towards the CSF-1 (Jones et al. 2003; Webb et al. 1996). In macrophages Rac1 is activated by acute stimulation with CSF-1 (Allen et al. 1998; Wells et al. 2004). Rac1 null macrophages have reduced membrane ruffling, spreading and chemotaxis in response to CSF-1 stimulation (Wells et al. 2004). Microinjection of constitutively active and dominant negative Cdc42 into the Bac1 macrophage cell line inhibited CSF-1 induced chemotaxis. Intriguingly dominant negative Cdc42 increases the speed of macrophage migration and increases the width of the lamella, although filopodia are absent (Allen et al. 1998). Macrophages that lack N-WASP activity are unable to chemotax towards CSF-1 and have defects in the dynamics of their actin cytoskeleton (Jones, 2000). This suggests that Cdc42 is essential for polarisation towards a CSF-1 gradient in BMM and that activation of the

Cdc42 target WASP is essential for generation of actin polymerisation required for cell motility in macrophages. The effect of CSF-1 stimulation on RhoA activity has not been characterised in macrophages as yet although C3-transferase inhibits CSF-1 induced migration (Allen et al. 1997).

1.19 **Aims**

In humans there are at least 20 Rho family GTPases, yet the majority of the work about the role of Rho GTPases in migration has been limited to RhoA, Rac1 and Cdc42. It is often assumed that because the siblings of the big three are highly homologous in amino acid sequence they will be functionally redundant. This project aims to investigate the function of RhoB, a homologue of RhoA, and where possible compare the contribution of RhoA and RhoB to cell migration and morphology.

RhoB was chosen in particular because a RhoB-null mouse was generated by the Prendergast laboratory, mainly for transformation studies (see section 1.10.4). Initial characterisation of *RhoB*$^{-/-}$ mouse embryonic fibroblasts showed that there was a defect in their migration into a scratch wound and adhesion to fibronectin. A RhoA-null mouse was unfortunately not available for comparison as deletion of RhoA causes death in the very early embryo (Wei et al. 2002). Therefore, where possible, small molecule inhibitors of Rho function were used, C3-transferase, which inhibits all Rho activity and Y27632 which inhibits ROCK activity. By comparison and correlation of results cell phenotypes dependent on RhoA or RhoB or both RhoA and B could be deduced. Over-expression studies were avoided in this study as it was felt that over-expression would simply swamp the cell with Rho protein and the activity of signalling scaffolds in specific places in the cell that Rho participates in would be lost (Chapter 1.14).

The macrophage was chosen as a tool for study of Rho GTPase function because:

- It is a single cell motile system whose movement is independent of other cells
- Macrophage motility is regulated by Rho GTPases.
- Macrophages have several functions that can be assessed for each cell individually and correlated to show the behaviour of the whole population.
- Macrophages can be derived from a murine source, purified and stored which allows repetition of experiments using cells from the same source under different conditions.

2 Materials and Methods

2.1 General reagents

50 Bp DNA ladder	Invitrogen	http://www.invitrogen.com
β-mercaptoethanol	Sigma	http://www.sigmaaldrich.com
BioRad protein assay reagent	BioRad Laboratorys	http://Bio-Rad.com
Bovine serum albumin	Sigma	http://www.sigmaaldrich.com/
Carboxyfluorescein diacetate succinimidyl ester (CSFE)	Molecular Probes	http://www.probes.com/
Coomassie Brilliant Blue (R250)	BioRad Laboratorys	http://Bio-Rad.com
CSF-1	R and D systems	http://www.rndsystems.com/
DAKO Mounting Medium	DAKO-cytomation inc	http://www.dakocytomation.us/
Dimethylsulphoxide (DMSO) cat no D2650	Sigma	http://www.sigmaaldrich.com/
Dried skimmed milk	Tesco	http://www.tesco.com/
ECL (Enhanced chemi-luminescence kit)	Amersham Biosciences	http://www.amershambiosciences.com
Endo-free maxi prep kit	Qiagen	http://www.qiagen.com/
Glutathione Sepharose Beads	Amersham Biosciences	http://www.amershambiosciences.com
LY294002	Calbiochem	http://www.calbiochem.com
Multimark protein size markers	Invitrogen	http://www.invitrogen.com
NuPage protein electrophoresis system	Invitrogen	http://www.invitrogen.com
Oligonucleotides	Sigma	http://www.sigmaaldrich.com/
Protein size marker RPN 756	Amersham Biosciences	http://www.amershambiosciences.com
PAK1 Pak binding domain agarose	Upstate Biotechnology	http://www.upstate.com/
Rhotekin Rho binding domain agarose	Upstate Biotechnology	http://www.upstate.com/
Super RX medical X Ray film	Fugi	http://www.fujifilm.com
Superscript RT PCR Kit	Invitrogen	http://www.invitrogen.com
Sure2 super-competent bacteria	Stratagene	http://www.stratagene.com/
Taq DNA polymerase kit	Invitrogen	http://www.invitrogen.com
Thiazolyl blue (MTT)	Sigma	http://www.sigmaaldrich.com/
XL1 Blue super-competent bacteria	Invitrogen	http://www.invitrogen.com
Y27632	Calbiochem	http://www.calbiochem.com

2.2 Cell culture

2.2.1 Materials

Phosphate buffered saline (PBS)	Invitrogen	http://www.invitrogen.com
100x Non-essential amino acids	Invitrogen	http://www.invitrogen.com
100 mM Sodium pyruvate	Invitrogen	http://www.invitrogen.com
Versene	Invitrogen	http://www.invitrogen.com
RPMI 1640 + 1% glutamine	Invitrogen	http://www.invitrogen.com
Dulbecco's minimum essential medium	Invitrogen	http://www.invitrogen.com
Donor calf serum	Invitrogen	http://www.invitrogen.com
Trypsin/EDTA	Invitrogen	http://www.invitrogen.com
Goat serum	Invitrogen	http://www.invitrogen.com
Foetal calf serum (FCS)	Helena Biosciences	http://www.helena-biosciences.com/

2.2.2 Components of medium

i) Macrophage growth medium

RPMI 1640 supplemented with 10% (v/v) FCS heat inactivated by incubation at 70°C for 30 min, 100 IU/ml Penicillin and 100 μg/ml Streptomycin, 1x non-essential amino acids (v/v), 1mM sodium pyruvate (v/v), 8.5μl β-mercaptoethanol supplemented with 10% L-cell conditioned medium

ii) Macrophage starve medium

As macrophage growth medium without the addition of L-cell conditioned medium.

iii) Macrophage freezing medium

Macrophage starve medium supplemented with 10% DMSO.

iv) Macrophage spreading medium

Macrophage medium containing 0.5% FCS without the addition of L-cell conditioned medium.

v) NIH 3T3 Medium

DMEM supplemented with 10% DCS (v/v) and 100 IU/ml penicillin and 100μg/ml streptomycin.

vi) L Cell conditioned medium

L-cell conditioned medium was kindly prepared by R. Garg.

L-cells were grown to confluence in DMEM, 10% heat inactivated FCS and 100 IU/ml penicillin and 100 μg/ml streptomycin. The lids of the flasks the cells were grown in were closed and incubated for 3 weeks at 37°C, 10% CO_2. The L-cell conditioned medium was sterilised by filtration through a 0.25–μm filter and stored at 4°C for up to 6 months.

2.2.3 Isolation of murine bone marrow-derived macrophages (BMM)

Femoral bone marrow cells were isolated from 6- to 8-week-old wild-type (Wt) or RhoB-null Sv129 mice (Figure 3.1 and Chapter 3.2). Mice from the same strain were used in these studies to control for allelic variation in expressions of genes between strains. The generation of RhoB-null mice is described in Liu and Prendergast (Liu et al. 2001). Bone marrow cells were flushed from excised fibulae of recently culled mice. These cells were seeded at $1x10^6$ cells/ml in 25 cm^2 bacteriological plastic dishes in macrophage growth medium supplemented with 10% L cell-conditioned medium as a source of CSF-1. They were incubated in a humidified atmosphere at 37°C, 10% CO_2. After 3 days, non-adherent cells were collected and were cryogenically stored in freezing medium. These cells are then seeded at 10^6 cells/ml in bacteriological petri dishes and incubated for a further 4-5 days, when 90% of cells are adherent. At this point cells were considered, for the purpose of the experiments described in this thesis, to be fully differentiated BMM.

2.2.4 Culture of BMM

BMM were cultured in macrophage growth medium, fresh 10% L-cell medium was added every 3 days. To passage, BMM were washed once with Versene and incubated in Versene for 15 min at 37°C and 10% CO_2. If cells had not detached at this point the cells were removed from the bacteriological plastic by pipeting with Versene. When all cells had detached macrophage medium was added to Versene at a 1:1 dilution and cells were collected by centrifugation at 1000g for 5 min. As BMM alter their physiological properties with age, cells were not used for more than 14 days after initial seeding onto bacteriologocal plastic.

2.2.5 Starvation and CSF-1 stimulation of BMM

Growth medium was removed and BMM were washed one or two times with starve medium. BMM were then incubated for 18 h in starve medium. BMM were stimulated using 33 ng/ml CSF-1 in growth medium for the time points indicated on the figures.

2.2.6 Treatment of BMM with inhibitors

Inhibitor	Target	Final Concentration	Incubation time
LY294002	PI 3-Kinases	10 nM	30 min
Y27632	Rho-Kinase	10 μM	30 min
C3-Tat	RhoA, B, C	5 μg/ml	4 h

Table 2.1. Conditions of inhibitor use

Cells were treated with inhibitors as follows: prior to addition of inhibitor BMM growth medium was removed and BMM were washed once with PBS. Growth medium with inhibitor was then added to BMM (Table 2.1). Cells were incubated for the indicated time prior to lysis or fixation. To washout inhibitor growth medium with inhibitor was removed and BMM were washed twice with growth medium and incubated in growth medium for 30 min.

2.2.7 Culture of NIH3T3 fibroblasts

NIH-3T3 fibroblasts were grown in NIH medium in 10 cm^2 tissue culture dishes in a humidified atmosphere at 37°C and 10% CO_2. For passaging, cells were washed in PBS and incubated with 3 ml trypsin/EDTA at 37°C and 10% CO_2 until cells had detached. NIH medium was added to inactivate trypsin and cells were collected by centrifugation at 1000g for 3 min. Cells were then diluted according to their growth rate between 1:5 and 1:10 in growth medium.

2.3 Molecular Biology (RNA and DNA methods)

2.3.1 Materials

Ampicillin	50 mg/ml stock in ddH_20
DEPC-treated Water autoclaved	1% DEPC (v/v), incubated overnight then
6x DNA loading buffer	30% Glycerol (v/v), 0.25% Bromophenol blue (w/v) 0.25% Xylene cyanol (w/v)
IPTG	0.5 M stock in ddH_20
LB	25 g per litre of Premix
LB Agar	15 g per litre Bacto agar added to LB
LB/AMP	LB supplemented with 50μg/ml Ampicillin
10x TBE buffer	960 mM Tris, 890 mM Boric Acid, 20 mM EDTA
T.E. pH 8	100 mM Tris Cl, 10 mM EDTA (pH 8.0) adjust pH if needed using 1M NaOH or 4 M HCl

2.3.2 Plasmids and constructs:

pGEX GST RhoA	Ridley Laboratory
pGEX GST RhoB	" "
pGEX GST RhoC	" "
pGEX Wasp-CRIB	Gift from Dr D. Sacks
pC3-Tat	Gift from Prof Chris Marshall

2.3.3 Primers

Primer Name	Sequence
RhoA Forward	GGAAGAAACTGGTGATTGTT
RhoA Reverse	TTCTAAACTATCAGGGCTGTCA
RhoB Forward	GGCAAGACGTGCCTGCTGATCG
RhoB Reverse	TGGCCGAGCACTCGAGGTAGTC
Rho C Forward	GGTGCCTGTGGGAAGACCTGCC
RhoC Reverse	TCTTGGCCAGCTCTCTCCTGGT

2.3.4 Extraction of plasmid DNA from bacteria

All plasmid DNA used was produced on a large scale using an ENDO-free plasmid maxi kit according to the manufacturers instructions (Section 2.1). Briefly, 5 ml of LB/Amp were inoculated with *Escherischa coli* from a glycerol stock and grown for 8 h at 37°C with vigorous shaking. The starter culture was then diluted 1:40 and grown overnight in LB/Amp. The bacterial cells were collected by pelleting in a Sorvall RC5C

centrifuge (Rotor-SS34) for 15 min. The cells were resuspended, lysed and the DNA precipitated using alkaline lysis. DNA was collected using 2 pre-equilibrated columns. DNA was precipitated using 0.7 volumes of isopropanol and collected by centrifugation at 1000g for 30 min, 4°C, in a Beckman J-6M/E centrifuge. The pellet was then washed with 70% ethanol and air-dried. The DNA pellet was then resuspended in 50 to 100µl of 100 mM TE 8.0 and the concentration calculated.

2.3.5 Determination of RNA/ DNA concentration

The RNA and DNA concentration of aqueous solutions was determined by placing the sample in a quartz cuvette. The optical density at 260 nm and 280 nm was measured using a Biorad spectrophotometer. The concentration of DNA and RNA was calculated as follows:

$Conc_{DNA}$ mg/ml = OD 280 x 50

$Conc_{RNA}$ mg/ml = OD 260 x 40

2.3.6 Isolation of total cellular RNA and production of cDNA

A confluent 5 cm dish of BMM (10^6 BMM) was lysed in 0.5 ml Trizol and incubated at room temperature (RT) for 5 min. 0.1ml chloroform was added and the suspension was mixed vigorously for 15 sec and incubated at RT for 15 min. The suspension was then centrifuged at 12000g for 15 min, at 4°C, in an Eppendorf mini-centrifuge 5417R, and the upper, aqueous phase was transferred to a 1.5 ml microfuge tube. 0.75 ml isopropanol at -20°C was then added, the sample was mixed by inversion to avoid shearing of DNA and incubated at RT for 10 min. RNA was collected by centrifugation at 12000g for 15 min at 4°C. The RNA pellet was washed once with 75% ethanol and air dried. The RNA was then resuspended in 50 to 100 µl DEPC H_2O and incubated at 55 -60°C until completely dissolved.

cDNA was synthesised using the SUPERSCRIPT kit, briefly total cellular RNA was treated with DNase to remove any residual genomic DNA. Total cellular RNA was then primed with oligo-dT primers and incubated with reverse transcriptase for 50 min at 42°C. The reverse transcriptase was inactivated by incubation at 70°C for 15 min and the concentration of cDNA was calculated.

2.3.7 Design of PCR primers

The *Mus musculus* and *Homo sapiens* genome was searched for RhoA, B, C using the nucelotide programme which is part of the NIH Pubmed website (Tatusova and Madden, 1999). 20-22mers of RhoA, B and C were chosen for RT-PCR primers which were identical in human and mouse. The Blast (http://www.ncbi.nlm.nih.gov/BLAST/) database was then searched by BLAST to ensure that these sequences were unique to RhoA, RhoB and RhoC.

2.3.8 Polymerase chain reaction

For cDNA amplification by PCR 10 to 50 ng of template cDNA, 40 μM of forward and reverse primers, 200 μM of each dNTP, 2 μM $MgCl_2$ were incubated in a total of 20 μl 1x PCR buffer. Immediately prior to PCR 0.4 μl Taq polymerase was added to the reaction. To denature the DNA each reaction was heated to 95°C for 2 min. 30 cycles of:

Denaturation: 95 °C 30 sec,
Annealing: 30 seconds 52°C (RhoA and B), 58°C RhoC
Elongation: 72 °C 1 min
were than carried out. RhoA, RhoB and RhoC primers yielded PCR fragments of 250, 450 and 350 bp respectively. The PCR products were analysed by agarose gel electrophoresis.
For each PCR reaction a positive control of human cDNA from RhoA, RhoB and RhoC in a pGEX2T plasmid was used.

2.3.9 Agarose gel electrophoresis

PCR products were analysed by size separation in 2% TBE agarose gels. To prepare gels 2 g of electrophoresis grade agarose was resuspended in 100 ml TBE and dissolved by boiling in a microwave oven. After cooling to 50°C 0.5 μg/ml ethidium bromide was added to allow visualisation of PCR products under a UV illumination (254 nm). The gel was poured into a gel cassette containing a well comb and allowed to set. The set gel was then placed in a gel tank containing 1x TBE running buffer, the well comb was removed and a DNA sample supplemented with 6x DNA loading buffer was added to

each well. DNA ladder (50 bp, 5 µl) was added to the first well to allow the size of the DNA products to be determined. The DNA was then electrophoresed across the gel at 100 volts until the xylene cyanol dye in the loading buffer reached the edge of the gel. The gel was photographed using a dual intensity UV transillumination box (GRI) and a Syngene camera (Sony).

2.4 Protein biochemistry

2.4.1 Buffers and solutions

2x SDS PAGE sample loading buffer	0.125 M Tris-Cl pH 6.8 4% SDS (w/v) 20% Glycerol (v/v) 1.41 M β-mercaptoethanol 0.04% Bromophenol blue (w/v)
10x SDS PAGE running buffer	4% SDS (w/v) 250 mM Tris-Cl 1.92 M Glycine
MOPS running buffer	50 mM morpholinepropanesulfonic acid (MOPS) 50 mM Tris-Cl pH 7.6 0.1% SDS (v/v) 1mM EDTA pH 8.0
SDS PAGE separation gel	3.75 mM Tris-Cl pH 8.8, 10 or 12% Acrylamide (v/v), 1% SDS (v/v)
SDS PAGE stack gel	630 µM Tris-Cl pH 6.8, 10% Acrylamide (v/v) 0.05% SDS (v/v)
Strip buffer	2% SDS (v/v) 62.5 mM Tris-Cl pH 6.8, 0.7% (v/v) β–mercaptoethanol
1x SDS PAGE transfer buffer	25 mM Tris Cl, 192 mM Glycine 20% Methanol (v/v)
TBS 0.5% Tween	25 mM Tris-Cl pH 7.6, 50 mM NaCl, 0.5% Tween 20 (v/v)
RIPA buffer	50 mM Tris-Cl pH 7.2 1% Triton X-100 (v/v) 0.1% SDS (v/v) 500 mM NaCl 10 mM $MgCl_2$ 10% Glycerol (v/v) 10 µg/ml DTT Protease inhibitor cocktail
1% NP-40 lysis buffer	50mM Tris-Cl pH 7.6 2 mM EDTA pH 8.0 150 mM NaCl

	10 mM $MgCl_2$ 1% NP-40 (v/v) 10% glycerol (v/v) 10 µg/ml DTT Protease inhibitor cocktail
Rac2 lysis buffer	10 mM Tris-Cl pH 7.5 0.1 mM EDTA pH 8.0 0.1 mM EGTA 0.5% SDS (v/v) 10 µg/ml DTT Protease inhibitor cocktail.
Protease inhibitor cocktail	1 µg/ml Leupeptin 1 mM PMSF 1 mM Sodium vanadate 0.72 TIU Apotinin 1 mM Sodium fluoride
Coomassie Blue destain	15% Methanol (v/v) 5% Acetic Acid (v/v)
Coomassie Blue stain	15% Methanol (v/v) 5% Acetic Acid (v/v) 0.025% Coomassie blue (w/v)
GST fusion protein lysis buffer	50 mM Tris-Cl pH 7.6 50 mM NaCl 5 mM $MgCl_2$ 10 µg/ml DTT 1mM PMSF

Software:

Program	**Manufacturer**	**Address**
Quantity one	Bio-Rad Laboratories Ltd	http://Bio-Rad.com

2.4.2 Antibodies used for western blotting

Western Blotting						
Antibody	Reactivity	Approx size (kDA)	Block	Dilution	Source	Address
4G10-pY	Mouse	NA	5% BSA	1:1000	Upstate Biotecnology	http://www.upstate.com
β–Actin	Mouse	40	5% Milk	1:4000	Sigma-Aldrich	http://www.sigmaaldrich.com
pS473 AKT	Rabbit	65	5% BSA	1:1000	Cell Signaling Technology	http://www.cellsignal.com
AKT	Rabbit	65	5% BSA	1:1000	Cell Signaling Technology	http://www.cellsignal.com
Cdc42	Mouse	21	5% Milk	1:2000	Santa Cruz Biotechnology	http://www.scbt.com
pT202/Y204 ERK1/2	Rabbit	42 + 44	5% Milk	1:4000	Cell Signaling Technology	http://www.cellsignal.com
Erk1	Rabbit	42 + 44	5% Milk	1:1000	Santa Cruz Biotechnology	http://www.scbt.com
pT 505/508 LIMK1/2	Rabbit	65	5% BSA	1:1000	Cell Signaling Technology	http://www.cellsignal.com
LIMK 1	Rabbit	65	5% BSA	1:1000	Cell Signaling Technology	http://www.cellsignal.com
pS19 MLC	Rabbit	21	5% BSA	1:500	Santa Cruz Biotechnology	http://www.scbt.com
MLC	Rabbit	21	5% BSA	1:500	Santa Cruz Biotechnology	http://www.scbt.com
pY118-paxillin	Rabbit	68	5% Milk	1:1000	Biosource	http://www.biosource.com
Paxillin	Mouse	68	5% Milk	1:1000	BD Pharmingen	http://www.bdbiosciences.com/pharmingen
Prk1	Mouse	120	5% Milk	1:1000	BD Pharmingen	http://www.bdbiosciences.com/pharmingen
Rac1	Mouse	21	5% Milk	1:1000	BD Pharmingen	http://www.bdbiosciences.com/pharmingen
Rac2	Mouse	21	5% Milk	1:1000	Santa Cruz Biotechnology	http://www.scbt.com
RhoA	Mouse	21	5% Milk	1:500	Santa Cruz Biotechnology	http://www.scbt.com
RhoB	Mouse	23	5% BSA	1:250	Santa Cruz Biotechnology	http://www.scbt.com
RhoB	Mouse	23	5% Milk	1:2000	Bethyl Laboratories	http://www.bethyl.com
RhoC	Rabbit	21	5% Milk	1:500	Gift from Dr S. Meravjer	
β–Tubulin	Mouse	55	5% Milk	1:4000	Sigma-Aldrich	http://www.sigmaaldrich.com

Table 2.2: Conditions of primary antibody use for western blotting, Milk=dried skimmed milk, BSA= Bovine serum albumin.

Secondary antibody	Source	Address
Horse radish peroxidase conjugated (HRP) anti- mouse, rabbit	Amersham Biosciences	http://www.amershambiosciences.com

Table 2.2b: Conditions of secondary antibody use for western blotting,

2.4.3 Cell lysis for analysis of cellular proteins

BMM were grown in bacteriological plastic dishes until confluence. Cells were then washed 1x with cold PBS and lysed on ice in an appropriate volume of lysis buffer (for a 5cm dish 250 µl lysis buffer was used). For analysis of Rho proteins RIPA lysis buffer was used as RhoB is not soluble in NP40 lysis buffer and RIPA lysis buffer efficiently removed of RhoB from cellular membranes. For analysis of proteins other than Rho proteins NP40 lysis buffer was used. Lysates were incubated on ice for 5 min prior to centrifugation, at 10,000g for 10 min at 4°C. The supernatant was then transferred to a fresh microfuge tube and the insoluble pellet fraction discarded. The protein concentration of the supernatant was calculated, then 2x sample loading buffer was added and the samples boiled at 100°C for 5 min and stored at -20°C.

2.4.4 Biorad protein assay

A 5 µl sample of cell lysate was diluted in 795 µl of ddH_2O. Biorad protein assay dye was added (200 µl) and the solution mixed by inversion. A blank was made with a 5 µl sample of the lysis buffer, 200 µl of Biorad protein assay dye and 795 µl of ddH_20. The absorbance of each sample was measured at 595 nm using a plastic cuvette and a Biorad spectrophotometer. The protein concentration was determined using a calibration curve made from known concentrations of BSA ranging from 0.01 µg/ml to 10 µl/ml.

2.4.5 SDS-PAGE

Proteins were separated by SDS-PAGE using a minigel apparatus (Mini-Protean Cell, Biorad). A separation gel of 1.5 mm thickness was cast, which contained 10 or 12% acrylamide to achieve maximum separation of proteins sized approximately between 15 and 97 kDa. The gel was overlayed with ddH_2O and allowed to set at RT. After the separation gel had set a stack gel containing 10% acrylamide was layered on top of the separation gel and a gel comb added to create wells for loading of protein samples. The

set gel was then placed into a gel tank containing 1x SDS-PAGE running buffer and electrophoresed at 120 volts for 1 h or until the bromophenol blue in the 2x sample buffer ran off the bottom of the gel.

2.4.6 Nu-PAGE electrophoresis

For more accurate separation of RhoA and RhoB proteins the NU-PAGE (Invitrogen) electrophoresis system was used according to manufacturers' instructions. Briefly, cell lysates were added to pre-cast Bis-Tris SDS-PAGE cells with a gradient of 4-12% acrylamide. The samples were electrophoresed in an X-Cell II gel tank in fresh 1xMOPS running buffer at 200 volts for 30 min. The gels were then western blotted in the same way as a SDS-polyacrylamide gel.

2.4.7 Coomassie blue staining to assay for protein concentration

To visualise protein levels by Coomassie Brilliant Blue, gels were incubated in Coomassie blue stain solution for 1 h with agitation. The gel was then washed several times with coomassie destain solution until bands were visible. Protein concentration of samples was determined by electrophoresing known concentrations of BSA (0.01-10 μg/ml) on the gels.

2.4.8 Western blotting

Following separation of proteins in cell lysates by electrophoresis, proteins were transferred onto polyvinylidene fluoride (PVDF) membranes (Immobilon-P) by wet transfer. Protein gels were overlaid on PVDF membrane (which had been pre-soaked in methanol), equilibrated in transfer buffer and sandwiched between two sheets of Whatmann 3 mm paper. Air bubbles were removed from between the gel and membrane and finally the whole was placed between two sponges that had also been pre-soaked in transfer buffer and placed in a Mini Protean II transfer case. The case was then placed into a gel tank filled with 1x transfer buffer. Proteins were transferred at 4°C at 100 volts for 1 h. The PVDF membrane was then blocked in either 5% non-fat dried milk or 5% BSA (as appropriate for the antibody to be used see section 2.4.2) for 30 min at RT with agitation. The membrane was then washed 3 to 4 times in TBS 0.5% Tween and incubated with 0.1-0.5μg/ml primary antibody in appropriate block for

either 1 h at RT or overnight at 4°C with agitation. The membrane was then washed 3 to 4 times in TBS 0.5% Tween and incubated with HRP-conjugated secondary antibody in appropriate block for 1 h at RT with agitation. The membrane was then washed 3 to 4 times in TBS 0.5% Tween, developed with ECL according to manufacturers' instructions and exposed to X-Ray film in the dark.

2.4.9 Stripping western blots

PVDF membranes were placed in 10 ml SDS strip buffer and incubated in an oven at 65°C for 15 min with agitation. Membranes were then washed 5 times with TBS 0.5% Tween and reblocked with 5% non-fat milk for 30 min and developed according to the standard western protocol.

2.4.10 Purification of GST fusion proteins

A scrape of glycerol stock was inoculated into 5ml LB/Amp and agitated at 37°C for 6 to 8 h. This culture was diluted 1:20 into L broth/100 μg/ml ampicillin and shaken overnight at 37°C. The solution was then diluted 1:10 into fresh, pre-warmed LB/Amp and grown for 1 h. Protein expression was induced with IPTG (0.2 mM) for 3 h. Bacterial cells were collected by centrifugation for 10 min, at 4000g, 4°C and resuspended in 6 ml of cold GST fusion protein lysis buffer. Bacterial cells were sonicated on ice at 1000 Hz for 3 times 45 sec with 1 min between each burst (Vibra-cell, Fischer scientific) until the bacterial solution became slightly viscous and opaque. The sonicated samples were then centrifuged at 10 K, 10 min, 4°C. The supernatant was added to glutathione-Sepharose beads which had been pre-equilibrated in lysis buffer and beads/supernatant were incubated with mild agitation for 60 min at 4°C. The beads were collected by centrifugation at 1000g for 2 min at 4°C and washed 3 times with 5 ml if ice-cold lysis buffer without PMSF to remove unbound proteins. The beads were then resuspended in an appropriate volume of lysis buffer with PMSF, a 5 μl aliquot was removed for analysis of protein concentration using Coomassie blue staining and the remainder was stored in 10 μl aliquots at -80°C.

2.4.11 GTPase activation assays (Pull-downs)

Pull-down assays were carried out using the method described by Ren and Schwartz (Ren and Schwartz, 2000). GST fusion proteins of PAK-CRIB or Rhotekin-RBD (Upstate) or the CRIB domain of WASp were used for Rac, Rho and Cdc42 pull-downs respectively. A near- confluent 25 cm^2 dish of BMM was used for each pull down. For RhoA and RhoB pull downs cells were lysed on ice using 250 µl of ice-cold RIPA cell lysis buffer. Cell lysate was immediately centrifuged in a prechilled microfuge at 10000g for 10 min at 4°C. For Rac1 and Cdc42 pull downs, cells were lysed on ice using 250 µl of ice-cold NP-40 cell lysis buffer. Cell lysates were immediately centrifuged et 10000g in a prechilled microfuge for 3 min, at 4°C. 200µl of cell lysate was added to 20 µg of the GST-fusion protein bead slurry and the lysate and bead slurry was incubated with mild agitation for 60 min at 4°C. The beads were collected by centrifugation at 10000g for 1 min at 4°C and washed 3 times with 0.5 ml cold lysis buffer to remove unbound proteins. The beads were then resuspended in 30 µl 2x SDS PAGE sample loading buffer. The 50 µl aliquot of cell lysate which had not been applied to beads was kept to analyse total Rho/Rac/Cdc42 level and determine protein concentration using a Bradford assay. Using the data from the Bradford protein assay, volumes corresponding to equal amounts of proteins were loaded onto NU-Page Bis-Tris gels. The gels were electrophoresed, western blotted and the X-ray films of the blots were quantitated using a Densitometer (Biorad) and Quantity one software. For the purposes of quantitation Wt BMM in starve medium were assigned a value of 1, and the Rho or Rac GTPase activity of other samples was determined as a quotient of this. To ensure that the Rho pulldowns were working, BMM lysates were incubated with EDTA and 100µM GTPγS or 1 mM GDPβS respectively at 30°C for 15 min with vigorous shaking. The reactions were stopped with the addition of $MgCl_2$ to a final concentration of 60 mM. Rho-GTP or Rac-GTP was precipitated by incubation of the loaded lysates with 20 µg GST-RBD or GST-PBD respectively. Western blotting of these control experiments showed that the GTPγS loaded Rho and Rac bound to the Rhotekin or PAK-Crib beads. Whereas the GDPβS loaded Rho and Rac did not bind to the Rhotekin or PAK-Crib beads (data not shown). These results showed that the pulldown assay were working correctly. ANOVA and Students T tests were used to compare GTPase activity between different samples. Statistical significance was accepted at $p>0.05$.

2.5 Bioinformatics

Software	Source	Address
Nucleotide	Part of Entrez/Pubmed	http://www.ncbi.nlm.nih.gov/entrez
Blast	National institute of Health USA	http://www.ncbi.nlm.nih.gov/BLAST
Uniprot	European Bioinformatics institute	http://www.ebi.uniprot.org
Protein explorer	(http://molvis.sdsc.edu/protexpl/frntdoor.htm)	

Amino Acids 1- 90, which contain the majority of the GTPase domain, of RhoA was compared to the proteins of all organisms sequenced to date using the UNIPROT database (see above). The results were exported into Microsoft Excel and then sorted according to organism. The full length amino acid sequences of the RhoA, RhoB and RhoC like GTPases of each organism were then compared to the full length sequences of Human RhoA, RhoB and RhoC using Pairwise BLAST. This allowed the number of Rho family GTPases in total to be determined and also the number of GTPases that specifically corresponded to RhoA RhoB or RhoC to be assigned for each organism.

2.6 Cell Biology

2.6.1 Materials

Primary antibodies				
Antibody	Reactivity	Dilution	Source	Address
βTubulin	Mouse	1:250	Sigma-Aldrich	http://www.sigmaaldrich.com
Paxillin	Mouse	1:50	BD Pharmingen	http://www.bdbiosciences.com/pharmingen/
pY118-Paxillin	Rabbit	1:200	Biosource	http://www.biosource.com/
PYK2	Mouse	1:50	BD Pharmingen	http://www.bdbiosciences.com/pharmingen/

Secondary Antibodies		
Antibody	Source	Address
FITC conjugated anti mouse	Southern Biotechnology Associates	http://www.southernbiotech.com
Cy5 conjugated anti rabbit	Jackson Immuno-Research	www.jacksonimmuno.com/
Rhodamine-conjugated Phalloidin	Sigma Aldrich	http://www.sigmaaldrich.com

Table 2.3: Conditions of antibody use for cell biology

Microscopes

Equipment	Manufacturer	Address
LSM 510 Confocal Microscope	Carl Zeiss	http://www.zeiss.com
KPM1E/K-S10 CCD Camera	Hitachi Denshi	http://www.hdal.com
BX-50 Microscope	Olympus	http://www.olympus-global.com
CoolSnap FX CCD camera	Roper Scientific	http://www.roperscientific.com

Software

Equipment	Source	Address
LSM5 software	Carl Zeiss	http://www.zeiss.com
Motion analysis	Kinetic Imaging Ltd	http://www.kineticimaging.com
Metamorph	Universal Imaging Systems	http://www.image1.com/products/metamorph
ImageJ	National Institute of Health USA	http://rsb.info.nih.gov/ij
Mathematica 5.0	Wolfram Research	http://www.wolfram.com
Adobe Photoshop 6.0	Adobe systems Inc.	http://www.adobe.com

2.6.2 Analysis of random migration

BMM were seeded onto 25 cm^2 dishes at 1 or $2x10^4$ cells/ml. Tissue culture plastic (Nunc) dishes which had been precoated with 10μg/ml fibronectin (Sigma) or glass-bottomed dishes (MatTek Corporation) were used as indicated. After seeding, cells were incubated in a humidified atmosphere for at least 18 h and no more than 72 h at 37°C, 10% CO_2, prior to timelapse microscopy. BMM were observed to become less motile with age and time, so all experiments were carried out within a strict time frame to ensure that all cells filmed had comparable motility. During the time-lapse experiments cells were incubated in a humidified chamber at 10% CO_2. A heated stage set at 37°C was used to control the temperature of the environment. Phase contrast micrographs of live cells were taken using a KPM1E/K-S10 Hitachi Denshi 768x576 pixel, 8 bit CCD camera using an x10 Plan/Neofluar N.A. 0.30 lens (Zeiss). Data sets were collected using Kinetic Imaging Motion analysis software. Frames were collected every 5 min for 5.5 h for random migration studies.

2.6.3 Chemotaxis assays

To study chemotaxis, cells were seeded on acid-washed 22 x 22 mm coverslips at a density of $2x10^4$ cells/ml in macrophage growth medium and incubated overnight. The coverslips were then mounted onto Dunn chemotaxis chambers (Fig 4.7) (Wells and Ridley, 2004) using recombinant murine CSF-1 (33 ng/ml) as the chemoattractant, and were sealed using imaging wax which consists of (1: 1: 1) lanolin, vaseline and paraffin wax. Dunn chambers were incubated at 37°C and phase contrast images were collected every 10 min for 16.5 h (see section 2.6.2). Mathematical analysis was then carried out using Mathematica 6.0 (Wolfram Research Institute) workbooks and Microsoft Excel (Allen et al. 1998; Wells and Ridley, 2004).

2.6.4 Migration analysis.

To quantitate migration the movement of the nucleus of individual BMMs was tracked using Motion analysis software. Cells that appeared to enter mitosis or moved off or onto the field of view during the course of the time-lapse video were excluded from the analysis. Data about the x and y co-ordinates of the cells tracked in each frame and the displacement of the cell in pixels frame to frame was recorded and exported as

Microsoft Excel compatible files (.xld). Mathematical data regarding the speed and direction of the migration of a population of BMM was generated using software written for Mathematica 6.0 by G.Dunn (Zicha et al. 1997). ANOVA and Students t-tests were used to compare the speeds of migration between different populations of BMM. Statistical significance was accepted for $p<0.05$.

Using this software it is possible to set an event horizon for migration of cells (Fig 2.1) The percentage migratory cells in a population could be calculated by setting the event horizon at 25 μm. A cell is defined as migratory if it has moved more than 25 μm from its starting point. By increasing the event horizon in increments of 25 μm it was possible to calculate the percentage of a given population of cells that had moved beyond there. Time-lapse movies were edited for presentation using ImageJ and Metamorph.

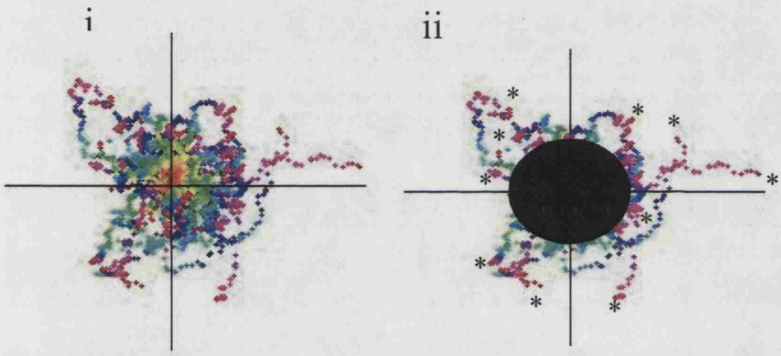

Figure 2.1: Illustration of the event horizon.
(i) A scatter plot of migrating BMM. (ii) The scatter plot with a 100 μm event horizon added, to show the number of cells whose path of migration is more than 100 μm away from their original location. The end of the track of each cell is indicated in purple and by *.

2.6.5 Calculation of turning during migration

To provide an indication of the amount that BMM turn during random migration, a quotient was calculated. This correlates the total distance a cell has moved during the time lapse film with the displacement from its origin (Fig 4.4B). The motion analysis software was used to calculate the displacement, frame to frame, in the time-lapse movie for each cell during its migration. This was then recorded in a Microsoft Excel

compatible file (.xld). A computer program for Excel was written based on the formula below to allow calculation of the turning quotient for a population of cells.

$$T.Q_n = \frac{\text{total distance a cell (n) has moved } \{(\delta x,y_{f1}) + (\delta x,y_{f2}) + ...(\delta x,y_{f3})\}^n}{\text{Displacement of a cell (n) from its origin}(x_{ff},y_{ff} - x_{f1},y_{f1})}$$

Where: n = an individual cell

$x_f y_f$ = Coordinates of cell for a particular frame

x_{ff},y_{ff} = final coordinates of cell

$$T.Q_{pop} = \frac{\Sigma\, T.Q.n_{f1}+n_{f2}..n_{ff.}}{n_{pop}}$$

Students t-tests were used to compare the speeds of migration between different populations of BMM. Statistical significance was accepted for $p<0.05$.

2.6.6 Immunofluorescent staining of cells

24 h prior to fixation 2 x 10^4 BMM were seeded onto 13 mm diameter glass coverslips. For visualisation of F-actin, paxillin and Pyk2, BMM were fixed in 3.7% formaldehyde in PBS for 20 min. For visualisation of β-tubulin, cells were fixed in 3.7% formaldehyde in PBS containing 3% sucrose. Cells were permeabilised in 0.5% Triton X-100 in PBS for 5 min. Prior to staining BMM were blocked with 20% goat serum in PBS for 30 min at room temperature. This was done to inhibit the Fc receptors expressed on the surface of macrophages promiscuously binding to the primary antibodies. Paxillin was visualised with mouse anti-paxillin antibody, paxillin phosphorylated on tyrosine 118 (pY118 paxillin) with rabbit anti-phosphoY118 paxillin antibody, β-tubulin with mouse anti-tubulin antibody, and Pyk2 was visualised using mouse anti-Pyk2. Cells were incubated with primary antibodies in a humidified chamber for 1 h. BMM were then washed thoroughly and incubated with FITC-labeled anti-mouse antibody and Cy5-labelled anti-rabbit antibody. F-actin was visualised using rhodamine-conjugated phalloidin.

2.6.7 Confocal microscopy

Images were generated with a Zeiss LSM510 confocal laser-scanning microscope, using an oil immersion 40x / 1.30 N.A. plan neofluar objective and the accompanying Zeiss software. Table 1 describes the settings of the confocal for each fluorophore used. Interchannel crosstalk was insignificant as previously determined by Dr Alan Entwistle (Wojciak-Stothard et al. 1998).

Flurophore	Laser used	Excitation λ (nm)	Emission λ (nm)	Filter used (nm)
FITC	Argon	488	520	Band Pass 505-550
TRITC/ Rhodamine	Helium/Neon	543	570 / 590	Long Pass 560
Cy5	Helium/Neon	650	670	Long Pass 680

Table 2.4: Configuration of confocal microscope filters

Image files were collected as a matrix of 1024x1024 pixels that described the average of 8 frames scanned at 0.062Hz; these files were then exported into 16 bit .tif files, which were used for image analysis.

2.6.8 Analysis of podosome localization and distribution

40 h before analysis of podosomes, 2 x 10^4 BMM were seeded onto 13 mm diameter glass coverslips in four-well multi-dishes (Nunc). A podosome was defined as a punctate focus of F-actin and paxillin. For quantitative analysis of podosomes the cells were visualised using an oil immersion 63x / 1.40 NA plan apochromat objective. Values represent the mean +/- S.E.M of at least 3 experiments. ANOVA and Students t-tests were used to compare different populations. Statistical significance was accepted for $p<0.05$.

2.6.9 Quantification of cell adhesive area and elongation ratio

For analysis of cell adhesive area and elongation ratio cells were seeded on 13 mm coverslips at a density of $2x10^4$ cells/ml and incubated overnight. Cells were then treated as indicated on the figure legend. In general BMM were incubated in: starve medium for 18 h, with growth medium supplemented with 5μM Y27632 for 30 min, with growth medium supplemented with 5μg/ml tat-C3-transferase for 4 h. BMM were fixed

in 3.7% formaldehyde and stained for F-actin using rhodamine-conjugated phalloidin. To analyse to adhesive area and elongation of BMM, digital images were acquired by confocal microscopy (section 2.6.8). Images were converted into 8 bit .tif files and preprocessed using Adobe photoshop 6.0 and ImageJ. Images were then quantitated using Metamorph 3.1. Briefly, images were passed through a medium filter using a 3x3 kernal to remove interference from background light. The image was then converted into a binary thresholded image in which all pixels above a certain grey-scale value (determined by the user) are considered to be of interest and assigned a value of 1. All other pixels are considered to be background and assigned a value of 0. Thus all pixels assigned a value of 1 should correspond to pixels within the basal spread area of a cell. The Metamorph program then measured the area of the cell, the longest chord through this area and the widest point perpendicular to this point (Fig. 2.2) using the integrated morphometry analysis add-in. Occasionally background pixels were present in the analysis image. To compensate for this an event horizon was placed in the morphometric analysis program to ignore coagulates of less than 250 pixels (corresponding to 5 μm^2). The numerical data from analysis of cell area, length and breadth was exported from Metamorph to Microsoft Excel. The elongation of the cell was calculated by dividing the length of the longest chord of each cell by its breadth at the widest point. The value of this was designated as Aspect (Fig 4.10b). Statistical analysis of spread area and elongation was calculated using Microsoft excel, ANOVA and Students *t*-test were used to compare differences between groups. Statistical significance was accepted for $p<0.05$. Data is presented as means ± s.e.m.

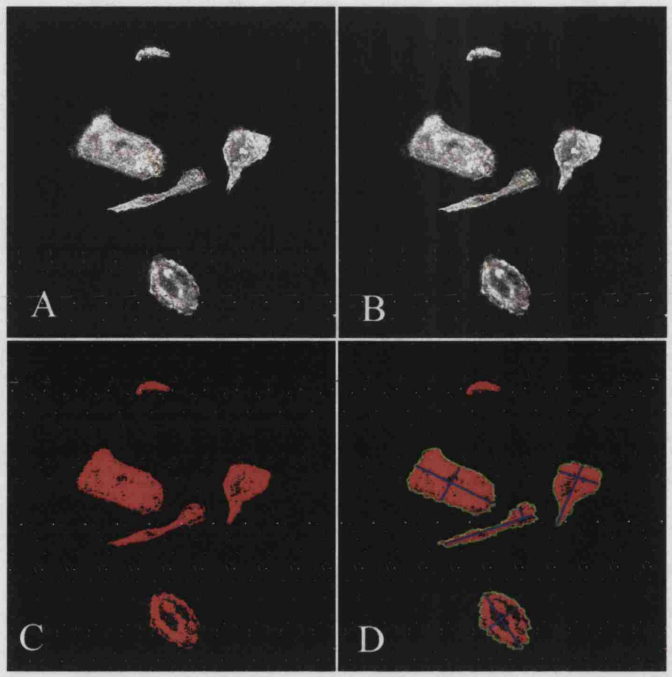

Figure 2.2: Quantification of cell adhesive area and elongation ratio

(A) Confocal image of growing BMM stained for F-actin stored as an 8-bit .tif file.

(B) Image (A) put through a Median filter with a 3x3 kernal.

(C) Binary thresholded image of (B)

(D) Shows the area measured by the integrated morphometry analysis in Metamorph. The spread area measured is indicated in red, the longest chord through the cell and the widest distance perpendicular to that is indicated in blue

2.6.10 Quantification of ruffling

40 h before analysis of ruffles, 2 x 10^4 BMM were seeded on 13 mm diameter glass coverslips. Cells were then treated as described in the figure legends (incubated in starve medium and restimulated with 33ng/ml recombinant CSF-1 for the time period indicated). A ruffle was defined as an F-actin-rich undulating membrane protrusion on the dorsal surface of a cell using fluorescence microscopy. BMM were scored as ruffling if one or more dorsal ruffle was present. For quantitative analysis of ruffles the F-actin on the apical surface of BMM was analysed. Values represent the mean +/- S.E.M of 3 experiments. ANOVA and Students t-test was used to compare different populations. Statistical significance was accepted for $p<0.05$.

2.6.11 Quantification of tail length

BMM were seeded onto fibronectin-coated tissue culture plastic and incubated overnight as described above. Cells were then treated as described in the figure legends (in starve medium or medium enriched in Y27632 or Tat-C3). To analyse tail lengths, stills from the first frame of time-lapse movies was used. Tail length was calculated as the distance in μm from the nucleus of the cell to the edge of the trailing end of a cell. Tail length was measured using ImageJ software and exported into a Microsoft Excel workbook. Values represent the mean +/- S.E.M of 3 experiments. Students t-test was used to compare different populations. Statistical significance was accepted for $p<0.05$

2.6.12 Adhesion and proliferation assay

The colourimetric assay for cell proliferation and adhesion is based on the ability of a mitochondrial dehydrogenase enzyme from viable cells to cleave the tetrazolium rings of the pale yellow 3,4,5-dimethylthiazol-2,5-diphenyltetrazolium bromide (MTT) and form dark blue formazan crystals that are not membrane permeable, this results in the accumulation of formazan salts inside metabolically active cells (Mosmann, 1983). Solubilisation of the cells by the addition of a detergent, such as SDS, results in the liberation of the crystals. The number of live cells is directly proportional to the level of the formazan product created. The colour is then quantified using absorbance at 595 nm. In this study BMM growing on 50 mm bacteriological plastic dishes were washed once and passaged with Versene (Section 2.2.4). BMM were collected by centrifugation at 1000g for 5 min. Cells were then seeded at $5x10^4$ cells/ml onto either 33 mm diameter plastic dishes precoated with 10 μg/ml fibronectin for 15 min or onto 13 mm diameter glass coverslips some of which were precoated with 10 μg/ml ICAM-1 overnight. Cells were then incubated in a humidified atmosphere at 37°C and 10% CO_2 for the time periods indicated: for proliferation assays 18, 24, 48 and 72 h, for adhesion assays 5, 15, 30 and 60 min. Cells were then washed twice in PBS and incubated in growth medium supplemented with 50μg/ml MTT for 3 h. 0.5 volumes of 10% SDS was added for lysis and cells were incubated for a further 1 h. The absorbance of the cell lysate was then measured at 595 nm and compared to a blank, which contained growth medium, MTT and 0.5 volumes of SDS alone.

2.7 Flow cytometry.

2.7.1 Materials

Buffers and solutions

FACS buffer	5% endotoxin free BSA (v/v) PBS

Software

Programme	Manufacturer	Address
FACsDiva	Becton Dickenson	http://www.bd.com/
CellQuest	Becton Dickenson	http://www.bd.com/

Antibodies used for flow cytometry

FACS				
Antibody	Reactivity	Dilution	Source	
FITC β1 Integrin	Rat	1:100	BD Pharmingen	http://www.bdbiosciences.com/pharmingen/
PE β2 Integrin	Mouse	1:100	BD Pharmingen	http://www.bdbiosciences.com/pharmingen/
β3 Integrin	Hamster	1:100	Serotec	http://www.serotec.co.uk/
cFMS	Rat	1:100	Santa Cruz Biotechnology	http://www.scbt.com/
FITC-F4/80	Rat	1:100	Serotec	http://www.serotec.co.uk/
FITC anti Mouse	Rabbit	1:100	Jackson Immuno research	www.jacksonimmuno.com/

Table 2.3: Conditions of antibody use for flow cytometry

2.7.2 Protocol used for flow cytometry

BMM were grown to confluence and passaged in Versene (Section 2.2.4). Cells were collected by centrifugation at 1000g for 5 min, resuspended into FACS buffer (PBS containing 0.5% endotoxin free BSA) and aliquoted into 1.5 ml microfuge tubes at a concentration of $5x10^5$ cells/ml. Cells were then stained with 1 μg/ml antibody for 30 min prior on ice and washed twice in FACS buffer. Most antibodies used for flow cytometry were conjugated to a fluorophore. However if this was not the case the cells were then incubated for 30 min with a secondary antibody conjugated to a fluorophore. BMM were then fixed in 4% paraformaldehyde for 10 min and cell surface fluorescence

was measured using a flow cytometer (Becton Dickenson FACScanto) and analysed using either Cell Quest software or FACSDiva software

2.8 Total internal reflection fluorescent microscopy

2.8.1 Materials: As described in 2.6

This method was developed in collaboration with B. Dubin-Thaler and M. Sheetz and is adapted for BMM from their method published in the Biophysical Journal (Dubin-Thaler et al. 2004). All experiments using this technique were carried out in the laboratory of Prof M. Sheetz at the University of Columbia N.Y. USA, using technology developed there.

2.8.2 Coverslip preparation

22 mm^2 glass coverslips were acid-washed and treated with hexamethyl disilazane, creating a highly hydrophobic surface that prevents nonspecific receptor activation and adhesion (Altankov and Groth, 1996). Coverslips were then incubated with 10 µg/ml fibronectin for 1 h at 37°C.

2.8.3 Staining of the cell membrane of BMM.

BMM were passaged in Versene and collected by centrifugation for 5 min at 1000g. Cells were then resuspended in spreading medium with 1µg/ml of the cell membrane dye CSFE and incubated for 15 min at 37°C. Cells were washed once in spreading medium without CFSE, centrifuged and resuspended at $5x10^4$ cells/ml in spreading medium and seeded onto the fibronectin-coated coverslips.

2.8.4 TIRF Microscopy

A custom-designed prism-based TIRF microscope was built by members of M.Sheetz laboratory, using an upright Olympus microscope. The standard stage was replaced with a sample holder situated above a Dove prism. A 488 nm laser line was generated from a Melles Griot (Carlsbad, CA) argon-ion laser and was guided through telescoping lenses and then into the beveled side of the prism. The angle of incidence and diameter of the beam was controlled by altering the position of mirrors guiding the laser beam. A rotating difuser was placed in the beam path to blur out laser interference patterns.

Adjusting the angle that the beam made with the top surface of the prism to be less than the critical angle of incidence resulted in the laser rising through the prism, totally reflecting at its top surface, and creating an evanescent wave that penetrated upwards out of the top surface for approximately 100 nm (Fig. 5.5). ECM-coated cover glass was placed on a motorized sample holder so that the cover glass was suspended above the prism. Coupling the prism to the cover glass using standard immersion oil resulted in a refractive interface between the top of the borosilicate cover glass and the aqueous sample (situated on top of the cover glass), causing the reflection of the laser beam to occur at the surface upon which the cells spread and exposing the cells to the evanescent wave (Fig. 5.5).

An Olympus 25x/ 0.95-NA water immersion objective was then lowered into the aqueous sample. The field of view through this objective was 400 μm across, and the diameter of the laser beam (and resulting evanescent wave) was adjusted to these dimensions by adjusting the magnification of the laser telescope. Temperature control of the sample was achieved by constructing a plexiglas box around the sample holder and stage, which was heated remotely by a hairdryer. Major sources of vibration, such as the heater, were mechanically isolated from the vibration isolation air table upon which the microscope sat to reduce sample movement during measurement. The objective was heated to 37°C by attaching a thermocouple to it.

2.8.5 Protocol for analysis of cell spreading

Fluorescently labeled cells suspended in spreading medium were added to the cover glass on the TIRF microscope and allowed to sediment onto the coated surface. A Roper Scientific cooled charge-coupled device (CCD) camera captured 12-bit digital 1300 x 1030-pixel grayscale images from the TIRF-illuminated cells every 5 s for 10 min. These images were stored to a computer hard disk drive running custom image capture software operating as a plug-in from within the open-source ImageJ software package. Exposure time for each image was typically 250 ms and the TIRF laser was shuttered with a Uniblitz (Rochester, NY) shutter between exposures to reduce photo-damage and photobleaching effects.

2.8.6 Image analysis

Cells were chosen for analysis if they initiated and completed spreading during the observation period of 10 min after plating. These cells were cropped from the full-size images and a medium n filter with a radius of 1 pixel was applied frame-by-frame to the images to reduce noise without altering the position of the cell edge (Section 2.6.9). A modified open source Java image segmenter (Dubin-Thaler et al. 2004), was used to process individual fluorescent TIRF images of a spreading cell. This resulted in the generation of a program which could differentiate the edge of the cell from the background. The program placed a binary threshold on the cell and assigning grey-scale values above a certain limit as cell and those below the limit as background (Cell Outliner program used in ImageJ). Running this program allowed the TIRF movie to be converted into a binary movie that showed only the outline of the edge of the cell membrane during spreading (Fig. 5.6).

2.8.7 Polar coordinate representation of cell edge

The cell outline was processed via two custom C programs that calculated the distance from the centroid of the outline to the outline edge along rays pointing outwards at evenly spaced angles using a cubic spine interpolation package (Dubin-Thaler et al. 2004). 360 such rays were sampled for each outline, and this process was repeated for each frame in the time-lapse sequence, using the centroid of the first outline in the sequence as the origin of the polar coordinate system to maintain a fixed reference frame throughout time. Further visualization and analyses were carried out using Mathematica software.

2.8.8 Measure of spreading versus attachment

Cells plated for the spreading assay were generally surveyed 60 min after plating. The CFSE-loaded cells in bright-field and TIRF images captured at this time point were identified as either spread or not spread. Cells exhibiting a TIRF footprint >200 μm^2 were considered to be spread (section 2.6.9). The number of spread cells was then compared to the total number of cells that appear in the bright-field images (Fig 5.5).

Chapter 3. The macrophage as a model for study of Rho GTPases

3.1 Introduction

In this study a detailed analysis of Rho GTPase expression in bone marrow derived macrophages (BMM) was carried out. The cytoskeleton of BMM was characterised and compared with that of fibroblasts. Previous studies have shown that the morphology and motility of fibroblasts is highly dependent on the Rho family of GTPases (Ridley, 2001a). Analysis of embryonic fibroblasts derived from the RhoB-null mice shows that they have defects in spreading, adhesion and migration but their peripheral actin structures are unaffected (Liu et al. 2001; Sandilands et al. 2004). Macrophages have some unique cytoskeletal features and function which fibroblasts do not share (Ridley, 2001c). For example cells of the myeloid lineage, including monocytes, macrophages and dendritic cells, form punctuate adhesive foci called podosomes. Podosomes are actin-based structures between 0.2 and 1 μm in diameter and 0.5 μm depth located on the basal plane of cells. Podosomes in BMM are shown here to have a similar organisation of proteins to podosomes described in other myeloid cells (Linder and Aepfelbacher, 2003). Recent studies of podosome dynamics show that podosomes, like focal adhesions, are transient structures, that do not translocate with the cell body (Evans et al. 2003; Small and Kaverina, 2003). Studies in osteoclasts and dendritic cells suggest that there may be a relationship between polarisation and podosome formation (Calle et al. 2004; Saltel et al. 2004). Here the relationship between polarisation of BMM and podosomes is investigated in depth.

In order to characterise the roles of RhoA and RhoB in podosome formation, RhoB-null macrophages were generated and the Rho inhibitor C3-transferase was used. RhoB-null macrophages were characterised and shown to express the cell surface markers which are consistent with fully differentiated macrophages. Deletion of *RhoB* did not affect podosome formation. Treatment of BMM with C3-transferase caused a decrease in the number of podosomes present in BMM suggesting that RhoA is required for maintenance of podosomes and RhoB is not involved in the regulation of podosome dynamics.

3.2 Generation of macrophages

The purification of bone marrow macrophages is described in detail in chapter 2.2. Briefly, 4 to10 week-old mice were culled and the hind limbs were excised. Fibulae were dissected out and the bone marrow flushed out which yields a variety of cells. The fully differentiated myeloid cells in the bone marrow express β2 integrin and will adhere to bacterial plastic. Haematopoetic precursor cells can be primed to become macrophages by incubation with a source of CSF-1 (Paulnock, 2000). Bone marrow cells undergo a marked population shift when cultured in the presence of L-cell conditioned media (which is enriched in CSF-1). After 2 to 3 days erythrocytes and lymphocytes disappear (Gordon, 1995). Macrophages express specific markers and the level of expression of these markers varies through the differentiation process. F4/80, a cell surface marker of unknown function, is expressed only by macrophages and is expressed early on in the differentiation process (Gordon, 1992). Fully differentiated macrophages are strongly adherent, highly phagocytic and express cell-surface F4/80, Mac-1 (αMβ2 integrin, which allows BMM to adhere to bacterial plastic) and c-FMS, the CSF-1 receptor (Fig. 3.1A). Both Wt and *RhoB*$^{-/-}$ BMM were analysed for expression of F4/80, β2 integrin and c-Fms (Fig. 3.1B, Fig. 5.3B and Fig. 6.5A). All of these markers of macrophage differentiation were expressed by Wt and *RhoB*$^{-/-}$ BMM, indicating that the cells used in this study are fully differentiated BMM.

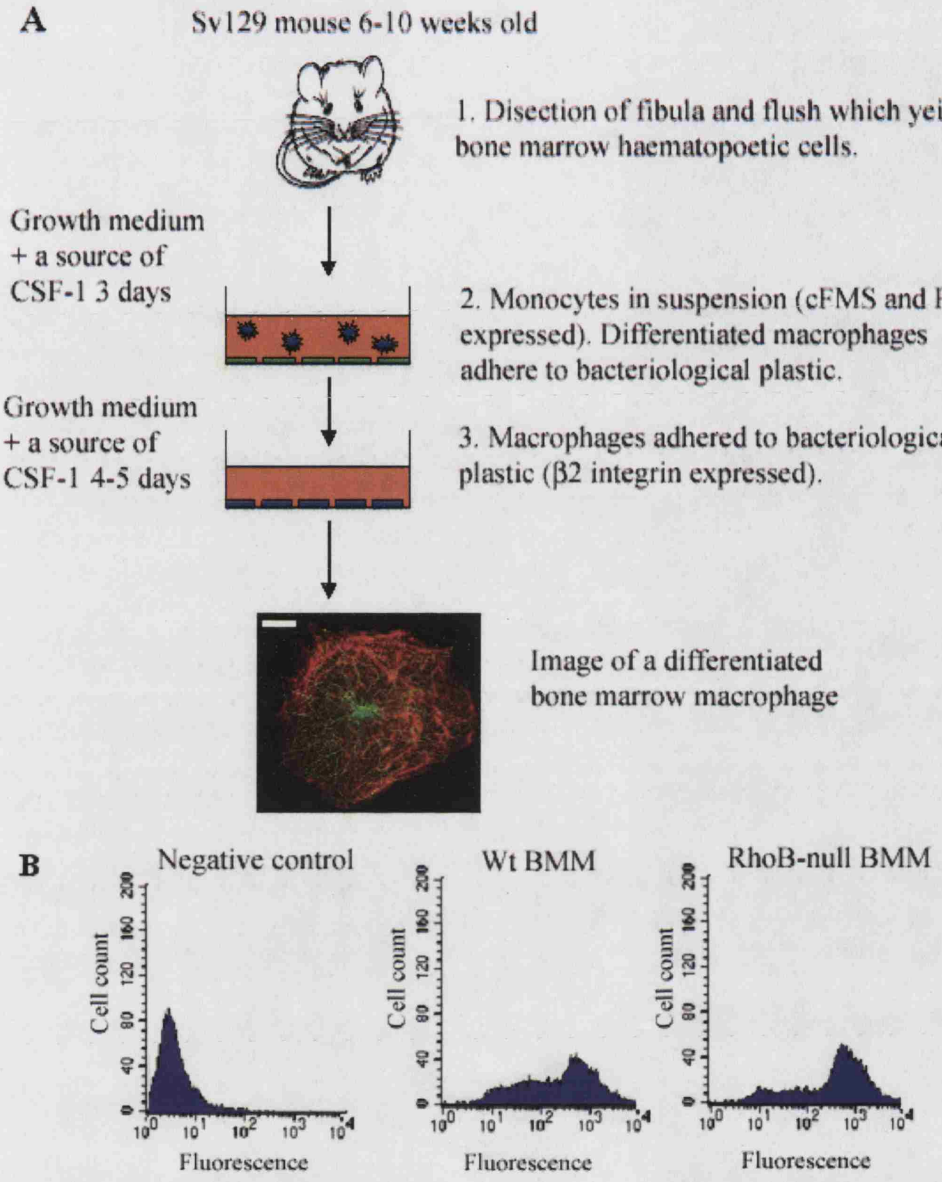

Figure 3.1: The generation of bone marrow-derived macrophages:

(A) Schematic diagram showing the differentiation of bone marrow-derived macrophages (BMM) and noting the cell surface markers expressed at different stages of maturation. (B) Flow cytometry analysis showing expression of F4/80 on BMM derived from Wt and RhoB-null mice.

3.3 The expression of Rho GTPases in BMM

Western blotting was used to determine the expression of Cdc42 and different isoforms of Rho and Rac in macrophages (Fig. 3.2A). It has been previously shown that BMM express Rac1 and Rac2 but not Rac3 (Wells et al. 2004). Rac1 and Rac2 were expressed in both Wt (Fig. 3.2A) and *RhoB*$^{-/-}$ BMM (data not shown). It was not clear from the western blot whether RhoC was expressed in BMM or not as the antibody gave several non-specific bands near to 21kDa, the molecular weight that corresponds to RhoC (Fig. 3.2A). To clarify this RT-PCR analysis was used to analyse the presence of *RhoA, RhoB* and *RhoC* mRNA in an asynchronous growing population of both Wt (Fig. 3.2B) and *RhoB*$^{-/-}$ BMM. *RhoA* mRNA was present in both Wt and *RhoB*$^{-/-}$ BMM, *RhoB* mRNA was present in Wt BMM but not *RhoB*$^{-/-}$ BMM (Fig. 3.3 B). The RhoC mRNA was not detectably present in Wt or *RhoB*$^{-/-}$ BMM. This showed that BMM only expressed RhoA and RhoB. Deletion of *RhoB* does not cause an in increase in RhoA mRNA or promote expression of RhoC mRNA. Deletion of *RhoB* also did not affect the expression of RhoA, Rac1 or Cdc42 although it could alter the activity of these proteins (Fig. 6.1B, C and D).

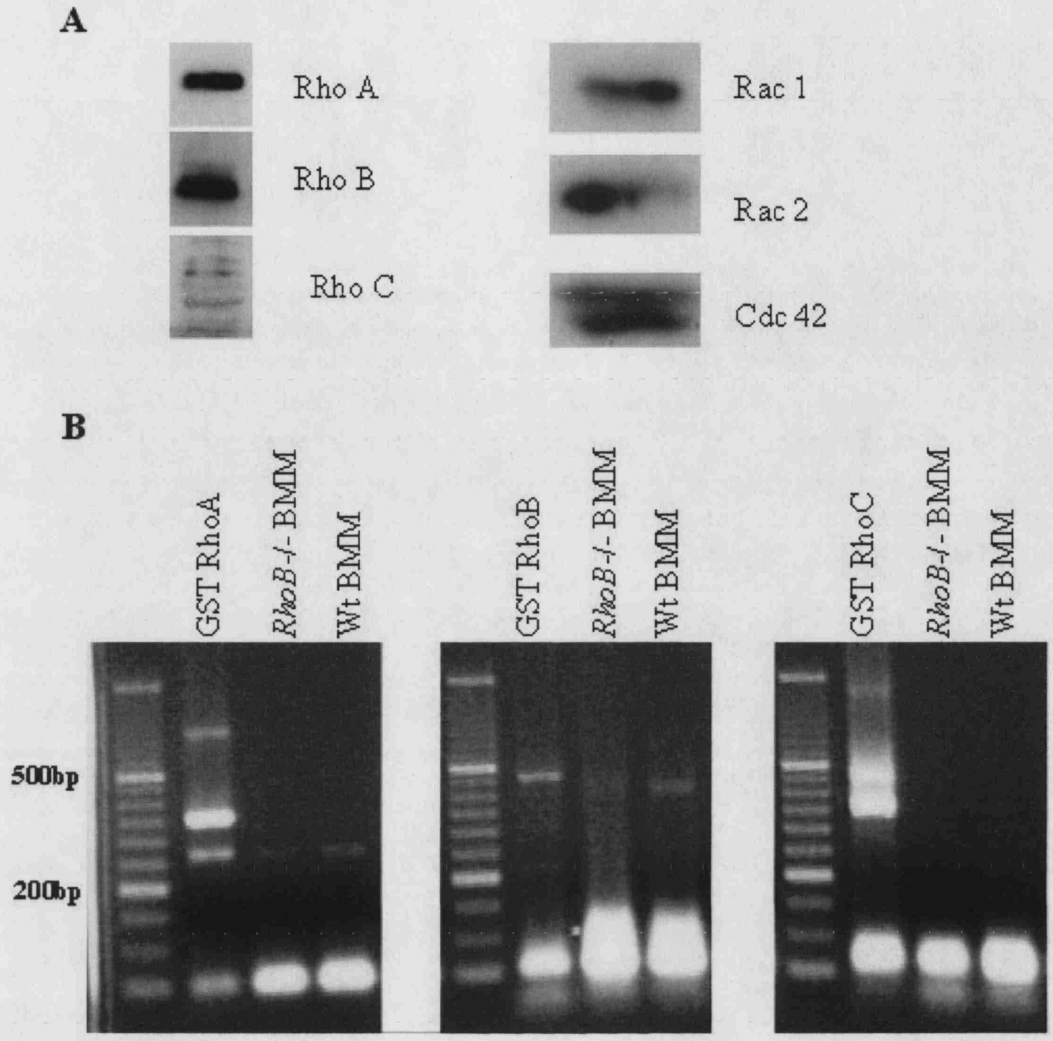

Figure 3.2: The expression of Rho GTPases in BMM

(A) Western blots of whole cell lysate of Wt BMM showing expression of RhoA, RhoB, RhoC Rac1, Rac2 and Cdc42. (B) RT-PCR analysis of *RhoA, RhoB* and *RhoC* transcription in Wt and *RhoB*$^{-/-}$ BMM. PCR products were separated on a 2% agarose gel. A 50 bp ladder is used to determine size of PCR product. Plasmids encoding GST-RhoA, GST-RhoB and GST-RhoC were included as positive controls. Expected product size: *RhoA* = 260 bp, *RhoB* = 470 bp and *RhoC* = 450 bp

3.4 The expression pattern of RhoA, RhoB and RhoC in different tissue types

Use of GeneNote expression analysis showed that RhoA, RhoB and RhoC mRNAs were expressed in many tissue types, particularly those which contain macrophages such as bone marrow, spleen, thymus, liver and lung (Genecards and Fig. 3.3A). It is interesting to note that RhoA mRNA appeared to be expressed at similar levels in all tissue types examined. The expression of RhoB and RhoC mRNA varies dependent on the tissue type examined. RhoB also appears to be generally expressed at a lower levels than RhoA and C. Interestingly in bone marrow RhoA and B were expressed at comparatively high levels but RhoC was not (Fig. 3.3A).

It was necessary to determine the specificity of the RhoA and RhoB antibodies for analysis of RhoA and RhoB protein expression in different cell types (Fig. 3.3C). These antibodies were also required to determine the activation state of RhoA and RhoB specifically in BMM under different conditions (Chapter 6). The specificity of three antibodies was tested: 2 monoclonal antibodies raised against RhoA and B and a polyclonal antibody raised against RhoB. GST-fusion proteins of RhoA, RhoB and RhoC were expressed in *E. coli* and the reaction of each antibody with them was examined. The monoclonal RhoA and B antibodies from Santa Cruz Biotechnologies slightly cross-reacted with other Rho isoforms. Whereas the polyclonal RhoB antibody from Bethyl did not cross-react with other Rho isoforms (Fig. 3.3B).

The expression of RhoA and B in several cell lines and tissues including BMM was examined (Fig. 3.3C). The hippocampus appeared to express RhoB at high levels, consistent with the implication of RhoB in long term potentiation in the hippocampus and in the nervous system (Conway et al. 2004; O'Kane et al. 2004) (Fig. 3.3A). RhoB is also expressed at high levels in cells with cell-cell junctions (such as epithelial cells and endothelial cells) (Fig 3.3C). RhoA is expressed in all cell types at similar levels. Macrophages express RhoA at a similar level to other cell types whereas the expression of RhoB was lower in macrophages compared to other cell types. Interestingly mouse T cells express RhoB at lower levels than BMM.

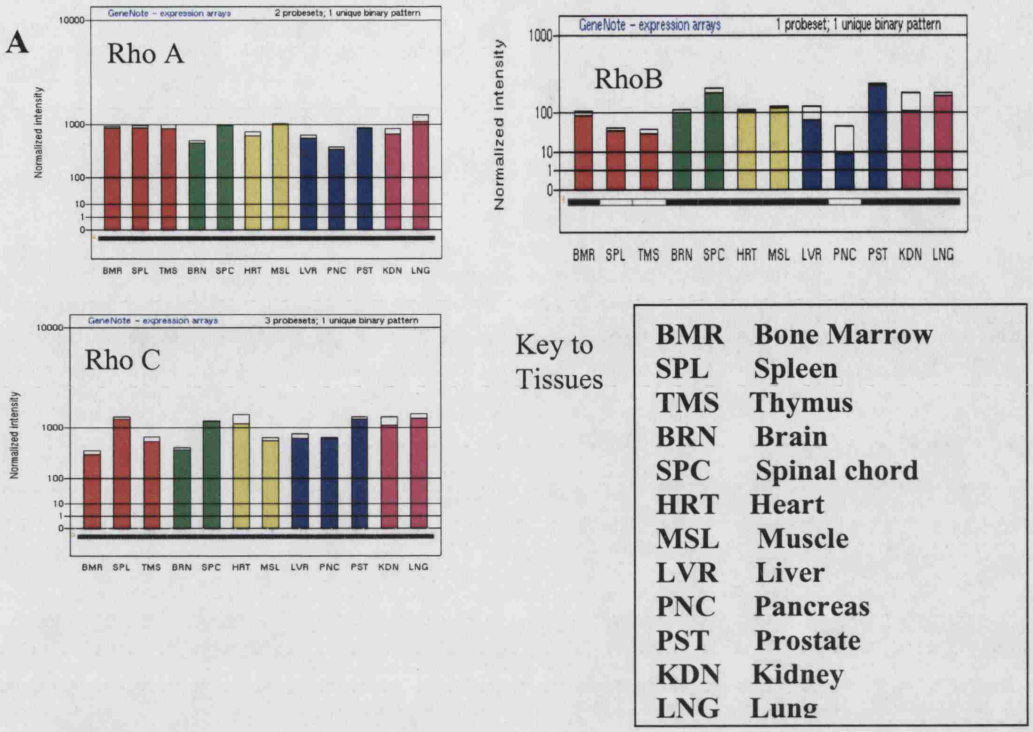

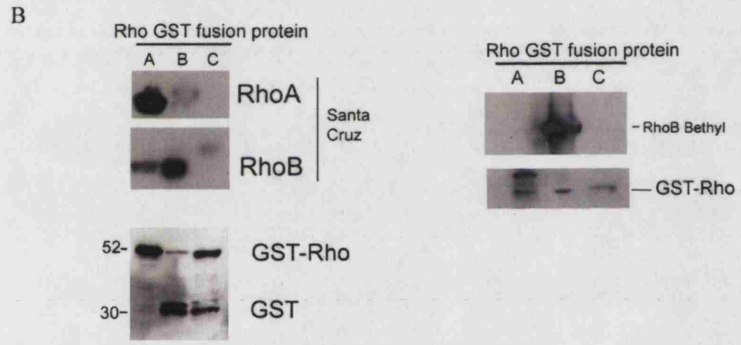

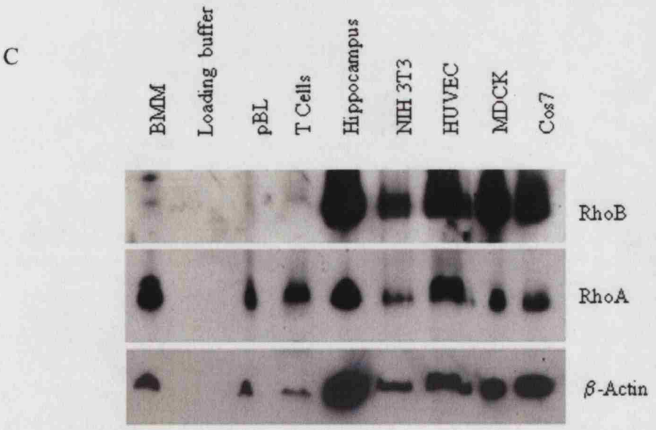

Figure 3.3: The expression of RhoA, B and C:

(A) Expression of RhoA, RhoB and RhoC in different tissue types. Data was obtained from the Genecards website, http://bioinfo.weizmann.ac.il/cards/index.shtml (Chapter 2.5) describing the hybridisation of cDNA derived from tissue homogenate to Affimetrix gene chips. (B) The activity of mouse monoclonal anti-RhoA and anti-RhoB antibodies and a rabbit polyclonal anti-RhoB antibody was tested against recombinant-GST fusion proteins of RhoA, B and C. The lower panels show recombinant GST-RhoA, GST-RhoB and GST-RhoC proteins separated on a 12% acrylamide gel. Proteins were visualised using Coomassie-Blue staining (C) Western blot analysis of expression of RhoA and RhoB in cell lysates from leukocytes, brain, fibroblasts, endothelial cells, epithelial cells and Cos-7 cells. The membrane was probed with a mouse monoclonal anti-RhoA and rabbit polyclonal anti-RhoB antibodies.

3.5 Comparison of the macrophage and fibroblast cytoskeletons

The fibroblast is widely studied in the analysis of cytoskeletal mechanics. RhoA has been shown to be important in the regulation of cell tension and adhesion turnover in fibroblasts (Hall and Nobes, 2000). The cytoskeleton of *RhoB*$^{-/-}$ fibroblasts has been briefly analysed. Although no major defects in the actin cytoskeleton were seen, *RhoB*$^{-/-}$ fibroblasts did have adhesion defects (Liu et al. 2001). This indicated that RhoA and RhoB may play different roles in regulation of cytoskeletal mechanics in fibroblasts. Confocal images of BMM and NIH3T3 fibroblasts were used to compare the cytoskeleton of fibroblasts and macrophages. Low magnification images clearly showed that the morphology of fibroblasts is very different to BMM. BMM and fibroblasts are similar in size and both BMM and NIH3T3 cells could form actin-rich structures such as lamellae (Fig. 3.4Ai). A higher magnification image showed that the actin cytoskeleton of BMM was very differently organised to that of a fibroblast (Fig. 3.4Aii). BMM lacked actin stress fibres and did not have the peripheral actin filaments that fibroblasts contain. BMM contained structures, such as dorsal ruffles and punctate F-actin structures, which were seen less frequently in fibroblasts (Fig. 3.4A, B). The microtubule cytoskeletons appeared similarly organised in fibroblasts and BMM, in as much as the microtubules were concentrated in the centre of the cell and radiated out to the periphery (with fewer microtubules being seen in the periphery of both cell types). Both BMM and fibroblasts contained a MTOC-like structure close to the nucleus (Fig. 3.5B), although staining with γ-tubulin would be required to confirm this. Antibodies to tyrosine phosphorylated-paxillin (pY-118 paxillin), a component of several types of cellular adhesions (Small and Kaverina. 2003), were used to analyse adhesion structures in BMM and NIH3T3 fibroblasts. The pY-118 paxillin staining in NIH3T3 cells was not evenly distributed. At the periphery of the fibroblasts, particularly in corners, larger tick like structures are present, these may correspond to focal adhesions (Small and Kaverina. 2003). Around the centre of the cell pY-118 paxillin enriched puncta were visible, which may correspond to focal contacts or vesicles. BMM organised their adhesions, as indicated by pY-118 paxillin staining, very differently to NIH3T3 cells. BMM contained tiny focal contacts, these were evenly distributed throughout the basal layer of the cell and also located at the very periphery of the cell membrane (Allen et al. 1997; Williams and Ridley, 2000) (Fig 3.4B). Circular foci containing F-actin and pY118-paxillin were present in the lamellae of some BMM (Indicated on Fig. 3.4B by

arrows), these structures, which correspond to podosomes (Linder and Aepfelbacher, 2003), were absent from NIH3T3 cells.

Figure 3.4: A comparison of the cytoskeleton of fibroblasts and BMM

(Ai) Low power images of the actin cytoskeleton of BMM and NIH3T3 fibroblasts in growth medium. Rhodamine phalloidin was used to visualise the acin cytoskeleton. (Bi) Cross sections of the basal plane of Wt BMM and a NIH3T3 fibroblast show the actin and microtubule cytoskeletons and adhesions. BMM and NIH3T3 cells were formaldehyde fixed and stained with rhodamine phalloidin to visualise the actin cytoskeleton, β-tubulin antibodies to visualise the microtubule cytoskeleton and pY118-paxillin antibodies to visualise adhesions. Red arrows indicate podosomes in BMM. (Bii) Merged image of (Bi) showing the interaction between the actin and microtubule cytoskeletons and cell adhesions. F-actin is shown in red, microtubules are shown in green and pY118-paxillin in blue. In all images bar = 10 μm.

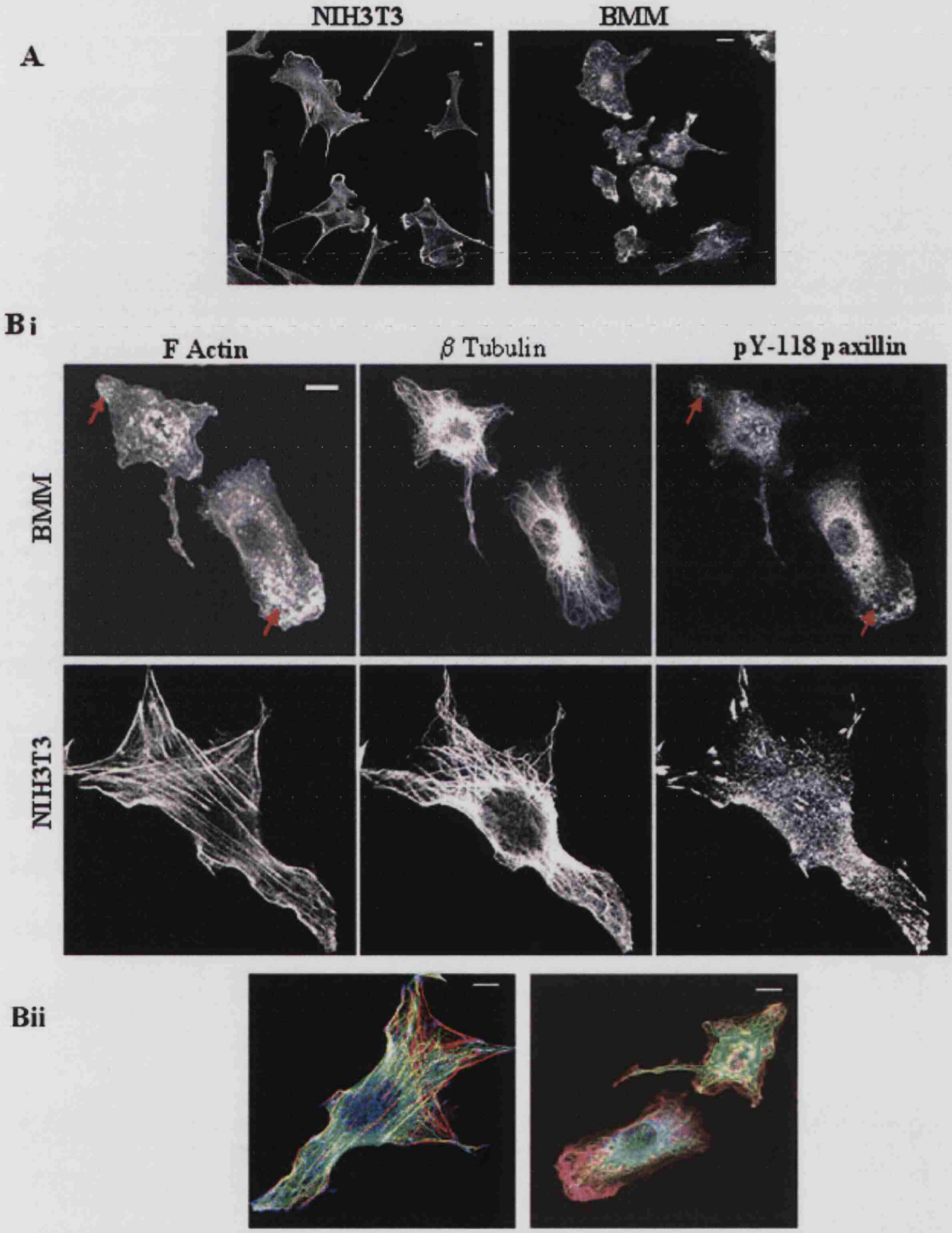
A
NIH3T3
BMM
Bi
F Actin
β Tubulin
pY-118 paxillin
BMM
NIH3T3
Bii

3.6 Characterisation of podosomes in BMM

Previous work in human macrophages, osteoclasts, dendritic cells and Src-transformed fibroblasts has shown that podosomes are F-actin-rich puncta containing integrins and integrin-associated proteins, tyrosine kinases, and proteins associated with the regulation of the actin cytoskeleton (Burns et al. 2001; Linder and Aepfelbacher, 2003; Pfaff and Jurdic, 2001). BMM were found to have podosomes with a similar structure to those identified in other myeloid cell types.

3.6.1 The structure of podosomes in BMM

For the purposes of this analysis, a podosome was defined as a small punctate focus of F-actin and paxillin juxtaposed to the substratum between 0.2 and 1 μm in diameter (Fig. 3.5 A). Higher magnification showed that podosomes consist of a core of F-actin surrounded by a peripheral paxillin ring. Tyrosine phosphorylated paxillin (pY118 paxillin) was present in podosomes (Fig. 3.5B). The tyrosine kinase Pyk2 co-localized with F-actin and pY118 paxillin in podosomes and also in membrane ruffles at the periphery of BMM (Fig. 3.5C). Paxillin and Pyk2 have been shown to localise with F-actin foci in podosomes of other myeloid cells (Duong et al. 1998; Linder and Aepfelbacher, 2003). Microtubules have been shown to be required for podosome assembly in macrophages and osteoclasts (Destaing et al. 2003; Linder et al. 2000). Microtubules were found to be present in peripheral areas of the cell that contain in podosomes (Fig. 3.5D). High magnification images show that microtubules are found in close proximity to podosomes but it is not clear whether they directly contact or are involved in podosomes formation from the confocal images (Fig. 3.5E). These results confirmed that the structures observed in BMMs are similar to podosomes in other cell types.

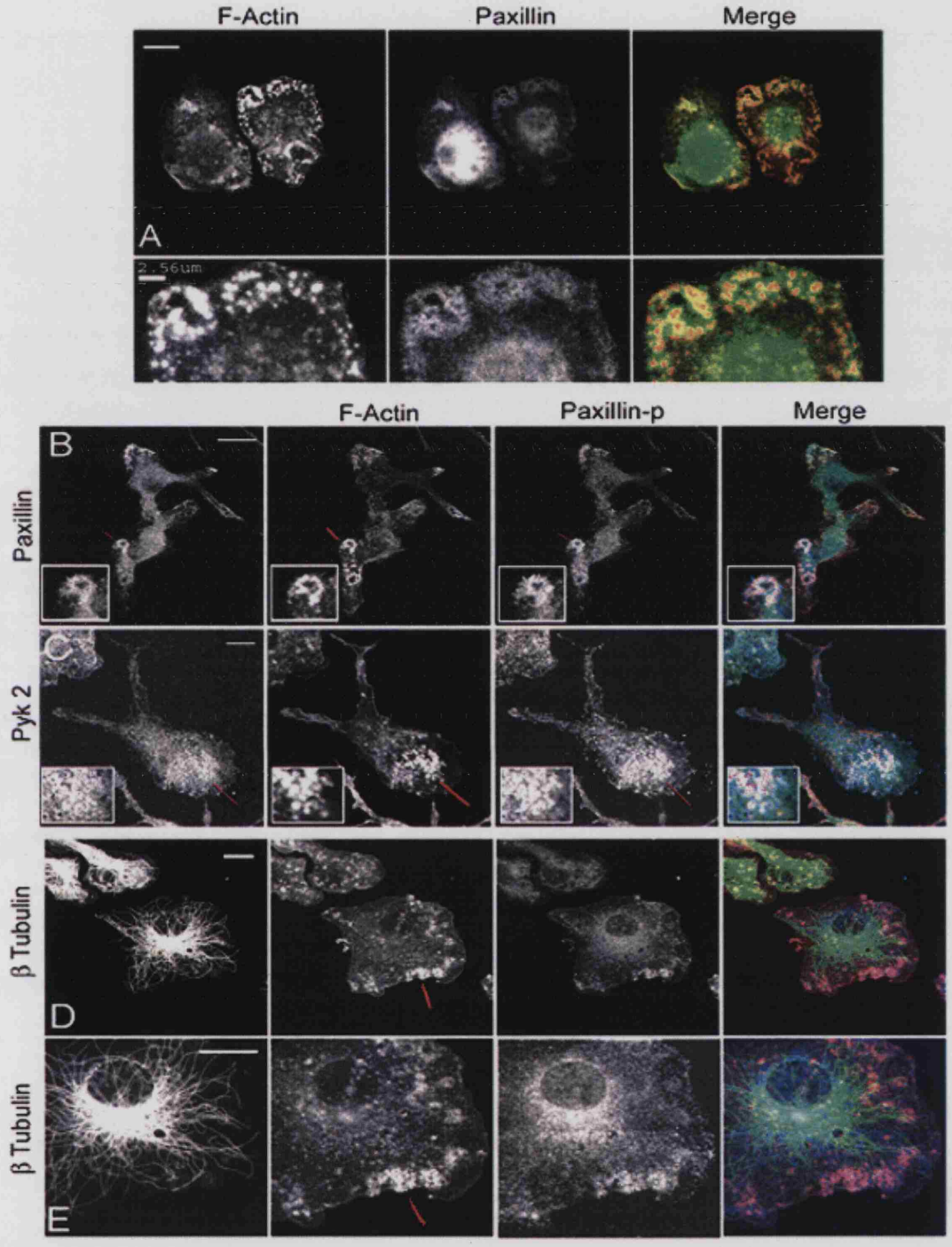
F-Actin
Paxillin
Merge
A
2.56um
F-Actin
Paxillin-p
Merge
Paxillin
B
Pyk 2
C
β Tubulin
D
β Tubulin
E

Figure 3.5: The composition of podosomes:

(A) Confocal images of Wt BMM showing that podosomes consist of a core of F-actin surrounded by a peripheral cloud of paxillin. In the merged image F-actin visualised using rhodamine phalloidin is shown in red and paxillin, visualised by anti paxillin antibodies is shown in green. (B) BMM were fixed and stained for: F-actin, paxillin and pY118 paxillin, (C) and Pyk 2. Enlarged images of podosomes are shown in bottom left corners. (D + E) BMM were formaldehyde fixed and stained with rhodamine phalloidin and β-tubulin and pY118 paxillin antibodies to show F-actin, microtubules and paxillin. Arrows indicate arrays of podosomes. In all parts of the figure the merged images show F-actin in red, pY118 paxillin in blue and paxillin, β-tubulin and Pyk2 are shown in green. Red lines indicate arrays of podosomes, bar = 10 μm unless otherwise indicated.

3.6.2 Podosomes are predominantly found in polarised BMM

The distribution of podosomes within an asynchronous population of BMM in growth medium was quantitated to find out if there was a connection between cell morphology and podosome number. A polarised cell was defined as one having a migratory morphology (Ridley et al. 2003). The anterior region was spread and contained the MTOC, lamellipodia and other protrusions; the posterior region was contracted with respect to the anterior end and contained the cell's tail and retraction fibres (Fig. 3.6A). A non-polarised cell was defined as a cell with no distinguishable anterior or posterior or no lamellae or trailing edges. In a population of growing BMMs 70% of the cells were polarised (Fig 3.5.2B). Polarised cells were highly enriched in podosomes compared to non-polarised cells. Significantly ($p<0.01$) more polarised cells contained podosomes than non-polarised cells (Fig. 3.8.2C). This may indicate that there is a link between cell polarisation and podosomes.

Figure 3.6 The relationship between cell shape and podosome distribution:

(A) BMMs were defined as polarised or non-polarised. A polarised cell is one with a migratory morphology with a lamellae at the front and the MTOC, indicated with arrows, in front of the nucleus. The actin cytoskeleton, visualised with rhodamine phalloidin is shown in red. The microtubule cytoskeleton, visualised with anti-β tubulin antibodies is shown in green (B) Graph showing the proportion of polarised and non polarised BMM containing podosomes. A BMM with one or more podosome was scored as a cell containing podosomes. (C) Graph showing the proportion of BMM containing 10 or more podosomes from the total population of BMM containing podosomes in polarised and non-polarised cells.* = a significant difference $p < 0.05$ between polarised and non-polarised cells, $n = 1200$.

A

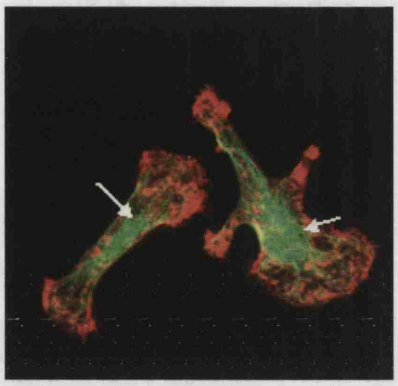

B

The relationship between polarisation of BMM and podosomes

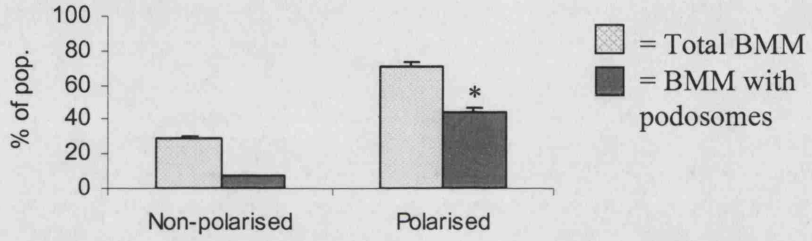

C

The relationship between polarisation of BMM with podosomes and the number of podosomes they contain.

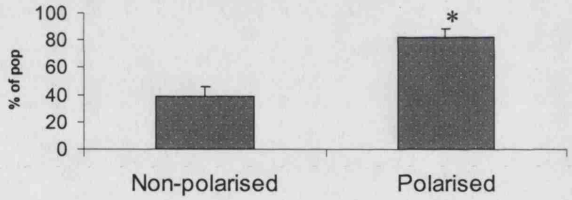

3.6.3 Relationship between podosome distribution and cell polarisation

To further investigate the relationship between podosomes and polarisation the intracellular distribution of podosomes was analysed. Cells with arrays of podosomes were assigned to one of four classification groups based on the organisation and localisation of the podosomes. These groups were as follows: circular arrays of podosomes, diffusely distributed podosomes, localised areas of podosomes in non-polarised cells and podosomes in protrusive regions of polarised cells (Fig. 3.7A-D). Cells defined as polarised and non-polarised were included in the analysis. When a cell was found to have two types of arrays of podosomes (Fig. 3.7B) the formation with most podosomes was scored. The BMM shown in Fig 3.7B would be scored as containing podosomes circular arrays as most podosomes in that cell are found in the circular arrays.

Both polarised and non-polarised cells primarily had organised arrays of podosomes (Fig. 3.6A and C). Only 2% of BMMs had podosomes that are diffusely distributed on the ventral membrane, and this arrangement of podosome is mainly confined to non-polarised cells (data not shown). This indicates that cells normally generate podosomes in defined locations (Fig. 3.6E). Circular arrays of podosomes were found in 9% of BMMs and contained on average 10 to 30 podosomes. Circular arrays could be localised anywhere on the ventral membrane of BMM except under the nucleus (Fig. 3.5B). In polarised cells, 75% of podosome arrays were in the main leading lamella (Fig. 3.7C and E) or in multiple protrusions (Fig. 3.7A). Podosomes were generally spread along the whole length of the lamella just behind but not in the lamellipodium. From this analysis it is clear that podosome localisation is usually highly organised in BMM. Their enrichment in polarised cells and close proximity to areas of active membrane extension is consistent with them playing a role in cell migration.

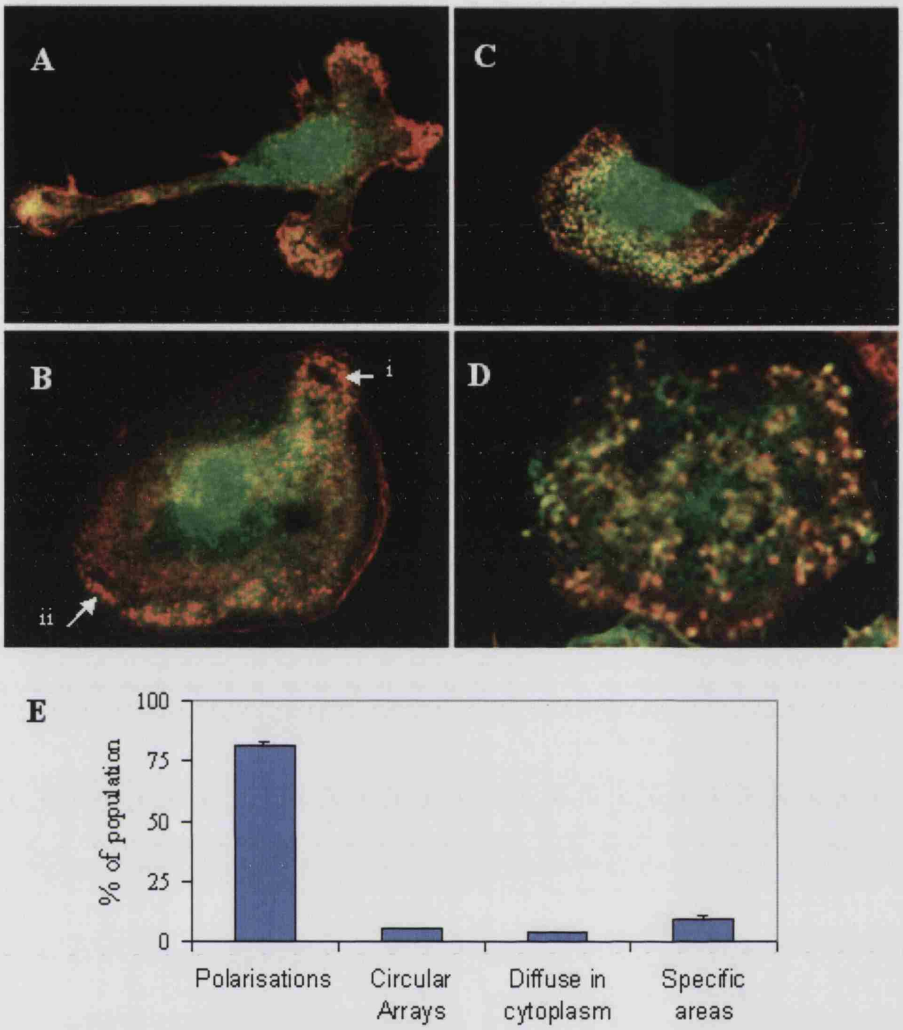

Figure 3.7 The intracellular distribution of podosomes:

(A) Arrays of podosomes within the cell was classified into 4 groups: (A) in multiple protrusions, (B i) in circular arrays, (B ii) specific areas in non polarised cells, (C) in lamellae, (D) diffuse in cytoplasm. Podosomes in multiple protrusions or lamellae (A+C) are considered for quantitative analysis to be one group designated 'polarisations'. (E) Graph showing that for BMM in growth medium podosomes are mainly localised in the polarising regions. Data is pooled from five independent experiments, n =600.

3.7 CSF-1 stimulation promotes cell polarisation and podosome formation

The effect of CSF-1 on podosome number and distribution was investigated. Previous work has shown that removal of CSF-1 from macrophages caused a decrease in their spread area, a reduction in dynamic actin cytoskeletal structures including lamellipodia and membrane ruffles and a decrease in cell migration speed (Fig. 3.8D and Chapter 4.5) (Allen et al. 1998; Jones et al. 2003; Wells and Ridley, 2004). Stimulation of BMM with CSF-1 was shown to alter the percentage of BMM containing podosomes significantly using an analysis of variance statistical test (ANOVA). Withdrawal of CSF-1 reduced the number of cells containing podosomes (Fig. 3.8A). Stimulation of BMMs with CSF-1 for 5 minutes promoted extensive and rapid morphological changes in BMM but no increase in podosomes (Fig. 3.8B and D). At 30 min after CSF-1 stimulation the majority of cells had a polarised morphology, and had more than 10 podosomes (Fig. 3.8B and D). 30 minutes of CSF-1 stimulation caused a slight, but statistically significant increase in circular arrays of podosomes in the cytosol (Fig. 3.8C). By 60 min of CSF-1 stimulation the number and distribution of podosomes returned to a similar level seen in growth medium (Fig3.6A, C). The actin cytoskeleton in cells stimulated with CSF-1 for 60 min was spread and in some cells lamellae were present however, the actin cytoskeleton was not the same as that of asynchronous cells (Fig. 3.8D). From this we conclude that there is a strong correlation between the BMM polarisation and increased podosome assembly.

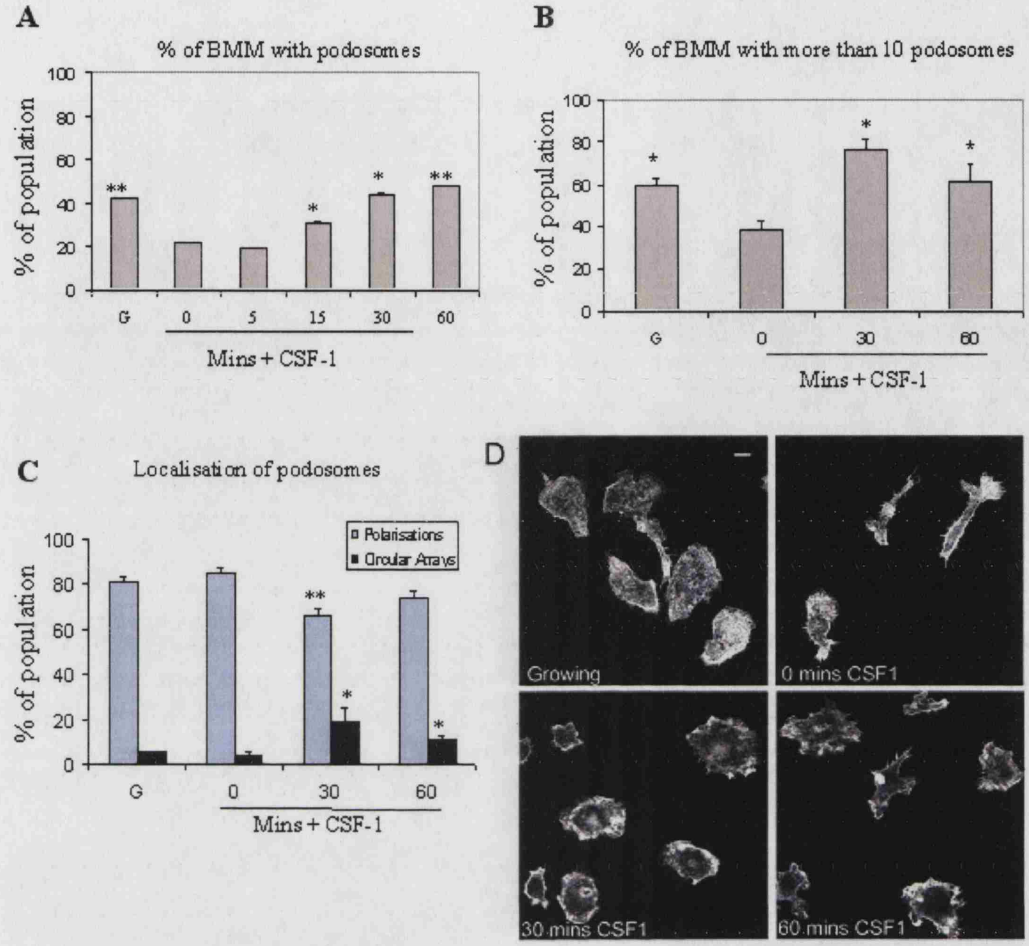

Figure 3.8 CSF-1 affects the number and distribution of podosomes:

(A) The percentage of a BMM population containing podosomes in growth medium (+CSF-1), starve medium (-CSF-1) and stimulated with 33ng/ml CSF-1 for 5, 15, 30 and 60 min. There is a significant difference in the number of BMM containing podosomes following CSF-1 stimulation, $p= 5x10^{-7}$ by ANOVA. (B) Graph showing that the proportion of BMM with podosomes containing 10+ podosomes significantly changes with CSF-1 stimulation, p=0.01 by ANOVA. (C) Graph showing that CSF-1 changes the intracellular distribution of podosomes. p=0.001 by ANOVA. Data shown is pooled from at least 3 independent experiments, n=600. The student t test was used to compare BMM starved of CSF-1 with all other conditions * = $p<0.05$. (D) Confocal images of the F- actin in BMM taken in growth and starve medium, and after 30 and 60 min of CSF-1 stimulation. F-actin was visualised using rhodamine phalloidin, bar = 10μm.

3.8 PI 3-kinases are essential for cell polarisation and podosome assembly

PI 3-kinases are involved in many aspects of cell behaviour, in macrophages they have been shown to contribute to migration, chemotaxis, phagocytosis and mitogenic signalling (Kelley et al. 1999; Leverrier and Ridley, 2001; Vanhaesebroeck et al. 1999). PI 3-kinases activate the serine/threonine kinase Akt, and this promotes Akt phosphorylation on Ser 473. Starvation of BMMs of CSF-1 for 18 h led to dephosphorylation of Akt (Fig. 3.9A), indicative of a reduction in PI 3-kinase activity. LY294002 is known to inhibit the activity of PI 3-kinases and signalling through Akt one of the pathways which is stimulated by CSF-1-R (Adi et al. 2001) (Fig. 6.6A). LY294002 has previously been shown to inhibit BMM migration to CSF-1 (Jones et al. 2003). BMM in growth medium treated with LY294002 for 30 minutes had reduced spread area and few protrusions, such as lamellae and ruffles. Most BMM had adopted either a rounded or an elongated morphology (Fig. 3.9B). LY294002 also induced disassembly of podosomes (Fig. 3.9C). The effects of LY294002 were reversible, as when it was washed out and BMMs treated with CSF-1 for 30 min, cells increased their spread area, extended protrusions and reassembled podosomes (Fig. 3.9B and C). These results indicate that podosome formation is dependent on PI 3-kinase activity and that loss of lamellae coincides with loss of podosomes.

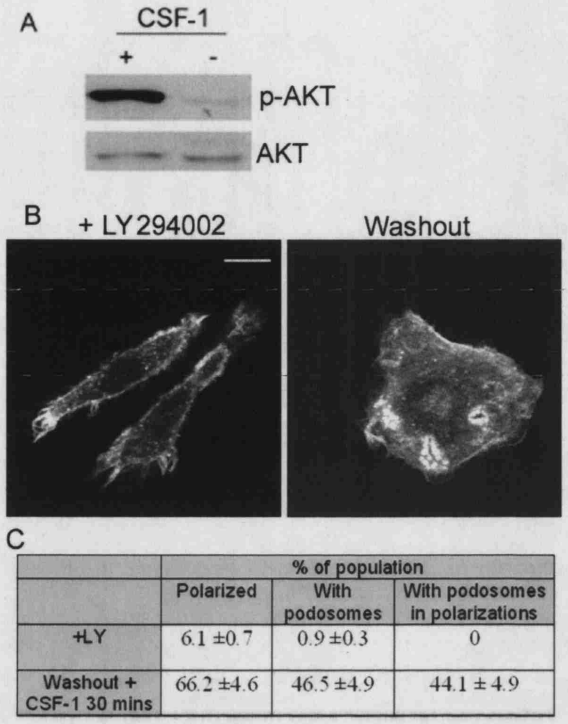

C

	% of population		
	Polarized	With podosomes	With podosomes in polarizations
+LY	6.1 ±0.7	0.9 ±0.3	0
Washout + CSF-1 30 mins	66.2 ±4.6	46.5 ±4.9	44.1 ± 4.9

Figure 3.9 PI 3-Kinases are required for podosome assembly:

(A) BMM in growth medium (+CSF-1) or starve medium (-CSF-1) were lysed, cell lysates were western blotted and probed for phospho-AKT and AKT. (B) Confocal images of the actin cytoskeleton of BMM incubated with 10μM LY294002 for 30 min and after washout of LY294002 stimulation of cells with 33 ng/ml CSF-1 for 30 min. Rhodamine phalloidin was used to visualise the actin cytoskeleton, bar = 10μm. (C) Quantitation of podosome number and polarisation shows that treatment of BMM with 10 μM LY294002 for 30 min causes loss of lamellae and other protrusions and loss of podosomes. Podosomes reformed after washout of LY294002 and 30 min stimulation of cells with CSF-1. Data is pooled from three independent experiments. The percentage of BMM with podosomes with and without LY294002 is significantly different, $p<0.01$ using Students t test.

3.9.1 Analysis of the role of Rho GTPases in podosome formation

Rho GTPases have been shown to regulate the formation and disassembly of focal adhesions in fibroblasts (Ridley et al. 2003). Although podosomes are not identical to focal adhesions they do contain some of the same proteins such as paxillin, vinculin and tyrosine kinases (FAK or Pyk2) and their formation is also regulated by Rho GTPases (Linder and Aepfelbacher, 2003). Treatment of BMM with the 10 ng of the pan-Rho GTPase inhibitor *Clostridium botulinum* Toxin B caused loss of cell protrusions and podosomes in BMM, as well as cell retraction and rounding (Fig 3.10). Over-expression of RhoA has been shown to promote podosome formation in endothelial cells and Src-transformed fibroblasts (Berdeaux et al. 2004; Moreau et al. 2003). To determine the role of Rho isoforms in podosome formation two approaches were taken. Firstly podosome distribution was analysed in RhoB-null BMM and secondly in BMM treated with C3-transferase, which inhibits RhoA, RhoB and RhoC (Aktories et al. 2004).

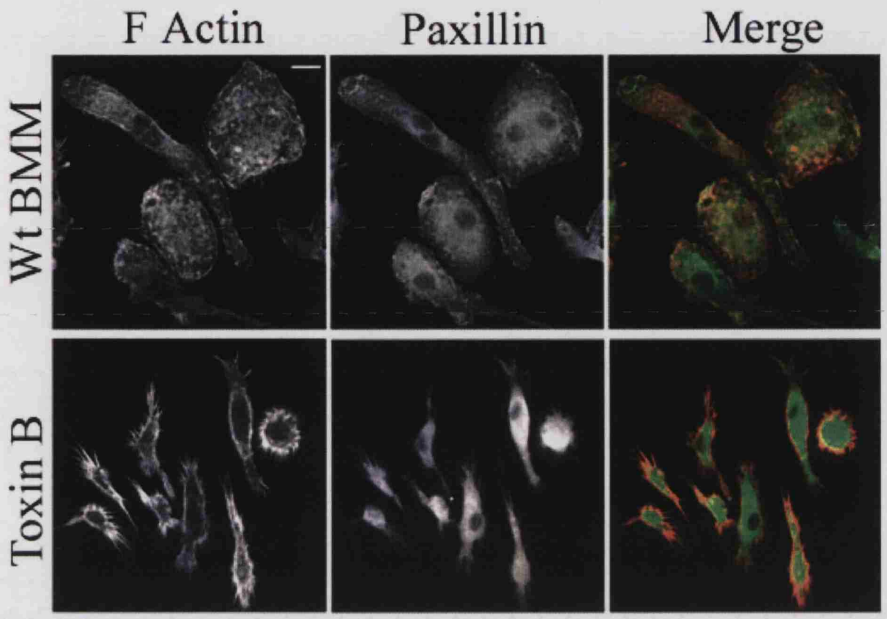

Figure 3.10: Characterisation of the effect of Toxin B on BMM and podosomes:

Confocal images of the basal plane of Wt BMM treated for 60 min with 10ng/ml Toxin B. Cells were formaldehyde fixed and stained with rhodamine phalloidin to visualise F-actin and anti paxillin antibodies to visualise paxillin. In the merged image F-actin is shown in red and paxillin in green, bar =10 μm.

3.9.2 Deletion of RhoB does not affect podosome dynamics.

Deletion of *RhoB* did not perturb the organisation of the actin cytoskeleton overall in BMM. Polarised structures such as lamellae, dorsal ruffles and formation of tails were all present $RhoB^{-/-}$ BMM (this is discussed at greater length in Chapter 4). Analysis of confocal images of the basal plane of BMM showed the structure of podosomes in $RhoB^{-/-}$ BMM was indistinguishable from that of Wt BMM (Fig. 3.11A). In an asynchronous growing population podosomes were present in an equal proportion of the $RhoB^{-/-}$ BMM as in Wt BMM and the presence of podosomes was significantly affected by CSF-1 in both Wt BMM (Fig. 3.11B). In growth medium both Wt BMM and $RhoB^{-/-}$ BMM had a similar pattern of distribution and localisation (Fig 3.8B, C, D and Fig. 3.11B, C and D). CSF-1 significantly affected the percentage of the Wt BMM population containing podosomes, as determined by ANOVA, ($p=7.57x10^{-5}$) but not $RhoB^{-/-}$ BMM (p=0.1918) (Fig. 3.11C). In fact there was no significant reduction in the percentage of $RhoB^{-/-}$ BMM that contained podosomes in starve medium, unlike Wt BMM (Fig 3.11C). However, the number of BMM containing 10 or more podosomes was significantly altered by CSF-1 stimulation in Wt BMM (p=0.008) and $RhoB^{-/-}$ BMM (p=0.01), although there was a slight lag in the recovery of podosomes in $RhoB^{-/-}$ BMM restimulated with recombinant CSF-1 (Fig 3.11C). In addition CSF-1 caused a significant change in the distribution of podosomes in Wt BMM (p=0.049) and $RhoB^{-/-}$ BMM (p=0.002). CSF-1 stimulation significantly reduced the number of podosomes found in the polarisations of Wt BMM (Fig 3.11D). This was not observed in $RhoB^{-/-}$ BMM (Fig 3.11D), but this might be again due to a lag in the response to stimulation with CSF-1 (Fig. 3.11.C, D). Deletion of RhoB therefore slightly alters CSF-1 induced changes to podosomes.

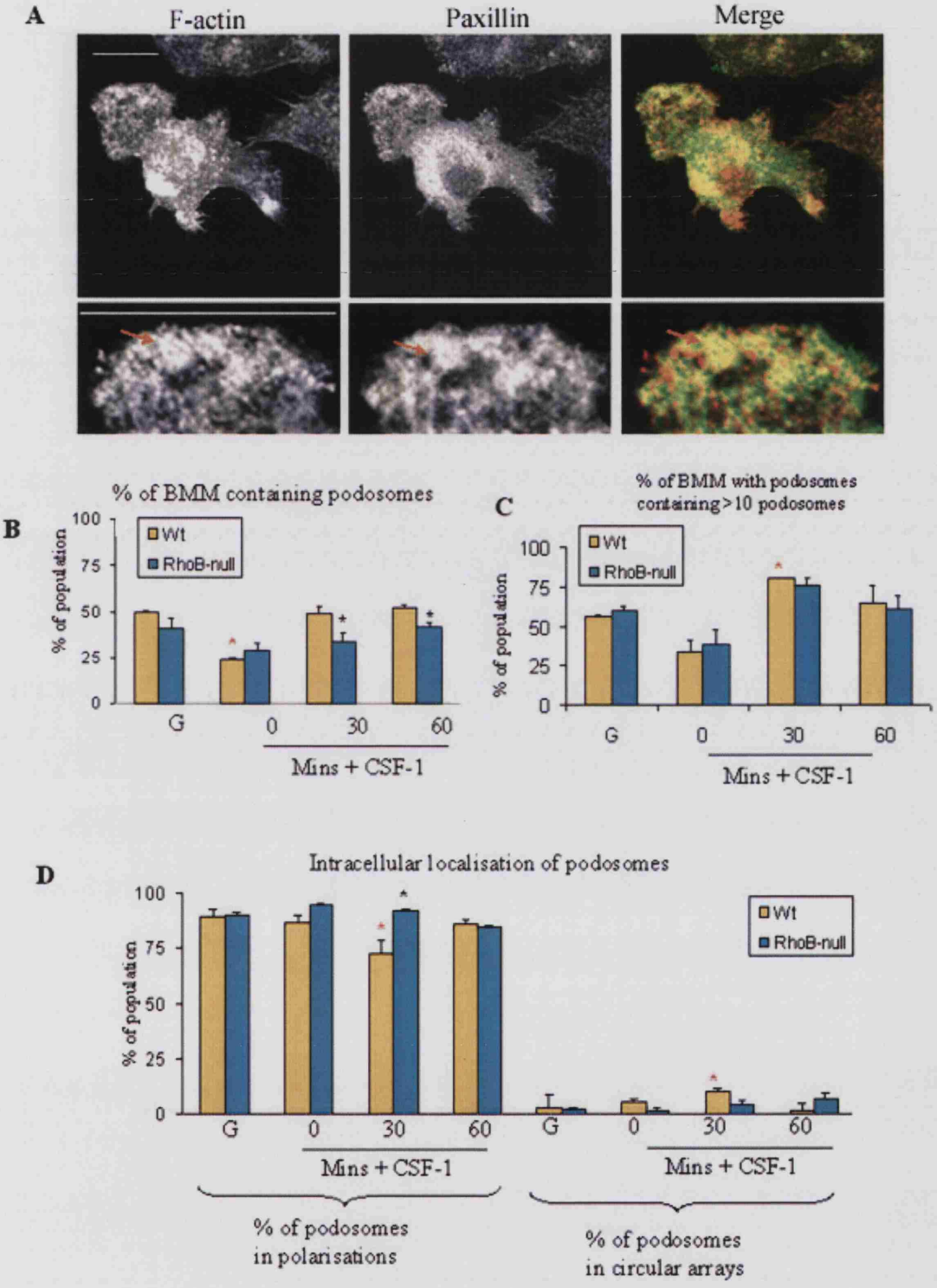
A
F-actin
Paxillin
Merge
B
% of BMM containing podosomes
% of population
Wt
RhoB-null
G
0
30
60
Mins + CSF-1
C
% of BMM with podosomes containing >10 podosomes
% of population
Wt
RhoB-null
G
0
30
60
Mins + CSF-1
D
Intracellular localisation of podosomes
% of population
Wt
RhoB-null
G
0
30
60
Mins + CSF-1
% of podosomes in polarisations
% of podosomes in circular arrays

Figure 3.11: Characterisation of the effect of deletion of *RhoB*$^{-/-}$ on podosomes

(A) Confocal images of podosomes in *RhoB*$^{-/-}$ BMM stained for F-actin and paxillin. Podosomes are indicated on the higher magnification image by red arrows, bar =10 μm. (B) Graph showing the percentage of BMM containing podosomes (Wt and *RhoB*$^{-/-}$ BMM). (C) Graph showing the proportion of BMM with podosomes containing more than 10 podosomes (Wt and *RhoB*$^{-/-}$ BMM). (D) Graph showing the intracellular distribution of podosomes in Wt and *RhoB*$^{-/-}$ BMM. In (B-D) the podosomes of Wt and *RhoB*$^{-/-}$ BMM in growth medium (G), starve medium (0 min CSF-1) and stimulated with CSF-1 for 30 and 60 min were analysed. In all cases BMM were formaldehyde fixed and stained with anti-paxillin antibodies, to visualise paxillin and rhodamine phalloidin to visualise F-actin. A focus where F-actin and paxillin co-localised was considered to be a podosome (Chapter 2.6.8). Data is shown mean ± SEM pooled from 3 independent experiments, n =100. * = a significant difference $p < 0.05$. *= difference between Wt and *RhoB*$^{-/-}$ BMM *= difference between Wt BMM in growth medium and any other condition.

3.10 C3-transferase causes a decrease in the prevalence of podosomes in a population of BMM.

C3-transferase is an exoenzyme produced by *Clostridium botulinum* and irreversibly inhibits the activity of all three isoforms of Rho. C3 itself is not cell permeableB by fusing a portion of the HIV transcriptional activation (Tat) protein to C3-transferase a recombinant tat-C3 protein is made which is cell-permeable (Sahai and Marshall, 2002b). Treatment of BMMs for 4 hours with 5 μg/ml tat-C3-transferase (Sahai and Marshall, 2002b) caused BMM to spread (Fig. 3.12Ai). This change in cell morphology was suggestive of a decrease in cell contractility, which is attributed to inhibition of RhoA activity caused by C3-transferase (Aktories et al. 2004; Sahai and Marshall. 2002b). C3-transferase caused several changes in the morphology of BMM (discussed in Chapter 4.10) and significantly affected podosome distribution ($p=0.01$) (Fig 3.12B). The shape of podosomes is not affected by C3-transferase treatment: a focus of F-actin surrounded by a paxillin ring was still clearly present in C3-treated BMM (Fig. 3.12Aii). Podosomes were still predominantly located in polarisations in BMM in C3-treated BMM (Fig. 3.12 Ai and B). However, the number of BMM containing podosomes was reduced by 50% compared to untreated cells (Fig. 3.12 B). There was a significant decrease in the percentage of BMM containing 10 or more podosomes in tat-C3-treated cells ($p=0.01$) (Fig. 3.12B). These results suggest a complex role for RhoA in podosome formation. RhoA is not essential for maintenance of podosomes but it may play a role in podosome turnover or dynamics or it may be that C3-treated cells have fewer protrusions and there are less polarised cells.

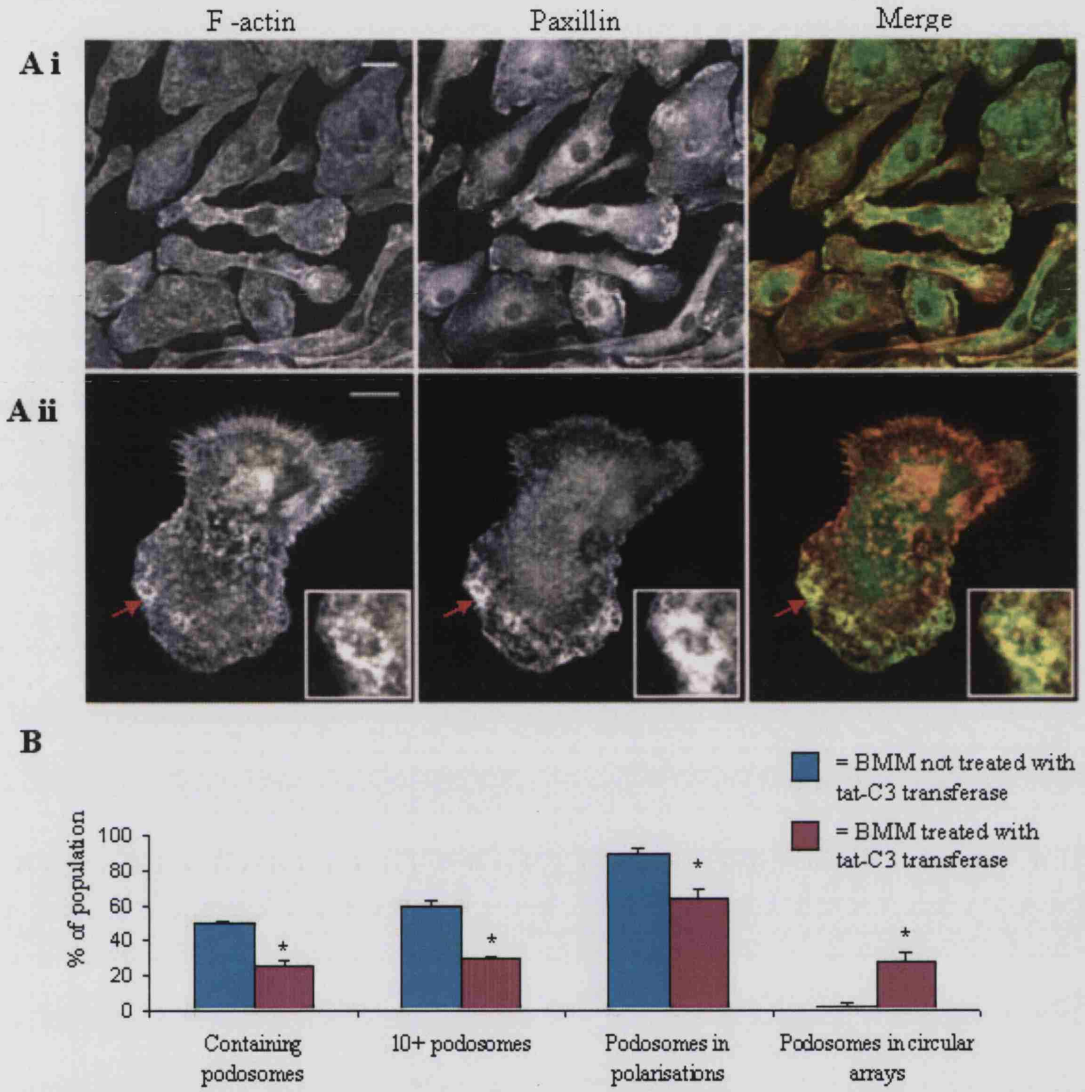

Figure 3.12 Characterisation of the effects of C3-transferase on podosomes

(Ai) Confocal images of the basal plane of Wt BMM treated for 4 h with 5 μg/ml tat-C3-transferase, fixed with formaldehyde and stained for F-actin using rhodamine phalloidin and paxillin using anti-paxillin antibodies. (Aii) A higher magnification image of podosomes in C3-transferase treated Wt BMM; podosomes are indicated by the red arrow. (B) Quantitation of podosomes of Wt BMM either in growth medium or in growth medium containing 5 μg/ml tat-C3-transferase for 4h. Data shown is mean ± SEM pooled from 3 independent experiments. Wt BMM in growth medium and Wt BMM in medium containing 5 μg/ml tat-C3-transferase were compared by the Student t test; * = a significant difference $p = 0.05$ between Wt and tat-C3-transferase treated BMM.

3.11 Conclusions and discussion

There are clear differences between the three isoforms of Rho in terms of tissue and cell type-specific expression. RhoA is expressed in every tissue and cell type examined at a similar level. RhoB and RhoC on the other hand exhibit cell type and tissue type variations in expression. This indicates that the functions of RhoB and RhoC may be more specialised than RhoA. RhoB is expressed at high levels in tissues from the nervous system, and in cells with cell-cell junctions, many of which have apical-basal polarity. The role of RhoB in trafficking of vesicles may be important in these cells (Symons and Rusk, 2003). The function of RhoB in the nervous system may well also be related to trafficking as RhoB has been shown to be involved in the trafficking of acetylcholine rich vesicles in the neuromuscular junction (Ishida et al. 2004). The function of RhoC is less well characterised, but it is interesting to note that RhoC is not detectably expressed in BMM as it has been shown to be associated with an increase in migratory and metastatic potential in cancerous cells (Wu et al. 2004). Unfortunately a RhoC antibody is not yet commercially available, and this limited the extent to which RhoC function could be studied here.

Studies using C3-transferase and overexpression of RhoA show that Rho is involved in the regulation of the cytoskeleton and cell motility in macrophages (Ridley, 2001c). The cytoskeleton of macrophages is differently organised to that of fibroblasts. Most notably BMM lack stress fibres and focal adhesions, which have been characterised in great detail in fibroblasts. The function of RhoB has been previously characterised in cultured fibroblasts and epithelial cells (Adini et al. 2003; Liu et al. 2001; Sandilands et al. 2004), but not in leukocytes (Chapter 1.10). *RhoB*$^{-/-}$ cells and Wt cell expressed similar levels of macrophage cell surface markers (Introduction 1.16) indicating deletion of RhoB causes minimal defects in macrophage maturation. The lack of RhoC in BMM makes analysis of isoform function far easier, as any Rho-dependent function will be due to RhoA or RhoB. By comparing Wt BMM with *RhoB*$^{-/-}$ BMM and BMM treated with the Rho inhibitor C3-transferase it was possible to assign an effect to a specific Rho isoform. As Wt BMM have both RhoA and RhoB activity, *RhoB*$^{-/-}$ BMM have only RhoA activity and BMM treated with C3-transferase have no Rho activity.

In this study podosomes in BMM were characterised. Podosomes are found in cells of the myeloid lineage and transformed fibroblasts (McNiven et al. 2004), but not found in non-transformed fibroblasts such as NIH3T3 cells. Similarly to other cell types podosomes in BMM were shown to contain Pyk2 (a kinase which is homologous to FAK), and paxillin, an adaptor protein involved in integrin-mediated adhesion, which was tyrosine phosphorylated.

The precise role of podosomes in cells of monocytic lineage is still poorly understood. In dendritic cells and immature osteoclasts application of maturation factors, LPS and RANK-ODF induce the formation of podosomes. These podosomes are often seen within polarised regions of the cells and their formation is transient. Cells which are unable to form lamellae correctly. For instance macrophages and dendritic cells that lack WASP, a protein which is involved in regulation of F-actin polymerisation (Chapter 1.11.1), and osteoclasts which are null for Gelsolin, an F-actin-severing protein, lack podosomes (Calle et al. 2004; Chellaiah et al. 2000a). Study of podosome distribution in a population of growing Wt BMM showed that podosomes are most abundant in macrophages with a polarised migratory morphology. Further investigation of the localisation of podosomes within these polarised cells showed that podosomes occurred mainly in protrusive regions. Non-polarised cells on the other hand had few podosomes, and these were found mainly in restricted regions of the cell (perhaps in regions of the cells that were about to polarise). CSF-1 stimulation induced changes to the the actin cytoskeleton, leading to cell polarisation and spreading (Wells et al. 2004). Podosomes were also affected by CSF-1. After 30 min of CSF-1 stimulation Wt BMM began to form a polarised morphology and this was accompanied by a transient increase in podosome number and a redistribution of podosomes. Agents that induced loss of migratory morphology, either through loss of polarised protrusions through treatment of cells with LY294002, or by cell spreading triggered by C3-transferase, caused a large decrease in podosomes. This suggests that the polarised, migratory morphology is linked to podosome formation and function.

Inhibition of PI 3-kinase activity using LY294002 induced loss of podosomes within a population of BMM. This indicated that PI 3-kinase activity is essential for podosome formation. However, as use of LY294002 also caused loss of protrusions in BMM and washout of LY294002 allowed reformation of lamellae and consequent formation of

podosomes, it is difficult to determine whether loss of protrusions lead to loss of podosomes or vice versa.

Rho GTPases have been shown to regulate podosomes, but most studies have used inhibitors of Rho GTPases or dominant negative Rho GTPases. Inhibition of Rac and Cdc42 prevents formation of new podosomes in dendritic cells (Burns et al. 2001). Little is known about the role of the different isoforms of Rho in podosome formation. Increasing RhoA activity (either through over-expression or by use of fast cycling RhoA) in both Src-transformed cells and endothelial cells induced formation of podosomes (Berdeaux et al. 2004; Moreau et al. 2003). Interestingly the podosomes induced by expression of fast cycling (T37N) RhoA in endothelial cells form in circular arrays, similar to those seen after 30 min of CSF-1 stimulation.

Use of BMM derived from knockout mice allows different isoforms of Rho GTPases to be assigned a specific role in podosome function. In *RhoB*$^{-/-}$ BMM and C3-transferase treated BMM there were no differences in the ultrastructure of podosomes. Thus RhoA and RhoB did not have a role in the localisation of F-actin and paxillin within an individual podosome. Deletion of RhoB affected the response of BMM to CSF-1. It is difficult to discern whether the reduced response *RhoB*$^{-/-}$ BMM to CSF-1 is due to the formation of podosomes being directly affected by lack of RhoB (perhaps due to adhesion defects), or an effect caused by defective CSF-1 signalling in *RhoB*$^{-/-}$ BMM. Podosome distribution in BMM in growth medium in *RhoB*$^{-/-}$ BMM was similar to Wt BMM. Therefore all the effects on podosome localisation and dynamics caused by C3-transferase treatment of BMM in growth medium, such as reduction in podosome number and decrease in podosome localisation in protrusions, can be directly attributed to RhoA (as RhoC is not expressed in BMM). The decrease in podosome number in C3-transferase treated cells is in agreement with the increase in podosome number seen in endothelial cells with increased RhoA activity (Moreau et al. 2003). As podosomes were reduced but not completely lost in C3-transferase treated BMM it is possible that RhoA is involved in podosome assembly. Alternatively C3-transferase induced cell spreading and loss of protrusions (Chapter 4.10 and Fig 3.12A) and this could be connected with loss of podosomes.

In summary the results in this chapter suggest that there is a link between podosome formation in BMM and cell protrusion and polarisation. RhoB slightly affect CSF-1

induced changes to podosomes, whereas RhoA inhibition generally reduces podosome assembly.

Chapter 4. The roles of RhoA and RhoB in macrophage motility

4.1 Introduction

Macrophages form part of the innate immune response: they are professional phagocytes and their function is to destroy pathogens and apoptotic cells. Tissues that are prone to frequent attack from pathogens contain resident populations of macrophages (Chapter 1.16). Monocytes arise within the bone marrow and then circulate through the blood. Similarly to other leukocytes, monocytes migrate to their site of action by attachment to the endothelium, diapedesis and then crawling through the extracellular matrix of tissues (Chapter 1.1) Directed migration towards a site of infection in response to chemo-attractants released by the injured tissue is an essential part of macrophage function. Macrophages respond to several chemoattractants including, bacterial products such as LPS, chemokines such as MCP-1, cytokines such as CSF-1 and complement (Ridley, 2001c). Of these the response of macrophages to the cytokine CSF-1 is particularly well documented (Pixley and Stanley, 2004). Stimulation of macrophages with CSF-1 causes an increase in the dynamics of the actin cytoskeleton, including formation of lamellipodia, filopodia and dorsal ruffles (Jones et al. 2003; Wells and Ridley, 2004). The Rac family of Rho GTPases and Cdc42 are required for a complete response to CSF-1 in macrophage cell lines and BMM (Allen et al. 1998; Jones et al. 2003; Wells and Ridley, 2004). Use of C3-transferase proved Rho to be essential for the regulation of morphology and migration of macrophages from the BAC1 cell lines (Allen et al. 1997) (See Chapter 3.9 and Chapter 1.16.2). However, the role of the three separate isoforms of Rho in macrophage motility or in their response to CSF-1 has not been analysed. BMM do not detectably express RhoC (Chapter 3.2) so an approach combining use of BMM derived from a *RhoB*$^{-/-}$ mouse, BMM treated with C3-transferase, and Y27632, an inhibitor of ROCK, was used to analyse the relative contribution of RhoA and RhoB and ROCK to macrophage motility.

Results

4.2 RhoA activity is essential for BMM migration.

To investigate the roles of RhoA and RhoB in the regulation of BMM migration the speed of migration of Wt BMM, *RhoB*$^{-/-}$ BMM, BMM treated with 5 μg/ml tat-C3-transferase (t-C3) (see chapter 3.9) and BMM treated with 5 μM Y27632 on fibronectin was measured. BMM change their morphological and migratory properties with age (personal communication, Dr Y.Leverrier and Dr C.Wells). All BMM in these experiments were therefore used only up to 8 days after differentiation (Chapter 2.2.3) Analysis of migration speed by ANOVA showed that there was a significant difference ($p=3.4x10^{-4}$) in the speed of migration between each population of BMM analysed. Wt BMM migrated at 0.6 μm/min in growth medium and *RhoB*$^{-/-}$ BMM migrated slightly more rapidly at 0.85 μm/min (Fig. 4.1A). In both Wt and *RhoB*$^{-/-}$ BMM treated with Y27632 and t-C3, the speed of migration was significantly reduced (Fig. 4.1A). Student t-tests showed that there was no significant difference in speed between Wt and *RhoB*$^{-/-}$ BMM in any condition but t-C3 and Y27632 treated BMM moved significantly slower than Wt BMM in growth medium. This suggests that RhoA and ROCK are both essential for migration. Absence of RhoB had the opposite effect to inhibition of RhoA activity causing cells to migrate more rapidly.

Most Wt BMM had a classical migratory morphology with a spread lamella at the back and a contracted tail at the rear (Abercrombie et al. 1971; Ridley et al. 2003) and go through a migratory cycle (Chapter 1.1), consisting of formation of lamellipodia and protrusion of lamellae (often several lamellae are formed, although ultimately one is chosen to generate persistent migration), elongation of the cell and translocation of the cell body followed by retraction of the cell tail. BMM were very heterogeneous in size and consequently the time taken for an individual BMM to go through a migration cycle and the size of lamellae and tails formed varied considerably from cell to cell (Fig. 4.1B and Movie 4.1). The morphology of *RhoB*$^{-/-}$ BMM was more rounded and phase bright, this indicated that these cells were more spherical than Wt BMM. *RhoB*$^{-/-}$ BMM appeared to 'hop' from one location to another in the time-lapse movie, probably because the cells moved further in the interval between frames than Wt BMM. (Fig. 4.1B and Movie 4.1). Migration of both Wt and *RhoB*$^{-/-}$ BMM treated with Y27632 and t-C3-transferase was severely compromised. Many t-C3 and Y27632 treated BMM had

tail retraction defects although the lamellae of these cells still moved forwards (Fig. 4.1B and Movies 4.2 and 4.3). t-C3 and Y27632 treated cells lost phase brightness during the course of the time-lapse experiments, which indicated that the cells had become more flattened (Fig. 4.1B and Movie 4.3). This could be due to a loss of cell contractility

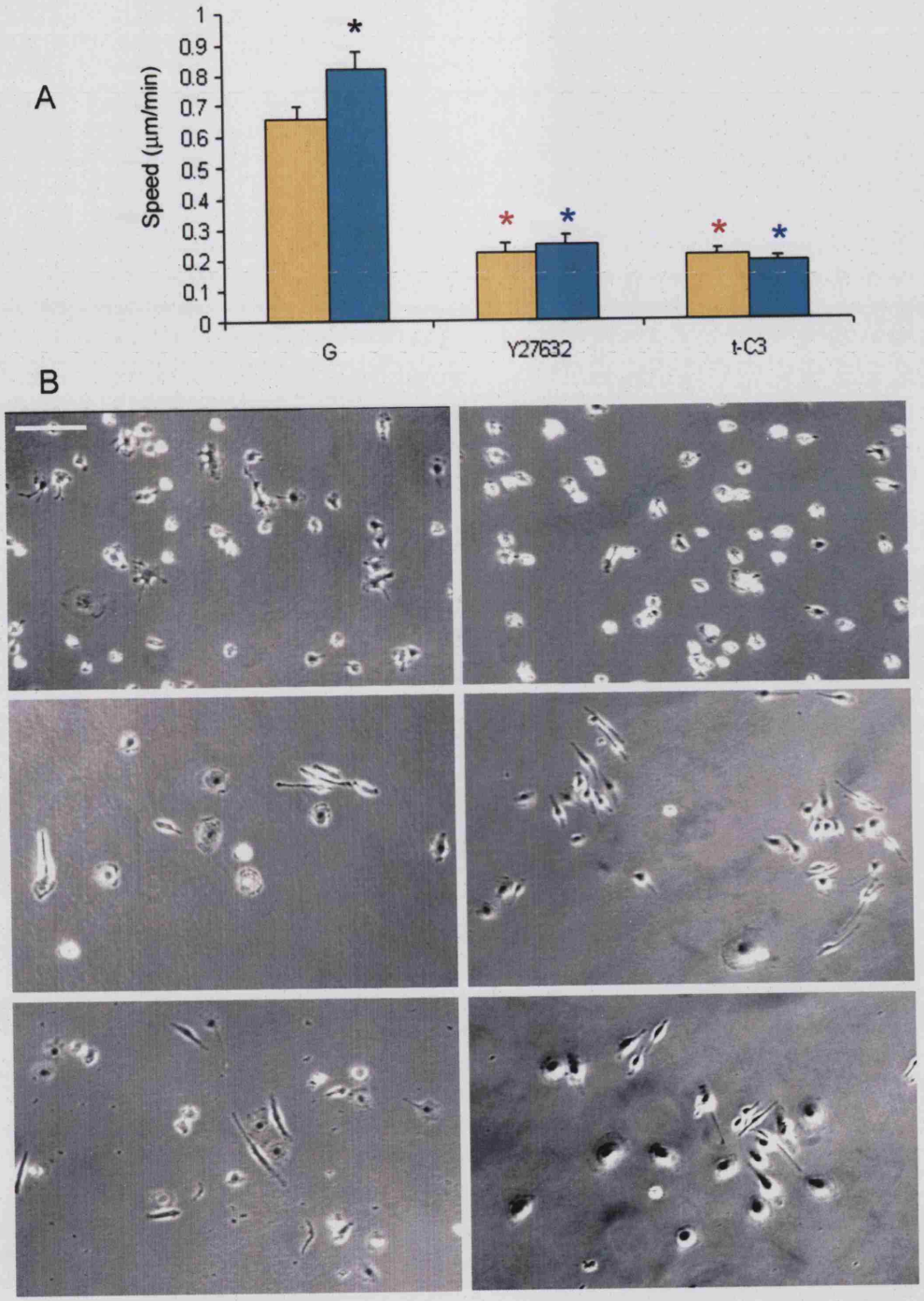

Figure 4.1. Effect of inhibition of Rho and ROCK on BMM migration

(A) Chart showing the speed of migration in mm/min of Wt and *RhoB*$^{-/-}$ BMM on fibronectin coated plastic in: growth medium, treated with: 5 µM Y27632, 5 µg/ml tat- C3-transferase. (B) Phase contrast images of Wt and *RhoB*$^{-/-}$ on fibronectin-coated plastic in growth medium (G), treated with Y27632, 5 µg/ml tat-C3-transferase. Bar = 100µm. Data is shown mean ± SEM pooled from 3 independent experiments n=100 cells. * = a significant difference, $p < 0.05$. *= difference between Wt and *RhoB*$^{-/-}$BMM *= difference between Wt BMM in growth medium and any other condition. *= difference between *RhoB*$^{-/-}$ BMM in growth medium and any other condition.

4.3 Withdrawal of CSF-1 decreases the distance BMM move.

Analysis of the speed of BMM in growth medium and starve medium showed that withdrawal of CSF-1 for 18 hours significantly reduced the speed of Wt and *RhoB*$^{-/-}$ BMM (Fig 4.2A). However, the *RhoB*$^{-/-}$ BMM migrated at a significantly faster speed than Wt cells in starve medium (Fig 4.2A). Wt BMM incubated in starve medium became more elongated though some retained a polarised morphology (Wells et al. 2004) (Fig 4.2B) and their nuclei often shuttled between each end of the cell (Movie 4.4). The method of tracking used in this analysis involved following the movement of the nucleus through a time lapse movie. Tracking BMM in which the nucleus shuttled from one end of an elongated cell to the other can give a false indication of cell migration. To differentiate between cells that shuttle their nuclei and cells that actually migrate, the displacement of BMM was analysed (Chapter 2.6.4). For the purposes of this analysis a cell that had displaced its nucleus more than 30 μm (a length that corresponds to the average length of a BMM, Chapter 4.10) is regarded as having translocated away from its initial position and therefore considered to be motile. A similar proportion of Wt and *RhoB*$^{-/-}$ BMM were motile in growth medium (Table 4.1). Treatment of Wt and *RhoB*$^{-/-}$ BMM with Y27632 or t-C3 caused an approximately 75% decrease in the motile population, and the majority of the population was therefore considered to be non migratory (Table 4.1). Most Wt BMM did not translocate in starve medium, and thus the speed of migration calculated by tracking of the nuclei of Wt BMM must be mainly due to nuclear shuttling.

After 18 hours incubation in starve media *RhoB*$^{-/-}$ BMM did not appear to have elongated as much as Wt BMM although they were noticeably smaller (Fig. 4.2B and 4.10). Quantitation of displacement of the *RhoB*$^{-/-}$ BMM revealed that they were still able to migrate in starve medium (Table 4.1). The proportion of motile *RhoB*$^{-/-}$ BMM fell to 55% of that in growth medium, suggesting that *RhoB*$^{-/-}$ BMM may not shuttle their nuclei as much in the absence of CSF-1 as Wt BMM. Lack of CSF-1 did not reduce the displacement of *RhoB*$^{-/-}$BMM as markedly as Wt BMM (Fig. 4.2D). This suggests that RhoB normally acts to reduce cell translocation.

	+ CSF-1		-CSF-1		Y27632		T-t-C3	
Genotype	*Wt*	*RhoB-/-*	*Wt*	*RhoB-/-*	*Wt*	*RhoB-/-*	*Wt*	*RhoB-/-*
% Population translocated >30 μm	76	75	25	41	12	25	20	19

Table 4.1 Percentage of BMM that migrate further than 30 μm during 6.5 h on fibronectin coated plastic. Data is pooled from three independent experiments, n = 100 cells.

Figure 4.2. BMM migration is slowed by withdrawal of CSF-1

(A) The speed of migration in μm/min of Wt and *RhoB-/-* BMM on fibronectin in growth medium (+CSF-1) and starve medium (-CSF-1). (B) Phase contrast micrographs of Wt and $RhoB^{-/-}$ BMM on fibronectin in growth and starve medium; bar = 100μm. (C) Graph showing the percentage of the Wt and $RhoB^{-/-}$ BMM population migrating on fibronectin that translocated beyond a fixed distance, during the course of the 6.5 h movie. Persistence of migration is shown for Wt and $RhoB^{-/-}$ BMM in growth medium and starve medium. Data is pooled from 3 independent experiments n=100 cells. * = a significant difference, $p < 0.05$. *= difference between Wt and $RhoB^{-/-}$BMM

4.4 All BMM have random migration on fibronectin

Using software designed for analysis of chemotaxis it is possible to identify if a statistically significant number of BMM are moving in a specific direction (Webb et al. 1996; Wells and Ridley, 2004). A vector plot shows the trajectories of BMM from their origin. The horizon was set to 30 μm as BMM that translocated more than this distance were considered to be migratory (Section 4.2). As expected in the absence of chemoattractant, both Wt and *RhoB*$^{-/-}$ BMM did not migrate persistently in one particular direction on fibronectin. Vector plots of *RhoB*$^{-/-}$ BMM and BMM treated with t-C3 or Y27632 also showed that these cells had migrated randomly on fibronectin (Fig. 4.3). This indicated that neither RhoA nor RhoB promoted directional migration in the absence of a chemokine stimulus.

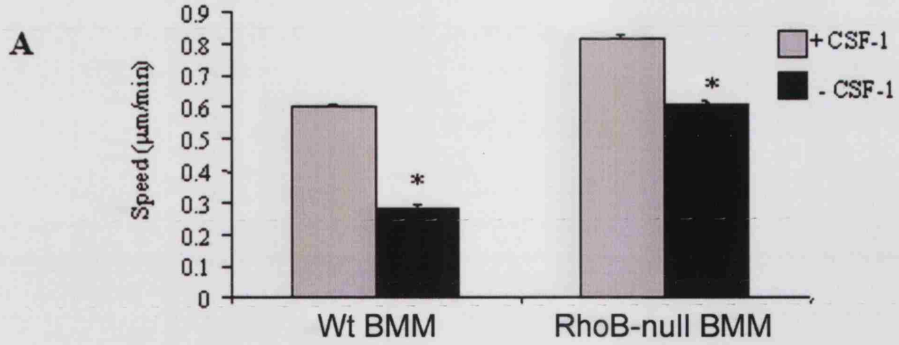
A
Speed (µm/min)
0.9
0.8
0.7
0.6
0.5
0.4
0.3
0.2
0.1
0
+ CSF-1
- CSF-1
*
*
Wt BMM
RhoB-null BMM

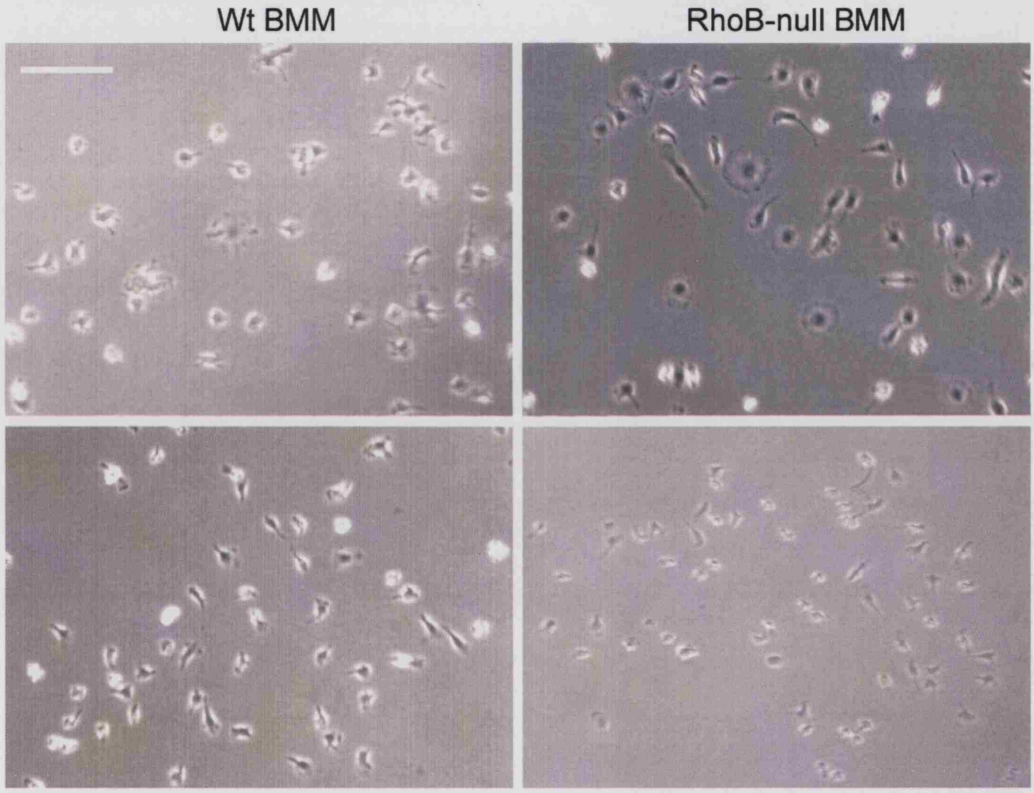
Wt BMM
RhoB-null BMM

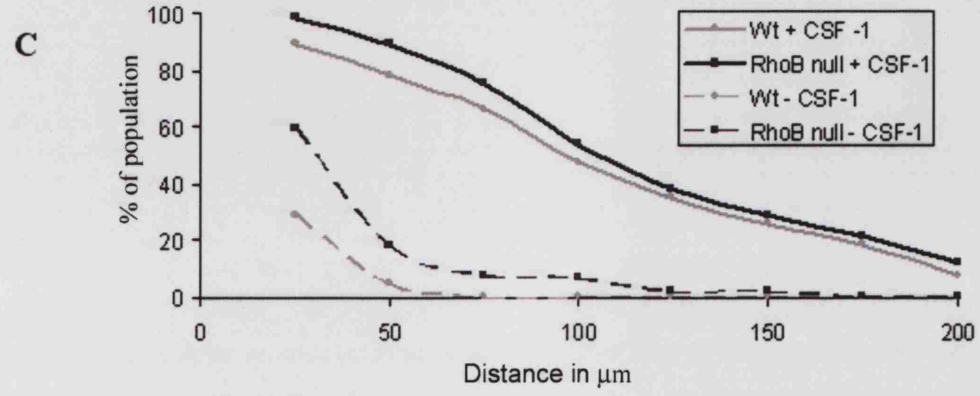
C
% of population
100
80
60
40
20
0
0
50
100
150
200
Distance in µm
Wt + CSF -1
RhoB null + CSF-1
Wt - CSF-1
RhoB null - CSF-1

	Wt BMM	No of cells	*RhoB*$^{-/-}$ BMM	No of cells
+ CSF-1	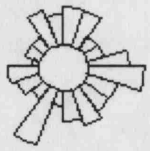	76	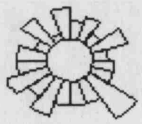	75
-CSF-1		25		41
Y27632	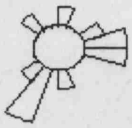	12	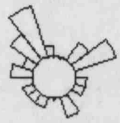	25
tat-C3	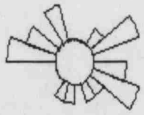	20	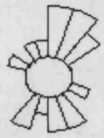	19

Figure 4.3: BMM migrate randomly on fibronectin

Vector plots, with the horizon set to 30 μm show the combined direction of migration on fibronectin of all BMM analysed. The angle of migration is shown for both Wt and *RhoB*$^{-/-}$ BMM in: growth (+CSF-1) and starve medium (-CSF-1) and for BMM in growth medium supplemented with 5 μM Y27632 or 5 μg/ml tat-C3-transferase. The migration of BMM was analysed for 6.5 hours. Data is pooled from 3 independent experiments.

4.5 Withdrawal of CSF-1 causes RhoB$^{-/-}$ BMM to turn more

The scatter plots with traces of migratory paths can be used as an indication of cell turning. The path of migration is represented as a temperature scale with the start of the path of cell migration shown in red and the end indicated by purple (Fig. 4.4A). This gives a qualitative indication of cell displacement. The scatter plots indicated that both Wt and *RhoB*$^{-/-}$ BMM were not displaced as far in starve medium as in growth medium (Fig. 4.4A). To determine whether this was due to an increase in cell turning a quotient of turning was determined. The turning quotient was calculated by dividing the total distance travelled by a migrating cell during a movie by the displacement from its origin. The closer this quotient was to 1 the fewer times the cell had turned (Fig. 4.4B). In this analysis very few BMM treated with t-C3 and Y27632 were considered to be motile, therefore they were not included in this analysis. In growth medium Wt and RhoB$^{-/-}$ BMM had similar turning quotients (Fig. 4.4C). In starve medium the turning of Wt BMM increased slightly, but as few of these cells were motile, this could be a result of increased nuclear shuttling (Fig. 4.2B and Movie 4.4). The *RhoB*$^{-/-}$ BMM in starve medium had a significantly increased turning quotient compared to both *RhoB*$^{-/-}$ BMM and Wt BMM in growth medium (Fig. 4.4C).

A

	Wt	No	*RhoB*$^{-/-}$	No
+CSF1	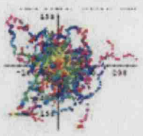	76	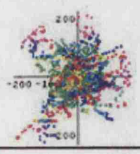	75
-CSF1	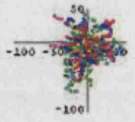	25	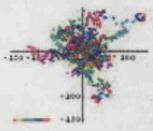	41
Y27632	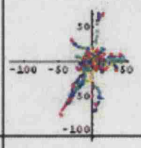	12	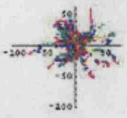	25
C3	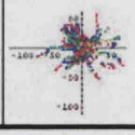	20	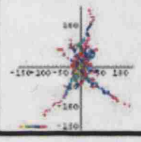	19

B

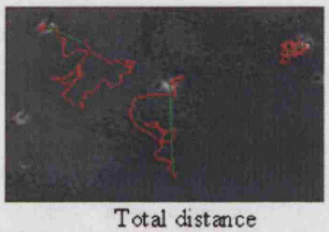

$$\text{Turning Quotient} = \frac{\text{Total distance moved by cell (red)}}{\text{Displacement from starting point (green)}}$$

C

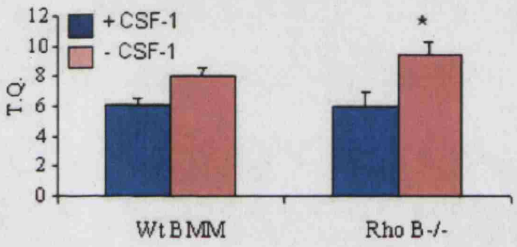

Figure 4.4: Withdrawal of CSF-1 causes RhoB$^{-/-}$ BMM to turn more

(A) Scatter plots of Wt and *RhoB*$^{-/-}$ BMM migrating on fibronectin are shown for the following conditions: growth medium (+CSF-1), starve medium (-CSF-1), growth medium supplemented with 5 μM Y27632 or 5 μg/ml tat-C3-transferase. (B) Phase contrast micrograph of a migrating cell to illustrate method of calculation of the turning quotient. The path taken by the migrating cell during the 6.5 hour experiment is shown in red. The final displacement of the cell from its origin is shown in green. (C) Graph of the turning quotients of Wt and *RhoB*$^{-/-}$ BMM moving on fibronectin in growth (+ CSF-1) and starve medium (-CSF-1). Data is pooled from 3 independent experiments; n=100 cells * = a significant difference $p < 0.05$ between Wt and *RhoB*$^{-/-}$BMM

4.6 Wt BMM migrate more rapidly on glass than *RhoB*$^{-/-}$ BMM

The migratory properties of fibroblasts, T cells and neutrophils are known to be dependent on the substrate they migrate upon (Friedl et al. 1998a; Hogg et al. 2002; Ware et al. 1998). To determine whether the migration of BMM was also substrate-dependent the migration of Wt and *RhoB*$^{-/-}$ BMM was measured on glass (Movie 4.5 and 4.6). In growth medium Wt BMM migrated at a higher speed on glass compared to fibronectin-coated plastic (Fig 4.1A and 4.5A). *RhoB*$^{-/-}$ BMM, on the other hand, moved more slowly on glass compared to fibronectin. In starve medium the speed of migration of both Wt and *RhoB*$^{-/-}$ BMM was decreased. In Wt BMM this was highly significant ($p=0.001$) decrease to a speed similar to that of Wt BMM in starve medium migrating on fibronectin (Fig 4.2A). *RhoB*$^{-/-}$ BMM also slowed down in starve medium but statistical analysis shows that this was not a significant reduction ($p>0.05$) in speed compared to that of *RhoB*$^{-/-}$ BMM moving in growth medium (Fig. 4.5A) possibly due to variablility between experiments. From the phase contrast micrographs it can be seen that the migratory morphology of Wt and *RhoB*$^{-/-}$ BMM appears qualitatively similar on glass to that seen on fibronectin (Fig. 4.4B and 4.2B). Some BMM on both substrata had a clearly polarised migratory morphology with a lamella at the front and a tail at the rear, and BMM clearly moved through a similar migratory cycle on both glass and fibronectin (Movie 4.5 and 4.6). However the details of the migration process such as exact area of extension of lamellae, time for turnover of adhesions and tail retraction could not be measured accurately by low power phase-contrast microscopy. The major differences between BMM migration on glass and on fibronectin may lie in these details.

Displacement analysis (Section 4.2) was applied to BMM migrating on glass. It showed that 60% of Wt BMM population were motile compared to 52% of *RhoB*$^{-/-}$ BMM population in growth medium (Fig 4.5C). The proportion of BMM that migrated in starve medium was identical in both Wt and *RhoB*$^{-/-}$ BMM (Fig 4.5C). Intriguingly the proportion of the motile population in *RhoB*$^{-/-}$ BMM is the same as Wt BMM in starve medium on glass (Table 4.2).

	+CSF-1		-CSF-1	
Genotype	*Wt*	*RhoB-/-*	*Wt*	*RhoB-/-*
% Population translocated >30μm	60	52	24	22

Table 4.2 Percentage of BMM measured that migrate further than 30 μm on glass in growth medium (+CSF-1) and starve medium (-CSF-1). Data is pooled from three independent experiments, *n*=100 cells.

Figure 4.5: Wt BMM migrate more rapidly on glass than *RhoB*$^{-/-}$ BMM

(A) The speed of migration in μm/min of Wt and *RhoB*$^{-/-}$ BMM on glass in growth medium (+CSF-1) and starve medium (-CSF-1). (B) Phase contrast image of Wt and *RhoB*$^{-/-}$ BMM in growth medium and starve medium. (C) A graph showing the percentage of the population of Wt and *RhoB*$^{-/-}$ BMM migrating on glass ± CSF-1 who have migration more then a fixed distance. Data is representative of 3 independent experiments, *n*=100. * = a significant difference $p < 0.05$. *= difference between Wt and *RhoB*$^{-/-}$ BMM *= difference between Wt BMM in growth medium and any other condition. *= difference between *RhoB*$^{-/-}$ BMM in growth medium and any other condition.

A

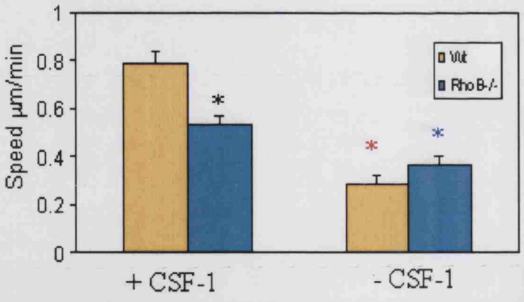
Speed µm/min
1
0.8
0.6
0.4
0.2
0
Wt
RhoB-/-
*
*
*
+ CSF-1
- CSF-1

B

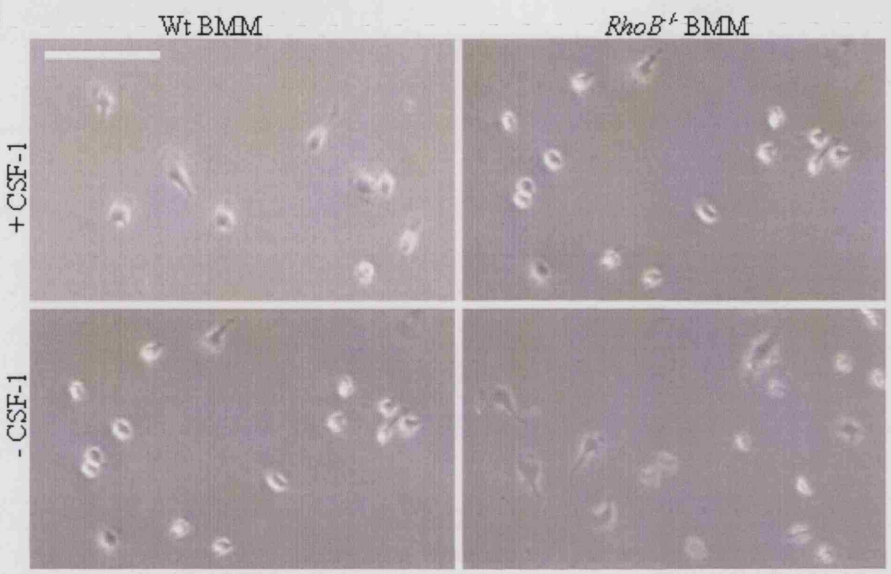
Wt BMM
RhoB-/- BMM
+ CSF-1
- CSF-1

C

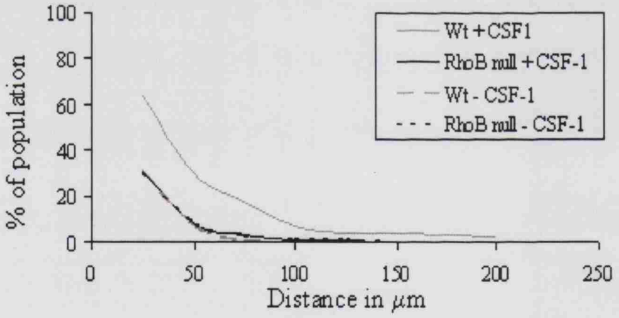
% of population
100
80
60
40
20
0
0
50
100
150
200
250
Distance in µm
Wt + CSF1
RhoB null + CSF-1
Wt - CSF-1
RhoB null - CSF-1

4.7 BMM have an increased turning quotient on glass.

As expected in the absence of chemoattractant migration on glass was non-directional in both growth and starve medium (Fig. 4.6A) for Wt and *RhoB*$^{-/-}$ BMM. Analysis of the scatter plots of BMM moving on glass shows their displacement was significantly smaller than that of BMM moving on fibronectin. The migration paths shown on the scatter plots (Fig. 4.6B) were also compacted together compared to the migration paths of BMM moving on fibronectin coated plastic which suggests the BMM on glass are either not migrating as far or that they are turning more. To distinguish between these, firstly the number of BMM that move further than 30 μm from their starting point was calculated (Table 4.2). This showed that 50 to 60% of the population of Wt and *RhoB*$^{-/-}$ BMM migrated on glass, which was less than were seen migrating on fibronectin (Table 4.4a)

The turning quotient of BMM moving on glass was calculated. Wt BMM migrating in growth medium had a very high turning quotient, which was significantly reduced in starve medium. The opposite effect was observed for *RhoB*$^{-/-}$ BMM (Fig 4.6b). A comparison of turning quotients of Wt and *RhoB*$^{-/-}$ BMM on different substrates showed that the migration of Wt BMM was significantly ($p<0.01$) more persistent on fibronectin than on glass in growth medium. Withdrawal of CSF-1 caused an increase in turning quotient of *RhoB*$^{-/-}$ BMM regardless of substrate. However in starve medium the turning quotient of Wt BMM was reduced on glass to a similar level seen on fibronectin. This may be due to a decrease in the proportion of cells migrating on both substrates (Table 4.3).

Genotype	CSF-1	Turning quotient		T Stat (2 tailed)	Significant Difference
		Glass	Fibronectin		
Wt	+	12.0	6.0	0.0001	Y
	-	7.5	8.0	0.4841	N
RhoB-/-	+	7.0	6.0	0.1747	N
	-	13.0	10.5	0.0642	N

Table 4.3: The turning quotients of Wt and *RhoB*$^{-/-}$ BMM on fibronectin and glass. In growth medium (+CSF-1) and starve medium (-CSF-1). Data is pooled from 3 independent experiments, n=100 cells.

A

	Wt	No	*RhoB-/-*	No
+ CSF-1	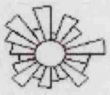	60		52
-CSF-1	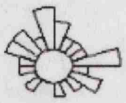	24	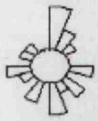	22

B

+ CSF-1	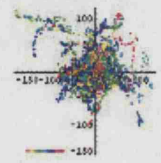	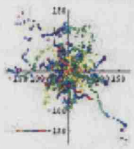
-CSF-1	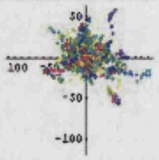	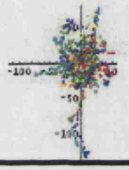

C

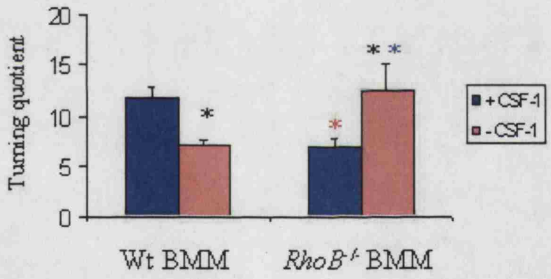

Figure 4.6: BMM have an increased turning quotient on glass

(A) Vector and (B) Scatter plots, where horizon is set to 30 μm, of the combined migration paths of Wt and *RhoB*$^{-/-}$ BMM on glass in growth (+CSF-1) and starve (-CSF-1) medium. (C) Graph of the turning quotients (T.Q.) of Wt and *RhoB*$^{-/-}$ BMM in growth and starve medium moving on glass. Data is pooled from 3 independent experiments, n=100. * = a significant difference $p<0.05$. *= difference between Wt and *RhoB*$^{-/-}$ BMM *= difference between Wt BMM in growth medium and any other condition. *= difference between *RhoB*$^{-/-}$ BMM in growth medium and any other condition.

4.8 Deletion of *RhoB* does not affect chemotaxis

The Dunn chamber can be used to visualise chemotaxis and to generate a variety of information about the chemotactic properties of cells (Wells and Ridley, 2004). The Dunn chamber consists of 2 concentric rings bored into a glass coverslip (Fig. 4.7). The rings are separated by a raised bridge, and it is possible to visualise cells migrating on this using an inverted microscope. The inner ring is filled with medium lacking chemokine, the outer ring contains medium with chemokine (in this case CSF-1), and if cells are capable of chemotaxis they will migrate across the bridge towards the chemokine source. A coverslip with BMM attached was placed over the concentric rings and sealed (Section 2.6.3 contains a more detailed methodology). The camera was oriented so that top of the field of view was medium containing CSF-1 and the bottom was starve medium, if BMM positively chemotaxed they would move 'upwards' towards the chemokine (Fig. 4.7A, C). Vector analysis of the cell tracks (Section 4.3) showed the average trajectory as upwards in chemotaxing cells. A custom C program then correlates the trajectory of the cell populations and through statistical analysis identifies whether a significant proportion ($p<0.05$) of a cell population are moving in a specified direction. The red arrow indicates the significant direction of cell movement and the 95% confidence limits of the mean are shown by the green triangle on the vector plot. A red arrow on the vector analysis plots pointing upwards therefore indicated BMM were chemotaxing towards a CSF-1 source (Allen et al. 1998; Wells and Ridley, 2004; Zicha et al. 1997) (Fig 4.7B). Quantitation of chemotaxis of Wt and *RhoB*$^{-/-}$ BMM showed that they both positively chemotaxed towards a medium containing 33 ng/ml recombinant CSF-1 (Fig 4.7C). The speed of migration was significantly faster in *RhoB*$^{-/-}$ BMM and more of the population of *RhoB*$^{-/-}$ BMM translocated 25 μm than Wt BMM, though this is probably due to the increased speed of migration of the *RhoB*$^{-/-}$ BMM in Dunn chambers (Fig 4.7C and Video 4.7).

A

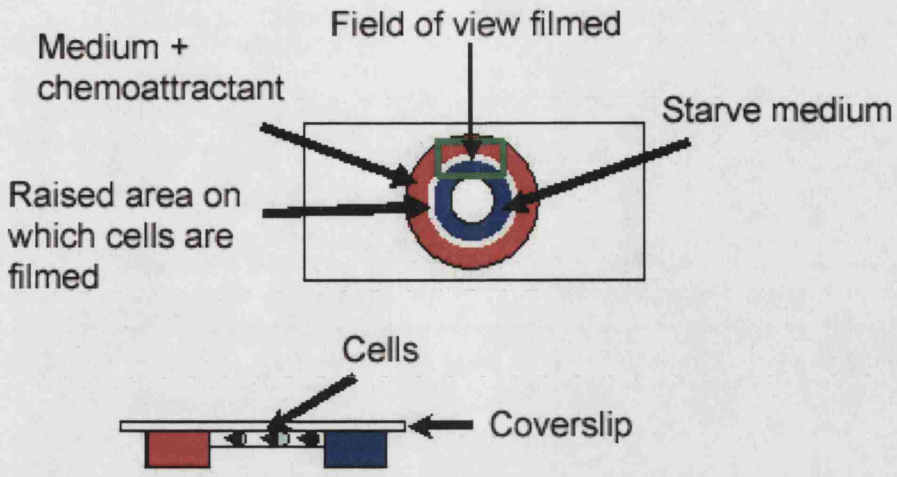

B

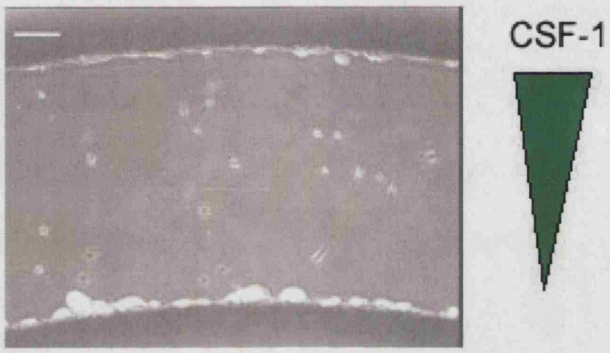

C

Wt BMM
horizon = 25 µm
p = 0.005
n = 40

RhoB-null BMM
horizon = 25 µm
p = 0.0001
n = 57

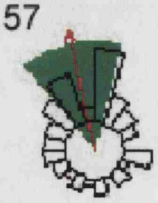

Speed of migration µm/min

Wt BMM	*RhoB*$^{-/-}$ BMM
0.018 ± 0.003	0.026 ± 0.003

Figure 4.7: Deletion of *RhoB* does not affect chemotaxis

(A) A schematic diagram of the Dunn chemotaxis chamber. Starve medium is shown in blue, medium with chemo attractant is shown in red. The field of view used in the time-lapse analysis is shown by the green box. (B) Phase contrast image of Wt BMM in a Dunn chamber, bar = 100μm. (C) Vector analysis of Wt and $RhoB^{-/-}$ BMM in Dunn chambers moving towards a source of recombinant CSF-1 The direction of positive chemotaxis is indicated by the red arrow and 95% confidence limits are shown by the green triangle. Cells were filmed for 16.5 hours, with 1 frame taken every 10 minutes. Data is pooled from 3 independent experiments, n=78.

4.9 *RhoB* deletion does not affect the organisation of the F-actin and microtubules

Study of the actin and microtubule cytoskeletons did not reveal any obvious defects in the *RhoB*$^{-/-}$ BMM. Both Wt and *RhoB*$^{-/-}$ BMM had a diversity of cell shapes (Fig 4.8A) but were able to assume a migratory morphology with a clear lamella at the front of the cell and a tail at the rear (Fig 4.8B). A structure corresponding to the MTOC was in front of the nucleus in the cells with a migratory morphology (Fig 4.8B). Wt and *RhoB*$^{-/-}$ BMM had a concentration of microtubules in the centre of the cell and peripheral microtubules extending to the edge of the cells. The actin cytoskeleton also appeared to be organised similarly in *RhoB*$^{-/-}$ BMM and Wt BMM. Cells had F-actin structures that corresponded to ruffles on the dorsal surface and contained lamellipodia and tails (Fig. 4.8B).

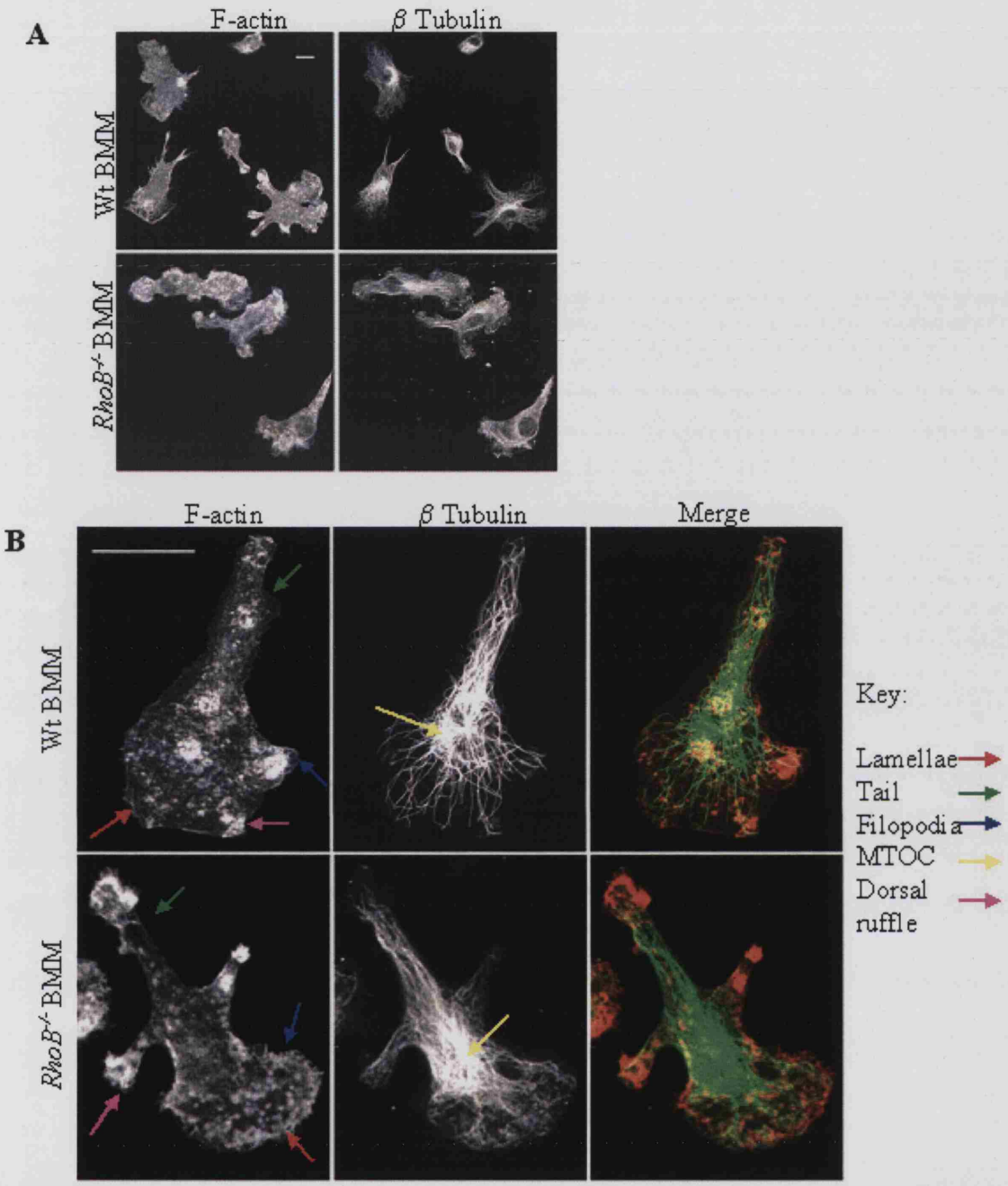

Figure 4.8: Comparison of the actin and microtubule cytoskeletons in Wt and *RhoB*$^{-/-}$ BMM

(A) Low power confocal images of the actin and microtubule cytoskeletons of Wt and *RhoB*$^{-/-}$ BMM in growth medium. (B) High power image of a Wt and *RhoB*$^{-/-}$ BMM with a polarised migratory morphology. Cytoskeletal features are indicated by arrows. Bar = 10 μm. In the merged image microtubules, visualised using anti-β tubulin antibodies, are shown in green. F-actin, visualised using rhodamine phalloidin, is shown in red.

4.10 C3-transferase and Y27632 cause rearrangements in the actin cytoskeleton

To investigate the relative contributions of RhoA and RhoB to BMM morphology the actin cytoskeleton of Wt and *RhoB*$^{-/-}$ BMM was studied in growth and starve medium and in the presence of Y27632 and t-C3 (the same conditions as were used to analyse migration). Wt BMM in growth medium had a heterogeneous range of morphologies (chapter 3.5 and Fig 4.8A); including large cells with a clearly migratory morphology, elongated cells and small rounded cells (Fig 4.9). The *RhoB*$^{-/-}$ BMM displayed an equal degree of heterogeneity (although they were slightly smaller in spread area Fig 3.8.2). In starve medium Wt BMM decreased their spread area, appeared to decrease the size of their lamellae and became elongated (Chapter 3.5 and Fig. 4.10A). *RhoB*$^{-/-}$ BMM reduced their spread area in starve medium but fewer cells become elongated compared to Wt BMM (Fig 4.9A and 4.10A). Treatment of Wt and *RhoB*$^{-/-}$ BMM with t-C3 and Y27632 caused cell flattening and some of the BMM had very elongated tails. The organisation of the actin cytoskeleton was altered by t-C3 and Y27632 in both Wt and *RhoB*$^{-/-}$ cells: there was a decrease in dorsal ruffles and rings of F-actin formed at the apical plane around the nucleus. Lamellae and lamellipodia were less obvious in these cells, however filopodia were still present (Fig 4.9).

Figure 4.9: C3-transferase and Y27632 cause rearrangements in the actin cytoskeleton

Confocal images of the basal plane of the cells showing the actin cytoskeleton of Wt and *RhoB* $^{-/-}$ BMM in: growth medium (+CSF-1), starve medium (-CSF-1), and growth medium supplemented with 5 μM Y27632 or 5 μg/ml tat-C3-transferase. Features of the actin cytoskeleton are indicated by arrows, bar = 10 μm, magnification is identical in all images. Rhodamine phalloidin was used to visualise F-actin.

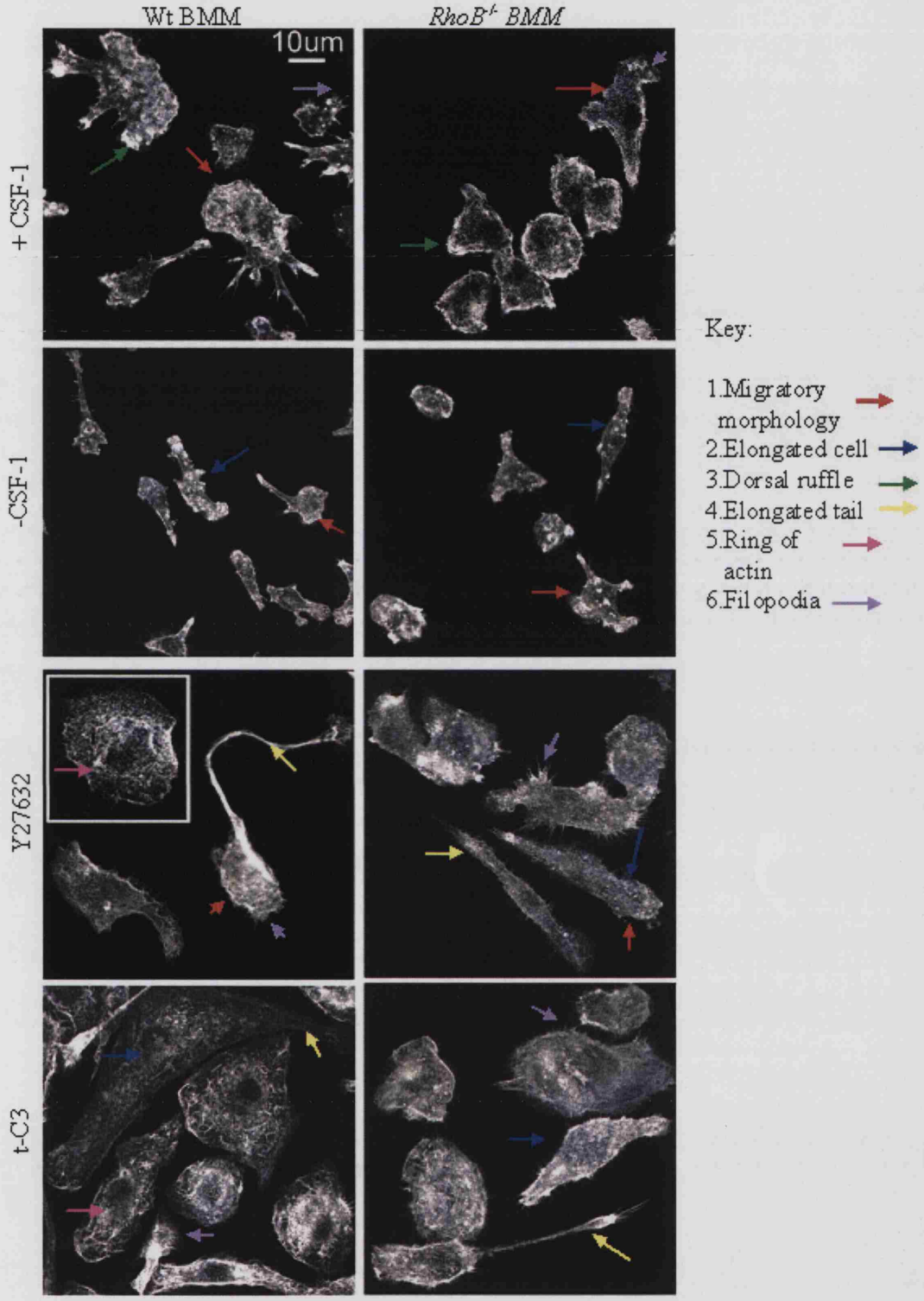
Wt BMM
RhoB-/- BMM
10um
+ CSF-1
-CSF-1
Y27632
t-C3
Key:
1.Migratory morphology
2.Elongated cell
3.Dorsal ruffle
4.Elongated tail
5.Ring of actin
6.Filopodia

4.11 Quantitative morphological analysis of C3-transferase and Y27632 treated BMM

The spread area and elongation of BMM was compared. Wt and *RhoB*$^{-/-}$ cells in growth medium had a heterogeneous array of morphologies (Fig 4.9). Therefore data from many cells was collected for morphological analysis. *RhoB*$^{-/-}$ BMM in growth medium had a slightly, but significantly, smaller spread area than Wt BMM (Fig 4.10A). Wt and *RhoB*$^{-/-}$ BMM in starve medium both had reduced spread areas. Treatment with Y27632 and t-C3 caused an increase in the spread area of both Wt and *RhoB*$^{-/-}$ BMM. This response to t-C3 and Y27632 is likely to be due to a loss of cell tension in the cells caused by inhibition of Rho (Kaibuchi et al. 1999; Narumiya et al. 1997). The final spread area in both Wt and *RhoB*$^{-/-}$ BMM treated with Y27632 was relatively similar and only slightly larger than the normal spread area of BMM in growth medium. t-C3 caused a doubling of cell spread area in Wt and *RhoB*$^{-/-}$ BMM; the final spread size of t-C3 treated *RhoB*$^{-/-}$ BMM was far smaller than the Wt BMM although the percentage increase in area was quite similar (Fig 4.10A and Table 4.4).

	- CSF-1		Y27632		t-C3 Transferase	
	Wt	*RhoB*$^{-/-}$	Wt	*RhoB*$^{-/-}$	Wt	*RhoB*$^{-/-}$
% Change in spread area	87	85	129	123	235	206

Table 4.4: The change in spread area from the spread area in growth medium of Wt and *RhoB*$^{-/-}$ BMM under different conditions. ANOVA was used to show that there were highly significant variations in the spread area of BMM ($p= 1x10^{-17}$). The spread areas of Wt and *RhoB*$^{-/-}$ BMM in each condition were compared by the Student t test. Data is representative of 3 independent experiments n=300 cells per condition.

The elongation of the BMM was measured by calculation of Aspect, which is an indication of 'roundness' of the cell. Aspect is the ratio of the longest chord through the cell and the widest span of the cell perpendicular to it. The nearer the value of aspect is to 1 the rounder the cell is. As aspect has no units it can be used to correlate elongation in a population that is heterogeneous in size (Wells et al. 2004) (Fig 4.10B). There was no significant difference in the aspect of *RhoB*$^{-/-}$ and Wt in growth medium ($p>0.05$). This indicated that deletion of RhoB did not affect cell elongation in growth conditions. Withdrawal of CSF-1 caused a statistically significant increase in elongation of Wt

BMM ($p=8.2x10^{-5}$), which made cells approximately twice as long as they were wide (Fig. 4.10C). This effect was not seen in *RhoB*$^{-/-}$ BMM, showing that *RhoB*$^{-/-}$ BMM did not elongate in starve medium, although they did decrease their spread area (Fig 4.10C and Table 4.4). Wt BMM became significantly more elongated than *RhoB*$^{-/-}$ BMM when treated with t-C3 (Fig 4.10A,C and Fig 4.9). Treatment of both Wt and *RhoB*$^{-/-}$ BMM with Y27632 caused cells to elongate equally (Fig 4.10). The aspect of Y27632 treated BMM was not as high as might be expected, considering that Y27632 treatment of fibroblasts, neutrophils and T cells caused tail retraction defects (Niggli, 2003; Smith et al. 2003; Tsuji et al. 2002). There are two reasons why the aspect may be not a great as would be expected. Firstly Y27632 treatment caused some cells to spread (Fig 4.10A) and gain a round morphology that would give an aspect close to 1. Secondly measurement of aspect is fully automated, so if the tails of Y27632 cells are thin or not straight (see Fig 4.9 for examples of this) they may not be included in the 'longest chord'. It is clear from statistical analysis that inhibition of RhoA, RhoB and ROCK activity caused a significant difference in both spread area and elongation of BMM. Deletion of RhoB had the opposite effect to inhibition of ROCK activity on spread area and elongation. Inhibition of RhoA and B activity by t-C3 caused stronger effects than inhibition of ROCK upon cell spreading and elongation particularly in Wt BMM.

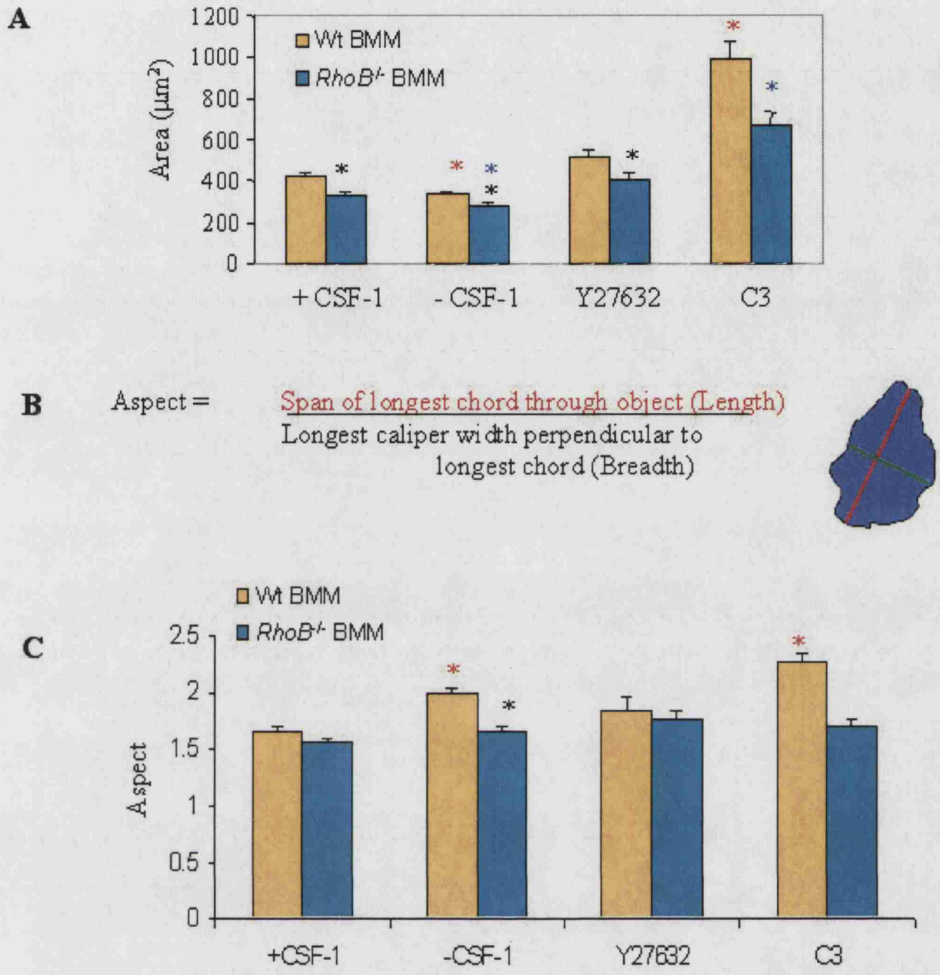

Figure 4.10: Quantitative morphological analysis of BMM

(A) Chart showing quantitative analysis of the spread area of the basal plane of Wt and *RhoB-/-* BMM in growth medium (+CSF-1), starve medium (-CSF-1), and treated with 5 μM Y27632 and 5 μg/ml tat-C3. (B) Schematic diagram showing calculation of aspect, which is division of the longest chord through the cell, shown in green, by the widest span perpendicular to it, shown in red. (C) Chart showing analysis of aspect in Wt and *RhoB*$^{-/-}$ BMM in growth medium, starve medium, and treated with 5 μM Y27632 and 5 μg/ml tat-C3-transferase. Data is representative of 3 independent experiments, n =100. * = a significant difference $p < 0.05$. *= difference between Wt and *RhoB*$^{-/-}$ BMM *= difference between Wt BMM in growth medium and any other condition. *= difference between *RhoB*$^{-/-}$BMM in growth medium and any other condition

4.12 Reduction of RhoA activity causes a decrease in dorsal ruffling and tail retraction.

To analyse the actin cytoskeleton two morphological features associated with an active actin cytoskeleton were analysed: formation of dorsal ruffles and tail retraction. For analysis of ruffling, cells were scored based on whether BMM contained 1 or more dorsal ruffles. BMM are known to form dorsal actin ruffles in response to CSF-1 stimulation (Fig 4.11A) and so ruffling was quantitated in starve medium and after 30 minutes of CSF-1 stimulation in Wt and *RhoB*$^{-/-}$ BMM. There was no significant difference in the ruffling response to CSF-1 stimulation between Wt and *RhoB*$^{-/-}$ BMM ($p > 0.05$) (Fig 4.11B). Indeed statistical analysis showed that the dorsal ruffling of *RhoB*$^{-/-}$ BMM was identical to that of Wt BMM even when BMM were incubated with inhibitors of Rho and ROCK ($p>0.05$). This showed that RhoB was not required for dorsal ruffling in BMM (Fig. 4.11B). In both Wt and *RhoB*$^{-/-}$ BMM in growth medium treated with Y27632 and t-C3 dorsal ruffling was significantly reduced ($p=2.15\times10^{-5}$), although this may have been due to the increase in cell spread area, which could have impeded dorsal ruffling. The dorsal ruffling in cells starved of CSF-1, of cells in growth medium treated with t-C3 and Y27632 was similar. Rac activity, which regulates dorsal ruffling, and is reduced by removal of CSF-1 (Fig. 6.1) may also be reduced by inhibition of Rho and ROCK (Fig 4.11B).

In a normally migrating cell the tail is retracted as part of translocation (Chapter 1.11.3). This effect is known to be dependent on cell contractility mediated by the RhoA-ROCK pathway (Kaibuchi et al. 1999). Wt BMM in growth medium, similar to migrating fibroblasts, had variable tail lengths. Y27632 treatment of fibroblasts caused tail retraction defects giving rise to elongated tails (Narumiya et al. 1997). Analysis of the movies of Y27632-treated BMM indicated that Y27632 had a similar effect on tail retraction in BMM (Fig 4.11C and Movie 4.1 and 4.3). Tail length was analysed by measurement of the distance from the nucleus to the end of the tail using stills from the time-lapse series (Fig 4.1B). There was no significant difference in tail retraction of *RhoB*$^{-/-}$ BMM under all conditions ($p>0.05$). This demonstrated that RhoB did not contribute to tail retraction in BMM (Fig. 4.11D). Inhibition of RhoA and ROCK activity though treatment of BMM with t-C3 and Y27632 respectively caused an increase in tail length (Fig 4.11D). This shows that both RhoA and ROCK activity are required for tail retraction in BMM.

Figure 4.11: Reduction of RhoA activity alters ruffling and tail retraction

(A) Confocal image of the dorsal surface of Wt BMMs showing F-actin ruffles. (B) Graph showing percentage of the population of Wt and *RhoB*$^{-/-}$ BMM ruffling in Growth medium (G), starve medium (S), 30 min stimulation with CSF-1, Growth medium treated with 5 μM Y27632 or 5 μg/ml tat-C3. (C) Phase contrast image of Wt BMM in growth medium and Wt BMM in growth medium treated with 5 μM Y27632 for 4 hours. (D) Graph showing length from nucleus to end of cell tail of Wt and *RhoB*$^{-/-}$ BMM in growth medium (control) and growth medium treated with 5 μM Y27632 or 5 μg/ml tat-C3 both for 4 hours. Data is shown mean ± SEM pooled from 3 independent experiments, n =100. * = A significant difference $p < 0.05$. *= Difference between Wt and *RhoB*$^{-/-}$ BMM *= Difference between Wt in growth medium and any other condition. *= Difference between *RhoB*$^{-/-}$ BMM in growth medium and any other condition

A

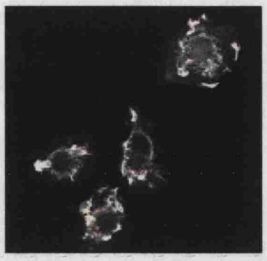

B

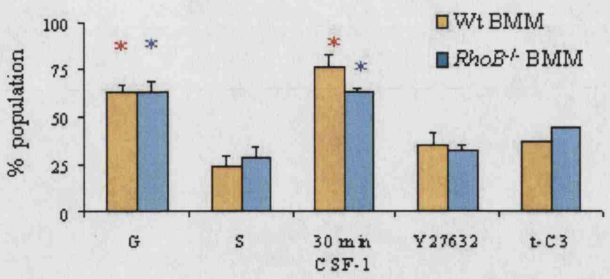
% population
100
75
50
25
0
Wt BMM
RhoB-/- BMM
G
S
30 min CSF-1
Y27632
t-C3

C

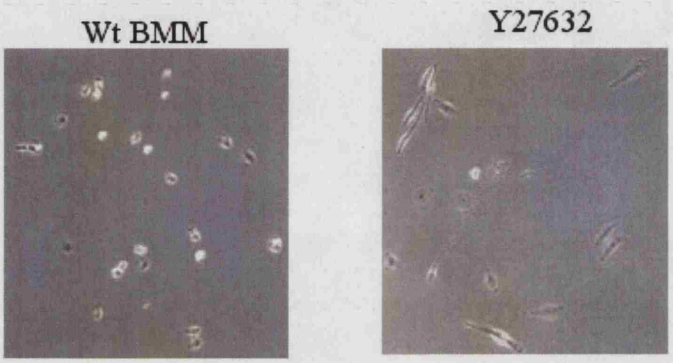
Wt BMM
Y27632

D

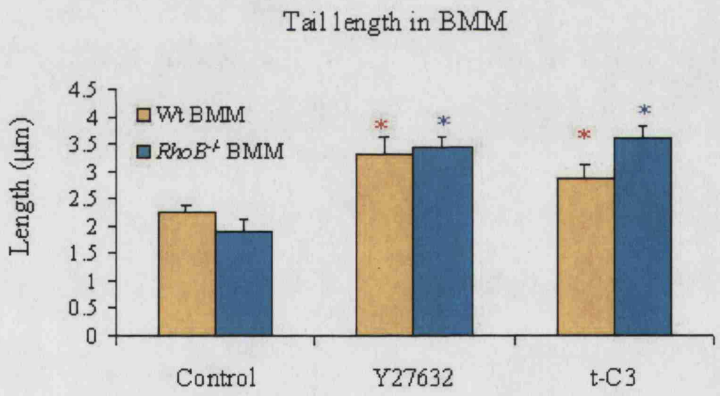
Tail length in BMM
Length (µm)
4.5
4
3.5
3
2.5
2
1.5
1
0.5
0
Wt BMM
RhoB-/- BMM
Control
Y27632
t-C3

4.13 Conclusions and discussion:

The results described in this chapter show that the process of BMM migration is similar to other cells types and is affected by external environmental features such as; substrate, withdrawal of growth factors and chemoattractants (Friedl, 2004; Hogg et al. 2002). It is also clear that a dynamic actin cytoskeleton is essential for migration of BMM and that Rho family GTPases, similarly to fibroblasts, neutrophils and neurons, play a key role in this (Govek et al. 2005; Hall and Nobes, 2000).

The chemokine CSF-1 is known to promote chemotaxis and promote cell spreading and formation of dorsal ruffles in BMM (Wells et al. 2004). Withdrawal of CSF-1 from BMM caused reduced migration and a change their morphology: they become elongated, lose lamellae and reduce dorsal ruffling (Wells et al. 2004). This indicates that it is probably the first stage of cell migration, cells polarising to form a migratory morphology (Ridley et al. 2003), which is affected most by withdrawal of CSF-1. Rac and Cdc42 have been shown to play a central role in polarisation of several cell types including leukocytes (Etienne-Manneville, 2004; Weiss-Haljiti et al. 2004), and are known to be required for macrophage chemotaxis to CSF-1 (Ridley, 2001c). Intriguingly in neutrophils and T-cells it is clear that the Rac1 and Rac2 isoforms each have an individual function in migration and chemotaxis (Chapter 1.14) (Gu et al. 2003), and in macrophages there is evidence that this is also the case (Jones et al. 2003; Weiss-Haljiti et al. 2004). Rac1-null BMM are more elongated but their migration and chemotaxis is unaffected (Wells et al. 2004).

Deletion of *RhoB* appears to enhance rather than reduce cell migration. This suggests that RhoB may be acting as a brake on the process of cell migration. The *RhoB*$^{-/-}$ BMM do not adopt as clear a migratory morphology as the Wt cells probably because they are moving more quickly through the cycle of migration. In support of this hypothesis *RhoB*$^{-/-}$ BMM do not reduce their motility or change their morphology in starve medium to the same degree that Wt BMM do. Therefore either the 'starvation' phenotype, seen in the absence of CSF-1, is either reduced in *RhoB*$^{-/-}$ BMM or occurs more slowly (Chapter 3.8).

Deletion of RhoB did not alter the dynamic properties of the actin cytoskeleton in BMM, formation of dorsal ruffles, retraction of tails and cell elongation was the same as

seen in Wt BMM. *RhoB*$^{-/-}$ BMM also had the same positive response to CSF-1 stimulation as Wt BMM. They were able to chemotax towards a CSF-1 source and form dorsal ruffles and podosomes in response to stimulation with CSF-1 (Chapter 3.8). Indeed several cell types that lack RhoB activity do not seen to have any apparent differences in the organisation of the actin cytoskeleton under growth conditions (Adini et al. 2003; Conway et al. 2004; Sandilands et al. 2004). A clue to which processes are regulated by RhoB may lie in the fact *RhoB*$^{-/-}$ BMM are less well spread and seem to have different migratory properties (such as speed of migration and turning) on different substrata. In fibroblasts derived from *RhoB*$^{-/-}$mice spreading and adhesion defects are also reported (Liu et al. 2001; Sandilands et al. 2004). This may implicate RhoB in the regulation of cellular adhesion rather than actin dynamics (this is addressed further in chapter 5).

Inhibiting Rho activity with C3-transferase, had a very strong negative impact on macrophage migration. Since deletion of RhoB did not inhibit cell migration, and BMM do not express RhoC this means that RhoA activity is specifically required for cell migration. Inhibition of Rho activity reduces cell migration and chemotaxis in several leukocytes (Ashida et al. 2001; Chellaiah et al. 2000b; Saito et al. 2002; Smith et al. 2003; Vicente-Manzanares et al. 2002). But this is the first indicatation that RhoA activity specifically, rather than RhoB or RhoC, is essential for BMM migration.

Y27632 inhibits Rho signalling to cell contractility via the ROCK and myosin light chain (MLC) pathway (Uehata et al. 1997). Similarly to neutrophils, monocytes, T cells and fibroblasts, Y27632 treated BMM are capable of forming a migratory morphology and also are able to move their nucleus, which shows that the ROCK activity is not required for cell polarisation (Niggli, 2003; Nobes and Hall, 1999; Smith et al. 2003, Worthylake et al. 2001), although this is not the case in endothelial cells (Wojciak-Stothard and Ridley, 2003). Inhibition of ROCK does impede tail retraction in BMM and cause cell spreading, similarly to T cells, monocyte and neutophils (Niggli, 2003; Smith et al. 2003, worthylake et.al 2001). Indeed in monocytes, both Y27632 and C3 transferase inhibited transendothelial migration as the tails of these cells cannot be retracted (Worthylake et.al. 2001, Worthylake and Burridge. 2003). Y27632-treated BMM were unable to migrate, which suggests that tail retraction is rate-limiting for cell migration in BMM. The impact of Y27632 treatment on cell migration varies depending upon cell type; in fibroblasts Y27632 promotes cell migration (Nobes and Hall, 1999;

Tsuji et al. 2002), whereas in leukocytes including T cells, osteoclasts, neutrophils and BMM Y27632 inhibits migration (Chellaiah et al. 2000b; Niggli, 2003; Smith et al. 2003). Intriguingly in monocytes the effect of Y27632 treatment on monocyte morphology and migration is substrate dependant. On non-charged substrates such as poly-l-lysine monocytes have a spread morphology very similar to that observed in the BMM in this study. On ICAM-1 or VCAM monocytes exhibit membrane protrusions (Worthylake and Burridge. 2003). It would be interesting to determine whether Y27632 causes defects in actomyosin contractility that then inhibit the turnover of adhesions or vice versa in BMM .

RhoA plays an important role in the organisation of the actin cytoskeleton, unlike RhoB. Overexpression of RhoA in fibroblasts is known to promote formation of stress fibres, focal adhesions and to increase cellular contractility (Kaibuchi et al. 1999; Ridley and Hall, 1992). Inhibition of Rho activity in several cell types causes cell spreading, loss of stress fibres, fine actin cables and promotes cell spreading (Ridley, 2001b), in epithelial cells and fibroblasts inhibition of Rho activity has been correlated with a complete loss of in cellular tension (Kaibuchi et al. 1999). Little is known about the effect of C3-transferase on primary macrophages. In macrophage cell lines microinjection with C3-transferase caused cell spreading and loss of fine actin filaments across the cells (these fine actin filaments are not as apparent in BMM) (Allen et al. 1997). Structures that may correspond to filopodia in BMM treated with C3-transferase were still apparent. In contrast to Bac1 macrophages (Allen et al. 1997), C3-transferase treated BMM had such a flattened morphology that no obvious lamellae were present in the cells. Indeed, BMM treated with C3-transferase were generally unable to form dorsal ruffles and changed their actin organisation significantly. These changes could be considered to be caused by a loss of acto-myosin based tension.

In conclusion, RhoA and RhoB play very distinct roles in the process of cell migration. RhoA activity is essential for cell migration whereas RhoB activity is not. Morphologically, *RhoB*$^{-/-}$BMM are less well spread than Wt BMM which may suggest changes in cellular adhesion or increased contractility. BMM lacking RhoA and ROCK activity have reduced contractility and cannot retract their trailing ends. It is possible that RhoB may be acting as a negative modifier of RhoA activity (Prendergast, 2001). C3-transferase treated BMM (with no Rho activity) have elongated tails but deletion of RhoB alone does not affect the length of cell tails. This suggests that RhoA alone may

be responsible for signalling to this pathway. ROCK activity is also required for tail retraction in BMM showing that; ROCK is primarily regulated by RhoA and not RhoB in the process of tail retraction in BMM.

Chapter 5: The role of RhoB in BMM adhesion and spreading

5.1 Introduction

For a migrating cell the regulation of adhesion is a delicate balance: the cell must adhere to its surroundings sufficiently strongly to generate the frictional forces necessary for migration without becoming immobilized. Adhesion between a cell and the ECM is mediated through transmembrane proteins such as integrins and proteoglycans such as lectins and syndecans (Hynes. 2002; Ivetic and Ridley. 2004). Integrins are not only there for the purposes of attachment but are also signalling units that a cell uses to transduce information, which allows a cell to respond physically to its immediate environment (Hynes. 2002). Integrins are the principal receptors used by mammalian cells for binding extracellular matrix proteins; including collagens, fibronectin, and laminins. In several cell types the variation in affinity for a particular matrix has been correlated with the cell surface expression pattern of various integrins (Friedl et al. 1998a; Hogg et al. 2002; Worthylake and Burridge, 2001). Studies where integrin activity has been blocked using antibodies showed that integrin activity is required for cell adhesion and formation of adhesive structures. These studies also show that the integrins used for adhesion to a given substrate can vary between cell types. For instance, LFA-1 ($\alpha L\beta 2$) is used by T cells to adhere to ICAM-1 (Hogg et al. 2004), macrophages use Mac-1 ($\alpha M\beta 2$) as well as LFA1 for adhesion to ICAM-1 (Zen and Parkos, 2003). It is important to note that although a particular integrin pair may predominate in the adhesion to a given substrate other integrin pairs may be involved. For example $\alpha v\beta 3$ is important for adhesion to vitronectin but $\alpha v\beta 1$ and $\alpha v\beta 5$ integrins have also been shown to play a role in adhesion and migration on vitronectin (Delannet et al. 1994). Integrins associate with several signalling molecules which can promote reorganisation of the cytoskeleton, such as FAK, Src family proteins, MAPK family proteins and activators of Rho family GTPases (Burridge and Wennerberg, 2004; Geiger and Bershadsky, 2002; Hood and Cheresh, 2002).

Rho proteins are important for regulation of cell adhesion, RhoA is transiently inactivated during fibroblast adhesion (Arthur and Burridge, 2001). Activation of RhoA has been shown to promote disassembly of focal contacts in fibroblasts, the activity of Dia, the Rho effector is associated with formation of focal contacts at the leading edge of motile cells (Tsuji et al, 2002) (Chapter 1.11.3). Inhibition of Rho using C3-

transferase causes spreading in several different cell types (Ridley, 2001a). *RhoB*$^{-/-}$ fibroblasts have a decreased spread area on fibronectin although the mechanism that causes this is not known (Liu et al. 2001; Sandilands et al. 2004).

5.2 Deletion of RhoB does not affect proliferation of BMM

To obtain BMM, bone marrow haematopoietic cells were flushed from the fibula of Wt and *RhoB*$^{-/-}$ mice and were initially plated onto bacterial plastic (Chapter 2.2.3). After 3 days of differentiation in macrophage growth medium there were consistently fewer *RhoB*$^{-/-}$ pre-macrophage suspension cells than Wt (Fig. 5.1A). The second differentiation step of pre-macrophages in growth medium on bacterial plastic also yielded fewer *RhoB*$^{-/-}$ BMM than Wt BMM (data not shown). This effect could either be due to a proliferation defect or an adhesion defect. To differentiate between the two, the proliferation of Wt and *RhoB*$^{-/-}$ BMM on fibronectin-coated plastic and uncoated glass was assayed (Chapter 2.6.12). *RhoB*$^{-/-}$ BMM proliferated at the same rate as Wt BMM on both fibronectin-coated plastic and uncoated glass (Fig 5.1B,C). This showed that deletion of RhoB did not affect the proliferation of BMM.

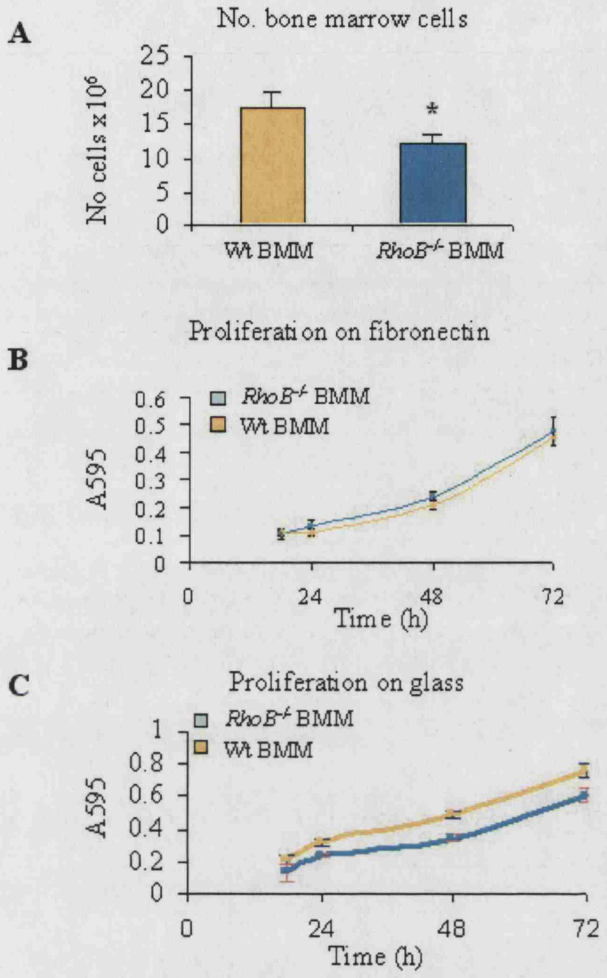

Figure 5.1: Proliferation of BMM is not affected by deletion of RhoB

(A) Bone marrow cells from a fibula flush were seeded at 10^6 cells/ml onto bacteriological plates and incubated for 3 days in growth medium. Cell number was determined using a haemocytometer. (B) Proliferation of Wt and *RhoB*$^{-/-}$ BMM in growth medium on fibronectin and (C) glass was measured using the adhesion/ proliferation assay (Section 2.6.12). Cell density was measured at 18, 24, 48 and 72 h after seeding. *= significant difference ($p>0.05$) between Wt and *RhoB*$^{-/-}$ BMM.

5.3 *RhoB*$^{-/-}$ BMM do not adhere to ICAM-1 and glass as well as wt BMM

The *in vivo* function of leukocytes requires attachment to endothelial membranes, and this has been shown to be mediated though ICAM-1, amongst other molecules (Hogg et al. 2002). For leukocytes to move to a site of infection they must attach to and migrate through blood vessels and the extracellular matrix between tissue cells (Worthylake and Burridge, 2001). The extracellular matrix is known to comprise of fibronectin and vitronectin amongst other molecules (Bosman and Stamenkovic, 2003). To determine if BMM adhere to different substrata equally efficiently the attachment of BMM to ICAM-1, fibronectin and glass was measured (N.B. in serum containing medium, glass is predominantly coated with the vitronectin present in serum (Hayman et al. 1983)). There was no difference in the adhesion of Wt and *RhoB*$^{-/-}$ BMM for fibronectin or the rate of attachment to fibronectin (Fig 5.2A). The *RhoB*$^{-/-}$ BMM had a reduced adhesion to both glass and ICAM-1 and their rate of attachment was also decreased (Fig 5.2B, C). A comparison of these adhesion assays shows that both Wt and *RhoB*$^{-/-}$ BMM have a higher adhesion to glass than both ICAM-1 and fibronectin. This might account for their high migratory rate upon fibronectin compared to glass (Chapter 4.2 and 4.6).

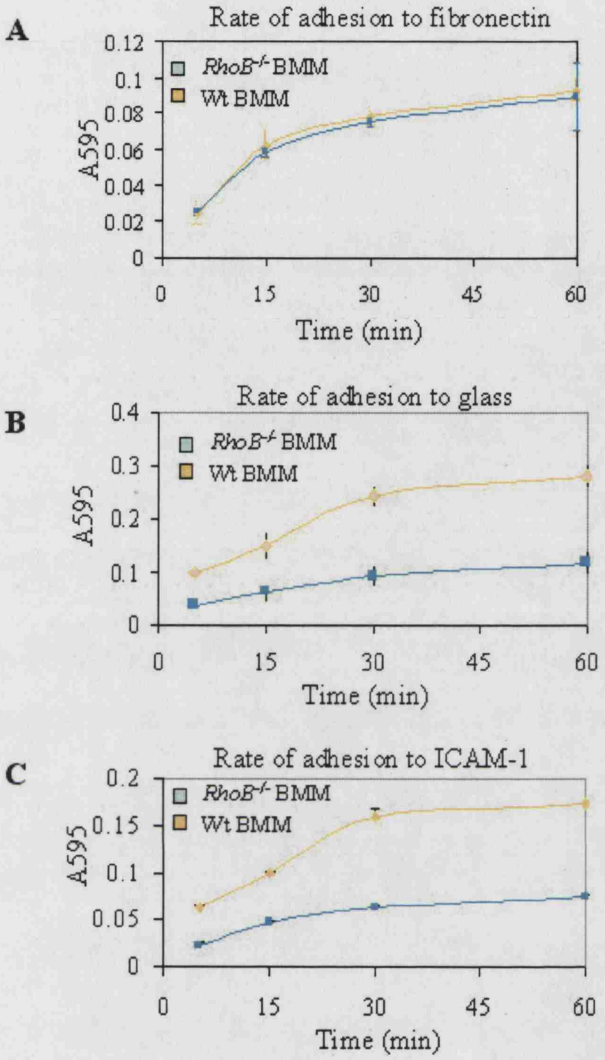

Figure 5.2: *RhoB*$^{-/-}$BMM do not adhere to ICAM-1 or glass as well as Wt BMM

(A) Wt and *RhoB*$^{-/-}$ BMM were subjected to adhesion assays on fibronectin (B) glass and (C) ICAM-1. Cells were seeded onto the substrates at $5x10^4$ cells/ml and cell density was measured at 5, 15, 30 and 60 min after seeding. Data shown mean ± SEM pooled from three independent experiments.

5.4 Analysis of integrin levels in BMM

Macrophages are known to express β1, β2 and β3 integrins (Zlotnik, 2000). To determine whether there was a link between the differences in adhesion observed in Wt and *RhoB*$^{-/-}$ BMM and integrin expression cell surface levels of β1, β2 and β3 integrins were analysed using flow cytometry (Two different flow cytometers were used for these experiments as the flow cytometer was upgraded during the time these experiments were carried out (Chapter 2.7). The data from the new machine is shown in Fig 5.3A. Data from the older machine is shown in Fig 5.3B. The data shown is representative of three separate experiments). Quantitation of the cell surface expression of integrins shows that the cell surface expression of β1 was similar in the Wt and *RhoB*$^{-/-}$ BMM (Fig. 5.3B), indeed there may be a slight increase in the cell surface expression of β1 integrin in *RhoB*$^{-/-}$ BMM (Fig. 5.3C). In contrast cell surface expression of β2 and 3 integrins was reduced in *RhoB*$^{-/-}$BMM. This can be seen by the left shift of the peak of fluorescence β2 (Fig. 5.3A) and β3 (Fig. 5.3B) integrins in *RhoB*$^{-/-}$ BMM. Quantitative analysis of fluorescence shows that both Wt and *RhoB*$^{-/-}$ BMM express β1, β2 and β3 integrins, however, the level of cell surface expression of both β2 and β3 integrin was decreased by approximately 35% in *RhoB*$^{-/-}$ BMM (Fig. 5.3C). β2 integrin is required for attachment of leukocytes to ICAM-1 and for BMM to bacteriological plastic (Hogg et al. 2004; Paulnock, 2000; Zen and Parkos, 2003). There are 3 types of β2 containing integrin pairs expressed on BMM αLβ2, αMβ2 and αDβ2. Reduced cell surface expression of β2 integrin in *RhoB*$^{-/-}$ BMM would account for the decrease in adhesion of these cells to ICAM-1 (Fig 5.2C) and explain why the yield of fully differentiated *RhoB*$^{-/-}$ BMM from a fibula flush was consistently lower than Wt BMM (Section 5.1). β3 integrin is the major integrin involved in adhesion to vitronectin, and therefore serum coated glass (it forms part of the vitronectin receptor αvβ3, (Zlotnik, 2000) and reduction in cell surface expression in *RhoB*$^{-/-}$ BMM would explain the adhesion defects of these cells to glass (Fig 5.2B).

A

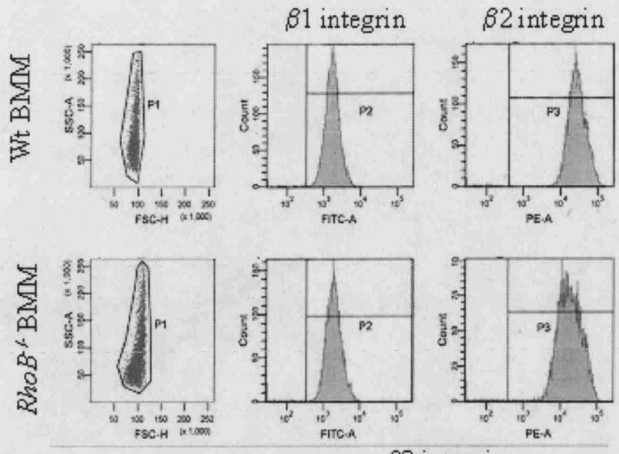

B

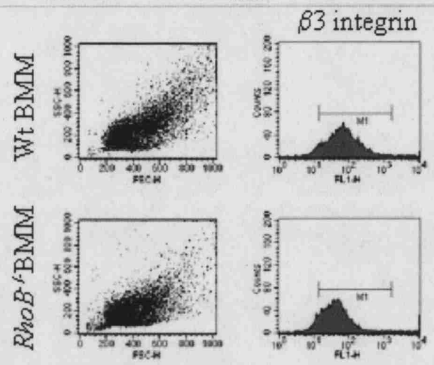

C

	β1 Integrin		β2 Integrin		β3 Integrin	
	% pop gated	Mean fluor	% pop gated	Mean fluor	% pop gated	Mean fluor
Wt BMM	99	1656	99	27273	93	67
RhoB$^{-/-}$ BMM	99	1918	98	17548	87	44

Figure 5.3: Analysis of integrin expression in Wt and *RhoB*$^{-/-}$BMM

(A) FACS analysis of an asynchronous growing population of Wt and *RhoB*$^{-/-}$ BMM for cell surface expression of β1, β2 integrin. Dot plots of cells are shown. (B) FACS analysis of an asynchronous growing population of Wt and *RhoB*$^{-/-}$ BMM for cell surface expression of β3 integrin. Dot plots of cells are shown. (C) Quantitation of geometric mean of the fluorescence from all samples. FACS plots shown are representative of three independent experiments. Data in (C) is pooled from three independent experiments.

5.5 Analysis of the changes in BMM morphology during spreading

RhoB$^{-/-}$ BMM have a defect in adhesion to glass, but does the adhesion defect affect the spreading process? To analyse this, the morphology of the actin cytoskeleton and formation of adhesions during cell spreading was studied after 10 and 30 min of spreading on glass. The co-localisation of F-actin and paxillin was used as to locate the basal plane of a cell. The same density of cells was used in these experiments as for the adhesion assays (described in section 5.2.). Analysis of the actin cytoskeleton in spreading Wt and *RhoB*$^{-/-}$ BMM showed that after 10 min after plating cells had spread slightly and had paxillin localised in the centre of the cell and on the edge of the membrane (Fig. 5.4A). Wt BMM after 30 min of spreading had maintained the same distribution of paxillin seen at 10 min of spreading, and had increased their spread area slightly and lamellipodia were also present (Fig. 5.4B). The *RhoB*$^{-/-}$ BMM conversely appeared to have a larger spread area and had distributed their paxillin more evenly across the basal surface of the cell (Fig. 5.4B). Paxillin forms part of focal adhesions (Turner. 2000), so the even distribution of paxillin across the basal surface of *RhoB*$^{-/-}$ BMM may suggest that these cell have more firmly attached to the glass than their Wt compatriots. Quantitation of spread area of Wt and *RhoB*$^{-/-}$ BMM during cell spreading showed that after 10 min of adhesion Wt and *RhoB*$^{-/-}$ cells spread to a similar area. *RhoB*$^{-/-}$ BMM have a slight but significant increase in spread area at 30 min compared to Wt BMM ($p<0.05$). The spread area of both Wt and *RhoB*$^{-/-}$ BMM at 24 h is significantly reduced compared to that of BMM at 10 and 30 min of spreading ($p=1.0\times10^{-10}$ calculated by ANOVA) (Fig 5.4C). Calculation of aspect (Chapter 2.6.9) shows that during the initial stages of spreading Wt and *RhoB*$^{-/-}$ BMM were rounded and they become more elongated by 24 h. There is a significant change in elongation of BMM during spreading ($p=4.4\times10^{-12}$ calculated by ANOVA) (Fig. 5.4D). Together this data indicated that the reduction of spread area observed in BMM spread for 24 h occurs concomitantly with an increase in cell elongation (Fig 5.4 C,D). This suggests that the reduction in spread area of BMM may be caused by shape change and the formation of a more elongated morphology. The distribution of tyrosine-118 phosphorylated paxillin (Y-118 paxillin), which has been found in small focal contact-like adhesions in BMM (Pixley et al. 2001), was compared in Wt and *RhoB*$^{-/-}$ BMM after 24 h of spreading (Fig 5.4E). There were no apparent differences in the size or distribution of the focal contacts in *RhoB*$^{-/-}$ BMM and Wt BMM.

Figure 5.4: Analysis of the changes in BMM morphology during spreading

Confocal images of the basal plane of Wt and *RhoB*$^{-/-}$ BMM in growth medium stained for F-actin and paxillin seeded for 10 min (A) and 30 min (B) onto glass to show the changes in morphology and cell adhesions during spreading. In the merged image paxillin, visualised using anti-paxillin antibodies, is shown in green. F-actin, visualised using rhodamine phalloidin, is shown in red, bar = 10 μm. (C) Graph showing quantitative analysis of the spread area of the basal plane of Wt and *RhoB*$^{-/-}$ BMM seeded onto glass for 10 min, 30 min and 24 h . (D) Graph showing analysis of aspect in Wt and *RhoB*$^{-/-}$ BMM seeded onto glass for 10 min, 30 min and 24 h . *= significant difference ($p>0.05$) between Wt and *RhoB*$^{-/-}$ BMM. Data is pooled from three independent experiments. (E) Confocal images of Wt and *RhoB*$^{-/-}$ BMM stained for pY118-paxillin to indicate the presence of focal contacts. Focal contacts indicated by red arrow, bar = 10 μm.

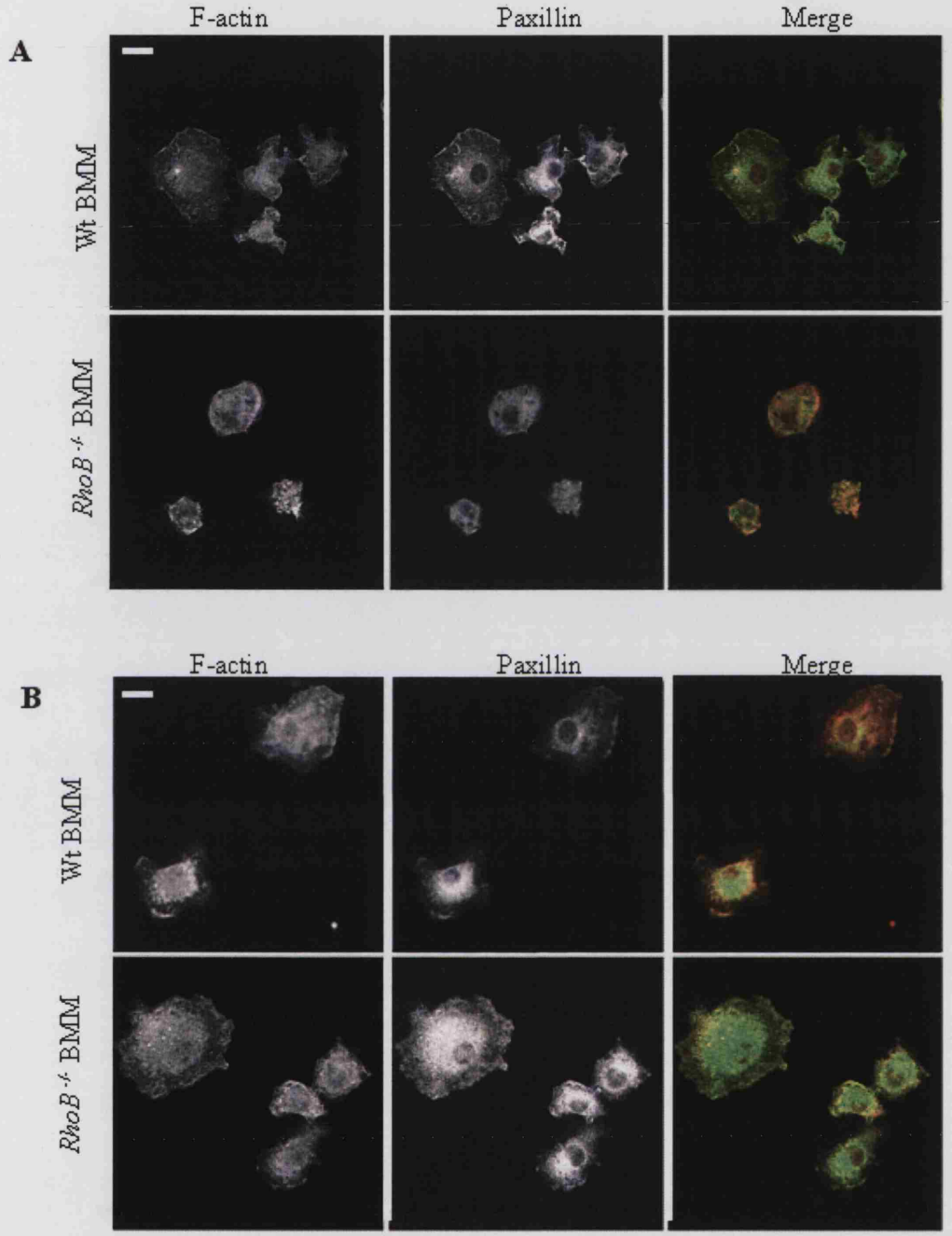
A
F-actin
Paxillin
Merge
Wt BMM
RhoB -/- BMM
B
F-actin
Paxillin
Merge
Wt BMM
RhoB -/- BMM

C

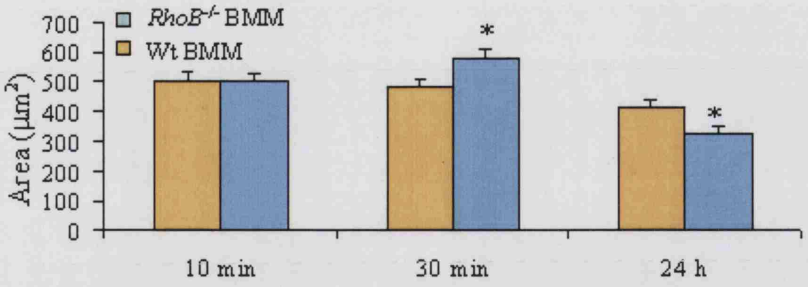
RhoB-/- BMM
Wt BMM
Area (µm2)
700
600
500
400
300
200
100
0
*
*
10 min
30 min
24 h

D

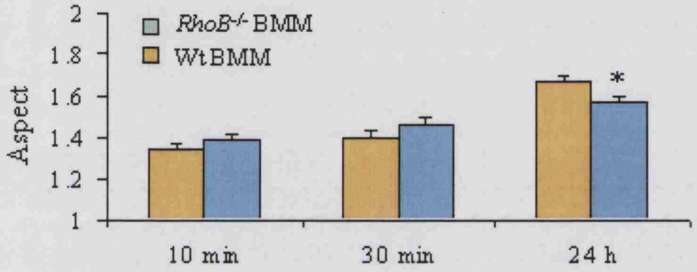
RhoB-/- BMM
Wt BMM
Aspect
2
1.8
1.6
1.4
1.2
1
*
10 min
30 min
24 h

E

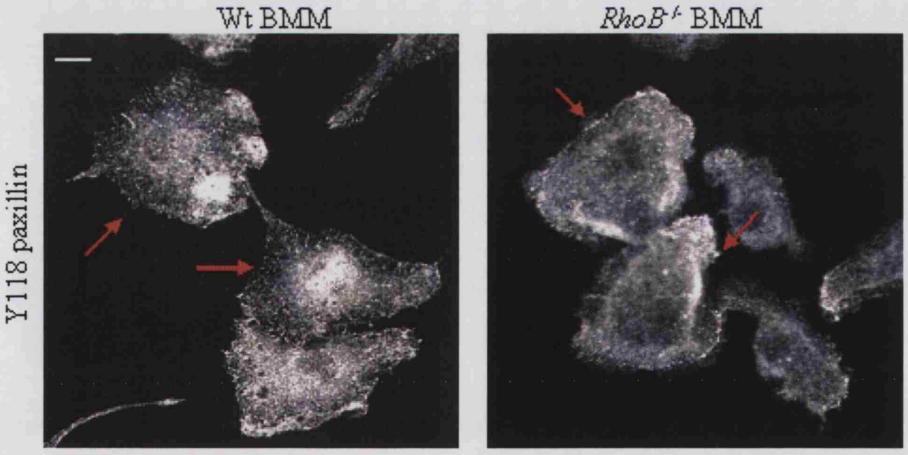
Wt BMM
RhoB-/- BMM
Y118 paxillin

5.6 The principles and application of total internal reflection fluorescent microscopy to cell spreading

To make a more detailed comparison of cell spreading between Wt and *RhoB*$^{-/-}$ BMM the movements of the cell membrane during cell spreading were quantitated and compared. This was done using total internal reflection fluorescence (TIRF) microscopy. The TIRF microscope works by directing a laser beam through a glass prism such that it is incident upon the aqueous medium in the cells are growing at a critical angle ($\alpha\theta$) (Fig. 5.5A). The light beam then totally internally reflects (rather then refracts) though the interface of glass and the aqueous phase. Totally internally reflected light generates an electromagnetic field that is very thin (200 nm at most) in the aqueous phase, which is at the same frequency as the incident light, exponentially decaying in intensity with distance from the surface. The electromagnetic field is capable of exciting fluorophores. Thus fluorophores that are located within the bottom 200 nm of the aqueous phase, which corresponds with the basal plane of the cells, are selectively excited (Lacey, 1999). This allows visualisation of events that occur close to or at the basal membrane only, which was useful for analysis of cell spreading. In these experiments BMM were stained to allow movements of the cell membrane during spreading to be visualised (Dubin-Thaler et al. 2004). The slight drawback of this system is that the coverslip used for the experiments must be of the same refractive index as the prism, so glass coverslips coated with fibronectin were used for all analyses. It would have been interesting to have conducted these experiements on glass alone and on ICAM-1 coated glass.

A combination of phase-contrast and TIRF microscopy was used to differentiate attachment of a cell to a substrate and the spreading of the cell on that substrate. For instance, a phase contrast image of Wt BMM that had been plated for 60 min shows that several cells had attached to the glass (Fig. 5.5B). The TIRF image of the same field of view shows that only a fraction of these cells had fully spread onto the glass (Fig. 5.5C,D). This method was used to compare the percentage of the population of Wt and *RhoB*$^{-/-}$ BMM that had attached and spread on fibronectin coated-glass. After 60 min significantly more of the *RhoB*$^{-/-}$ BMM had attached and spread to the fibronectin coated-glass than Wt (Fig. 5.5E). This showed that BMM in general do not necessarily spread immediately upon attachment to a substrate but *RhoB*$^{-/-}$ BMM were more likely to spread following attachment to fibronectin.

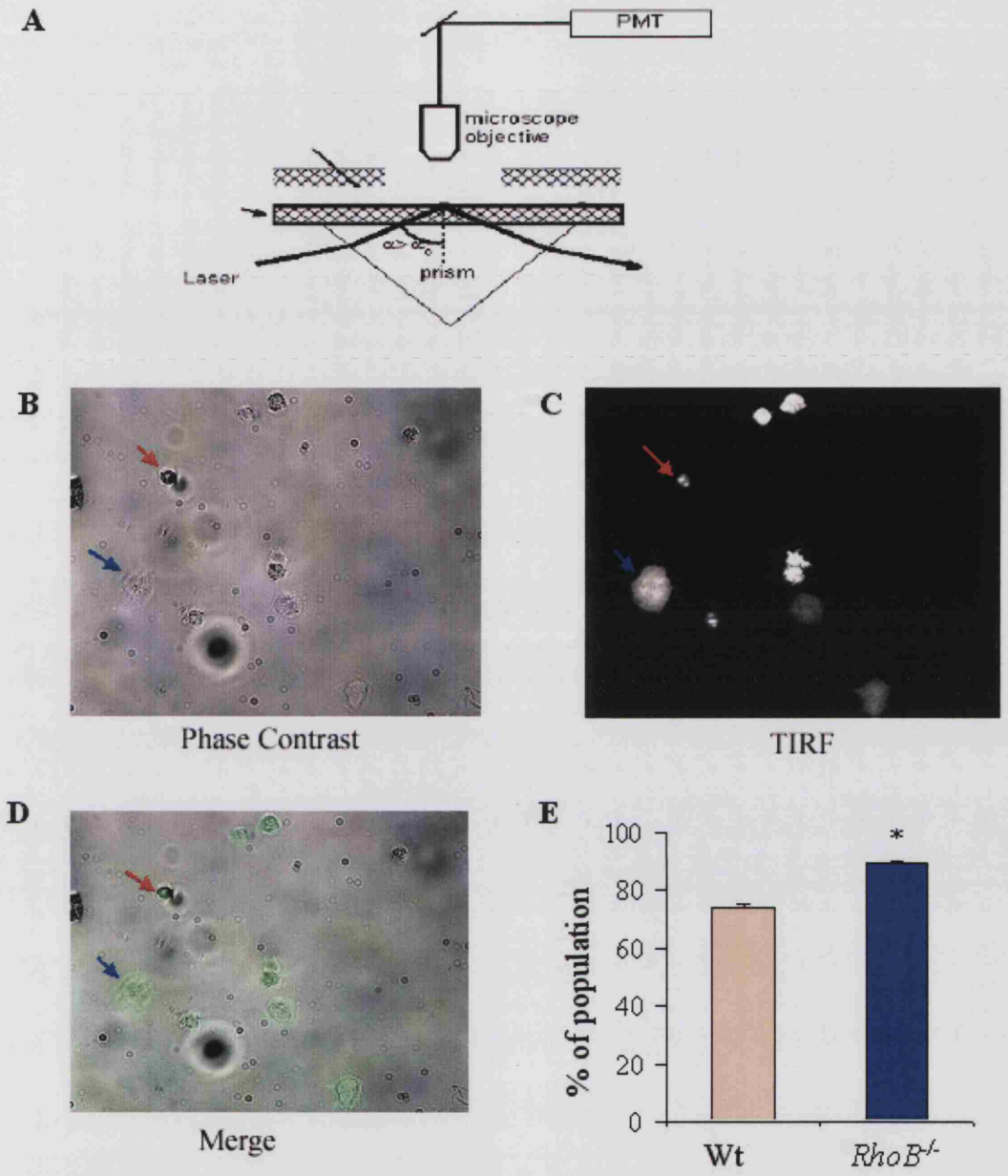

Figure 5.5. The principles and application of total internal reflection fluorescent microscopy to cell spreading

(A) Schematic diagram showing the principles of a TIRF microscope. (B) Phase contrast and (C) TIRF image of Wt BMM seeded onto fibronectin coated glass for 60 min. (D) Phase-contrast image of Wt BMM with TIRF image superimposed upon it, indicating a cells that has spread and giving a large TIRF signal (blue arrow) and a cell that has attached but not spread giving a small TIRF signal (red arrow). (E) Graph showing the percentage of a Wt and *RhoB*$^{-/-}$ BMM population that have attached and spread on fibronectin-coated glass 60 min after seeding. Data is pooled from 3 independent experiments, n=50 cells. *= significant difference between Wt and *RhoB*$^{-/-}$ BMM ($p>0.05$).

5.7 Analysis of the cell membrane movements on the basal plane of the cell during spreading.

The first 10 min of spreading 30 Wt and 30 *RhoB*$^{-/-}$ BMMs spreading was captured using TIRF time-lapse microscopy, (a representative image of a Wt and *RhoB*$^{-/-}$ BMM is shown in the figures) (Video 5.1 and 5.2, Fig. 5.6A). Differences in cell membrane movements were measured by generating a binary thresholded image of the spreading cell, in which the edge of the cell was defined manually using the Cell Outliner program (Dubin-Thaler et al. 2004) (Chapter 2.8.5). An image showing the edge of the cell membrane during cell spreading was then created for each cell (Fig. 5.6B). The edge of the cell was then broken down into 360 data points, corresponding to each degree of a circle (radians) (Fig 5.6C). The position of each radian in time for a spreading cell could be analysed using a custom C program, Creep (Dubin-Thaler et al. 2004) (Chapter 2.8.6). This gives information about the movement of each point (radian) of the cell membrane in time and space during cell spreading. A 3D graph shows displacement of the cell membrane during cell spreading on the z-axis plotted against points measured in the cell membrane (radians, x-axis) and elapsed time (y-axis) (Fig 5.6D). Analysis of this plot showed that the Wt BMM slowly increased its spread area over time and different parts of the cell membrane moved at different times during spreading, which has been termed non-isotropic spreading (Dobereiner et al. 2004). The *RhoB*$^{-/-}$ BMM increased its spread area more rapidly and all parts of the cell membrane appeared to move outwards at the same time during spreading, known as isotropic spreading. However this type of plot only gives a qualitative impression of cell spreading and the data from individual cells spreading cannot easily be cross-correlated to analyse variations between cells of a whole population moving.

A more analytically useful plot was the velocity density plot in which the rate of change of movement of the cell membrane (velocity) was plotted as a 'temperature scale' against time and radians (Fig 5.6E). The velocity density plots of two BMM of each genotype are shown to illustrate the variability of spreading within the population of Wt and *RhoB*$^{-/-}$ BMMs. Although the spreading between Wt and *RhoB*$^{-/-}$ was not obviously different in terms of periodicity of membrane movement, the *RhoB*$^{-/-}$ BMM appeared to extend and retract their membrane at a wider range of speeds compared to Wt BMM (shown as red and blue regions on the velocity density plot). The data from the velocity density plots is interesting but it only allows comparison of one Wt and one

RhoB$^{-/-}$ BMM. There was considerable variation in the dynamics of spreading between Wt and *RhoB*$^{-/-}$ BMM even within the 30 cells analysed, some cells rapidly spread to a large area and others only spread a small amount, some spread all parts of their membrane equally whereas other cells preferentially spread in one particular direction (Fig 5.6E). This is perhaps not surprising as the morphology of the basal plane of both Wt and *RhoB*$^{-/-}$ BMM after 10 min spreading was quite heterogeneous (Fig 5.4A and C).

Figure 5.6: Analysis of cell membrane movements on the basal plane of the cell during spreading

(A) Montage of TIRF images of Wt and *RhoB*$^{-/-}$ BMM stained with CFSE, spreading on fibronectin-coated glass. Time in seconds between images is indicated in the bottom right hand corner of the image. (B) Montage of binary thresholded images of the spreading Wt and *RhoB*$^{-/-}$ BMM shown as in (A) indicating the cell edge of the spreading cells as calculated by the Cell Outliner program (Chapter 2.8.7). (C) Schematic diagram showing the method of assigning a radian value to the edge of a spreading cell. (D) Plot of the radius as a function of time in Cartesian co-ordinates for Wt and *RhoB*$^{-/-}$ BMM shown in (A) and (B), time is shown in frame numbers 1 frame = 6 sec (E) Velocity density plot showing radial edge velocity plotted as a function of time and angle for two Wt and *RhoB*$^{-/-}$ BMMs (a) corresponds to the Wt and *RhoB*$^{-/-}$ BMM shown in (A) and (B).

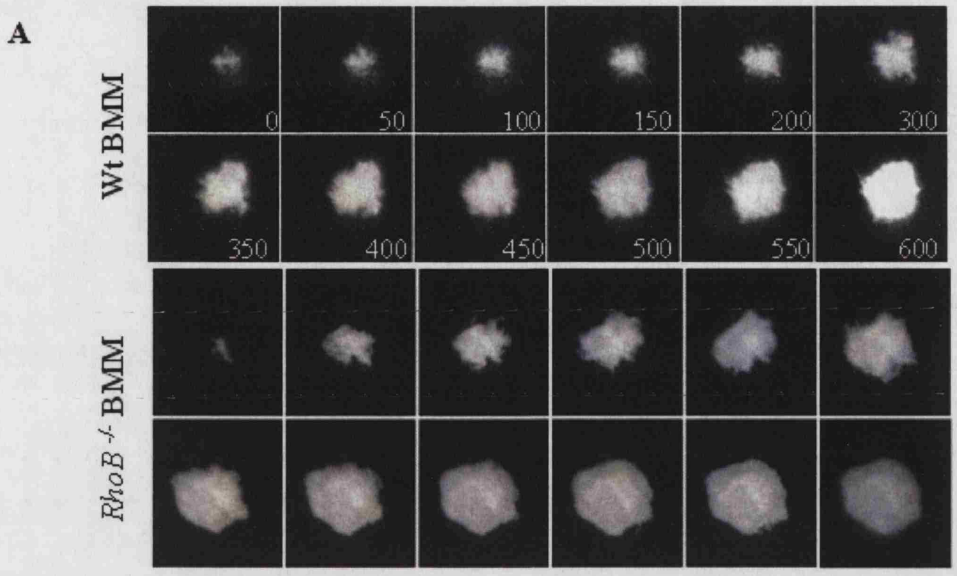
A
Wt BMM
0
50
100
150
200
300
350
400
450
500
550
600
RhoB -/- BMM

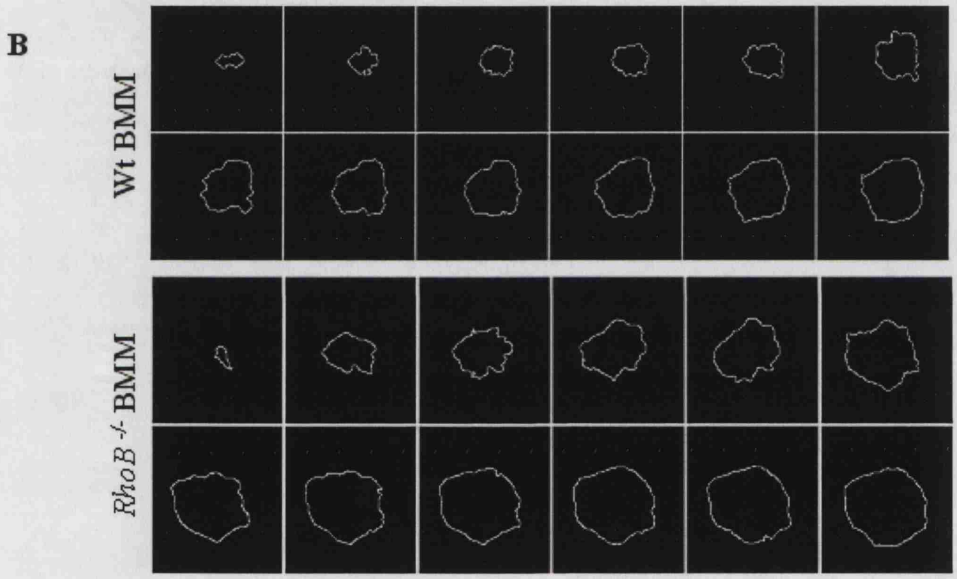
B
Wt BMM
RhoB -/- BMM

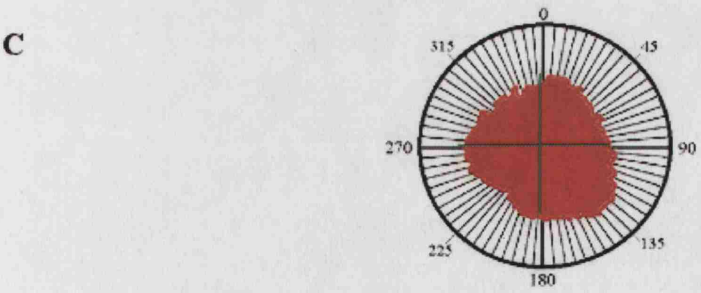
C
0
45
90
135
180
225
270
315

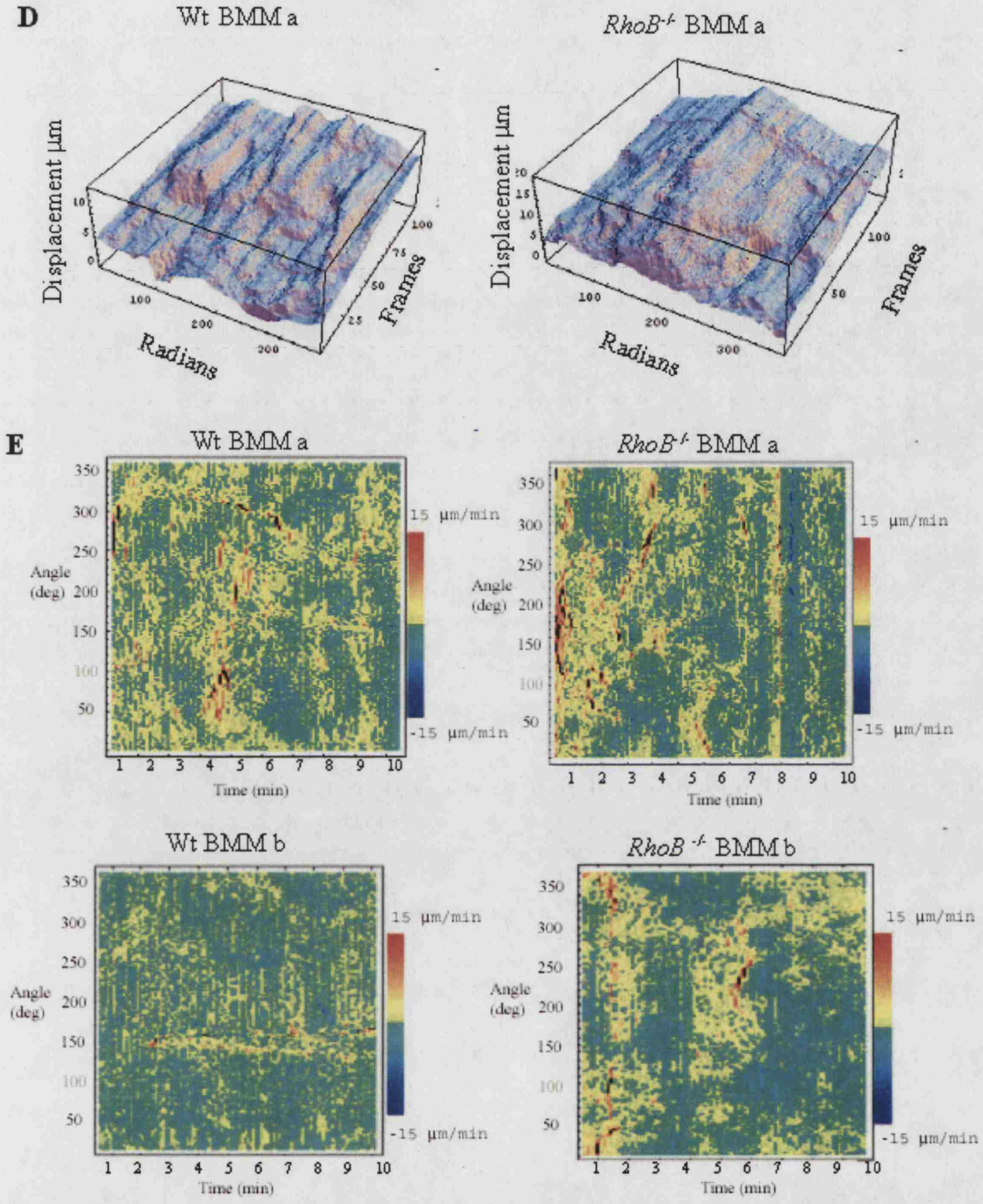
D
Wt BMM a
RhoB-/- BMM a
Displacement µm
Radians
Frames
E
Wt BMM a
RhoB-/- BMM a
Wt BMM b
RhoB -/- BMM b
Angle (deg)
Time (min)
15 µm/min
-15 µm/min

5.8 Comparison of the kinetics of the membrane movement during spreading in wild-type and *RhoB*$^{-/-}$ BMM

By combining the spreading data from all radians a comparison of the rate of change in total cell area and total velocity of the cell membrane movements can be made between the Wt cell and *RhoB*$^{-/-}$ cell (shown in Fig 5.6A,B). This showed that the Wt BMM went through 3 defined phases of cell spreading: A lag phase in which the cell did not increase its spread area greatly (1). This was then followed by a stage of rapid spreading (2) and finally a stage of slower spreading (3) (The changes in phases are marked by blue lines on Fig 5.7 for all cells shown). The time each of the 30 cells analysed spent in each of these three phases of spreading varied greatly (Fig 5.7A and B and data not shown). The *RhoB*$^{-/-}$ BMM appeared to follow a similar pattern, but in the majority of the *RhoB*$^{-/-}$ BMM analysed the initial lag phase was far shorter than that seen in the Wt BMM (Fig 5.7B and data not shown). The rate of area change in the Wt BMMs analysed was always positive; the rate of area change was more rapid in the second phase of cell spreading, which is consistent with data obtained from spreading fibroblasts (Dobereiner et al. 2004). The rate of area change in the *RhoB*$^{-/-}$ BMM was not always a positive number indicating that at certain times the cell membrane of the *RhoB*$^{-/-}$ BMM was retracting rather then expanding (Fig 5.7B). This could also be seen by the areas of darker blue on the velocity density plots (Fig 5.6E).

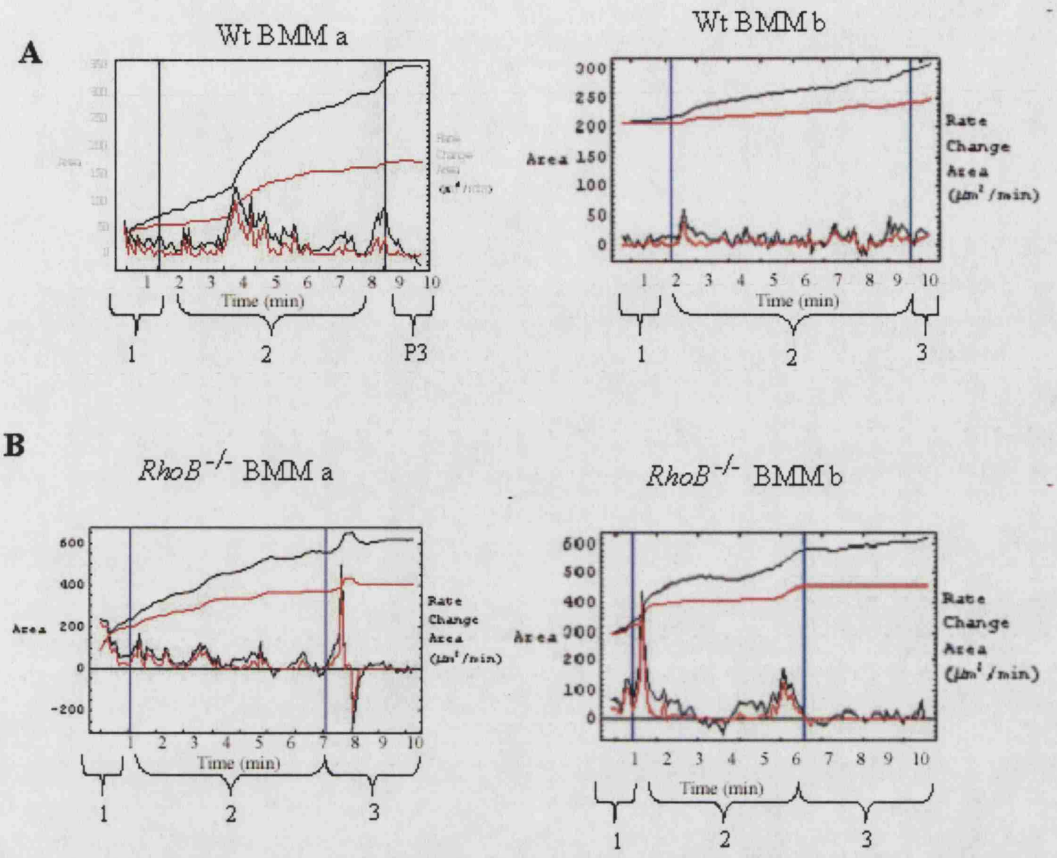

Figure 5.7: Comparison of the kinetics of membrane movement during spreading in wild-type and *RhoB*$^{-/-}$ BMM

Graphs showing the variation in total cell area and total change in radial edge velocity during spreading for two Wt (B) and *RhoB*$^{-/-}$ BMM (B). The phases of cell spreading: 1, 2 and 3 are indicated on each graph. The red line indicates the area thresholded in the Cell Outliner program. The black line indicates the total area as calculated by Creep. In each graph the top plot shows the total change in cell area through the spreading process, the bottom plot shows the total rate of change in area through the spreading process.

5.9 *RhoB*$^{-/-}$ BMM extend and contract their membrane more rapidly than wild-type BMM.

Analysis of the range of velocities of cell membrane movement for the Wt and *RhoB*$^{-/-}$ BMM (shown in Fig. 5.6) indicates that the average speed of membrane movement in RhoB$^{-/-}$ BMM was similar to that of the Wt BMM. The two *RhoB*$^{-/-}$ BMMs however had an slightly wider range of velocities the membrane movement than Wt's (Fig 5.8A)

Information about the mean and maximal protrusion and retraction velocity for each individual cell studied was obtained (30 Wt and *RhoB*$^{-/-}$ BMM) and then combined to give an indication of the mechanics of a population of spreading BMM. This pooled data shows that there was no difference in the mean velocity of membrane protrusion between Wt and *RhoB*$^{-/-}$ BMM. The maximum velocity at which the *RhoB*$^{-/-}$ BMM as a population extended and retracted their membranes during spreading was significantly higher than the Wt BMM (Fig. 5.8B). Unlike Wt BMM, the maximum velocity of membrane protrusion in *RhoB*$^{-/-}$ BMM, (15 μm/min) was actually faster than that of polymerisation of F-actin (Higgs and Pollard, 2001). This suggested that areas of cell membrane above the basal plane of the cell were sometimes collapsing onto the substrate, causing an abrupt increase in the spread area of the cell which was not due to de-novo actin polymerisation. This effect was observed in some time-lapse series of *RhoB*$^{-/-}$ BMMs spreading (Fig 5.8C).

Figure 5.8: *RhoB*$^{-/-}$ BMM extend and retract their membrane more rapidly than Wt BMM

(A) Histograms showing the range of radial edge velocities during spreading during the first 10 min of spreading for two Wt and *RhoB*$^{-/-}$ BMMs. Positive velocities indicate protrusion of the cell membrane; negative velocities indicate retraction of the cell membrane. (B) Graph showing the mean and maximal protrusion and retraction velocities for a population of BMM. Data is pooled from three independent experiments n= 30 cells. *= significant difference ($p>0.05$) between Wt and *RhoB*$^{-/-}$ BMM. (C) Montage of TIRF images of a *RhoB*$^{-/-}$ BMM showing collapse of the membrane, arrows indicate the area where membrane is collapsing. Time elapsed (sec) is indicated in the top left of each frame.

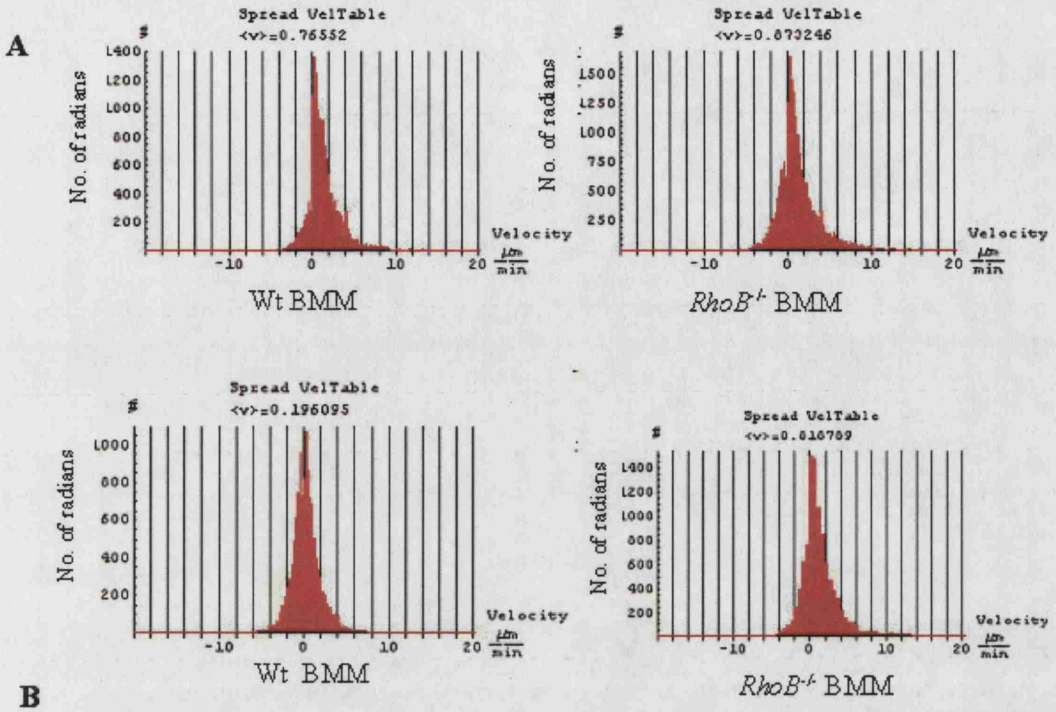
A
Spread VelTable
<v>=0.76552
No. of radians
Velocity
Wt BMM
Spread VelTable
<v>=0.673246
No. of radians
Velocity
RhoB-/- BMM
Spread VelTable
<v>=0.196095
No. of radians
Velocity
Wt BMM
Spread VelTable
<v>=0.616789
No. of radians
Velocity
RhoB-/- BMM

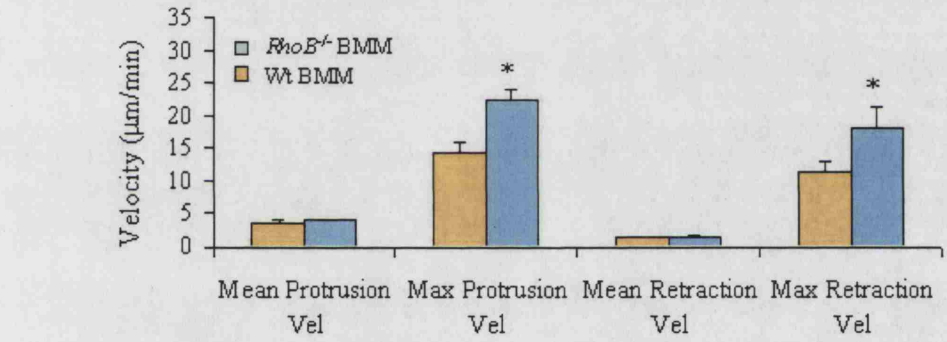
B
Velocity (µm/min)
RhoB-/- BMM
Wt BMM
Mean Protrusion Vel
Max Protrusion Vel
Mean Retraction Vel
Max Retraction Vel

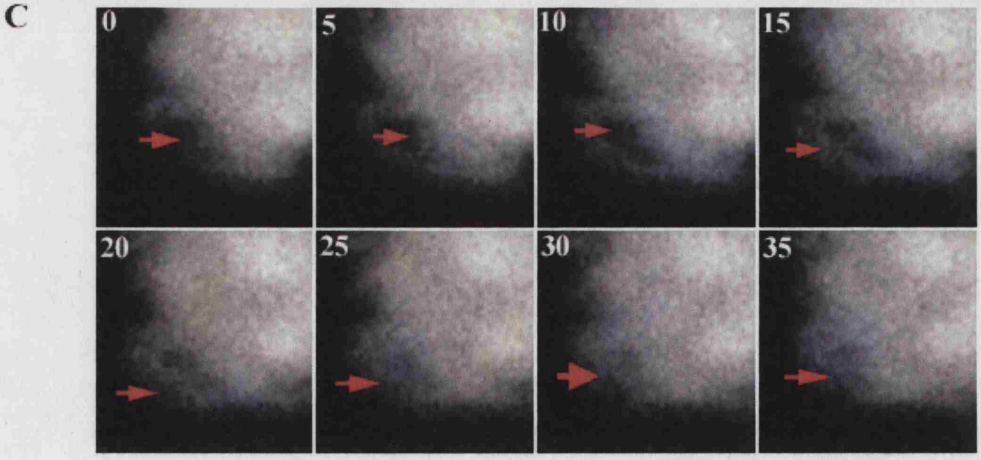
C
0
5
10
15
20
25
30
35

5.10 The persistence of membrane movement is not affected by deletion of RhoB.

The velocity density plots show that for each cell there was a periodicity to cell membrane extension (Fig. 5.9A), which correlates with observations in fibroblasts (Dobereiner et al. 2004). To analyse this periodicity of membrane extension the cell membrane was classified as active, moving at a velocity above 2 μm/min; or stationary, moving at a velocity below 2 μm/min. The average duration of the active and stationary phases of cell membrane movement for each cell was calculated. This showed that the membrane of Wt BMMs was active for 2.5 sec and stationary for 15 sec during the first 10 min of cell spreading. This division into active and stationary phases was not significantly altered in *RhoB*$^{-/-}$ BMM (Fig. 5.9B).

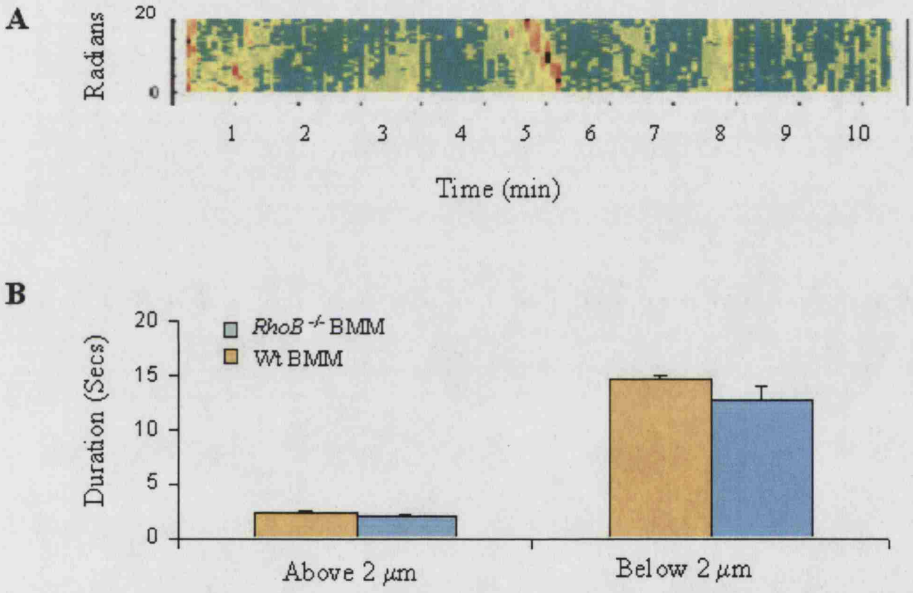

Figure 5.9: The persistence of membrane movements is not affected by deletion of RhoB

(A) Velocity density plot of 20 radians of a spreading Wt BMM indicating membrane extension cycles through stationary (green) and actively extending (yellow) periods during cell spreading. Arrows indicate the active phases. (B) Graph showing the average duration of periods of active membrane extension and pausing for spreading Wt and *RhoB*$^{-/-}$ BMM, n= 30 cells.

5.11 Conclusions and discussion

Deletion of RhoB appears not to affect the proliferation of BMM. C3 transferase is known to inhibit cell proliferation by inhibiting cytokinesis (Hall and Nobes, 2000) and RhoA mutants in *Drosophila* have cytokinesis defects (Magie et al, 1999). Indeed, fibroblasts where RhoA activity has been specifically knocked down using RNAi are multi-nucleate, where as RhoB RNAi treatment does not inhibit cytokinesis at all (data not shown). Consistent with this, no proliferative defects were reported in RhoB-null fibroblasts or endothelial cells (Adini et al. 2003; Liu et al. 2001), which suggests RhoB does not play a major role in the regulation of cell proliferation.

RhoB certainly has an important role to play in cell adhesion in BMMs. It has been previously shown that RhoB-null cells have decreased spread area and other defects attributable to defective adhesion (Adini et al. 2003; Liu et al. 2001; Sandilands et al. 2004). In fibroblasts, T cells, macrophage cell lines and BMM, inhibition of Rho activity through use of C3-transferase does not appear to inhibit cell adhesion although it promotes cell spreading (Allen et al. 1997; Nobes and Hall, 1999; Smith et al. 2003) (Chapter 4.11). In contrast *RhoB*$^{-/-}$ BMM have a reduced spread area and defects in adhesion to glass and ICAM-1. This suggests that RhoB may be playing a very different role in the regulation of cell spreading to RhoA. Using a combination of FACS and adhesion assays the defects in adhesion observed in *RhoB*$^{-/-}$ BMM could be attributed to decreased cell surface expression of integrins β2 and β3. The decrease in the cell surface expression of β2 is particularly interesting as αMβ2, αLβ2 and αDβ2 are important for macrophage adhesion. αMβ2 in particular is required for adhesion to bacteriological plastic (Paulnock, 2000). So reduced β2 expression may explain why fewer BMM were generated from fibula flushes of *RhoB*$^{-/-}$ mice. There is very little reported about the interaction between RhoB and integrins. It is clear that deletion of RhoB does affect cell surface expression of β2 and β3 integrins and this may be due to trafficking of integrins to the plasma membrane or alternatively as a 'knock-on' effect of the perturbation in the activity of Rac1 and RhoA in *RhoB*$^{-/-}$ BMM (chapter 6.2). It would be very interesting to analyse the impact of deletion of RhoA on cell surface integrin expression and adhesion but as yet a source of RhoA-null BMM is not available.

As with other cell types the adhesion of BMM is dependent on the substrate. BMM adhere more strongly to glass than fibronectin, but they migrate faster on fibronectin than glass (Chapter 4.2 and 4.6). Fibroblasts adhere more strongly to vitronectin than fibronectin and similarly to BMM they migrate rapidly on fibronectin (Ware et al. 1998). T cell and neutrophil adhesion to laminin, collagen and fibronectin varies in its avidity as well (Hogg et al. 2002). BMM do not have large focal adhesions observed in fibroblasts (Chapter 3.4). BMM have small, but visible by conventional confocal microscopy, focal contact-type structures distributed across the basal plane of the cell, which can be visualised by phospho-tyrosine 118 paxillin staining (paxillin is an adaptor protein found in several adhesion types, Chapter 1.13.1) (Pixley et al. 2001). The distribution or size of these on the basal surface of the cell does appear to be greatly perturbed by deletion of RhoB. This suggests that RhoB might be involved in the early processes of cell attachment and spreading, which may be affected primarily by the level of cell surface integrin. It would be interesting to study whether BMM have tiny integrin contacts too small to be discerned by conventional optical microscopy, described by Wiseman et al (Wiseman et al. 2004).

TIRF microscopy can be used to gain insights into the early stages of adhesion. Study of a single macrophage attaching and spreading can give a more detailed view of the process of adhesion. It appears that, similarly to fibroblasts (Dobereiner et al. 2004), adhesion has three clearly defined stages in BMM. Firstly the cell attaches to the substratum but does not begin to spread upon it. The time that Wt BMM remain in this state is variable. In the second stage the cell increases its spread area rapidly. In this stage paxillin is either perinuclear or localised around the edge of the cell membrane. Similarly to fibroblasts spreading in this stage the cell membrane is not always moving (Giannone et al. 2004). Instead, the membrane oscillates between active and stationary states and the duration of the active and stationary states is not affected by deletion of RhoB. These states may correspond to either to cycles of actin polymerisation regulated by Rac and Cdc42, or cycles of myosin based contractility within the cell (Millard et al. 2004) (Giannone et al, 2004). In the final stage of spreading the cell begins to form a more polarised morphology, after 30 min of spreading BMM become more elongated and paxillin is more evenly distributed over the basal plane of the cell, which suggests that the focal contacts seen in fully spread BMM begin to form.

On fibronectin *RhoB*$^{-/-}$ BMM appeared to move through these stages more rapidly than the Wt BMM. Notably, more *RhoB*$^{-/-}$ BMM have spread on fibronectin-coated glass after 60 min than Wt BMM. *RhoB*$^{-/-}$ BMM also had a larger area after 30 min spreading on glass, which appears an incongruous result as they have, in general a reduced adhesion to glass and a smaller spread area than Wt BMM after 24 h on glass. Although it is difficult to interpret these results one conclusion may be that there is a minimum level of cell surface integrin expression required for attachment. The *RhoB*$^{-/-}$ BMM had wider variation of cell surface integrin expression than Wt BMM. Presumably some *RhoB*$^{-/-}$ BMM express integrins at a sufficiently high level for attachment to a surface and these ones rapidly spread.

TIRF has been previously used to analyse the movements of only the basal membrane of spreading cells (Dobereiner et al. 2004; Giannone et al. 2004). Here, TIRF was used investigate why *RhoB*$^{-/-}$ BMM spread so rapidly. When Wt BMM were plated they generally spread by putting out small projections in the intended direction of spreading which were then enlarged. The cell membrane moved only moves to extend the spread area of the cell and Wt BMM rarely retracted their membrane during the second phase of spreading. In *RhoB*$^{-/-}$ BMM spreading included more rapid membrane extension and retraction and occasionally the membrane directly above the cell-substratum plane appeared to collapse into the basal 'spreading' plane. This collapse of cell membrane may account for the transient rapid increases in spread area of the cell. It also would account for the rapid rate of cell spreading of *RhoB*$^{-/-}$ BMM. This collapse of the cell membrane may suggest that the *RhoB*$^{-/-}$ BMM have reduced cell tension on this membrane compared to Wt BMM or that the integrin signalling in *RhoB*$^{-/-}$ BMM is perturbed during spreading.

In conclusion, a combined use of TIRF and fluorescence microscopy has allowed an in-depth characterisation of cell spreading in BMM. This showed that, overall, the deletion of *RhoB* slightly altered the mechanics of cell spreading in stage 2 (membrane extension) but had little effect on stage 3 (polarisation). However, the first stage of adhesion, that of attachment of a cell to the substratum, was most affected by deletion of RhoB. Although this was dependent on the substrate and may reflect differences in cell surface expression of certain integrins. It would be interesting to determine the connection between RhoB and cell surface expression of integrins in more depth and how this affects the mechanics of cell spreading on different substrates.

Chapter 6: The effect of deletion of RhoB on cell signalling

6.1 Introduction

The activity of RhoB in cell signalling is often regulated by its expression (Fritz et al. 1995; Jahner and Hunter, 1991; Zalcman et al. 1995), it is transiently increased in response to growth and stress stimuli (Fritz et al. 1999). The farnesylated form of RhoB is found on the plasma membrane of the cell and has been reported to be involved in neoplastic transformation and formation of stress fibres (Adamson et al. 1992; Prendergast, 2001). The activity of the geranyl-geranylated form of RhoB, which is localised on the early and late endosomes, has been reported to suppress transformation (Du and Prendergast, 1999). Endosomal RhoB also regulates trafficking of some cell surface receptors through the early endosome to lysosome transition (Rojas et al. 2004; Wherlock et al. 2004) and also controls the localisation of Akt and Src (Adini et al. 2003; Sandilands et al. 2004). Increasing the activity of RhoB retards trafficking of the EGF receptor, a receptor tyrosine kinase (RTK), which can activate a number of cellular signalling pathways including the PI 3-Kinase/Akt pathway (Gampel et al. 1999; Wyckoff et al. 2004). Intriguingly RhoB expression has been shown to be inhibited by the PI 3-Kinase / Akt pathway (Jiang et al. 2004b). This suggests that RhoB may be part of an intricate signalling loop, where its activity regulates and is regulated by its targets (Adnane et al. 2002; Jiang et al. 2004a; Sandilands et al. 2004). In macrophages CSF-1 signals to promote migration and proliferation via a RTK, c-Fms (Pixley and Stanley, 2004). Rac and Cdc42 are known to be involved in CSF-1 signalling but the role of RhoA and RhoB is currently not known (Allen et al. 1998; Webb et al. 1996; Wells et al. 2004). Therefore the effect of CSF-1 signalling on RhoA and RhoB activity and the impact of deletion of RhoB on CSF-1 signalling was investigated.

Results

6.2 Impact of deletion of RhoB on Rho family GTPase activity

When CSF-1 was withdrawn from Wt BMM their speed of migration decreased, BMM became elongated, lamellae were reduced and dorsal ruffling was decreased ((Wells et al. 2004) and Chapter 3.7 and 4.11). The decrease in migration speed and cell elongation was not as marked in *RhoB*$^{-/-}$ BMM although dorsal ruffling was not affected. These changes in cell morphology and migration are regulated through Rho GTPases (Fig. 4.2, 4.10 and 4.11). To determine whether the difference in behaviour of *RhoB*$^{-/-}$ BMM following withdrawal of CSF-1 could be attributed to differences in Rho GTPase activity, Rho activation assays (pull-down assays) were carried out. In pull down assays the association of a Rho protein with the GTPase binding domain of an effector is measured (Ren and Schwartz, 2000). A GST fusion of the GTPase-binding domain of the effector is bound to glutathione-Sepharose beads and then incubated with a cell lysate at 0°C. It is essential to keep this reaction cold to slow the hydrolysis of GTP bound to the Rho protein, which is promoted by GAPs (Chapter 1.3) as Rho can only associate with effectors in the GTP bound state (Bishop and Hall, 2000). The Rho protein bound to beads can be can be collected, or pulled down, using high-speed centrifugation of the beads. These assays can be used to measure the activity of Rho GTPases in the cell under different conditions (Fig. 6.1A and Chapter 2.4.11). Using these pull down assays it was shown, using ANOVA, that there is a significant difference in the activity of RhoA and Rac in Wt and *RhoB*$^{-/-}$ BMM between growth and starve medium ($p=0.02$ for RhoA and $p=0.01$ for Rac). Withdrawal of CSF-1 induced a decrease in the level of GTP-bound RhoA and Rac (Fig. 6.1B, C). The extent to which RhoA and Rac activity was reduced by withdrawal of CSF-1 varied between experiments, and the most representative of 3 experiments is shown. The reduction in RhoA and Rac activity was consistent with the decrease in dorsal ruffling and cell migration observed in CSF-1 starved BMM (Wells et al. 2004). RhoA activity was higher in *RhoB*$^{-/-}$ BMM in the presence (and absence) of CSF-1 compared to Wt BMM (Fig. 6.1B). On the other hand, Rac activity seemed slightly lower in the *RhoB*$^{-/-}$ BMM in the presence (and absence) of CSF-1 (Fig. 6.1C). Cdc42 activity was also up-regulated in the *RhoB*$^{-/-}$ BMM in growth medium (Fig.. 6.1D). Deletion of RhoB therefore affected the activity of RhoA, Rac and Cdc42 in BMM.

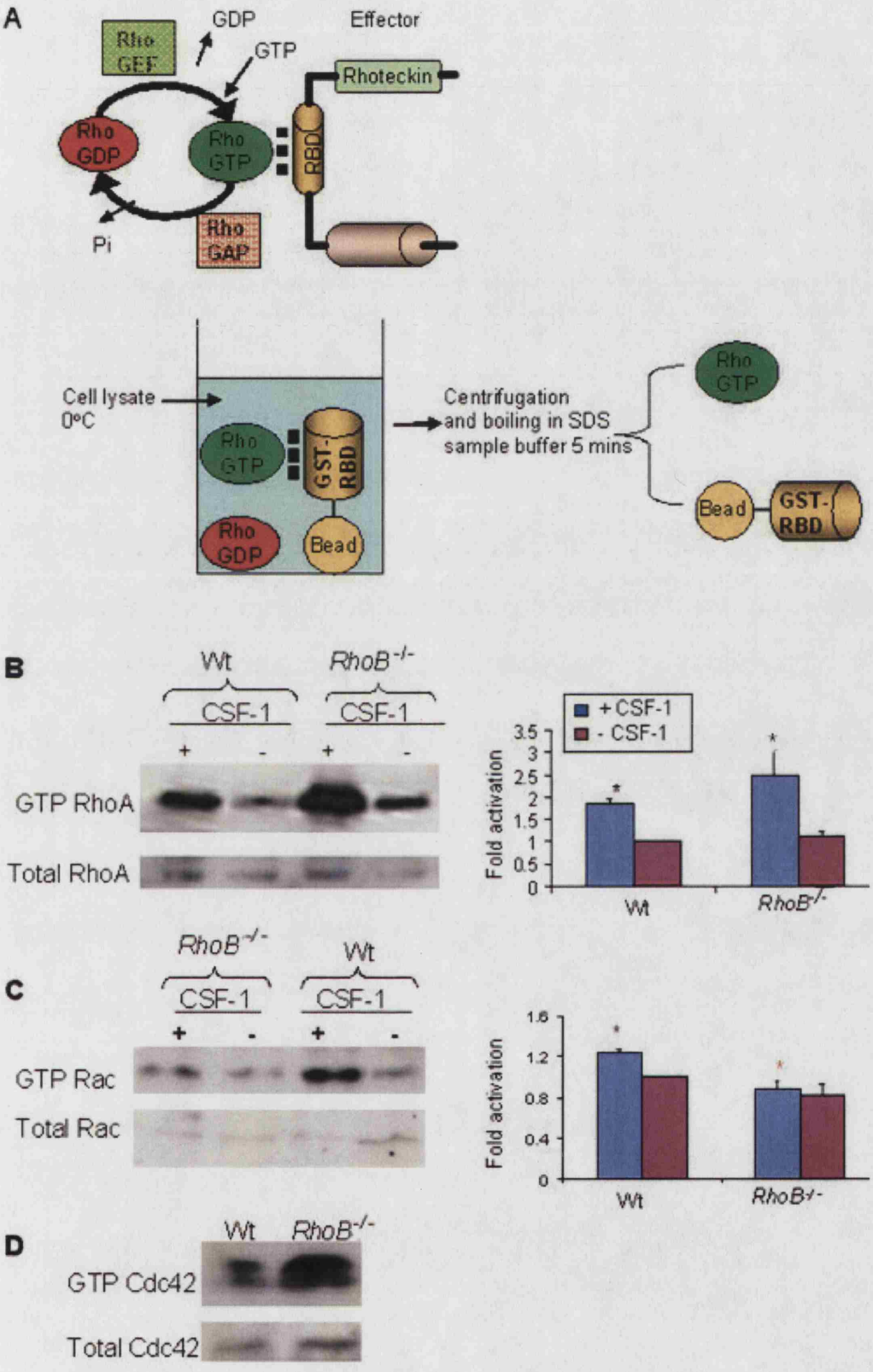
A
Rho GEF
GDP
GTP
Effector
Rhoteckin
Rho GDP
Rho GTP
RBD
Pi
Rho GAP
Cell lysate 0°C
Rho GTP
GST-RBD
Rho GDP
Bead
Centrifugation and boiling in SDS sample buffer 5 mins
Rho GTP
Bead
GST-RBD
B
Wt
RhoB-/-
CSF-1
CSF-1
+ - + -
GTP RhoA
Total RhoA
+CSF-1
- CSF-1
Fold activation
3.5
3
2.5
2
1.5
1
0.5
0
Wt
RhoB-/-
C
RhoB-/-
Wt
CSF-1
CSF-1
+ - + -
GTP Rac
Total Rac
Fold activation
1.6
1.2
0.8
0.4
0
Wt
RhoB-/-
D
Wt
RhoB-/-
GTP Cdc42
Total Cdc42

Figure 6.1: The impact of deletion of *RhoB* on Rho family GTPase activity

(A) Schematic diagram showing the principles of a pull down assay to determine Rho GTPase activity. RhoA binds to the Rho binding domain (RBD) on an effector protein. GST-RBD is then bound to glutathione-Sepharose beads and the GST-RBD-bead slurry is incubated with cell lysate where Rho-GTP binds to the RBD. Centrifugation is then used to harvest the beads and Rho is liberated from the beads by boiling in SDS sample buffer. (B) Pull down using GST-RBD beads showing activity of RhoA in Wt and *RhoB*$^{-/-}$ BMM in growth medium (+ CSF-1) and starve medium (- CSF-1) and graph showing quantitation of Rho activity. Cells were lysed and western blots were performed using an anti-RhoA-specific antibody. Western blots of whole cell lysates (Total RhoA) were performed using the same antibody (C) Pull down using GST-PAK-CRIB beads showing activity of Rac1 in Wt and *RhoB*$^{-/-}$ BMM in growth and starve medium. Cells were lysed and western blots were performed using an anti-Rac antibody. Western blots of whole cell lysates (Total Rac) were performed using the same antibody. Autoradiographs of the GST-RBD and GST PAK-CRIB pull-downs and the whole cell lysate blots were quantified using Quantity One (BioRad) software, and the level of GTP-bound RhoA or Rac was normalised to protein expression levels in the whole cell lysate. The induction of GTPase activity was determined by calculation of the ratio of the normalised level of RhoA in each condition with the normalised level of RhoA/Rac in Wt BMM in starve medium. Results shown are the mean± s.e.m. of three independent experiments. *= a significant difference from Rho or Rac activity of Wt BMM in starve medium $p>0.05$. (D) Pull down using GST-WASP-CRIB beads showing activity of Cdc42 in Wt and *RhoB*$^{-/-}$ BMM in growth medium (n=3).

6.3 The phosphorylation of MLC and LIMK in starve medium is altered in *RhoB*$^{-/-}$ BMM

The effect of deletion of RhoB on the proteins MLC and LIMK, which are known to signal from Rho to cell locomotion and the actin cytoskeleton (Maekawa et al. 1999), was analysed in growth and starve medium. LIMK, activated by Rac and PAK and also by RhoA and ROCK (Riento and Ridley, 2003), regulates actin polymerisation, and is involved in the formation of lamellipodia and cell shape change (Millard et al. 2004) (Chapter 1.11.1). MLC phosphorylation is co-ordinated by RhoA and ROCK and Ca^{2+}, regulates cell contractility and tail retraction, both of which are necessary for cell locomotion ((Riento and Ridley, 2003) and Chapter 1.2.2). Both MLC and LIMK are active when they are phosphorylated therefore phospho-specific antibodies were used to measure the activity of MLC and LIMK. The phosphorylation of MLC and LIMK both decreased when Wt BMM were starved of CSF-1 (Fig. 6.2 A, B). In *RhoB*$^{-/-}$ BMM the decrease in phosphorylation of MLC when CSF-1 was withdrawn was less, even though the activity of RhoA was decreased (Fig. 6.1B and 6.2B). This means that either MLC is not being dephosphorylated by MLC phosphatase or its phosphorylation (regulated by MLCK or ROCK), continues after CSF-1 is withdrawn. ROCK is known to regulate the activity of MLC-phosphatase and MLCK *in vitro* (Kaibuchi et al. 1999). However, it is not clear which of these processes would be altered by the deletion of RhoB.

LIMK was also not dephosphorylated to the same extent when CSF-1 was withdrawn in *RhoB*$^{-/-}$ BMM as it was in Wt BMM (Fig. 6.2B). This may either be due to continued PAK or ROCK activity in *RhoB*$^{-/-}$ BMM in the absence of CSF-1. Together, these results suggest a molecular mechanism that may be involved in maintenance of actin polymerisation and cell contractility in *RhoB*$^{-/-}$BMM even in the absence of CSF-1.

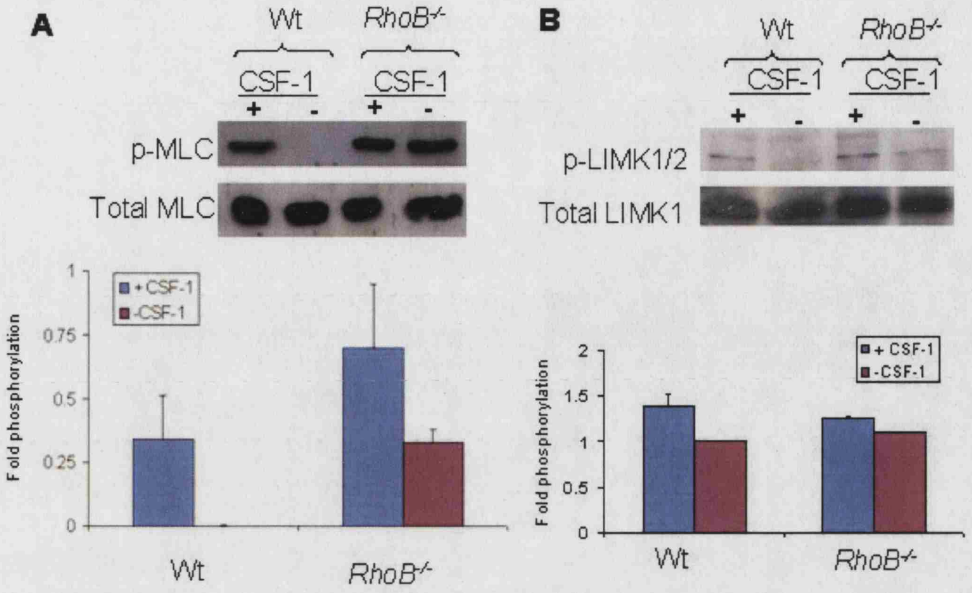

Figure 6.2: The phosphorylation of MLC and LIMK are perturbed in *RhoB*$^{-/-}$BMM

(A) Western blot showing phosphorylation of MLC and total MLC levels in Wt and *RhoB*$^{-/-}$BMM in growth (+ CSF-1) and starve medium (- CSF-1). (B) Western blot showing LIMK1 phosphorylation and LIMK 1/2 in Wt and *RhoB*$^{-/-}$ BMM in growth and starve medium. Autoradiographs of the phospho-MLC and phospho-LIMK1/2 and total MLC and LIMK1. blots were quantified using Quantity One (BioRad) software. The level of phospho-MLC or phospho-LIMK was normalised to total MLC or LIMK1 expression levels respectively. The activation levels of each sample +/- CSF-1 was determined by calculation of the ratio of the normalised level of phospho-MLC or phospho-LIMK in each condition with the normalised level of phospho-MLC or phospho-LIMK respectively in Wt BMM in starve medium. The blot shown is representative of 3 independent experiments. Data shown is means ±s.e.m of three independent experiments.

6.4 Expression of RhoA and RhoB following CSF-1 stimulation

The transcription of *RhoB* has been shown to increase in response to growth and stress stimuli (Fritz and Kaina, 2001). It has been shown that EGF and PDGF (both of which signal through receptor tyrosine kinases) increase the transcription of RhoB (Jahner and Hunter, 1991). To determine whether RhoA or RhoB expression was changed by CSF-1 stimulation Wt BMM were stimulated with CSF-1 over a 4-h time course. Expression of both RhoA and RhoB decreased slightly when BMM were starved of CSF-1 for 18 h. Expression of RhoB increased after 1 h of CSF-1 stimulation to control levels (Fig. 6.3). ANOVA showed that neither expression of RhoA nor RhoB was significantly affected by CSF-1 stimulation (Fig. 6.3). The decrease in expression of RhoA and RhoB when CSF-1 was withdrawn was very small, which may mean, in terms of cell signalling, that this effect is not relevant.

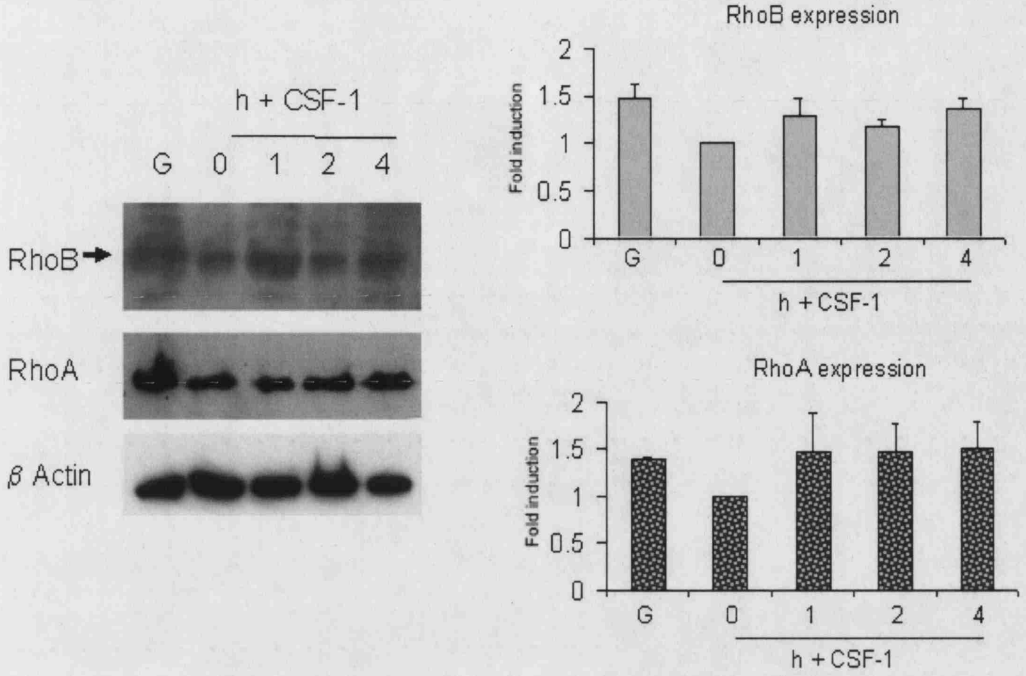

Figure 6.3: Expression of RhoA and RhoB following CSF-1 stimulation

Western blot showing the level of expression of RhoA and RhoB protein in Wt BMM in growth medium (G), after incubation of BMM for 18 h in starve medium (0) and following stimulation with 33 ng/ml recombinant CSF-1 for 1, 2 and 4 h. The blot was reprobed with anti -β actin antibodies to show equal loading. The blot shown is representative of 3 independent experiments. Autoradiographs of the RhoA and RhoB blots were quantified using Quantity One (BioRad) software, and the level of RhoA or RhoB was normalised to β actin expression levels. The protein levels of each sample were determined by calculation of the ratio of the normalised level of RhoA or RhoB in each condition with the normalised level of RhoA or RhoB respectively in starve medium. The blot shown is representative of 3 independent experiments. Data shown is means ±s.e.m of three independent experiments.

.

6.5 Activation of RhoA and RhoB following CSF-1 stimulation

CSF-1 stimulation of BMM causes changes in the actin cytoskeleton of BMM (Jones et al. 2003; Wells et al. 2004), and this is accompanied by an increase in the activity of Rac1 (personal communication Dr E. Prigmore). In contrast it was not known whether the activity of RhoA or RhoB was increased in response to CSF-1 stimulation. To determine the effect of CSF-1 stimulation upon RhoA and RhoB, pull-down assays were carried out (see Fig. 6.4A). BMM were stimulated with CSF-1 and the levels of GTP-bound RhoA and RhoB were measured over a 60 min time course. The activity RhoA altered slightly during CSF-1 stimulation. Its activation was always reduced in the absence of CSF-1, although the extent of this reduction was variable and not statistically significant. The activity of RhoA increased after 5 min of CSF-1 stimulation and was then maintained at the same level, although again the extent of activation of RhoA by CSF-1 was variable (Fig. 6.4A and C). The activity of RhoB was slightly different to that of RhoA in response to CSF-1. In cells starved of CSF-1 the activity of RhoB was not markedly reduced, however after 5 min of CSF-1 stimulation its activity was increased. The activation of RhoB then decreased after 15 min of CSF-1 stimulation and returned to the level observed in growing cells at 30 min of CSF-1 stimulation and was then reduced at 60 min (Fig. 6.4B and C). BMM express PRK1, an effector of RhoA and RhoB. PRK1 has been implicated in regulation of cytokine receptor trafficking with RhoB (Mellor et al. 1998; Zeng et al. 2003). The expression of PRK1 was slightly decreased by withdrawal of CSF-1 but was not affected by stimulation of BMM with CSF-1 (Fig. 6.4D).

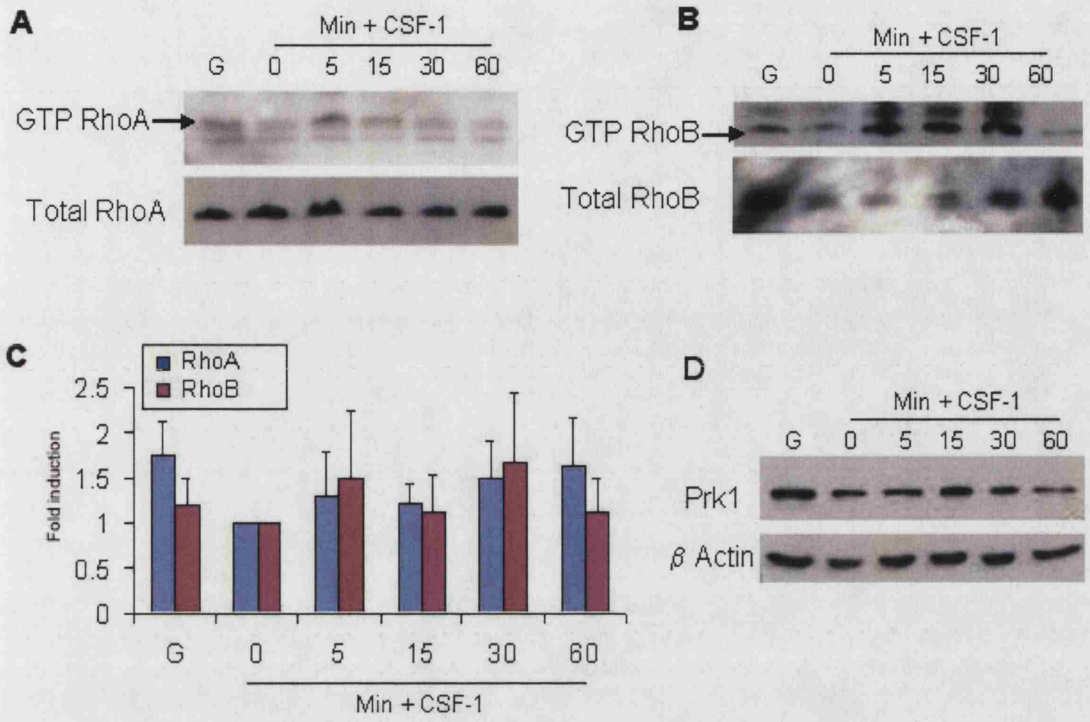

Figure 6.4: Activation of RhoA and RhoB following CSF-1 stimulation.

(A and B) Pull down assays were carried out using GST-TBRD beads to show the activity and expression of (A) RhoA and (B) RhoB in growth medium (G), after incubation of BMM for 18 h in starve medium (0) and following stimulation with 33ng/ml recombinant CSF-1 for 5, 15, 30 and 60 min in Wt BMM. Cells were lysed in RIPA buffer and separated using Nu-PAGE (Chapter 2.4.6). Western blots show the activity (upper blot) and expression (lower blot) of RhoA (A) and RhoB (B). (C) Autoradiographs of the activity and expression blots (A+B) were quantified using Quantity One (BioRad) software, and data from the activity blots was normalised to protein expression levels. The induction of RhoA or RhoB activity for each sample was determined by calculation of the ratio of the normalised level of RhoA or RhoB in each condition with the normalised level of RhoA or RhoB in starve medium. Results shown are the mean±s.e.m. of three independent experiments. (D) The expression levels of PRK1, an effector of RhoB is shown by western blotting of whole cell lysates stimulated as in (A and B). The blot was reprobed with anti -β actin antibodies to show equal loading. The blot shown is representative of 3 independent experiments. Data shown is means ±s.e.m of three independent experiments.

6.6 CSF-1 induced protein tyrosine phosphorylation is not affected in *RhoB*$^{-/-}$ BMM.

RhoB has been shown to retard the trafficking of EGF-R though the endocytic pathway. Stimulation of fibroblasts with EGF has been shown to increase the extent of protein tyrosine phosphorylation. In HeLa cells overexpressing RhoB the signalling from EGF-R is altered (Gampel et al. 1999). To investigate whether the CSF-1 signalling pathway was regulated by RhoB, signalling induced by CSF-1 stimulation was compared between Wt and *RhoB*$^{-/-}$ BMM. The first aspect of the CSF-1 signalling pathway to be analysed was cell surface expression of the CSF-1 receptor, c-Fms. Flow cytometry showed that there was no difference in the cell surface expression of c-Fms in an asynchronous population of Wt and *RhoB*$^{-/-}$ BMM in growth medium (Fig. 6.5A) To determine whether deletion of RhoB altered tyrosine kinase signalling the tyrosine phosphorylation status of proteins was measured following CSF-1 stimulation of Wt and *RhoB*$^{-/-}$ BMM. After CSF-1 had been withdrawn for 18 h, Wt BMM had a decreased level of protein tyrosine phosphorylation (Fig. 6.5B). Restimulation of Wt BMM with recombinant CSF-1 induced an increase in tyrosine phosphorylation with maximal changes between 5 and 30 min after stimulation. In *RhoB*$^{-/-}$ BMM the effect of CSF-1 stimulation on tyrosine phosphorylation was the same as seen in Wt BMM (Fig. 6.5B).

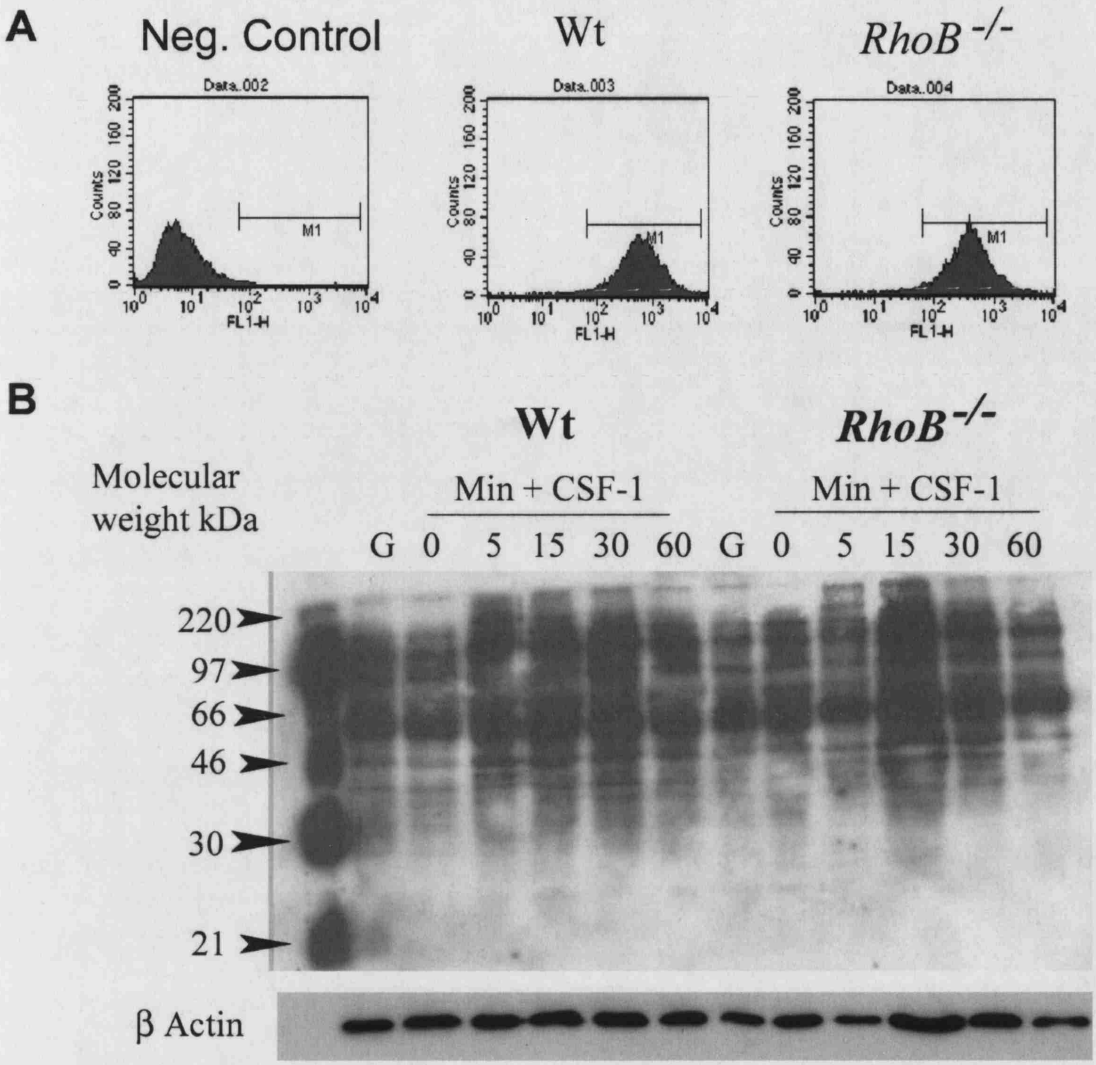

Figure 6.5: CSF-1 induced protein tyrosine phosphorylation is not affected in *RhoB*$^{-/-}$ BMM.

(A) Flow cytometry was used to analyse cell surface expression of the CSF-1 receptor c-Fms in Wt and *RhoB*$^{-/-}$ BMM. (B) Western blot of whole cell lysates from Wt and *RhoB*$^{-/-}$ in growth medium (G), after incubation for 18 h in starve medium (0) and following stimulation with 33 ng/ml recombinant CSF-1 for 5, 15, 30 and 60 min, showing protein tyrosine phosphorylation using the 4G10 anti-phospho-tyrosine antibody. The blot was reprobed with anti -β actin antibodies to show equal loading (lower panel). The blot shown is representative of 3 independent experiments.

6.7 The kinetics of Erk and Akt activation were not altered in *RhoB*$^{-/-}$ BMM

CSF-1 signalling was known to stimulate the Erk/MAPK signalling cascade and PI 3-kinases and Akt (Pixley and Stanley, 2004). Activation of the PI 3-kinase pathway in neutrophils and *Dictyostelium* is known to contribute to chemotaxis (Merlot and Firtel, 2003; Xu et al. 2003). The Erk/MAPK pathway is also known to be activated in response to chemokine signalling in macrophages and monocytes and to contribute to cell motility (Ashida et al. 2001; Wells et al. 2004). Deletion of *RhoB* did not affect the kinetic of CSF-1 phosphorylation of Akt although the level of phosphorylation of Akt was reduced in *RhoB*$^{-/-}$ BMM (Fig. 6.6A). In *RhoB*$^{-/-}$ BMM, CSF-1 induced phosphorylation of ERK and the kinetics of ERK activation was not affected (Fig. 6.6B). There was an increase in phosphorylation of Akt and ERK in response to CSF-1 stimulation in both Wt and *RhoB*$^{-/-}$ BMM in all experiments. This indicates that deletion of RhoB does not affect the kinetics of Akt or ERK phosphorylation in response to CSF-1 signalling. This is consistent with data that shows that there is no chemotaxis defect in *RhoB*$^{-/-}$ BMM (Fig. 4.7).

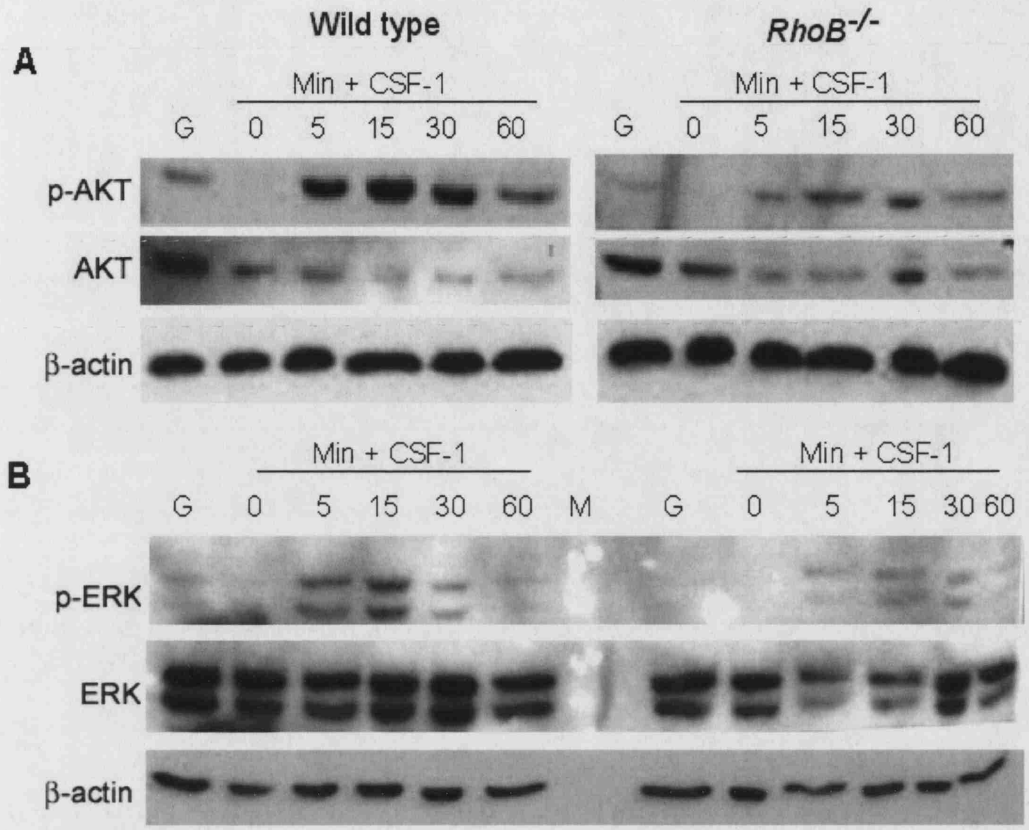

Figure 6.6: The kinetics of Erk and Akt activation were not altered in *RhoB*$^{-/-}$BMM

Western blots of Wt and *RhoB*$^{-/-}$ in growth medium (G), after incubation of BMM for 18 h in starve medium (0) and following stimulation with 33 ng/ml recombinant CSF-1 for 5, 15, 30 and 60 min showing phosphorylation of Akt and Akt levels (A) and phosphorylation of ERK and ERK1 levels (B). Blots were probed with antibodies to phospho-ERK and phospho-Akt, stripped and reprobed with antibodies to ERK and Akt. The blots were lastly reprobed with anti -β actin antibodies to show equal loading (lower panel). The blots shown are representative of 3 independent experiments. M represents the protein size markers on the ERK blots.

6.8 The phosphorylation of paxillin was not affected by deletion of RhoB

CSF-1 signalling is known to promote cell spreading and adhesion (Pixley and Stanley, 2004) and was observed to induce a rearrangement in podosomes (Fig. 3.7). Tyrosine phosphorylated paxillin is localised to adhesions in macrophages (Pixley et al. 2001, Turner. 2000), including podosomes (Fig. 3.1). Therefore, the impact of CSF-1 signalling on phosphorylation of paxillin in Wt and *RhoB*$^{-/-}$ BMM was determined. In Wt BMM the tyrosine phosphorylation of paxillin was slightly decreased in the absence of CSF-1. Paxillin can be phosphorylated on tyrosines, serines and threonines, and higher mobility of paxillin in BMM starved of CSF-1 and restimulated with CSF-1 may correspond to changes in the serine and threonine phosphorylation in paxillin (Fig. 6.7). Y-118 phosphorylation of paxillin increased after 5 min of CSF-1 stimulation in Wt BMM (Fig. 6.7A). In *RhoB*$^{-/-}$ BMM the kinetics of Y-118 paxillin phosphorylation following CSF-1 stimulation was slightly delayed compared to Wt BMM (Fig. 6.7). Confocal images showed that paxillin is found in both the perinuclear region and on the plasma membranes in BMM (Fig. 3.1). It would be interesting to fractionate BMM into membrane and cytosolic fractions to see if paxillin phosphorylation is increased in the membrane fraction in response to CSF-1 stimulation.

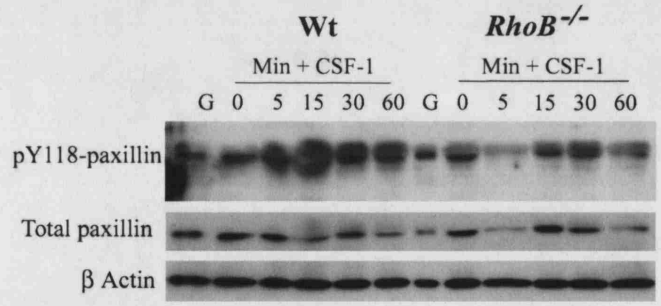

Figure 6.7: The phosphorylation of paxillin was not affected by deletion of RhoB

Western blot of cell lysates of Wt and *RhoB*$^{-/-}$ BMM, in growth medium (G), after incubation of BMM for 18 h in starve medium (0) and following stimulation with 33 ng/ml recombinant CSF-1 for 5, 15, 30 and 60 min. Blots were probed with antibodies toY-118 paxillin (upper panel), stripped and reprobed with antibodies to paxillin. The blot was reprobed with anti -β actin antibodies to show equal loading. The blot shown is representative of 3 experiments.

Conclusions and discussion

CSF-1 acts through the receptor tyrosine kinase c-Fms and thus following CSF-1 stimulation the level of protein tyrosine phosphorylation in cells in increased (Yeung and Stanley, 2003). This CSF-1 induced protein tyrosine phosphorylation was associated with the activation of signalling complexes within the cytoskeleton (Pixley and Stanley, 2004). Withdrawal of CSF-1 from BMM was accompanied by a decrease in protein tyrosine phosphorylation and a decrease in the dorsal ruffling, cell migration and spreading and elongation of BMM (Figure 4.10 and 4.11). GTPase activation assays showed that this decrease in the activity of the cytoskeleton was concomitant with a decrease the activity of RhoA and Rac in Wt BMM. Stimulation of BMM with CSF-1 promotes acute activation of Rac and increased formation of lamellipodia and membrane ruffles (Wells et al. 2004). Interestingly the activity of Cdc42 in the whole cell is not changed following CSF-1 stimulation (Wells et al, 2004) although microinjection of dominant negative Cdc42 inhibits chemotaxis in Bac1 macrophages and causes dendritic cells to lose polarity (Allen et al. 1998; Burns et al. 2001). It may be that Cdc42 activation is confined to specific regions of the cells which could not be shown using pull-downs. It would be interesting to use FRET based analysis of Cdc42 activation in BMM in a chemokine gradient to investigate this. CSF-1 signalling therefore causes changes in the cytoskeleton that are mediated at least in part through Rho GTPases (Pixley and Stanley, 2004; Ridley, 2001c) (Fig.6.8).

Unlike Rac, the activity of RhoA was not immediately increased by stimulation of BMM with CSF-1. This may indicate that CSF-1 stimulation leads to RhoA activity latently or that RhoA was activated in response to the other, Rac mediated, downstream effects of CSF-1 signalling, such as the formation of filopodia and lamellipodia. Rac and RhoA activity are usually inversely correlated in cellular processes and the CSF-1 stimulation of BMM is not exceptional to this. Both endothelial cells and fibroblasts decrease RhoA activity and increase Rac activity when they change shape (Burridge and Wennerberg, 2004; Wojciak-Stothard and Ridley, 2003). Growth factor signalling also causes early increase in Rac activity which is followed by a later increase in RhoA activity (Maddala et al. 2003). Indeed in several cellular processes, such as the regulation of cell-cell junctions, cell spreading and adhesion to substrates, neurite outgrowth and the epithelial-mesenchyme transition, it appears that Rac and Rho play opposing roles (Braga et al. 1999; Burridge, 1999; Burridge and Wennerberg, 2004;

Hall and Nobes, 2000; Rottner et al. 1999; Sander et al. 1999; Wojciak-Stothard and Ridley, 2003).

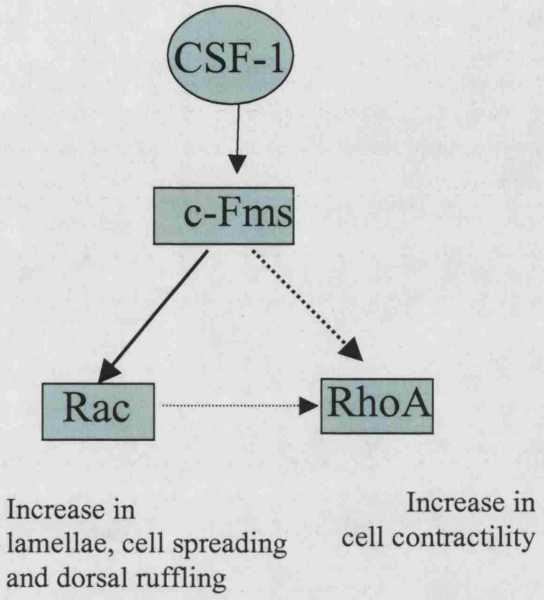

Figure 6.8: Schematic diagram showing the effects of CSF-1 stimulation mediated by RhoA and Rac

Study of Rac1-null BMM showed that the acute response of the actin cytoskeleton to CSF-1 was reduced. The increase in spread area and change in the elongation of Rac-1 null BMM was also significantly reduced compared to Wt BMM (Wells et al. 2004). This suggests that CSF-1 induced changes in elongation, promotion of spreading and dorsal ruffling are processes that are promoted through CSF-1 activation of Rac and do not require activation of RhoA activity (particularly RhoA activity is not increased following 60 min of CSF-1 stimulation). However, RhoA activity was found to be essential for cell migration (Chapter 4.1) Analysis of the migration of BMM in Dunn chemotaxis chambers showed that they did not become motile immediately following CSF-1 stimulation (See video 4.7), although they clearly formed lamellae, filopodia and began to adopt a polarised migratory morphology in the first hour of CSF-1 stimulation (Fig. 3.7) (Jones et al. 2003; Wells et al. 2004). It would be interesting to find out if the delayed increase in BMM motility after CSF-1 treatment is accompanied by an increase in RhoA activity.

RhoB activity is not markedly affected by CSF-1, consistent with this, deletion of *RhoB* does not affect the kinetics of stimulation of Akt phosphorylation, which is an indicator of PI 3-kinase activity (Vanhaesebroeck et al. 1999), or the of phosphorylation of ERK, which was involved in chemotaxis in macrophages and monocytes (Ashida et al. 2001; Wells et al. 2004). This suggests that RhoB does not play a direct role as an intermediate in CSF-1 dependent signalling. However, deletion of RhoB did affect the protein tyrosine phosphorylation levels in BMM following CSF-1 stimulation. As C-Fms, is a receptor tyrosine kinase, it is possible that either the tyrosine kinase activity of C-Fms, or the activity of downstream tyrosine kinases such as Src is decreased by deletion of RhoB (Sandilands et al. 2004). RhoB has previously been implicated in regulation of trafficking of receptor tyrosine kinases (Gampel et al. 1999; Rojas et al. 2004). c-Fms is localised in perinuclear structures, corresponding to endosomes or Golgi, 5-30 min after CSF-1 stimulation (Yeung and Stanley, 2003). It is interesting to note that RhoB, known to be localised on the endosomes (Wherlock et al. 2004), was activated 5-30 min after CSF-1 stimulation. This suggests that RhoB could be active during trafficking of C-Fms. PRK1, which has been shown to form a complex with RhoB that can retard trafficking of EGF through the endocytic pathway (Mellor et al. 1998), is expressed in BMM. It would be interesting to find out if RhoB and c-Fms co-localise on the endosomes, and whether deletion of RhoB alters the rate or pathways of trafficking of c-Fms.

Deletion of RhoB from BMM slightly alters the activation of RhoA, Rac and Cdc42. The phosphorylation of the downstream effectors of RhoA and Rac, MLC and LIMK, is also altered in *RhoB*$^{-/-}$ BMM when CSF-1 is withdrawn. It is interesting to note here that *RhoB*$^{-/-}$ BMM are still motile in the absence of CSF-1 (Fig. 4.2) and this might be due to the differences in the activity of MLC and LIMK in CSF-1 starved BMM. Both cell contractility, which is regulated by MLC phosphorylation (Kaibuchi et al. 1999) and actin polymerisation, which is regulated in part through LIMK (Millard et al. 2004) may still be active in CSF-1 starved *RhoB*$^{-/-}$ BMM. ROCK, a downstream effector or RhoA is known to promote phosphorylation of both MLC and LIMK, so perhaps ROCK activity is higher in *RhoB*$^{-/-}$ BMM starved of CSF-1.

To summarise RhoB does appear to regulate RhoA activity as its deletion causes an increase in RhoA activity. This then may well upset the equilibrium of Rho GTPase signalling within the whole cell. Deletion of RhoB affects protein tyrosine

phosphorylation and MLC and LIMK activities but not the other CSF-1 regulated pathways tested. It would be interesting to investigate the link between these changes and motility, adhesion and spreading in BMM.

Chapter 7: Concluding Remarks

7.1 Migration and adhesion

Macrophages are a key component of both the innate and acquired immune systems. Macrophages, derived from circulating monocytes are the major inflammatory cell type present in wounded tissue at the early proliferative stage of wound repair. The ability of macrophages to phagocytose and produce factors that regulate tissue repair and tissue remodelling is critical to their physiological function. The recruitment of macrophages to the wound depends upon adherence to the endothelium, the establishment of a gradient of chemoattractant and the ability of macrophages to migrate up this gradient (Gordon, 1995; Webb et al. 1996).

Wound repair requires the movement of four key cell types, neutrophils, lymphocytes, macrophages and tissue cells such as keratinocytes or fibroblasts. Each of these cell types has individual characteristics of cell shape, velocity and cytoskeletal organisation which are unique to that cell type (Friedl et al. 1998b). Neutrophils are the first cells to become recruited to a wound (Henderson et al. 2003), so it is perhaps not surprising that they migrate at a high speed (Table 7.1). Both neutrophils and T cells have an amoeboid migratory morphology with a uropod which projects above the cell surface at the rear of the cell, keratinocytes are spread and consist of a single large lamella, both macrophages and fibroblasts are multipolar, with a spread leading lamella and a contracted tail (Friedl et al. 1998b; Ridley et al. 2003). It is interesting to note here that both fibroblasts and macrophages have a relatively slow speed of migration compared to other leukocytes. Howener, the speed of macrophage migration, similarly to other cell types, does appear to depend on the substrate it is moving on (Chapter 4.1 and 4.6) (Friedl, 2004). What causes these cell types to adopt different migratory morphologies is currently not known (Ivetic and Ridley, 2004).

Cell type	Speed of migration μm/min
Neutrophil	9
Macrophage	0.6
T Lymphocyte	7.2
Fibroblast	0.2

Table 7.1: The approximate speed of different cell types on a 2D matrix taken from (Friedl et al. 1998b)

Both fibroblasts and macrophages form clusters of integrins (focal contacts) where they physically interact with the substratum. In fibroblasts these interactions are prominent at the leading edge of the cell and then mature to become focal adhesions as the cell moves forwards (Bershadsky et al. 2003; Friedl et al. 1998b; Linder et al. 2000). Conversely, neutrophils and T cells organise their adhesions differently to macrophages and fibroblasts. They do not cluster their integrins, except in the uropod, and adhesive foci are not visible using conventional microscopy in these cell types (Friedl et al. 1998b; Wiseman et al. 2004). Interestingly TIRF microscopy shows that macrophages and fibroblasts go through similar stages in cell spreading (Dobereiner et al. 2004) (Chapter 5.8). This may indicate that macrophages and fibroblasts may form their adhesions by a similar mechanism, but they mature their adhesions differently.

Leukocytes organise their actin cytoskeleton differently to fibroblasts, they lack actin stress fibres and large focal adhesions, instead they often have a cortical actin ring and fine actin filaments which surround the cells (Hogg et al. 2002; Ivetic and Ridley, 2004) (Chapter 3.5). Macrophages are similar to osteoclasts and dendritic cells as they adhere to the substratum using small adhesive foci which are distributed across the basal layer of the substratum (Burns et al. 2004; Pfaff and Jurdic, 2001). Similar to other myeloid cell types BMM also contain podosomes which, whilst they are not the primary mechanism for adhesion to the substratum, contain adhesive elements (Linder and Aepfelbacher, 2003). CSF-1 stimulation, which is known to promote chemotaxis, has been shown to promote podosome formation in BMM (Chapter 3.6). Other pro-inflammatory cytokines also promote formation of podosomes (Linder and Aepfelbacher, 2003; McNiven et al. 2004) which may suggest that podosome activity is part of the inflammatory response, perhaps allowing chemotaxing cells to breakdown the extracellular matrix.

7.2 Chemotaxis

Macrophages have been shown to chemotax towards CSF-1 (Allen et al. 1998; Jones et al. 2003; Webb et al. 1996; Wells et al. 2004), but their migration upon exposure to a gradient of CSF-1 does not occur immediately (Movie 4.7). This could be because other chemokine signals such as MCP-1 or CR5, which signal through G-protein coupled receptors (Ashida et al. 2001; Hogg et al. 2002; Jones et al. 2003), are required to reinforce the receptor tyrosine signalling stimulated by CSF-1, or alternatively as recruitment of monocytes to a wound is delayed until the late inflammatory / early proliferative phase (Gordon, 1995; Hogg et al. 2002), the delay in chemotaxtic response to CSF-1 is part of macrophage physiology. It is possible that the technique used with the Dunn chemotaxis chambers (Wells and Ridley, 2004), requires slight improvements to aid study of chemotaxis. Especially as chemotaxis towards MCP-1 is more rapid than chemotaxis towards CSF-1 (Jones et al. 2003).It would be interesting to investigate this in more depth.

Deletion of RhoB did not affect the ability of macrophages to chemotax, due to a lack of time, the ability of *RhoB*$^{-/-}$ BMM to phagocytose was not investigated. There have not been any reports of *RhoB*$^{-/-}$ mice having compromised immune function, although this has not been specifically tested, so it can be concluded that overall the impact of deletion of RhoB is not hugely deleterious to immune function. In fact *RhoB*$^{-/-}$ BMM had a slightly increased speed of migration on fibronectin. It is interesting to note that the *RhoB*$^{-/-}$BMM also had a decreased spread area. In other cell types such as fibroblasts where cell spread area has been decreased the speed of migration is also seen to increase (Nobes and Hall, 1999). Neutrophils and T-Lymphocytes are also cells with a small spread area and a fast speed of migration. It is likely that spread area and speed of migration are inversely correlated not only in fibroblasts (Friedl, 2004), but in all cell types.

7.3 Rho isoform specificity

RhoA is known, in fibroblasts, to regulate formation of stress fibres and cellular contractility (Narumiya et al. 1997; Ridley and Hall, 1992) and is localised on the plasma membrane (Adamson et al. 1992). RhoB has been shown to be localised both on

the plasma membrane and the endosomes and has been shown in epithelial cell lines to retard intracellular trafficking of EGF (Rojas et al. 2004; Wherlock et al. 2004). When RhoA and RhoB were overexpressed in fibroblasts they both promoted formation of stress fibres (Adamson et al. 1992). To determine whether RhoA and RhoB are indeed functionally redundant, loss of function studies can be a useful tool, such as use of genetic knockouts, mRNA silencing and small molecule inhibitors. C3 transferase inhibits cell migration in several cell types (Hall and Nobes, 2000; Saito et al. 2002; Smith et al. 2003; Tsuji et al. 2002), including BMM (Chapter 4.1). As *RhoB*$^{-/-}$ BMM migrate more rapidly than Wt BMM it is clear that cell migration is dependent on RhoA activity and not RhoB in BMM. Rac1-null macrophages did not have impaired migration, similarly the migration of Rac1- and Rac2- null neutrophils and T cells was not inhibited. However Rac1/Rac2 double knock out neutrophils had inhibited motility (Gu et al. 2003; Li et al. 2002; Wells et al. 2004). This indicates that in the case of Rac proteins one isoform can compensate for the loss of the other in the process of cell migration. For Rho proteins this appears not to be the case (Chapter 4.1 and 4.2) although it is possible that RhoA and RhoC are functionally redundant. To categorically prove this assertion it will be necessary to make inhibitors of individual isoforms of Rho, for example using RNAi technology.

Although RhoA activity is required for migration it does not appear to be required for cell adhesion, similarly to monocytes (Wothylake et al. 2001). C3 transferase treated BMM increased their spread area and did not detach from the substrate (Chapter 3.9 and 4.10), although they did lose podosomes. RhoA activity is known to be required for podosome organisation in several cell types (Berdeaux et al. 2004; Chellaiah et al. 2000b; Moreau et al. 2003). RhoB however is required for adhesion, deletion of RhoB reduces the cell surface expression of β2 and β3 integrins (chapter 5.3) and *RhoB*$^{-/-}$ BMM have defects in spreading (Chapter 5.8). It was not possible to determine impact of deletion of RhoA on integrin expression or cell spreading as a RhoA-null mouse has not been published.

RhoA and RhoB therefore appear to have opposing roles in migration and spreading, and the activity of RhoA in these is dominant. However, there are certain morphological phenomena in BMM upon which deletion of RhoB has no impact but that inhibition of Rho or ROCK alter dramatically, such as tail retraction, dorsal ruffling and podosome formation. This indicates that RhoB is not simply a negative modifier of RhoA function

in migration and adhesion, but also has functions which are independent of RhoA, these may be shown by the difference in the kinetics of protein tyrosine phosphorylation in BMM after CSF-1 stimulation and other differences noted in the CSF-1 response (Fig 6.5 and 3.9). RhoA activation assays showed that in *RhoB*$^{-/-}$ BMM RhoA activity was higher (Chapter 6.2), and the activity of both Rac and Cdc42 was also perturbed in *RhoB*$^{-/-}$ BMM (Chapter 6.2). This suggests that RhoB may indirectly affect the balance of GTPase signalling across the cell by its effects on integrin levels of cell shape (del Pozo et al. 2004; DeMali et al. 2003). Cross talk between GTPases, for instance RhoA and Rac1 has been shown in several cellular processes, either through interactions with GEFs and GAPS or effectors (Burridge, 1999; Hall, 2000; Nimnual et al. 2003; Tsuji et al. 2002). RhoB may act upon RhoA in this way by sequestering effectors or competing with RhoA for common exchange factors (Prendergast, 2001). In the absence of RhoB, RhoA will then have enhanced ability to bind these effectors and promote activation of their downstream targets (Fig. 7.1). The increase in phosphorylation of MLC and LIMK in *RhoB*$^{-/-}$ BMM would support this hypothesis.

7.4 RhoA, ROCK and motility

The mechanism through which RhoA mediates its activity appears to vary between cell types. In macrophages, T cells and neutrophils the ROCK inhibitor Y27632 causes an increase in cell spreading and a decrease in the rate of cell migration (Niggli, 2003; Smith et al. 2003), but in fibroblasts the opposite effect is observed (Nobes and Hall, 1999). The effect of Y27632 on monocytes is substrate dependent. On non-charged substrates monocytes display a similar morphology to that seen by BMM. However on VCAM, ICAM-1 and fibronectin monocytes extend lamellipodia and protrusions and develop podosome like structures (Worthylake and Burridge, 2003). In monocytes this is attributed to a destabilising of the cortical actin network and it would be interesting to identify if the effects of Y27632 varied with substrate in BMM as well.

It is not clear why Y27632 has a cell type and substrate type specific effect. It may be because cell types regulate the cortical actin network differently (Hall, 1998;Worthylake and Burridge 2003). The cortical actin network is corrdinated through the distribution of effectors of Rho within the cell. In fibroblasts dominant-negative mDia is known to be able to override the promotion of ruffling promoted by Y27632 treatment (Tsuji et al. 2002). Conversely, the inhibition of cell migration by dominant

negative mDia1 can be overcome by addition of Y27632 (Magdalena et al. 2003). In T cells, monocytes and fibroblasts ROCK has been

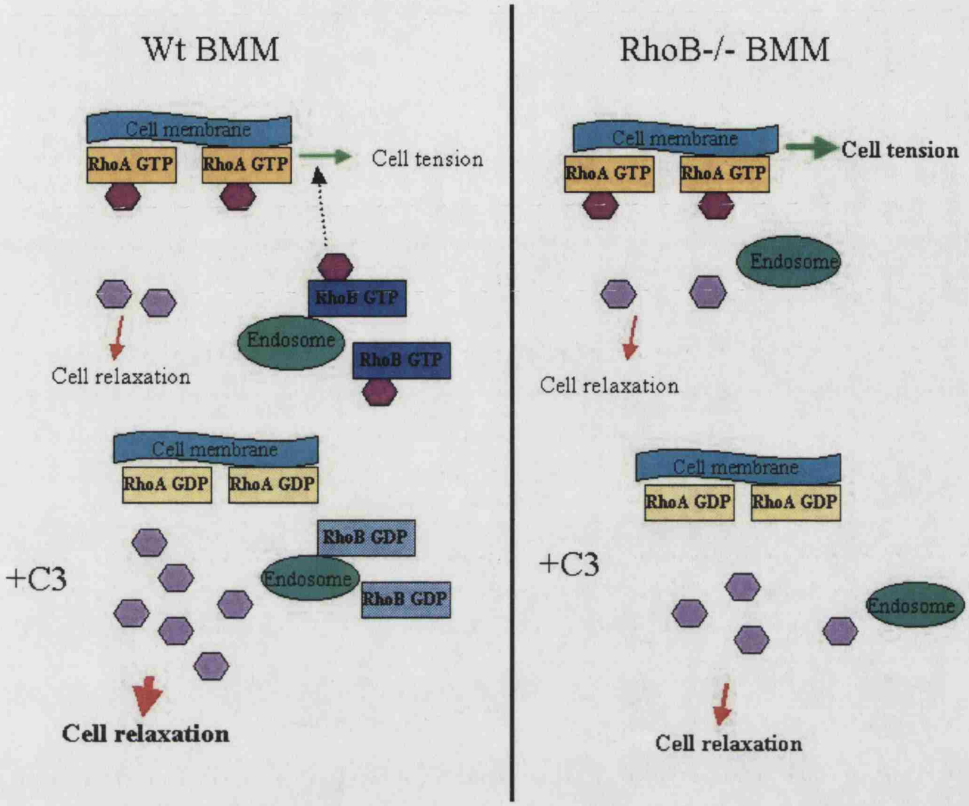

Figure 7.1: Schematic diagram showing how RhoA and RhoB compete for effectors.

shown to act at the rear of the cell where it is involved in tail retraction (Riento and Ridley, 2003).The localisation of mDia, Citron and other Rho effectors is not known in most cell types although BMM have been shown to express PRK1 (Chapter 6.5), which has been shown to be targeted to endosomes by RhoB (Mellor et al. 1998). RhoA is not the only Rho family GTPase that interacts with ROCK. Both Gem and RhoE are known to interact with ROCK and inhibit its downstream signaling (Olson, 2002; Riento and Ridley, 2003). The expression level of these other Rho family GTPases may be cell type specific (similarly to RhoB and RhoC), so it may be that the reported differences in the actions Y27632 are due to cell type-specific expression of Gem or RhoE.

7.5 RhoA, RhoB and CSF-1 signaling

Cell signalling stimulated by CSF-1 is essential to BMM function. CSF-1-null mice have compromised immune defence, potentially indicative of loss of macrophages, osteoporosis, fertility defects and tooth eruption failure. (Dai et al. 2002). Withdrawal of

CSF-1 from BMM causes reduction changes in morphology including a reduction in: membrane ruffling, cell spreading and the proportion of macrophages that migrate on both glass and plastic as well as elongation of BMM (Figures 4.2, 4.6, 4.10, 4.11) (Wells et al. 2004). The effect of withdrawal of CSF-1 on cell turning appears to depend on the substrate BMM are plated on. This may be due to differences in signalling from the integrin complexes involved in forming adhesions. The changes in morphology are accompanied by a decrease in RhoA and Rac GTPase activity in BMM. Stimulation of BMM with CSF-1 is known to cause an acute increase in Rac1 activity (Wells et al. 2004). This is accompanied by an increase in dorsal ruffling and formation of lamellae (Figure 3.7 and 4.10)(Wells et al. 2004). Interestingly RhoA activity is not altered increased upon acute CSF-1 stimulation (Figure 6.4). Rho activity has previously been shown to not be required for formation of dorsal ruffles and lamellae in macrophage cell lines (Allen et al. 1997), so perhaps it is not surprising that RhoA is not immediately activated upon CSF-1 stimulation. Interestingly, CSF-1 stimulation increases the number of BMM with podosomes to levels seen in growing cells with a similar kinetic to that of RhoA activation (Figure 3.7 and 6.4) and inhibition of RhoA causes a reduction in podosomes, further linking RhoA activity to podosome formation (Berdeaux et al. 2004; Chellaiah et al. 2000b; Moreau et al. 2003). The increase in RhoA activity also appears to occur at a similar time after CSF-1 stimulation to when BMM were observed to begin formation of a polarised migratory morphology (Figure 3.7). It would be very interesting to examine the link between CSF-1 stimulation, the activation status of Rho GTPases and the morphology of Wt BMM in much greater detail. This would allow deeper insights into the role of Rho GTPases in signaling to cell polarisation and migration.

Deletion of RhoB perturbed CSF-1 signaling in BMM, although it did not affect chemotaxis, or the PI 3-kinase-Akt and ERK/MAPK signaling pathways, which have been associated with to chemotaxis (Vanhaesebroeck et al. 1999; Xu et al. 2003). Most notably the proportion of *RhoB*$^{-/-}$ BMM which translocated more than 30 μm on both glass and fibronectin in the absence of CSF-1 was significantly higher than Wt BMM (Table 4.1 and 4.2). The fact that MLC phosphorylation is not decreased in *RhoB*$^{-/-}$ BMM in starve medium and LIMK phosphorylation is only slightly reduced may account for this (Chapter 6.3).

RhoB does, however, has a slightly different kinetic of activation to RhoA. Its activity appears to transiently increase, then decrease in response to CSF-1 (Chapter 6.5). A similar pattern of activation of RhoB has also been observed in EGF signaling (Gampel et al. 1999). Although *RhoB*$^{-/-}$ BMM do not appear to have any defects in membrane ruffling in response to CSF-1 stimulation (Chapter 4.12), they do have differences in podosome redistribution (Figure 3.7). It would be interesting to find out if the trafficking of the CSF-1 receptor is altered in *RhoB*$^{-/-}$ BMM, and if so how this affects cell signaling and what the consequences are for BMM migration and morphology, especially as the CSF-1 receptor, is known to be trafficked to the lysosome following stimulation (Yeung and Stanley, 2003).

In summary it can be said that this thesis shows that RhoA and RhoB are not functionally redundant in regulating macrophage morphology and migration although there is still much to investigate concerning the mechanisms through which RhoA and RhoB elicit their effects.

References

Abercrombie, M. Heaysman, J. E. and Pegrum, S. M. (1971). The locomotion of fibroblasts in culture. IV. Electron microscopy of the leading lamella. Exp Cell Res *67*, 359-367.

Adamson, P. Paterson, H. F. and Hall, A. (1992). Intracellular localization of the P21rho proteins. J Cell Biol *119*, 617-627.

Adi, S. Wu, N. Y. and Rosenthal, S. M. (2001). Growth factor-stimulated phosphorylation of Akt and p70(S6K) is differentially inhibited by LY294002 and Wortmannin. Endocrinology *142*, 498-501.

Adini, I. Rabinovitz, I. Sun, J. F. Prendergast, G. C. and Benjamin, L. E. (2003). RhoB controls Akt trafficking and stage-specific survival of endothelial cells during vascular development. Genes Dev *17*, 2721-2732.

Adnane, J. Seijo, E. Chen, Z. Bizouarn, F. Leal, M. Sebti, S. M. and Munoz-Antonia, T. (2002). RhoB, not RhoA, represses the transcription of the transforming growth factor β type II receptor by a mechanism involving activator protein 1. J Biol Chem *277*, 8500-8507.

Aktories, K. Wilde, C. and Vogelsgesang, M. (2004). Rho-modifying C3-like ADP-ribosyltransferases. Rev Physiol Biochem Pharmacol *152*, 1-22.

Allal, C. Pradines, A. Hamilton, A. D. Sebti, S. M. and Favre, G. (2002). Farnesylated RhoB prevents cell cycle arrest and actin cytoskeleton disruption caused by the geranylgeranyltransferase I inhibitor GGTI-298. Cell Cycle *1*, 430-437.

Allen, W. E. Jones, G. E. Pollard, J. W. and Ridley, A. J. (1997). Rho, Rac and Cdc42 regulate actin organization and cell adhesion in macrophages. J Cell Sci *110 (Pt 6)*, 707-720.

Allen, W. E. Zicha, D. Ridley, A. J. and Jones, G. E. (1998). A role for Cdc42 in macrophage chemotaxis. J Cell Biol *141*, 1147-1157.

Altankov, G. and Groth, T. (1996). Fibronectin matrix formation by human fibroblasts on surfaces varying in wettability. J Biomater Sci Polym Ed *8*, 299-310.

Arber, S. Barbayannis, F. A. Hanser, H. Schneider, C. Stanyon, C. A. Bernard, O. and Caroni, P. (1998). Regulation of actin dynamics through phosphorylation of cofilin by LIM-kinase. Nature *393*, 805-809.

Arthur, W. T. and Burridge, K. (2001). RhoA inactivation by p190RhoGAP regulates cell spreading and migration by promoting membrane protrusion and polarity. Mol Biol Cell *12*, 2711-2720.

Arthur, W. T. Ellerbroek, S. M. Der, C. J. Burridge, K. and Wennerberg, K. (2002a). XPLN, a guanine nucleotide exchange factor for RhoA and RhoB, but not RhoC. J Biol Chem *277*, 42964-42972.

Arthur, W. T. Noren, N. K. and Burridge, K. (2002b). Regulation of Rho family GTPases by cell-cell and cell-matrix adhesion. Biol Res *35*, 239-246.

Ashida, N. Arai, H. Yamasaki, M. and Kita, T. (2001). Distinct signaling pathways for MCP-1-dependent integrin activation and chemotaxis. J Biol Chem *276*, 16555-16560.

Ballestrem, C. Wehrle-Haller, B. and Imhof, B. A. (1998). Actin dynamics in living mammalian cells. J Cell Sci *111 (Pt 12)*, 1649-1658.

Bear, J. E. Svitkina, T. M. Krause, M. Schafer, D. A. Loureiro, J. J. Strasser, G. A. Maly, I. V. Chaga, O. Y. Cooper, J. A. Borisy, G. G. and Gertler, F. B. (2002). Antagonism between Ena/VASP proteins and actin filament capping regulates fibroblast motility. Cell *109*, 509-521.

Berdeaux, R. L. Diaz, B. Kim, L. and Martin, G. S. (2004). Active Rho is localized to podosomes induced by oncogenic Src and is required for their assembly and function. J Cell Biol *166*, 317-323.

Bershadsky, A. D. Balaban, N. Q. and Geiger, B. (2003). Adhesion-dependent cell mechanosensitivity. Annu Rev Cell Dev Biol *19*, 677-695.

Bhatt, N. Y. Kelley, T. W. Khramtsov, V. V. Wang, Y. Lam, G. K. Clanton, T. L. and Marsh, C. B. (2002). Macrophage-colony-stimulating factor-induced activation of extracellular-regulated kinase involves phosphatidylinositol 3-kinase and reactive oxygen species in human monocytes. J Immunol *169*, 6427-6434.

Bhattacharyya, R. and Wedegaertner, P. B. (2003). Characterization of G α 13-dependent plasma membrane recruitment of p115RhoGEF. Biochem J *371*, 709-720.

Bishop, A. L. and Hall, A. (2000). Rho GTPases and their effector proteins. Biochem J *348 Pt 2*, 241-255.

Biyasheva, A. Svitkina, T. Kunda, P. Baum, B. and Borisy, G. (2004). Cascade pathway of filopodia formation downstream of SCAR. J Cell Sci *117*, 837-848.

Bosman FT, Stamenkovic I. (2003). Functional structure and composition of the extracellular matrix.J Pathol. *200*:423-8.

Brach, M. A. Henschler, R. Mertelsmann, R. H. and Herrmann, F. (1991). Regulation of M-CSF expression by M-CSF: role of protein kinase C and transcription factor NF κB. Pathobiology *59*, 284-288.

Braga, V. M. Del Maschio, A. Machesky, L. and Dejana, E. (1999). Regulation of cadherin function by Rho and Rac: modulation by junction maturation and cellular context. Mol Biol Cell *10*, 9-22.

Burke, B. and Lewis, C. E. (2002). The macrophage, 2nd edn (Oxford, Oxford University Press).

Burns, S. Hardy, S. J. Buddle, J. Yong, K. L. Jones, G. E. and Thrasher, A. J. (2004). Maturation of DC is associated with changes in motile characteristics and adherence. Cell Motil Cytoskeleton *57*, 118-132.

Burns, S. Thrasher, A. J. Blundell, M. P. Machesky, L. and Jones, G. E. (2001). Configuration of human dendritic cell cytoskeleton by Rho GTPases, the WAS protein, and differentiation. Blood *98*, 1142-1149.

Burridge, K. (1999). Crosstalk between Rac and Rho. Science *283*, 2028-2029.

Burridge, K. and Wennerberg, K. (2004). Rho and Rac take center stage. Cell *116*, 167-179.

Calderwood DA, and Ginsberg MH (2003). Talin forges the links between integrins and actin. Nat Cell Biol *8*:694-7.

Calle, Y. Chou, H. C. Thrasher, A. J. and Jones, G. E. (2004). Wiskott-Aldrich syndrome protein and the cytoskeletal dynamics of dendritic cells. J Pathol *204*, 460-469.

Cannizzaro, L. A. Madaule, P. Hecht, F. Axel, R. Croce, C. M. and Huebner, K. (1990). Chromosome localization of human ARH genes, a ras-related gene family. Genomics *6*, 197-203.

Castellano, F. Chavrier, P. and Caron, E. (2001). Actin dynamics during phagocytosis. Semin Immunol *13*, 347-355.

Chang, J. H. Gill, S. Settleman, J. and Parsons, S. J. (1995). c-Src regulates the simultaneous rearrangement of actin cytoskeleton, p190RhoGAP, and p120RasGAP following epidermal growth factor stimulation. J Cell Biol *130*, 355-368.

Chang, L. and Goldman, R. D. (2004). Intermediate filaments mediate cytoskeletal crosstalk. Nat Rev Mol Cell Biol *5*, 601-613.

Chellaiah, M. Kizer, N. Silva, M. Alvarez, U. Kwiatkowski, D. and Hruska, K. A. (2000a). Gelsolin deficiency blocks podosome assembly and produces increased bone mass and strength. J Cell Biol *148*, 665-678.

Chellaiah, M. A. Soga, N. Swanson, S. McAllister, S. Alvarez, U. Wang, D. Dowdy, S. F. and Hruska, K. A. (2000b). Rho-A is critical for osteoclast podosome organization, motility, and bone resorption. J Biol Chem *275*, 11993-12002.

Chen, Z. Sun, J. Pradines, A. Favre, G. Adnane, J. and Sebti, S. M. (2000). Both farnesylated and geranylgeranylated RhoB inhibit malignant transformation and suppress human tumor growth in nude mice. J Biol Chem *275*, 17974-17978.

Chikumi, H. Barac, A. Behbahani, B. Gao, Y. Teramoto, H. Zheng, Y. and Gutkind, J. S. (2004). Homo- and hetero-oligomerization of PDZ-RhoGEF, LARG and p115RhoGEF by their C-terminal region regulates their in vivo Rho GEF activity and transforming potential. Oncogene *23*, 233-240.

Clark, E. A. Golub, T. R. Lander, E. S. and Hynes, R. O. (2000). Genomic analysis of metastasis reveals an essential role for RhoC. Nature *406*, 532-535.

Clark, E. A. King, W. G. Brugge, J. S. Symons, M. and Hynes, R. O. (1998). Integrin-mediated signals regulated by members of the rho family of GTPases. J Cell Biol *142*, 573-586.

Conway, A. M. James, A. B. O'Kane, E. M. Rakhit, S. and Morris, B. J. (2004). Regulation of myosin light chain phosphorylation by RhoB in neuronal cells. Exp Cell Res *300*, 35-42.

Correia, I. Chu, D. Chou, Y. H. Goldman, R. D. and Matsudaira, P. (1999). Integrating the actin and vimentin cytoskeletons. adhesion-dependent formation of fimbrin-vimentin complexes in macrophages. J Cell Biol *146*, 831-842.

Cox, A. D. and Der, C. J. (2002). Farnesyltransferase inhibitors: promises and realities. Curr Opin Pharmacol *2*, 388-393.

Croker, B. A. Handman, E. Hayball, J. D. Baldwin, T. M. Voigt, V. Cluse, L. A. Yang, F. C. Williams, D. A. and Roberts, A. W. (2002a). Rac2-deficient mice display perturbed T-cell distribution and chemotaxis, but only minor abnormalities in T(H)1 responses. Immunol Cell Biol *80*, 231-240.

Croker, B. A. Tarlinton, D. M. Cluse, L. A. Tuxen, A. J. Light, A. Yang, F. C. Williams, D. A. and Roberts, A. W. (2002b). The Rac2 guanosine triphosphatase regulates B lymphocyte antigen receptor responses and chemotaxis and is required for establishment of B-1a and marginal zone B lymphocytes. J Immunol *168*, 3376-3386.

Curtis, A. S. (1964). The Mechanism of Adhesion of Cells to Glass. A Study by Interference Reflection Microscopy. J Cell Biol *20*, 199-215.

Dai, X. M. Ryan, G. R. Hapel, A. J. Dominguez, M. G. Russell, R. G. Kapp, S. Sylvestre, V. and Stanley, E. R. (2002). Targeted disruption of the mouse colony-stimulating factor 1 receptor gene results in osteopetrosis, mononuclear phagocyte deficiency, increased primitive progenitor cell frequencies, and reproductive defects. Blood *99*, 111-120.

Danen, E. H. Sonneveld, P. Brakebusch, C. Fassler, R. and Sonnenberg, A. (2002). The fibronectin-binding integrins α5β1 and αvβ3 differentially modulate RhoA-GTP loading, organization of cell matrix adhesions, and fibronectin fibrillogenesis. J Cell Biol *159*, 1071-1086.

Del Barrio, M. G. and Nieto, M. A. (2004). Relative expression of Slug, RhoB, and HNK-1 in the cranial neural crest of the early chicken embryo. Dev Dyn *229*, 136-139.

del Pozo, M. A. Alderson, N. B. Kiosses, W. B. Chiang, H. H. Anderson, R. G. and Schwartz, M. A. (2004). Integrins regulate Rac targeting by internalization of membrane domains. Science *303*, 839-842.

Delannet, M. Martin, F. Bossy, B. Cheresh, D. A. Reichardt, L. F. and Duband, J. L. (1994). Specific roles of the αV β 1, αV β3 and αV β5 integrins in avian neural crest cell adhesion and migration on vitronectin. Development *120*, 2687-2702.

DeMali, K. A. Wennerberg, K. and Burridge, K. (2003). Integrin signaling to the actin cytoskeleton. Curr Opin Cell Biol *15*, 572-582.

Destaing, O. Saltel, F. Geminard, J. C. Jurdic, P. and Bard, F. (2003). Podosomes display actin turnover and dynamic self-organization in osteoclasts expressing actin-green fluorescent protein. Mol Biol Cell *14*, 407-416.

Dobereiner, H. G. Dubin-Thaler, B. Giannone, G. Xenias, H. S. and Sheetz, M. P. (2004). Dynamic phase transitions in cell spreading. Phys Rev Lett *93*, 108105.

Du, W. and Prendergast, G. C. (1999). Geranylgeranylated RhoB mediates suppression of human tumor cell growth by farnesyltransferase inhibitors. Cancer Res *59*, 5492-5496.

Dubin-Thaler, B. J. Giannone, G. Dobereiner, H. G. and Sheetz, M. P. (2004). Nanometer analysis of cell spreading on matrix-coated surfaces reveals two distinct cell states and STEPs. Biophys J *86*, 1794-1806.

Duong, L. T. Lakkakorpi, P. T. Nakamura, I. Machwate, M. Nagy, R. M. and Rodan, G. A. (1998). PYK2 in osteoclasts is an adhesion kinase, localized in the sealing zone, activated by ligation of α (v)β3 integrin, and phosphorylated by src kinase. J Clin Invest *102*, 881-892.

Edwards, D. C. Sanders, L. C. Bokoch, G. M. and Gill, G. N. (1999). Activation of LIM-kinase by Pak1 couples Rac/Cdc42 GTPase signalling to actin cytoskeletal dynamics. Nat Cell Biol *1*, 253-259.

Etienne-Manneville, S. (2004). Cdc42--the centre of polarity. J Cell Sci *117*, 1291-1300.

Evans, J. G. Correia, I. Krasavina, O. Watson, N. and Matsudaira, P. (2003). Macrophage podosomes assemble at the leading lamella by growth and fragmentation. J Cell Biol *161*, 697-705.

Fadok, V. A. Bratton, D. L. Konowal, A. Freed, P. W. Westcott, J. Y. and Henson, P. M. (1998). Macrophages that have ingested apoptotic cells in vitro inhibit proinflammatory cytokine production through autocrine/paracrine mechanisms involving TGF-β, PGE2, and PAF. J Clin Invest *101*, 890-898.

Franco, S. J. Rodgers, M. A. Perrin, B. J. Han, J. Bennin, D. A. Critchley, D. R. and Huttenlocher, A. (2004). Calpain-mediated proteolysis of talin regulates adhesion dynamics. Nat Cell Biol *6*, 977-983.

Friedl, P. (2004). Dynamic imaging of cellular interactions with extracellular matrix. Histochem Cell Biol *122*, 183-190.

Friedl, P. Brocker, E. B. and Zanker, K. S. (1998a). Integrins, cell matrix interactions and cell migration strategies: fundamental differences in leukocytes and tumor cells. Cell Adhes Commun *6*, 225-236.

Friedl, P. Zanker, K. S. and Brocker, E. B. (1998b). Cell migration strategies in 3-D extracellular matrix: differences in morphology, cell matrix interactions, and integrin function. Microsc Res Tech *43*, 369-378.

Fritz, G. Gnad, R. and Kaina, B. (1999). Cell and tissue-type specific expression of Ras-related GTPase RhoB. Anticancer Res *19*, 1681-1688.

Fritz, G. and Kaina, B. (2001). Transcriptional activation of the small GTPase gene rhoB by genotoxic stress is regulated via a CCAAT element. Nucleic Acids Res *29*, 792-798.

Fritz, G. Kaina, B. and Aktories, K. (1995). The ras-related small GTP-binding protein RhoB is immediate-early inducible by DNA damaging treatments. J Biol Chem *270*, 25172-25177.

Fuchs, E. and Cleveland, D. W. (1998). A structural scaffolding of intermediate filaments in health and disease. Science *279*, 514-519.

Fujiwara K, Tilney LG (1975). Substructural analysis of the microtubule and its polymorphic forms. Ann N Y Acad Sci.*253*, 27-50.

Fujisawa, K. Madaule, P. Ishizaki, T. Watanabe, G. Bito, H. Saito, Y. Hall, A. and Narumiya, S. (1998). Different regions of Rho determine Rho-selective binding of different classes of Rho target molecules. J Biol Chem *273*, 18943-18949.

Funamoto, S. Meili, R. Lee, S. Parry, L. and Firtel, R. A. (2002). Spatial and temporal regulation of 3-phosphoinositides by PI 3-kinase and PTEN mediates chemotaxis. Cell *109*, 611-623.

Gampel, A. Parker, P. J. and Mellor, H. (1999). Regulation of epidermal growth factor receptor traffic by the small GTPase rhoB. Curr Biol *9*, 955-958.

Geiger, B. Avnur, Z. Kreis, T. E. and Schlessinger, J. (1984). The dynamics of cytoskeletal organization in areas of cell contact. Cell Muscle Motil *5*, 195-234.

Geiger, B. and Bershadsky, A. (2002). Exploring the neighborhood: adhesion-coupled cell mechanosensors. Cell *110*, 139-142.

Giannone, G. Dubin-Thaler, B. J. Dobereiner, H. G. Kieffer, N. Bresnick, A. R. and Sheetz, M. P. (2004). Periodic lamellipodial contractions correlate with rearward actin waves. Cell *116*, 431-443.

Glantschnig, H. Fisher, J. E. Wesolowski, G. Rodan, G. A. and Reszka, A. A. (2003). M-CSF, TNFα and RANK ligand promote osteoclast survival by signaling through mTOR/S6 kinase. Cell Death Differ *10*, 1165-1177.

Glogauer, M. Marchal, C. C. Zhu, F. Worku, A. Clausen, B. E. Foerster, I. Marks, P. Downey, G. P. Dinauer, M. and Kwiatkowski, D. J. (2003). Rac1 deletion in mouse neutrophils has selective effects on neutrophil functions. J Immunol *170*, 5652-5657.

Gordon, S. (1992). Antigen markers of macrophage differentiation in murine tissues).

Gordon, S. (1995). The macrophage. Bioessays *17*, 977-986.

Govek, E. E. Newey, S. E. and Van Aelst, L. (2005). The role of the Rho GTPases in neuronal development. Genes Dev *19*, 1-49.

Gu, Y. Filippi, M. D. Cancelas, J. A. Siefring, J. E. Williams, E. P. Jasti, A. C. Harris, C. E. Lee, A. W. Prabhakar, R. Atkinson, S. J. *et al.* (2003). Hematopoietic cell regulation by Rac1 and Rac2 guanosine triphosphatases. Science *302*, 445-449.

Hall, A. (1998). RhoGTPases and the actin cytoskeleton. Science. *279*,509-14.

Hall, A. (2000). GTPases (Oxford, Oxford University Press).

Hall, A. and Nobes, C. D. (2000). Rho GTPases: molecular switches that control the organization and dynamics of the actin cytoskeleton. Philos Trans R Soc Lond B Biol Sci *355*, 965-970.

Hall, A. Paterson, H. F. Adamson, P. and Ridley, A. J. (1993). Cellular responses regulated by rho-related small GTP-binding proteins. Philos Trans R Soc Lond B Biol Sci *340*, 267-271.

Hannigan, M. Zhan, L. Li, Z. Ai, Y. Wu, D. and Huang, C. K. (2002). Neutrophils lacking phosphoinositide 3-kinase γ show loss of directionality during N-formyl-Met-Leu-Phe-induced chemotaxis. Proc Natl Acad Sci U S A *99*, 3603-3608.

Hayman, E. G. Pierschbacher, M. D. Ohgren, Y. and Ruoslahti, E. (1983). Serum spreading factor (vitronectin) is present at the cell surface and in tissues. Proc Natl Acad Sci U S A *80*, 4003-4007.

Henderson, R. B. Hobbs, J. A. Mathies, M. and Hogg, N. (2003). Rapid recruitment of inflammatory monocytes is independent of neutrophil migration. Blood *102*, 328-335.

Higgs, H. N. and Pollard, T. D. (2001). Regulation of actin filament network formation through ARP2/3 complex: activation by a diverse array of proteins. Annu Rev Biochem *70*, 649-676.

Hogg, N. Henderson, R. Leitinger, B. McDowall, A. Porter, J. and Stanley, P. (2002). Mechanisms contributing to the activity of integrins on leukocytes. Immunol Rev *186*, 164-171.

Hogg, N. Smith, A. McDowall, A. Giles, K. Stanley, P. Laschinger, M. and Henderson, R. (2004). How T cells use LFA-1 to attach and migrate. Immunol Lett *92*, 51-54.

Hood, J. D. and Cheresh, D. A. (2002). Role of integrins in cell invasion and migration. Nat Rev Cancer *2*, 91-100.

Hotchin, N. A. and Hall, A. (1995). The assembly of integrin adhesion complexes requires both extracellular matrix and intracellular rho/rac GTPases. J Cell Biol *131*, 1857-1865.

Houliston, E. Pickering, S. J. and Maro, B. (1987). Redistribution of microtubules and pericentriolar material during the development of polarity in mouse blastomeres. J Cell Biol *104*, 1299-1308.

Howard, J. (2001). Mechanics of motor proteins and the cytoskeleton (Sunderland, Mass. Sinauer Associates).

Hynes RO. (2002) Integrins: bidirectional, allosteric signaling machines.Cell.*110:*673-87.

Ihara, K. Muraguchi, S. Kato, M. Shimizu, T. Shirakawa, M. Kuroda, S. Kaibuchi, K. and Hakoshima, T. (1998). Crystal structure of human RhoA in a dominantly active form complexed with a GTP analogue. J Biol Chem *273*, 9656-9666.

Ishida, H. Zhang, X. Erickson, K. and Ray, P. (2004). Botulinum toxin type A targets RhoB to inhibit lysophosphatidic acid-stimulated actin reorganization and acetylcholine release in nerve growth factor-treated PC12 cells. J Pharmacol Exp Ther *310*, 881-889.

Ishizaki, T. Morishima, Y. Okamoto, M. Furuyashiki, T. Kato, T. and Narumiya, S. (2001). Coordination of microtubules and the actin cytoskeleton by the Rho effector mDia1. Nat Cell Biol *3*, 8-14.

Ivetic, A. and Ridley, A. J. (2004). Ezrin/radixin/moesin proteins and Rho GTPase signalling in leucocytes. Immunology *112*, 165-176.

Jahner, D. and Hunter, T. (1991). The ras-related gene rhoB is an immediate-early gene inducible by v-Fps, epidermal growth factor, and platelet-derived growth factor in rat fibroblasts. Mol Cell Biol *11*, 3682-3690.

Jiang, K. Delarue, F. L. and Sebti, S. M. (2004a). EGFR, ErbB2 and Ras but not Src suppress RhoB expression while ectopic expression of RhoB antagonizes oncogene-mediated transformation. Oncogene *23*, 1136-1145.

Jiang, K. Sun, J. Cheng, J. Djeu, J. Y. Wei, S. and Sebti, S. (2004b). Akt mediates Ras downregulation of RhoB, a suppressor of transformation, invasion, and metastasis. Mol Cell Biol *24*, 5565-5576.

Jones, G. E. (2000). Cellular signaling in macrophage migration and chemotaxis. J Leukoc Biol *68*, 593-602.

Jones, G. E. Prigmore, E. Calvez, R. Hogan, C. Dunn, G. A. Hirsch, E. Wymann, M. P. and Ridley, A. J. (2003). Requirement for PI 3-kinase γ in macrophage migration to MCP-1 and CSF-1. Exp Cell Res *290*, 120-131.

Kaibuchi, K. Kuroda, S. and Amano, M. (1999). Regulation of the cytoskeleton and cell adhesion by the Rho family GTPases in mammalian cells. Annu Rev Biochem *68*, 459-486.

Kaverina, I. Krylyshkina, O. and Small, J. V. (1999). Microtubule targeting of substrate contacts promotes their relaxation and dissociation. J Cell Biol *146*, 1033-1044.

Kelley, T. W. Graham, M. M. Doseff, A. I. Pomerantz, R. W. Lau, S. M. Ostrowski, M. C. Franke, T. F. and Marsh, C. B. (1999). Macrophage colony-stimulating factor promotes cell survival through Akt/protein kinase B. J Biol Chem *274*, 26393-26398.

Kemp BE, Pearson RB, House C. (1983). Role of basic residues in the phosphorylation of synthetic peptides by myosin light chain kinase. Proc Natl Acad Sci U S A. 80, 7471-7475.

Kimura, K. Ito, M. Amano, M. Chihara, K. Fukata, Y. Nakafuku, M. Yamamori, B. Feng, J. Nakano, T. Okawa, K. *et al.* (1996). Regulation of myosin phosphatase by Rho and Rho-associated kinase (Rho-kinase). Science *273*, 245-248.

Kiosses WB, Shattil SJ, Pampori N, Schwartz MA. (2001). Nat Cell Biol. 3:316-20.

Koch, G. Benz, C. Schmidt, G. Olenik, C. and Aktories, K. (1997). Role of Rho protein in lovastatin-induced breakdown of actin cytoskeleton. J Pharmacol Exp Ther *283*, 901-909.

Kozma, R. Ahmed, S. Best, A. and Lim, L. (1995). The Ras-related protein Cdc42Hs and bradykinin promote formation of peripheral actin microspikes and filopodia in Swiss 3T3 fibroblasts. Mol Cell Biol *15*, 1942-1952.

Kraynov, V. S. Chamberlain, C. Bokoch, G. M. Schwartz, M. A. Slabaugh, S. and Hahn, K. M. (2000). Localized Rac activation dynamics visualized in living cells. Science *290*, 333-337.

Krendel, M. Zenke, F. T. and Bokoch, G. M. (2002). Nucleotide exchange factor GEF-H1 mediates cross-talk between microtubules and the actin cytoskeleton. Nat Cell Biol *4*, 294-301.

Kunkel, E. J. and Butcher, E. C. (2002). Chemokines and the tissue-specific migration of lymphocytes. Immunity *16*, 1-4.

Lacey, A. J. (1999). Light microscopy in biology : a practical approach, 2nd edn (Oxford, Oxford University Press).

Laplante, I. Paquin, J. and Beliveau, R. (2001). RhoB expression is induced after the transient upregulation of RhoA and Cdc42 during neuronal differentiation and influenced by culture substratum and microtubule integrity. Brain Res Dev Brain Res *129*, 157-168.

Lauber, K. Bohn, E. Krober, S. M. Xiao, Y. J. Blumenthal, S. G. Lindemann, R. K. Marini, P. Wiedig, C. Zobywalski, A. Baksh, S. *et al.* (2003). Apoptotic cells induce migration of phagocytes via caspase-3-mediated release of a lipid attraction signal. Cell *113*, 717-730.

Lebowitz, P. F. Casey, P. J. Prendergast, G. C. and Thissen, J. A. (1997). Farnesyltransferase inhibitors alter the prenylation and growth-stimulating function of RhoB. J Biol Chem *272*, 15591-15594.

Lebowitz, P. F. and Prendergast, G. C. (1998). Non-Ras targets of farnesyltransferase inhibitors: focus on Rho. Oncogene *17*, 1439-1445.

Lee, Y. L. Shih, K. Bao, P. Ghirnikar, R. S. and Eng, L. F. (2000). Cytokine chemokine expression in contused rat spinal cord. Neurochem Int *36*, 417-425.

Leverrier, Y. and Ridley, A. J. (2001). Requirement for Rho GTPases and PI 3-kinases during apoptotic cell phagocytosis by macrophages. Curr Biol *11*, 195-199.

Li, S. Yamauchi, A. Marchal, C. C. Molitoris, J. K. Quilliam, L. A. and Dinauer, M. C. (2002). Chemoattractant-stimulated Rac activation in wild-type and Rac2-deficient

murine neutrophils: preferential activation of Rac2 and Rac2 gene dosage effect on neutrophil functions. J Immunol *169*, 5043-5051.

Li, Z. Hannigan, M. Mo, Z. Liu, B. Lu, W. Wu, Y. Smrcka, A. V. Wu, G. Li, L. Liu, M. *et al.* (2003). Directional sensing requires G β γ-mediated PAK1 and PIX α-dependent activation of Cdc42. Cell *114*, 215-227.

Lin EY, Nguyen AV, Russell RG, Pollard JW.(2001) Colony-stimulating factor 1 promotes progression of mammary tumors to malignancy. J Exp Med. *193*:727-40.

Linder, S. and Aepfelbacher, M. (2003). Podosomes: adhesion hot-spots of invasive cells. Trends Cell Biol *13*, 376-385.

Linder, S. Hufner, K. Wintergerst, U. and Aepfelbacher, M. (2000). Microtubule-dependent formation of podosomal adhesion structures in primary human macrophages. J Cell Sci *113 Pt 23*, 4165-4176.

Liu, A. Du, W. Liu, J. P. Jessell, T. M. and Prendergast, G. C. (2000). RhoB alteration is necessary for apoptotic and antineoplastic responses to farnesyltransferase inhibitors. Mol Cell Biol *20*, 6105-6113.

Liu, A. X. Rane, N. Liu, J. P. and Prendergast, G. C. (2001). RhoB is dispensable for mouse development, but it modifies susceptibility to tumor formation as well as cell adhesion and growth factor signaling in transformed cells. Mol Cell Biol *21*, 6906-6912.

Lu, B. Rutledge, B. J. Gu, L. Fiorillo, J. Lukacs, N. W. Kunkel, S. L. North, R. Gerard, C. and Rollins, B. J. (1998). Abnormalities in monocyte recruitment and cytokine expression in monocyte chemoattractant protein 1-deficient mice. J Exp Med *187*, 601-608.

Madaule, P. and Axel, R. (1985). A novel ras-related gene family. Cell *41*, 31-40.

Madaule, P. Furuyashiki, T. Reid, T. Ishizaki, T. Watanabe, G. Morii, N. and Narumiya, S. (1995). A novel partner for the GTP-bound forms of rho and rac. FEBS Lett *377*, 243-248.

Maddala, R. Reddy, V. N. Epstein, D. L. and Rao, V. (2003). Growth factor induced activation of Rho and Rac GTPases and actin cytoskeletal reorganization in human lens epithelial cells. Mol Vis *9*, 329-336.

Maekawa, M. Ishizaki, T. Boku, S. Watanabe, N. Fujita, A. Iwamatsu, A. Obinata, T. Ohashi, K. Mizuno, K. and Narumiya, S. (1999). Signaling from Rho to the actin cytoskeleton through protein kinases ROCK and LIM-kinase. Science *285*, 895-898.

Miralles, F. Posern, G. Zaromytidou, A. I. and Treisman, R. (2003). Actin dynamics control SRF activity by regulation of its coactivator MAL. Cell *113*, 329-342.

Mircescu, H. Steuve, S. Savonet, V. Degraef, C. Mellor, H. Dumont, J. E. Maenhaut, C. and Pirson, I. (2002). Identification and characterization of a novel activated RhoB binding protein containing a PDZ domain whose expression is specifically modulated in thyroid cells by cAMP. Eur J Biochem *269*, 6241-6249.

Mitchison TJ. (1995) Evolution of a dynamic cytoskeleton. Philos Trans R Soc Lond B Biol Sci. *349*:299-304.

Mitchison, T. J. and Cramer, L. P. (1996). Actin-based cell motility and cell locomotion. Cell *84*, 371-379.

Moreau, V. Tatin, F. Varon, C. and Genot, E. (2003). Actin can reorganize into podosomes in aortic endothelial cells, a process controlled by Cdc42 and RhoA. Mol Cell Biol *23*, 6809-6822.

Mosmann, T. (1983). Rapid colorimetric assay for cellular growth and survival: application to proliferation and cytotoxicity assays. J Immunol Methods *65*, 55-63.

Narumiya, S. Ishizaki, T. and Watanabe, N. (1997). Rho effectors and reorganization of actin cytoskeleton. FEBS Lett *410*, 68-72.

Nayal A, Webb DJ, Horwitz AF. (2004). Talin: an emerging focal point of adhesion dynamics. Curr Opin Cell Biol. *1*,94-8.

Niggli, V. (2003). Microtubule-disruption-induced and chemotactic-peptide-induced migration of human neutrophils: implications for differential sets of signalling pathways. J Cell Sci *116*, 813-822.

Nimnual, A. S. Taylor, L. J. and Bar-Sagi, D. (2003). Redox-dependent downregulation of Rho by Rac. Nat Cell Biol *5*, 236-241.

Nisimoto, Y. Freeman, J. L. Motalebi, S. A. Hirshberg, M. and Lambeth, J. D. (1997). Rac binding to p67(phox). Structural basis for interactions of the Rac1 effector region and insert region with components of the respiratory burst oxidase. J Biol Chem *272*, 18834-18841.

Nobes, C. D. and Hall, A. (1995). Rho, rac, and cdc42 GTPases regulate the assembly of multimolecular focal complexes associated with actin stress fibers, lamellipodia, and filopodia. Cell *81*, 53-62.

Nobes, C. D. and Hall, A. (1999). Rho GTPases control polarity, protrusion, and adhesion during cell movement. J Cell Biol *144*, 1235-1244.

Maesaki, R. Ihara, K. Shimizu, T. Kuroda, S. Kaibuchi, K. and Hakoshima, T. (1999). The structural basis of Rho effector recognition revealed by the crystal structure of human RhoA complexed with the effector domain of PKN/PRK1. Mol Cell *4*, 793-803.

Magdalena, J. Millard, T. H. and Machesky, L. M. (2003). Microtubule involvement in NIH 3T3 Golgi and MTOC polarity establishment. J Cell Sci *116*, 743-756.

Magie, C. R. Meyer, M. R. Gorsuch, M. S. and Parkhurst, S. M. (1999). Mutations in the Rho1 small GTPase disrupt morphogenesis and segmentation during early Drosophila development. Development *126*, 5353-5364.

Mallik R, and Gross SP. (2004) Molecular motors: strategies to get along. Curr Biol. *14*:R971-82.

Matsui, T. Amano, M. Yamamoto, T. Chihara, K. Nakafuku, M. Ito, M. Nakano, T. Okawa, K. Iwamatsu, A. and Kaibuchi, K. (1996). Rho-associated kinase, a novel serine/threonine kinase, as a putative target for small GTP binding protein Rho. Embo J *15*, 2208-2216.

Matsumura, F. Ono, S. Yamakita, Y. Totsukawa, G. and Yamashiro, S. (1998). Specific localization of serine 19 phosphorylated myosin II during cell locomotion and mitosis of cultured cells. J Cell Biol *140*, 119-129.

McNiven, M. A. Baldassarre, M. and Buccione, R. (2004). The role of dynamin in the assembly and function of podosomes and invadopodia. Front Biosci *9*, 1944-1953.

Mejillano, M. R. Kojima, S. Applewhite, D. A. Gertler, F. B. Svitkina, T. M. and Borisy, G. G. (2004). Lamellipodial versus filopodial mode of the actin nanomachinery: pivotal role of the filament barbed end. Cell *118*, 363-373.

Mellor, H. Flynn, P. Nobes, C. D. Hall, A. and Parker, P. J. (1998). PRK1 is targeted to endosomes by the small GTPase, RhoB. J Biol Chem *273*, 4811-4814.

Merlot, S. and Firtel, R. A. (2003). Leading the way: Directional sensing through phosphatidylinositol 3-kinase and other signaling pathways. J Cell Sci *116*, 3471-3478.

Millan, J. and Ridley, A. J. (2004). Rho GTPases and leukocyte-induced endothelial remodelling. Biochem J.

Millard, T. H. Sharp, S. J. and Machesky, L. M. (2004). Signalling to actin assembly via the WASP (Wiskott-Aldrich syndrome protein)-family proteins and the Arp2/3 complex. Biochem J *380*, 1-17.

Minamide, L. S. Painter, W. B. Schevzov, G. Gunning, P. and Bamburg, J. R. (1997). Differential regulation of actin depolymerizing factor and cofilin in response to alterations in the actin monomer pool. J Biol Chem *272*, 8303-8309.

O'Kane, E. M. Stone, T. W. and Morris, B. J. (2004). Increased long-term potentiation in the CA1 region of rat hippocampus via modulation of GTPase signalling or inhibition of Rho kinase. Neuropharmacology *46*, 879-887.

Okigaki, M. Davis, C. Falasca, M. Harroch, S. Felsenfeld, D. P. Sheetz, M. P. and Schlessinger, J. (2003). Pyk2 regulates multiple signaling events crucial for macrophage morphology and migration. Proc Natl Acad Sci U S A *100*, 10740-10745.

Olson, M. F. (2002). Gem GTPase: between a ROCK and a hard place. Curr Biol *12*, R496-498.

Palazzo, A. F. Eng, C. H. Schlaepfer, D. D. Marcantonio, E. E. and Gundersen, G. G. (2004). Localized stabilization of microtubules by integrin- and FAK-facilitated Rho signaling. Science *303*, 836-839.

Palazzo, A. F. Joseph, H. L. Chen, Y. J. Dujardin, D. L. Alberts, A. S. Pfister, K. K. Vallee, R. B. and Gundersen, G. G. (2001). Cdc42, dynein, and dynactin regulate MTOC reorientation independent of Rho-regulated microtubule stabilization. Curr Biol *11*, 1536-1541.

Parsons, J. T. (2003). Focal adhesion kinase: the first ten years. J Cell Sci *116*, 1409-1416.

Parsons, S. J. and Parsons, J. T. (2004). Src family kinases, key regulators of signal transduction. Oncogene *23*, 7906-7909.

Paulnock, D. M. (2000). Macrophages : a practical approach (Oxford, Oxford University Press).

Paul W.E. and Seder R.A. (1994) Lymphocyte responses and cytokines. Cell *76*, 241-251

Pfaff, M. and Jurdic, P. (2001). Podosomes in osteoclast-like cells: structural analysis and cooperative roles of paxillin, proline-rich tyrosine kinase 2 (Pyk2) and integrin αVβ3. J Cell Sci *114*, 2775-2786.

Pixley, F. J. Lee, P. S. Condeelis, J. S. and Stanley, E. R. (2001). Protein tyrosine phosphatase phi regulates paxillin tyrosine phosphorylation and mediates colony-stimulating factor 1-induced morphological changes in macrophages. Mol Cell Biol *21*, 1795-1809.

Pixley, F. J. and Stanley, E. R. (2004). CSF-1 regulation of the wandering macrophage: complexity in action. Trends Cell Biol *14*, 628-638.

Platko, J. V. Leonard, D. A. Adra, C. N. Shaw, R. J. Cerione, R. A. and Lim, B. (1995). A single residue can modify target-binding affinity and activity of the functional

domain of the Rho-subfamily GDP dissociation inhibitors. Proc Natl Acad Sci U S A *92*, 2974-2978.

Pollard, T. D. (1983). Measurement of rate constants for actin filament elongation in solution. Anal Biochem *134*, 406-412.

Prahlad, V. Yoon, M. Moir, R. D. Vale, R. D. and Goldman, R. D. (1998). Rapid movements of vimentin on microtubule tracks: kinesin-dependent assembly of intermediate filament networks. J Cell Biol *143*, 159-170.

Prendergast, G. C. (2001). Actin' up: RhoB in cancer and apoptosis. Nat Rev Cancer *1*, 162-168.

Pring, M. Evangelista, M. Boone, C. Yang, C. and Zigmond, S. H. (2003). Mechanism of formin-induced nucleation of actin filaments. Biochemistry *42*, 486-496.

Redd, M. J. Cooper, L. Wood, W. Stramer, B. and Martin, P. (2004). Wound healing and inflammation: embryos reveal the way to perfect repair. Philos Trans R Soc Lond B Biol Sci *359*, 777-784.

Reid, T. Furuyashiki, T. Ishizaki, T. Watanabe, G. Watanabe, N. Fujisawa, K. Morii, N. Madaule, P. and Narumiya, S. (1996). Rhotekin, a new putative target for Rho bearing homology to a serine/threonine kinase, PKN, and rhophilin in the rho-binding domain. J Biol Chem *271*, 13556-13560.

Ren, X. D. and Schwartz, M. A. (2000). Determination of GTP loading on Rho. Methods Enzymol *325*, 264-272.

Revenu, C. Athman, R. Robine, S. and Louvard, D. (2004). The co-workers of actin filaments: from cell structures to signals. Nat Rev Mol Cell Biol *5*, 635-646.

Ridley, A. J. (1997a). The GTP-binding protein Rho. Int J Biochem Cell Biol *29*, 1225-1229.

Ridley, A. J. (1997b). Signalling by Rho family proteins. Biochem Soc Trans *25*, 1005-1010.

Ridley, A. J. (2001a). Rho family proteins: coordinating cell responses. Trends Cell Biol *11*, 471-477.

Ridley, A. J. (2001b). Rho GTPases and cell migration. J Cell Sci *114*, 2713-2722.

Ridley, A. J. (2001c). Rho proteins, PI 3-kinases, and monocyte/macrophage motility. FEBS Lett *498*, 168-171.

Ridley, A. J. (2004). Rho proteins and cancer. Breast Cancer Res Treat *84*, 13-19.

Ridley, A. J. and Hall, A. (1992). The small GTP-binding protein rho regulates the assembly of focal adhesions and actin stress fibers in response to growth factors. Cell *70*, 389-399.

Ridley, A. J. Paterson, H. F. Johnston, C. L. Diekmann, D. and Hall, A. (1992). The small GTP-binding protein rac regulates growth factor-induced membrane ruffling. Cell *70*, 401-410.

Ridley, A. J. Schwartz, M. A. Burridge, K. Firtel, R. A. Ginsberg, M. H. Borisy, G. Parsons, J. T. and Horwitz, A. R. (2003). Cell migration: integrating signals from front to back. Science *302*, 1704-1709.

Riento, K. and Ridley, A. J. (2003). Rocks: multifunctional kinases in cell behaviour. Nat Rev Mol Cell Biol *4*, 446-456.

Rodriguez, O. C. Schaefer, A. W. Mandato, C. A. Forscher, P. Bement, W. M. and Waterman-Storer, C. M. (2003). Conserved microtubule-actin interactions in cell movement and morphogenesis. Nat Cell Biol *5*, 599-609.

Rojas, R. Ruiz, W. G. Wang, E. Kinlough, C. L. Poland, P. A. Hughey, R. P. Dunn, K. W. and Apodaca, G. (2004). RhoB-dependent modulation of early endocytic traffic in Madin-Darby canine kidney cells. J Biol Chem.

Rottner, K. Hall, A. and Small, J. V. (1999). Interplay between Rac and Rho in the control of substrate contact dynamics. Curr Biol *9*, 640-648.

Sahai, E. and Marshall, C. J. (2002a). RHO-GTPases and cancer. Nat Rev Cancer *2*, 133-142.

Sahai, E. and Marshall, C. J. (2002b). ROCK and Dia have opposing effects on adherens junctions downstream of Rho. Nat Cell Biol *4*, 408-415.

Saito, H. Minamiya, Y. Saito, S. and Ogawa, J. (2002). Endothelial Rho and Rho kinase regulate neutrophil migration via endothelial myosin light chain phosphorylation. J Leukoc Biol *72*, 829-836.

Saltel, F. Destaing, O. Bard, F. Eichert, D. and Jurdic, P. (2004). Apatite-mediated actin dynamics in resorbing osteoclasts. Mol Biol Cell *15*, 5231-5241.

Sander, E. E. ten Klooster, J. P. van Delft, S. van der Kammen, R. A. and Collard, J. G. (1999). Rac downregulates Rho activity: reciprocal balance between both GTPases determines cellular morphology and migratory behavior. J Cell Biol *147*, 1009-1022.

Sandilands, E. Cans, C. Fincham, V. J. Brunton, V. G. Mellor, H. Prendergast, G. C. Norman, J. C. Superti-Furga, G. and Frame, M. C. (2004). RhoB and actin polymerization coordinate Src activation with endosome-mediated delivery to the membrane. Dev Cell *7*, 855-869.

Schenkel, A. R. Mamdouh, Z. and Muller, W. A. (2004). Locomotion of monocytes on endothelium is a critical step during extravasation. Nat Immunol *5*, 393-400.

Schmidt, A. and Hall, A. (2002). Guanine nucleotide exchange factors for Rho GTPases: turning on the switch. Genes Dev *16*, 1587-1609.

Schneider, G. B. Gilmore, A. P. Lohse, D. L. Romer, L. H. and Burridge, K. (1998). Microinjection of protein tyrosine phosphatases into fibroblasts disrupts focal adhesions and stress fibers. Cell Adhes Commun *5*, 207-219.

Schratt, G. Philippar, U. Berger, J. Schwarz, H. Heidenreich, O. and Nordheim, A. (2002). Serum response factor is crucial for actin cytoskeletal organization and focal adhesion assembly in embryonic stem cells. J Cell Biol *156*, 737-750.

Settleman, J. (2001). Rac 'n Rho: the music that shapes a developing embryo. Dev Cell *1*, 321-331.

Shao, F. and Dixon, J. E. (2003). YopT is a cysteine protease cleaving Rho family GTPases. Adv Exp Med Biol *529*, 79-84.

Sharma, S. V. (1998). Rapid recruitment of p120RasGAP and its associated protein, p190RhoGAP, to the cytoskeleton during integrin mediated cell-substrate interaction. Oncogene *17*, 271-281.

Sheikine, Y. and Hansson, G. K. (2004). Chemokines and atherosclerosis. Ann Med *36*, 98-118.

Sherr, C. J. Rettenmier, C. W. Sacca, R. Roussel, M. F. Look, A. T. and Stanley, E. R. (1985). The c-fms proto-oncogene product is related to the receptor for the mononuclear phagocyte growth factor, CSF-1. Cell *41*, 665-676.

Small, J. V. and Kaverina, I. (2003). Microtubules meet substrate adhesions to arrange cell polarity. Curr Opin Cell Biol *15*, 40-47.

Smith, A. Bracke, M. Leitinger, B. Porter, J. C. and Hogg, N. (2003). LFA-1-induced T cell migration on ICAM-1 involves regulation of MLCK-mediated attachment and ROCK-dependent detachment. J Cell Sci *116*, 3123-3133.

Springer T.A. (1994). Traffic signals for lymphocyte recirculation and leukocyte emigration. The multistep paradigm. Cell *76*, 301-314.

Stamatakis, K. Cernuda-Morollon, E. Hernandez-Perera, O. and Perez-Sala, D. (2002). Isoprenylation of RhoB is necessary for its degradation. A novel determinant in the complex regulation of RhoB expression by the mevalonate pathway. J Biol Chem *277*, 49389-49396.

Stanley, E. R. Berg, K. L. Einstein, D. B. Lee, P. S. Pixley, F. J. Wang, Y. and Yeung, Y. G. (1997). Biology and action of colony--stimulating factor-1. Mol Reprod Dev *46*, 4-10.

Sun, C. X. Downey, G. P. Zhu, F. Koh, A. L. Thang, H. and Glogauer, M. (2004). Rac1 is the small GTPase responsible for regulating the neutrophil chemotaxis compass. Blood *104*, 3758-3765.

Svitkina, T. M. and Borisy, G. G. (1999). Arp2/3 complex and actin depolymerizing factor/cofilin in dendritic organization and treadmilling of actin filament array in lamellipodia. J Cell Biol *145*, 1009-1026.

Svitkina, T. M. Bulanova, E. A. Chaga, O. Y. Vignjevic, D. M. Kojima, S. Vasiliev, J. M. and Borisy, G. G. (2003). Mechanism of filopodia initiation by reorganization of a dendritic network. J Cell Biol *160*, 409-421.

Svitkina, T. M. Verkhovsky, A. B. McQuade, K. M. and Borisy, G. G. (1997). Analysis of the actin-myosin II system in fish epidermal keratocytes: mechanism of cell body translocation. J Cell Biol *139*, 397-415.

Symons, M. and Rusk, N. (2003). Control of vesicular trafficking by Rho GTPases. Curr Biol *13*, R409-418.

Tatusova, T. A. and Madden, T. L. (1999). BLAST 2 Sequences, a new tool for comparing protein and nucleotide sequences. FEMS Microbiol Lett *174*, 247-250.

Tolliday, N. VerPlank, L. and Li, R. (2002). Rho1 directs formin-mediated actin ring assembly during budding yeast cytokinesis. Curr Biol *12*, 1864-1870.

Tsuji, T. Ishizaki, T. Okamoto, M. Higashida, C. Kimura, K. Furuyashiki, T. Arakawa, Y. Birge, R. B. Nakamoto, T. Hirai, H. and Narumiya, S. (2002). ROCK and mDia1 antagonize in Rho-dependent Rac activation in Swiss 3T3 fibroblasts. J Cell Biol *157*, 819-830.

Turner, C. E. (2000). Paxillin and focal adhesion signalling. Nat Cell Biol. 2000:E231-6.

Uehata, M. Ishizaki, T. Satoh, H. Ono, T. Kawahara, T. Morishita, T. Tamakawa, H. Yamagami, K. Inui, J. Maekawa, M. and Narumiya, S. (1997). Calcium sensitization of smooth muscle mediated by a Rho-associated protein kinase in hypertension. Nature *389*, 990-994.

Vanhaesebroeck, B. Jones, G. E. Allen, W. E. Zicha, D. Hooshmand-Rad, R. Sawyer, C. Wells, C. Waterfield, M. D. and Ridley, A. J. (1999). Distinct PI(3)Ks mediate mitogenic signalling and cell migration in macrophages. Nat Cell Biol *1*, 69-71.

Vicente-Manzanares, M. Cabrero, J. R. Rey, M. Perez-Martinez, M. Ursa, A. Itoh, K. and Sanchez-Madrid, F. (2002). A role for the Rho-p160 Rho coiled-coil kinase axis in the chemokine stromal cell-derived factor-1α-induced lymphocyte actomyosin and microtubular organization and chemotaxis. J Immunol *168*, 400-410.

Wakatsuki, T. Wysolmerski, R. B. and Elson, E. L. (2003). Mechanics of cell spreading: role of myosin II. J Cell Sci *116*, 1617-1625.

Wallar, B. J. and Alberts, A. S. (2003). The formins: active scaffolds that remodel the cytoskeleton. Trends Cell Biol *13*, 435-446.

Wallis, J. W. Aerts, J. Groenen, M. A. Crooijmans, R. P. Layman, D. Graves, T. A. Scheer, D. E. Kremitzki, C. Fedele, M. J. Mudd, N. K. *et al.* (2004). A physical map of the chicken genome. Nature *432*, 761-764.

Wang, H. R. Zhang, Y. Ozdamar, B. Ogunjimi, A. A. Alexandrova, E. Thomsen, G. H. and Wrana, J. L. (2003a). Regulation of cell polarity and protrusion formation by targeting RhoA for degradation. Science *302*, 1775-1779.

Wang, L. Yang, L. Luo, Y. and Zheng, Y. (2003b). A novel strategy for specifically down-regulating individual Rho GTPase activity in tumor cells. J Biol Chem *278*, 44617-44625.

Ware, M. F. Wells, A. and Lauffenburger, D. A. (1998). Epidermal growth factor alters fibroblast migration speed and directional persistence reciprocally and in a matrix-dependent manner. J Cell Sci *111 (Pt 16)*, 2423-2432.

Watanabe, N. Madaule, P. Reid, T. Ishizaki, T. Watanabe, G. Kakizuka, A. Saito, Y. Nakao, K. Jockusch, B. M. and Narumiya, S. (1997). p140mDia, a mammalian homolog of Drosophila diaphanous, is a target protein for Rho small GTPase and is a ligand for profilin. Embo J *16*, 3044-3056.

Waterman-Storer, C. M. and Danuser, G. (2002). New directions for fluorescent speckle microscopy. Curr Biol *12*, R633-640.

Webb, S. E. Pollard, J. W. and Jones, G. E. (1996). Direct observation and quantification of macrophage chemoattraction to the growth factor CSF-1. J Cell Sci *109 (Pt 4)*, 793-803.

Wei, L. Imanaka-Yoshida, K. Wang, L. Zhan, S. Schneider, M. D. DeMayo, F. J. and Schwartz, R. J. (2002). Inhibition of Rho family GTPases by Rho GDP dissociation inhibitor disrupts cardiac morphogenesis and inhibits cardiomyocyte proliferation. Development *129*, 1705-1714.

Weiss-Haljiti, C. Pasquali, C. Ji, H. Gillieron, C. Chabert, C. Curchod, M. L. Hirsch, E. Ridley, A. J. van Huijsduijnen, R. H. Camps, M. and Rommel, C. (2004). Involvement of phosphoinositide 3-kinase γ, Rac, and PAK signaling in chemokine-induced macrophage migration. J Biol Chem *279*, 43273-43284.

Wells, C. M. and Ridley, A. J. (2004). Analysis of cell migration using the dunn chemotaxis chamber and time-lapse microscopy. Methods Mol Biol *294*, 31-42.

Wells, C. M. Walmsley, M. Ooi, S. Tybulewicz, V. and Ridley, A. J. (2004). Rac1-deficient macrophages exhibit defects in cell spreading and membrane ruffling but not migration. J Cell Sci *117*, 1259-1268.

Wherlock, M. Gampel, A. Futter, C. and Mellor, H. (2004). Farnesyltransferase inhibitors disrupt EGF receptor traffic through modulation of the RhoB GTPase. J Cell Sci *117*, 3221-3231.

Wherlock, M. and Mellor, H. (2002). The Rho GTPase family: a Racs to Wrchs story. J Cell Sci *115*, 239-240.

Williams, L. M. and Ridley, A. J. (2000). Lipopolysaccharide induces actin reorganization and tyrosine phosphorylation of Pyk2 and paxillin in monocytes and macrophages. J Immunol *164*, 2028-2036.

Wiseman, P. W. Brown, C. M. Webb, D. J. Hebert, B. Johnson, N. L. Squier, J. A. Ellisman, M. H. and Horwitz, A. F. (2004). Spatial mapping of integrin interactions and dynamics during cell migration by image correlation microscopy. J Cell Sci *117*, 5521-5534.

Wittmann, T. Bokoch, G. M. and Waterman-Storer, C. M. (2003). Regulation of leading edge microtubule and actin dynamics downstream of Rac1. J Cell Biol *161*, 845-851.

Wojciak-Stothard, B. Entwistle, A. Garg, R. and Ridley, A. J. (1998). Regulation of TNF-α-induced reorganization of the actin cytoskeleton and cell-cell junctions by Rho, Rac, and Cdc42 in human endothelial cells. J Cell Physiol *176*, 150-165.

Wojciak-Stothard, B. and Ridley, A. J. (2002). Rho GTPases and the regulation of endothelial permeability. Vascul Pharmacol *39*, 187-199.

Wojciak-Stothard, B. and Ridley, A. J. (2003). Shear stress-induced endothelial cell polarization is mediated by Rho and Rac but not Cdc42 or PI 3-kinases. J Cell Biol *161*, 429-439.

Wood, W. Jacinto, A. Grose, R. Woolner, S. Gale, J. Wilson, C. and Martin, P. (2002). Wound healing recapitulates morphogenesis in Drosophila embryos. Nat Cell Biol *4*, 907-912.

Worthylake, R. A. and Burridge, K. (2001). Leukocyte transendothelial migration: orchestrating the underlying molecular machinery. Curr Opin Cell Biol *13*, 569-577.

Worthylake, R. A. and Burridge, K. (2003). RhoA and ROCK promote migration by limiting membrane protrusions. J Biol Chem *278*, 13578-13584.

Worthylake, R. A. Lemoine, S. Watson, J. M. and Burridge, K. (2001). RhoA is required for monocyte tail retraction during transendothelial migration. J Cell Biol *154*, 147-160.

Wu, M. Wu, Z. F. Kumar-Sinha, C. Chinnaiyan, A. and Merajver, S. D. (2004). RhoC induces differential expression of genes involved in invasion and metastasis in MCF10A breast cells. Breast Cancer Res Treat *84*, 3-12.

Wyckoff, J. Wang, W. Lin, E. Y. Wang, Y. Pixley, F. Stanley, E. R. Graf, T. Pollard, J. W. Segall, J. and Condeelis, J. (2004). A paracrine loop between tumor cells and macrophages is required for tumor cell migration in mammary tumors. Cancer Res *64*, 7022-7029.

Xu, J. Wang, F. Van Keymeulen, A. Herzmark, P. Straight, A. Kelly, K. Takuwa, Y. Sugimoto, N. Mitchison, T. and Bourne, H. R. (2003). Divergent signals and cytoskeletal assemblies regulate self-organizing polarity in neutrophils. Cell *114*, 201-214.

Yamashiro, S. Yamakita, Y. Ono, S. and Matsumura, F. (1998). Fascin, an actin-bundling protein, induces membrane protrusions and increases cell motility of epithelial cells. Mol Biol Cell *9*, 993-1006.

Yeung, Y. G. Jubinsky, P. T. Sengupta, A. Yeung, D. C. and Stanley, E. R. (1987). Purification of the colony-stimulating factor 1 receptor and demonstration of its tyrosine kinase activity. Proc Natl Acad Sci U S A *84*, 1268-1271.

Yeung, Y. G. and Stanley, E. R. (2003). Proteomic Approaches to the Analysis of Early Events in Colony-stimulating Factor-1 Signal Transduction. Mol Cell Proteomics *2*, 1143-1155.

Yeung, Y. G. Wang, Y. Einstein, D. B. Lee, P. S. and Stanley, E. R. (1998). Colony-stimulating factor-1 stimulates the formation of multimeric cytosolic complexes of signaling proteins and cytoskeletal components in macrophages. J Biol Chem *273*, 17128-17137.

Yuruker, B. and Niggli, V. (1992). α-actinin and vinculin in human neutrophils: reorganization during adhesion and relation to the actin network. J Cell Sci *101 (Pt 2)*, 403-414.

Zalcman, G. Closson, V. Linares-Cruz, G. Lerebours, F. Honore, N. Tavitian, A. and Olofsson, B. (1995). Regulation of Ras-related RhoB protein expression during the cell cycle. Oncogene *10*, 1935-1945.

Zen, K. and Parkos, C. A. (2003). Leukocyte-epithelial interactions. Curr Opin Cell Biol *15*, 557-564.

Zeng, P. Y. Rane, N. Du, W. Chintapalli, J. and Prendergast, G. C. (2003). Role for RhoB and PRK in the suppression of epithelial cell transformation by farnesyltransferase inhibitors. Oncogene *22*, 1124-1134.

Zhang, J. Zhu, J. Bu, X. Cushion, M. Kinane, T. B. Avraham, H. and Koziel, H. (2004a). Cdc42 and RhoB Activation are Required for Mannose Receptor-Mediated Phagocytosis by Human Alveolar Macrophages. Mol Biol Cell.

Zhang, Y. Wang, H. R. and Wrana, J. L. (2004b). Smurf1: A Link between Cell Polarity and Ubiquitination. Cell Cycle *3*, 391-392.

Zheng, Y. Wong, M. L. Alberts, B. and Mitchison, T. (1995). Nucleation of microtubule assembly by a γ-tubulin-containing ring complex. Nature *378*, 578-583.

Zicha, D. Dunn, G. and Jones, G. (1997). Analyzing chemotaxis using the Dunn direct-viewing chamber. Methods Mol Biol *75*, 449-457.

Zlotnik A. and Yoshie O. (2000) Chemokines, A new classification system and their role in immunity. Immunity *12*, 121-127.

Zong, H. Raman, N. Mickelson-Young, L. A. Atkinson, S. J. and Quilliam, L. A. (1999). Loop 6 of RhoA confers specificity for effector binding, stress fiber formation, and cellular transformation. J Biol Chem *274*, 4551-4560.

Abbreviations

ADP	Adenosine diphosphate
ATP	Adenosine triphosphate
APS	Ammonium persulphate
BSA	Bovine serum albumin
BMM	Bone marrow derived macrophage
C terminal	Carboxyl terminus
t-C3	Tat *Chlostridium Botulinum* 3-transferase
cDNA	Complementary deoxyribose nucleic acid
CFSE	Carboxy-fluorescein diacetate succinimidyl ester
CO2	Carbon dioxide
CSF-1	Colony stimulating factor
DCS	Donor calf serum
DEPC	Diethylpyrocarbonate
Dia	Diaphanous
DMEM	Dulbecco's minimum essential medium
DMSO	Dimethyl sulphoxide
DNA	Deoxyribose nucleic acid
DRF	Diaphanous related formin
E.Coli	*Escherichia Coli*
ECM	Extracellular matrix
EDTA	Ethylene-diamine-tetra-acetic-acid
EGF	Epidermal growth factor
EGTA	Ethylene-glycol-tetra-acetic acid
Ena/VASP	Enabled/ vasodilator-stimulated phosphoprotein
ERK	Extracellular regulatory kinase
EST	Expressed sequence tag
F	Farnesylated
F-Actin	Filamentous actin
FAK	Focal adhesion kinase
FACS	Fluorescence assisted cell sorting
FCS	Foetal calf serum
FITC	Fluorescein isothiocyanate
FTI	Farnesyl transferase inhibitor

G-Actin	Globular actin
GAP	Guanine activator protein
GDI	Guanine dissociation inhibitor
GDP	Guanine di-phosphate
GEF	Guanine nucleotide exchange factor
GG	Geranylgeranylated
GST	Glutothione S-transferase
GTP	Guanine tri-phosphate
ddH2O	Double distilled water
HRP	Horseradish peroxidase
ICAM-1	Intracellular adhesion molecule 1
IPTG	Isopropylthiogalactopyranoside
IRM	Interference reflection microcopy
LIMK	Lim domain kinase
LPS	Lipopolysaccheride
MAPK	Mitogen activated protein kinase
MBS	Myosin binding subunit
MCP-1	Monocytic chemotactic peptide-1
MHC	Major histocompatibility complex
MIF	Macrophage inhibitory factor
MLC	Myosin light chain
MLCK	Myosin light chain kinase
mRNA	Messenger ribonucleic acid
MTOC	Microtubule organising centre
N terminal	Amino terminus
NP-40	Nonidet P-40
PAGE	Polyacrylamide gel electrophoresis
PAK	P21 activated kinase
PBS	Phosphate buffered saline
PCR	Polymerase chain reaction
PDGF	Platelet derived growth factor
PE	Phycoerythrin
PI 3-kinase	Phospho-inositide 3 kinase
PKC	Protein kinase C
PTEN	phosphatase and tensin homolog

pY118 paxillin	Phospho tyrosine-118 paxillin
RNA	Ribonucleic acid
RNAi	Ribonucleotide interference
ROCK	Rho-kinase
RT	Room Temperature
RT-PCR	Reverse transcriptase PCR
SDS	Sodium dodecyl sulphate
TBS	Tris buffered saline
TEMED	Tetramethylethylenediamine
TGF	Tumour growth factor
TIRF	Total internal reflection fluorescence
Tris	Trishydroxymethyalaminoethane
UV	Ultra-violet
WASP	Wiskott-Aldrich syndrome protein
Wt	Wild type
XPLN	Exchange factor found in platelets and leukemic and neuronal tissues

Acknowledgments:

Firstly I would like to thank Anne for all of her help, infinite patience and wise words through the last 4 years. It has been an inspiration and a pleasure to work under her supervision.

A big thankyou to the members of the Ridley lab old (Fig.1A), and new (Fig. 1B) for their support, tolerance and shared enthusiasm for tea and biscuits. In particular I would like to thank Claire Wells and Yann Levverier for teaching me the wily ways of macrophages, Stephen Smith and Parag Bhavsar for supplying macrophages, media and a listening ear in times of need and Aleks Ivetic and Priam Villalonga-Smith for help with all of the biochemistry and invaluable advice about how to get the pull downs working. Lastly, but by no means least Ritu Garg for constant technical support and encouragement.

I would like to express my gratitude to: the Laboratory of Molecular Cell Biology who co-ordinate the four year PhD programme and my PhD committee, Dr Kathy Barrett, Dr Kate Nobes, Prof. Steve Moss and Dr. Julie Pitcher for useful discussions and guidance. My collaborators; Dr George Prendergast and his laboratory (Lankenau institute, Pennsylvania) (Fig. 1C), Dr Brian Morris and Claire Guilding, Prof Michael Sheetz and Ben Dubin Thaler for giving me the space, time and technical assistance I needed with the TIRF microscopy (Fig 1D) and to Adam Meshel, Ana Kostic and other members of the Sheetz laboratory for making my time in New York so much fun.

Finally I'd like to thank Dr Jane Mellor for stimulating my enthusiasm for Biochemistry and Cell Biology. Thanks also to everyone in Kathy Barrett and Buzz Baums Lab for invaluable advice and emergency supplies (Fig 1E+F). A massive thankyou to all of my friends and family for the happy memories, tea and cake (the bastions of civilisation (Fig 1.G)), and of course to the Green Man for provision of beer in times of need.

This thesis is dedicated to the memory of James and Hilda McKinley.

Figure 1 Acknowledgements:

(A) The Ridley lab 2002. (B) The Ridley lab 2005. (C) Dr George Prendergasts Lab. (D) Ben Dubin Thalter and the TIRF microscope. (E) Dr Kathy Barretts Lab. (F) Dr Buzz Baums Lab. (G) Tea and cake.